Report No. FHWA-RD-77-127

DETERMINATION OF SEISMICALLY INDUCED SOIL LIQUEFACTION POTENTIAL AT PROPOSED BRIDGE SITES

Vol. 1 Theoretical Considerations
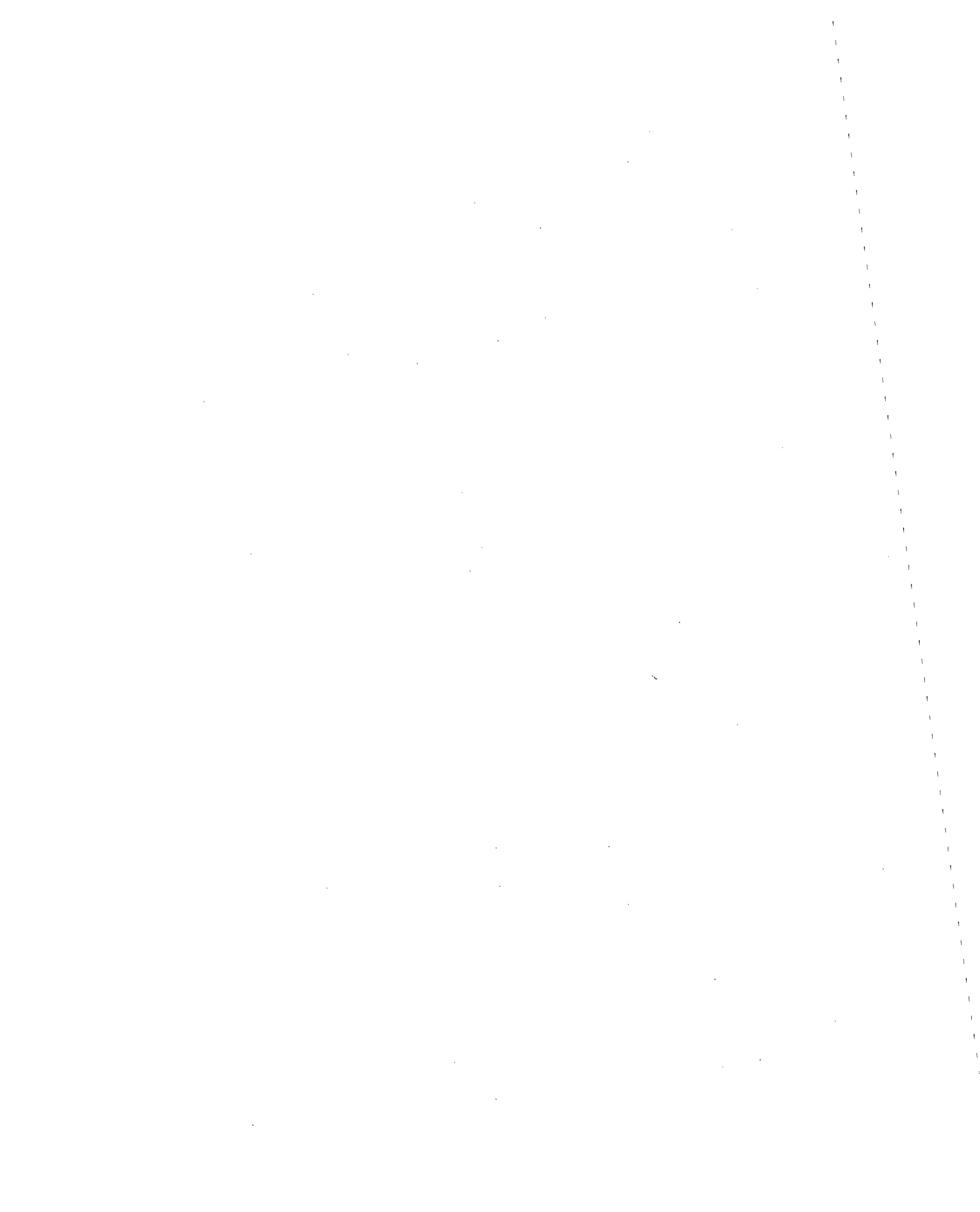
August 1977
Final Report

Prepared for

FEDERAL HIGHWAY ADMINISTRATION

Offices of Research & Development

Washington, D. C. 20590

1. Report No. FHWA-RD-77-127	2. Government Accession No.	3. Recipient's Catalog No. PB282354

4. Title and Subtitle DETERMINATION OF SEISMICALLY INDUCED SOIL LIQUEFACTION POTENTIAL AT PROPOSED BRIDGE SITES. Volume I - Theoretical Considerations	5. Report Date August 1977
	6. Performing Organization Code PB-282354

7. Author's) J. M. Ferritto and J. B. Forrest	8. Performing Organization Report No.

9. Performing Organization Name and Address CIVIL ENGINEERING LABORATORY Naval Construction Battalion Center Port Hueneme, California 93043	10. Work Unit No. (TRAIS) 35A2-082
	11. Contract or Grant No. 5-3-0208
	13. Type of Report and Period Covered

12. Sponsoring Agency Name and Address Offices of Research and Development Federal Highway Administration U.S. Department of Transportation Washington, D.C. 20590	Final Report 1 July 1975 - 30 June 1977
	14. Sponsoring Agency Code S0725

15. Supplementary Notes

FHWA contract manager: J. D. Cooper (HRS-11)

16. Abstract

The technical report contains two volumes. Volume I gives a technical treatment of seismically induced liquefaction of cohesionless saturated soils. Volume II presents data in a format to be of use as an aid to bridge planners. Specific information is given to estimate earthquake motion and soil strength.

Volume I is divided into nine chapters covering soil parameters which affect liquefaction, dynamic properties of soils, summary of methods to predict liquefaction, field and laboratory methods for determining soil parameters, site earthquake motion, soil displacement consequences of liquefaction, and observed bridge damage. Volume I presents a technique for evaluation of probability of liquefaction and possible criteria for siting of bridges.

17. Key Words Liquefaction, Earthquake, Soil dynamics, Bridges	18. Distribution Statement No restrictions. This document is available to the public through the National Technical Information Service, Springfield, Virginia 22151.

19. Security Classif. (of this report) Unclassified	20. Security Classif. (of this page) Unclassified	21. No. of Pages	22. Price

Form DOT F 1700.7 (8-72)

i

CONVERSION FACTORS, U.S. CUSTOMARY TO METRIC (SI) UNITS OF MEASUREMENT

U. S. customary units of measurement used in this report can be converted to metric (SI) units as follows:

Multiply	By	To Obtain
inches	2.54	centimetres
feet	0.3048	metres
miles (U. S. statute)	1.609344	kilometres
square miles (U. S. statute)	2.589988	square kilometres
pounds (mass)	0.4535924	kilograms
pounds (mass) per cubic foot	16.01846	kilograms per cubic metre
pounds (force) per square inch	6894.757	pascals
pounds (force) per square foot	47.88026	pascals
kips per square foot	47880.26	pascals
tons per square foot	9764.8548	pascals
feet per second	0.3048	metres per second
degrees (angle)	0.01745329	radians
inch/second^2	0.0254	metre/second^2
pound-force-second/foot^2	47.88026	pascal-second

TABLE OF CONTENTS

Volume I.

CHAPTER 2 (Continued)

CHAPTER 3 — PROCEDURES FOR ANALYSIS OF LIQUEFACTION OF SOILS

CHAPTER 3 (Continued)

CHAPTER 4 — FIELD DETERMINATION OF SITE AND SOIL CONDITIONS

CHAPTER 5 — LABORATORY INVESTIGATIONS

CHAPTER 8 — DAMAGE TO BRIDGE STRUCTURES CAUSED BY
EARTHQUAKE INDUCED LIQUEFACTION

CHAPTER 9 — RECOMMENDATIONS FOR LIQUEFACTION CRITERIA
FOR BRIDGE SITES

CHAPTER 9 (Continued)

APPENDIX

Chapter 1

HIGHWAY BRIDGE RESPONSE TO SEISMICALLY INDUCED SOIL LIQUEFACTION

INTRODUCTION

Significant documentation on the damage to highways, bridges, and embankments from seismically induced liquefaction of loose, saturated, cohesionless soils points out the need to develop criteria to identify the damage potential of both new and existing highway structures founded on these types of soils. The 1964 Alaska earthquake caused considerable highway damage resulting from liquefaction and differential ground settlement (Ross et al., 1973). Seismically induced soil-liquefaction potential exists in those areas where strong ground shaking and loose, saturated, cohesionless soil occur. Figure 1-1 shows several bridges of the many which collapsed. Prediction of structural damage from soil liquefaction will provide the design engineer with information on which to base a rational decision on the hazards associated with earthquakes.

The purpose of this report is to provide guidance to highway design engineers and planners to minimize the damage from seismically induced soil liquefaction. The report is divided into two volumes: the first contains a detailed treatment of liquefaction; the second contains a condensed guide for evaluation of liquefaction potential. It is not the intent of the report to be a design manual nor to be a state-of-the-art review. This report, hopefully, lies somewhere between the two. Much data have been reviewed and presented to give the reader an appreciation of the complexity of the problem. Guidance and recommendations are given to assist in the interpretation and use of the information.

Cohesionless soils that may provide adequate structural support under ordinary circumstances may result in liquefaction and settlement during an earthquake. When liquefaction occurs, settlements may be increased by at least one order of magnitude over static settlements. The highway-bridge design engineer is particularly interested in the differential ground settlement caused by earthquakes. Often, a bridge abutment supported on a pile foundation into firm material undergoes relatively small settlement compared to that of the backfill material that rests directly on the ground surface. Large backfill settlement
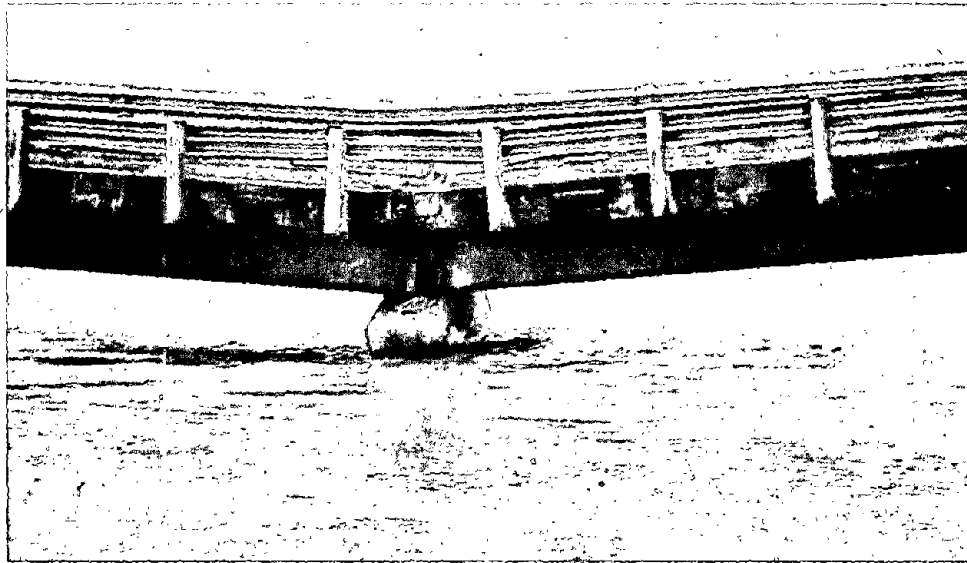
(a) Collapsed bent and deck of Copper River 5 Bridge, mile 35.0, Copper River Highway.
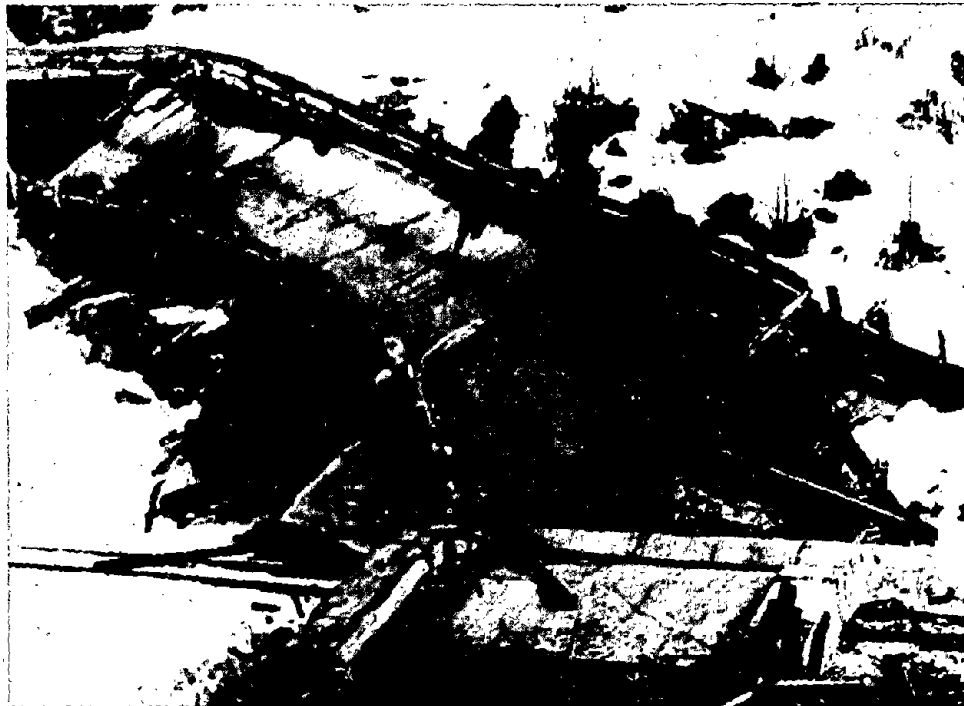
(b) East side of Snow River crossing, structure collapsed upon tracks of The Alaska Railroad.

2
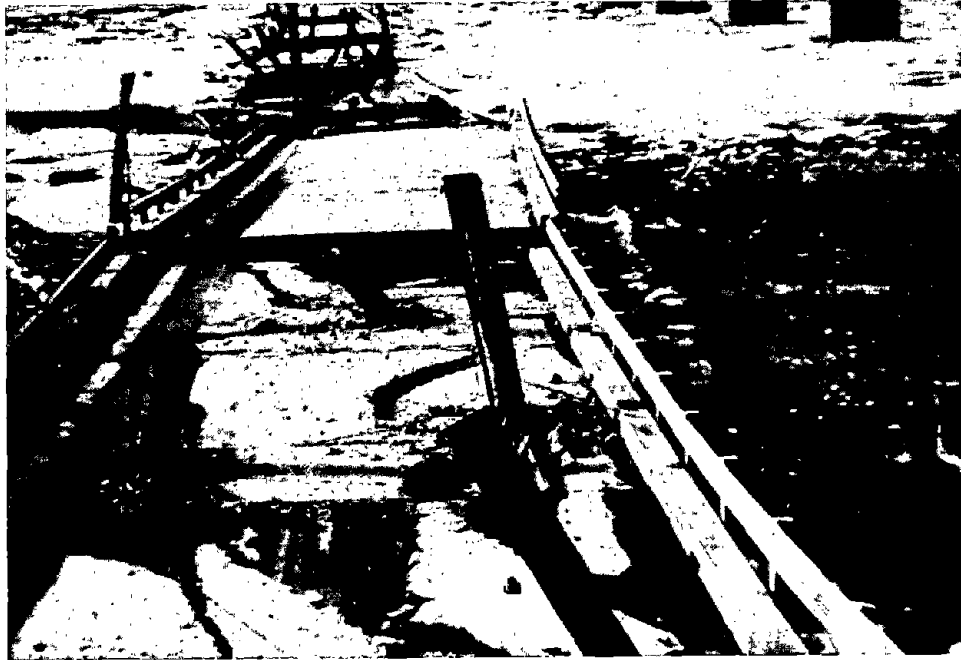
(c) Collapsed bridge across Twentymile River; railroad bridge
in upper right of photograph did not collapse.

Figure 1-1.   Liquefaction damage to bridges from Alaskan
earthquake, 1964.

of an area surrounding an abutment can render an important bridge in a
transportation network useless, creating personal as well as economic
hardship.

When a loose sand is subjected to seismically induced vibratory
motion, it tends to decrease in volume. If it is saturated and drainage
is impeded, then some of the interparticle stress is transferred to the
water. The transferred load causes a rise in the pore water pressure
(generally, the higher the intensity of vibration, the greater the poten-
tial for increase in pore water pressure). As the pore pressure approaches
the confining pressure on the soil, shear resistance is lost. As a con-
sequence the bridge substructure may tilt and settle, resulting in
differential motions that may cause severe bridge damage.

Soil borings normally taken at a bridge site provide information
on existing soil conditions. With proper analysis, this soil data can
give an indication of the liquefaction potential in earthquake-prone
regions. Based on the borings, a foundation system is normally designed
to support the bridge under static and traffic loads. However, when
soil liquefaction potential exists, the engineer has no means by which
to evaluate the associated structural hazard (risk assessment) that could
be caused by the earthquake.

Early quantitative studies of liquefaction pertained to natural earth slopes which became unstable from a gradual rise in the water table or tidal fluctuations which caused excess seepage pressures. Generally, a massive flow slide would begin, and the soil came to rest only when the slope angle had been reduced to a few degrees. To explain this phenomenon Casagrande (1936) proposed the "critical void ratio" concept. Subsequently, following extensive studies of numerous flow slides along the banks of the Mississippi River, empirical rules were developed by the Corps of Engineers to predict the likelihood of occurrence of such flow slides.

During the last 10 to 15 years, the term "liquefaction" has been extended to include soil behavior under cyclic loading conditions caused by earthquake vibrations. While the end result — loss of soil strength — is the same whether caused by static or dynamic loading, the shear stresses leading to liquefaction under cyclic loading conditions may be much lower than those required to cause liquefaction under static loading conditions. Under continuous vibrations cyclic stresses cause an incremental buildup of pore pressure which progressively reduces the effective strength.

The strength that a sand can mobilize to resist shearing along a given plane depends on the effective or intergranular pressure on the plane and the effective coefficient of friction. The shearing resistance or strength τ_f may be written

$$\tau_f = \sigma' \tan \phi'$$

in which σ' is the effective stress and ϕ' is the effective angle of internal friction. In a saturated sand the intergranular normal stress σ' is defined as

$$\sigma' = \sigma - u$$

where σ = the total normal stress

   u = the pore water pressure

Then

$$\tau_f = (\sigma - u) \tan \phi'$$

If water pressure u increases, while the total stress σ remains constant, the shear strength τ_f across any plane of failure decreases independent of the friction angle ϕ'. When u = σ, the τ_f = 0, and the sand has lost all its shear strength and is said to have liquefied. The sand is sometimes considered to have liquefied when large strains occur under applied loads. In soil mechanics practice, the term "soil liquefaction" may be defined by two criteria. One defines liquefaction in terms of loss of strength and material transformation of a granular material into a fluid. An alternate definition is expressed in terms of the amount of strain or deformation that is unacceptable from a structural viewpoint.

GENERAL PROCEDURE FOR EVALUATING SOIL LIQUEFACTION POTENTIAL

The general method proposed by Seed and Idriss (1970) summarizes the usual engineering approach.

    1. After establishing the soil conditions and the design earthquake, determine the time history of shear stresses induced by the earthquake ground motions at different depths within the deposits.

    2. By appropriate weighting of the stress levels involved in the various stress cycles throughout the earthquake, convert the stress history into an equivalent number of uniform stress cycles and plot the equivalent uniform stress level as a function of depth as shown in Figure 1-2. By this means the intensity of ground shaking, the duration of shaking, and the variation of shear stress with depth within the deposit are taken into account.

    3. By means of laboratory soil tests data, determine the cyclic shear stresses which would have to be developed at various depths to cause liquefaction in the same number of stress cycles as that determined in step (2) to be representative of the particular earthquake under consideration. The stresses required to cause failure may then be plotted as a function of depth as shown in Figure 1-2.

    4. By comparing the shear stresses induced by the earthquake with those required to cause liquefaction, determine whether any zone exists within the deposit where liquefaction can be expected to occur (induced stresses exceed those causing failure).

stress

depth

zone of liquefaction

cyclic stress causing
liquefaction in N cycles
(from testing program)

cyclic stress developed
for N cycles by earth-
quake motions
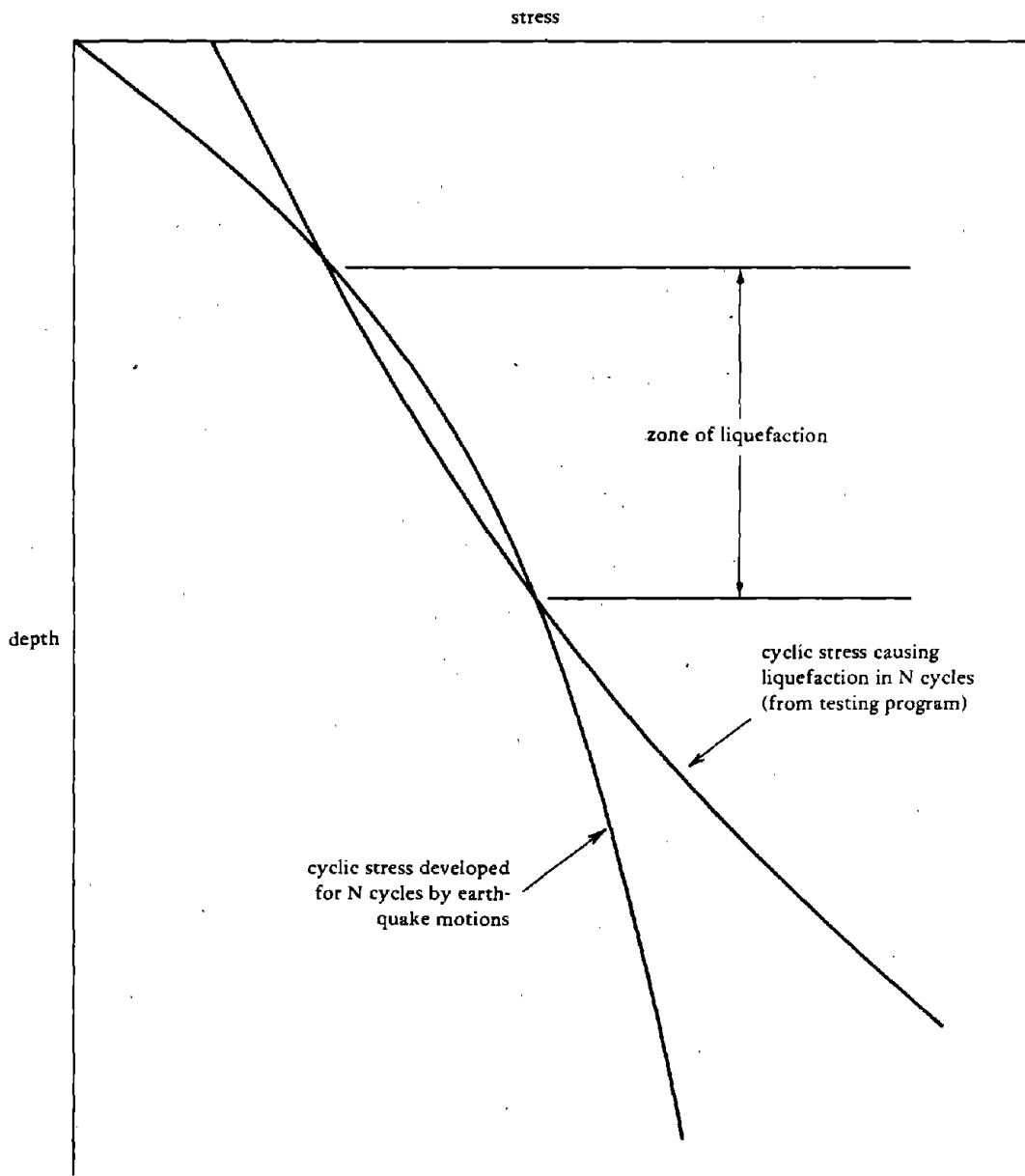
Figure 1-2. Method of evaluating liquefaction potential
(after Seed and Idriss, 1970).

6

SCOPE OF THIS REPORT

Volume I of this report will discuss in depth the soil properties and liquefaction analysis procedures. Chapter 2 presents soil parameters which affect liquefaction and the dynamic properties of soils required in analytical procedures. Chapter 3 presents hand and computer methods for the analysis of liquefaction. Chapter 4 presents field methods for determining the required soil parameters and geologic profiles used in the analytical procedures. Chapter 5 presents laboratory test procedures for required data and an evaluation of the test results. Chapter 6 gives methods to determine site earthquake motion. Chapter 7 discusses soil displacement prediction. Chapter 8 gives a summary of observed bridge damage. Chapter 9 presents recommendations.

Volume II of this report gives a design guide in a format to be of practical assistance to a highway engineer.

REFERENCES, CHAPTER 1

Casagrande, A. (1936) "Characteristics of cohesionless soils affecting the stability of slopes and earth fills," Contributions to Soil Mechanics, 1925-1940. Boston, Mass., Boston Society of Civil Engineering, 1940.

Ross, G. A., Seed, H. B., and Migliaccio, R. R. (1973) Performance of highway bridge foundations: The great Alaska earthquake of 1964. Washington, D.C., Engineering, National Academy of Sciences, 1973.

Seed, H. B., and Idriss, I. M. (1970) "A simplified procedure for evaluating soil liquefaction potential," Journal of the Soil Mechanics and Foundations Division, ASCE, vol 97, no. SM9, Sep 1970, pp 1249-1274.

Chapter 2

SOIL PARAMETERS AFFECTING LIQUEFACTION

LIQUEFACTION PHENOMENA

The introductory portion of this chapter is directed toward the reader who does not have first-hand familiarity with soil response. To provide a better understanding of the behavior of saturated granular soils under load, typical test data on both quasi-static (monotonic) and cyclically loaded soil specimens are discussed. This will provide insight into the undrained shear behavior and liquefaction of saturated sands and provide an understanding of the liquefaction phenomenon more satisfactory than that communicated by attempts at generalized or abstract definitions.

Monotonic Loading

Consider first the response of a saturated sand under monotonic loading in a standard undrained triaxial compression test. Three different types of material response (such as that presented by Castro 1969) will be illustrated qualitatively (Figures 2-1 and 2-2) to show the behavior of three specimens of sand at low, moderate, and high relative densities. Under increasing vertical (deviator) stress, each of these specimens exhibits a different type of behavior, depending upon its volumetric strain-shear stress coupling which is, in turn, a function of its initial density. The densest sample, test 3, does not undergo liquefaction, but exhibits an initial sharp rise in pore pressure with axial strain (Figure 2-1b); this corresponds to a decrease in effective stress (Figure 2-2) and a reduction in stiffness (deviator stress) (Figure 2-1a). The pore pressure rise and loss in stiffness is related to the tendency for the sand to initially compress under applied shear stress. At larger strains, the volumetric strain-shear strain coupling inherent in granular materials causes volume dilation to occur with attendant reduction in pore pressures (Figure 2-1b), increase in effective stress (Figure 2-2), and some increase in stiffness (see Figure 2-1a).
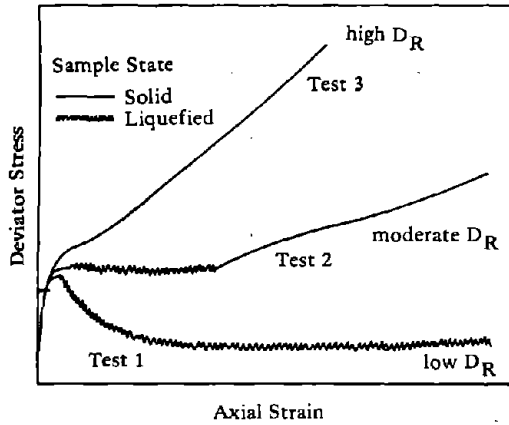
(a) Deviator Stress — Axial Strain.
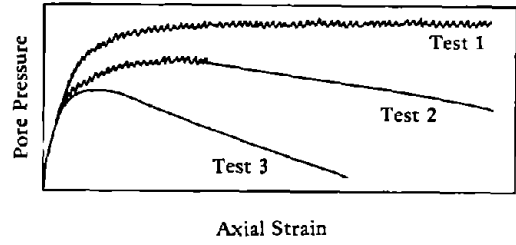
(b) Pore Pressure — Axial Strain.

Figure 2-1. Stress-strain curves for three monotonically loaded triaxial compression tests on undrained sample of sand.

Effective Spherical Pressure
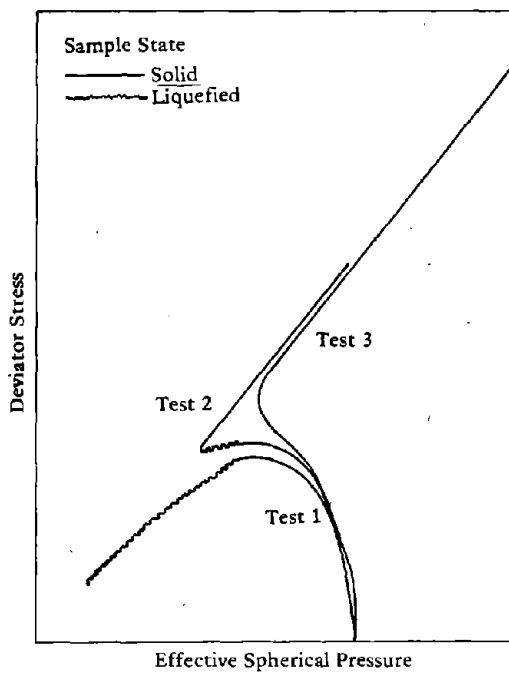
Figure 2-2. Stress paths for the three triaxial compression tests plotted in Figure 2-1.

9

Test 1 is an example of "unlimited flow." The specimen exhibits response behavior similar to that shown in test 3 up to the commencement of yielding (Figure 2-1a). Beyond this point, the specimen in test 1, because of its loose condition, does not dilate; hence, the pore water pressure approaches the initial confining chamber pressure, and the strength falls off dramatically.

The phenomenon of "limited flow" is demonstrated in test 2. In this test, initial specimen yielding (Figure 2-1a) did not occur until a considerable amount of strain (volumetric dilation) had occurred. This behavior is attributed to the fact that the density of the specimen was slightly looser than the specimen of test 3. At large axial strain, the test 2 specimen starts to dilate, causing a recovery of effective stress (Figure 2-2) and a re-establishment of some vertical load stiffness (Figure 2-1a).

Cyclic Loading Without Stress Reversal

Cyclically loaded tests demonstrate a different type of pore pressure generation and strength loss from those of monotonic tests. Figure 2-3 shows complete loss of effective stress, or unlimited flow, during cyclic loading of two triaxial specimens without stress reversal. With each application and release of the deviator stress, a residual pore pressure is generated, which results in an incremental reduction in the effective confining pressure. Following a certain number of cycles, depending upon the initial value of effective confining stress and the deviator (shear) stress level, a liquefaction condition is encountered, where the effective confining pressure is reduced to zero. It is interesting to note that the wavy lines in Figure 2-3 represent the yield envelope for these soil specimens; that is, the maximum obliquity or the shear-stress/normal-stress relationship for the material at failure. Such tests can also demonstrate "limited flow." The results of such a test are shown in Figure 2-4. During the first cycle of deviator loading (Path 0-ℓ-s-1) the specimen liquefied at a deviator stress of about 100 kN/m^2 and then restabilized by a dilation-associated increase in effective confining stress. Thereafter, the specimen remained within the stable domain as indicated by later load cycles (shown by numbers on the diagram). The reduction in deviator stress noted between successive cycles in Figure 2-4 is a result of the constant deviator load applied to a cross-sectional area that is increasing due to specimen deformation.

Information such as the foregoing has been used to support the conclusion that shear-stress reversals are necessary to produce repeated occurrences of liquefaction during cyclic loading (Seed and Lee, 1969).
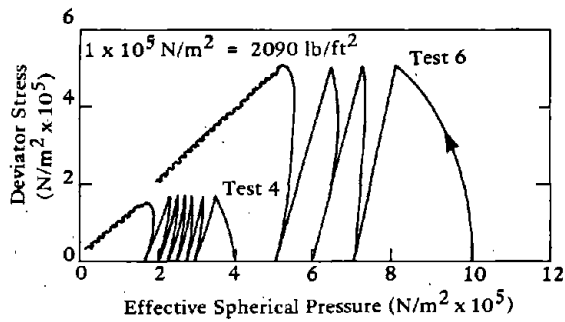
Figure 2-3. Liquefaction and unlimited flow generated by cyclic
loading (stress paths from cyclically loaded triaxial com-
pression tests without stress reversals). (Data from
L. T. Youd, 1973, in work published by Earth-
quake Engineering Research Institute.)
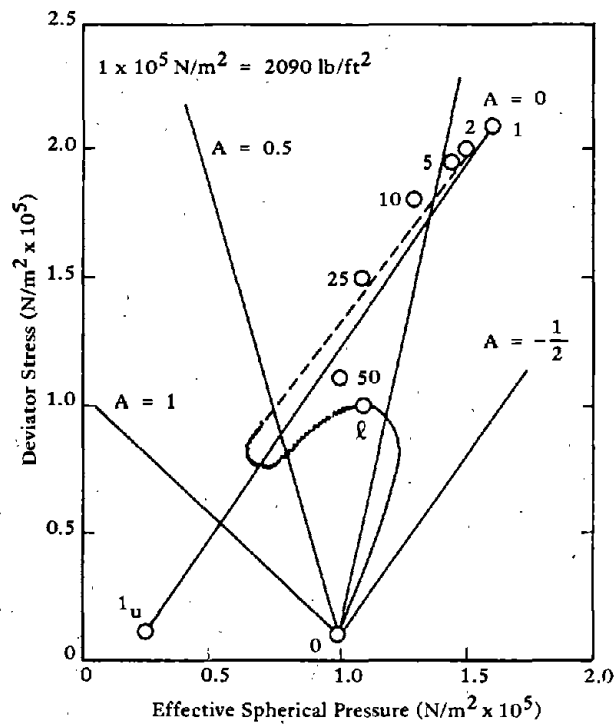
Figure 2-4. Stress path from a cyclically loaded triaxial com-
pression test without stress reversals; liquefaction and
limited flow occurred only during first loading (data
found in L. T. Youd, 1973, in work published by
Earthquake Engineering Research Institute).

11

It is interesting to consider Figure 2-4 in another context; the straight lines sloping upward from point 0 represent constant values of a parameter equivalent to Skempton's pore pressure parameter A. It is noted that, under initial loading, the value of A is approximately 0 (no pore pressure generation) and then increases to a value >1.0 (pore pressure generated faster than applied deviator stress) just prior to liquefaction (the specimen is attempting to compress). Thereafter, the specimen maintains an A value of about -0.5 during continued cycling. This latter implies that during application of compressive deviator load, the specimen is, in fact, dilating — hence, causing a negative change or reduction in pore pressure. During the unloading portion of the cycle, the specimen recovers some of its volume expansion, causing an increase in pore pressure. This is interesting in that it is not the normal behavior experienced under monotonic triaxial shear testing.

Cyclic Loading With Stress Reversal

In cyclic triaxial tests with stress reversals (i.e., those incorporating alternating tensile and compressive deviator stress), a type of limited flow referred to by Castro (1969) as cyclic mobility, is exhibited. A record from this type of test is shown in Figure 2-5. In this test the effective confining stresses are incrementally reduced by the increases in residual pore pressure with each load cycle. At some point, often during an extensional cycle, the effective confining stresses approach zero and liquefaction occurs. The specimen deforms rapidly, but then resolidifies from a dilatency-associated decrease in pore pressure. Upon the ensuing compressional cycle, the specimen again undergoes a period of limited flow, generally near peak deviator stress level, following which the specimen may again regain strength by a dilation-associated increase in effective stress. In this manner cyclic triaxial tests may undergo increasingly larger alternating vertical strain increments with each half-cycle, until the integrity of the specimen is completely destroyed.

The response of the soil specimen shown in Figure 2-5 suggests an initial value of an equivalent Skempton pore pressure coefficient A* during a double-amplitude strain cycle of about 0.2. This factor then increases progressively up to about 0.5 at large strain amplitudes. Replotting the data of Figure 2-5 in Figure 2-6 shows one interpretation of what is occurring in detail. The specimen, initially under an effective stress σ_3 undergoes a gradual increase in pore pressure, resulting in a decrease in average effective confining stress. At the same

---

*Skempton's A was not defined for situations involving stress reversals. The use of an equivalent "A" is introduced here as an aid to characterizing the soil response.

Test 85

e = 0.644

D_r = 55%

pore pressure

axial strain

deviator stress
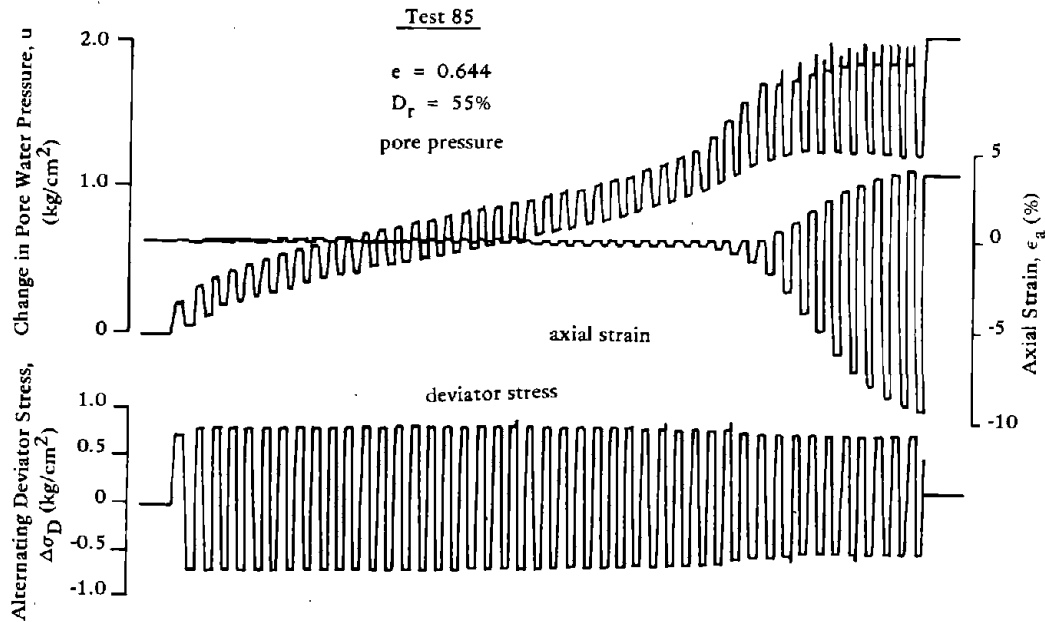
Figure 2-5. Data from a triaxial test on medium-dense Ottawa sand (from "Soil Dynamics Liquefaction of Sands," by W. L. Finn, p. 104, Figure 3, in Proceedings, International Conference on Microzonation for Safer Construction Research and Application, sponsored by American Society of Civil Engineers, 30 Oct-2 Nov 1972).

specimen begins large deflection under tensile loading

$\bar{\sigma}_1$

$\bar{\sigma}_3$

$\bar{\sigma}_0$

average effective confining stress

Number of Cycles
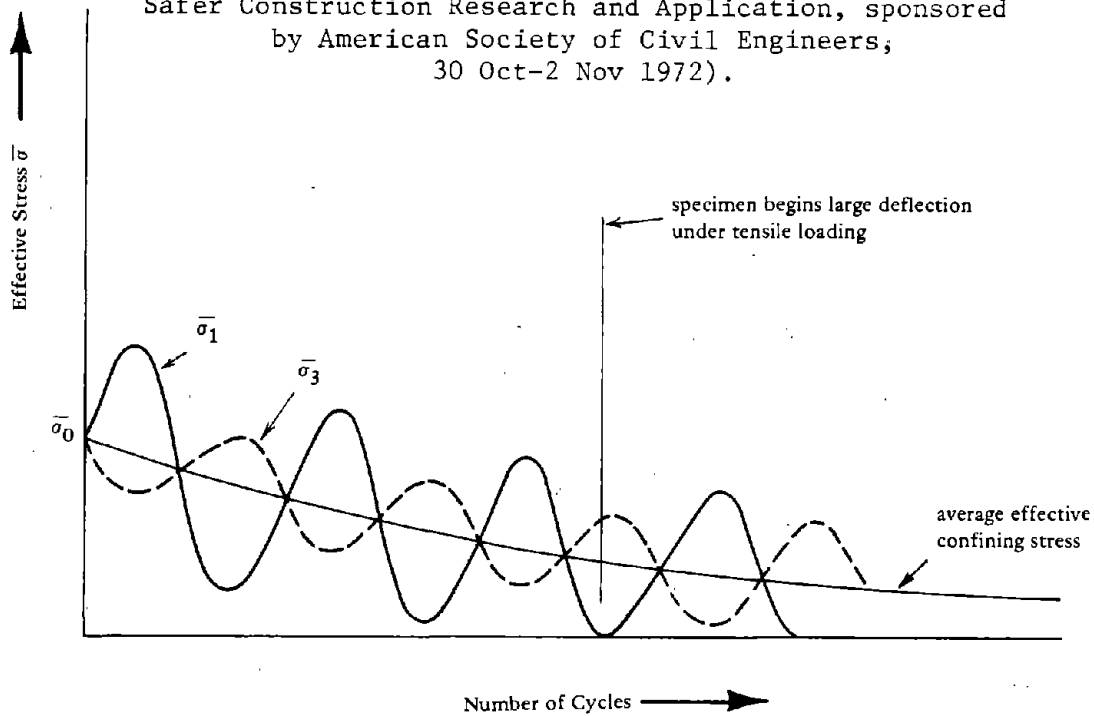
Figure 2-6. Plot of data in Figure 2-5.

13

time, the pore pressure coefficient A is gradually increasing, reducing the amplitudes of the vertical stress oscillations but increasing the magnitude of the lateral stress oscillations. At some point (noted in Figure 2-6 and in this example during an extensional cycle), the effective stress value attempts to go into tension. Since granular material has no effective tensile strength, unrestrained deformation commences.

This way of looking at deformations during cyclic loading can provide additional insight into the complexity of soil response. For example, traditional interpretation of triaxial test results has indicated a strong relationship between strength and ratio of effective principal stresses. This ratio is a direct function of the total applied stress levels and the pore water pressure parameter A. For example, for typical cyclic triaxial tests (Seed and Lee, 1966) values of equivalent A less than 0.5 would mean a greater effective principal stress ratio during the extensional phase of the loading cycle than during the compressional phase. Hence, such specimens would be expected to commence undergoing large deformations first in tension. Figure 2-7 shows results from shake table tests (DeAlba, Chan, and Seed, 1975) on a medium dense sand layer under a uniform vertical surcharge following the occurrence of cyclic mobility. The motion of the table is shown in Figure 2-7, and the reponse of the specimen may be visualized in terms of the relative ballast displacement, Figure 2-7c. The pore pressure level, as well as the total of confining pressure and back pressure for reference, is shown in Figure 2-7a. This test illustrates the following behavior, commencing our observation with the ballast and the table off center at an extreme position. The table motion changes direction; and, since dilation has caused a temporary reduction in pore pressure, the soil behaves as a solid and imparts a motion on the ballast. As the table commences to catch up with the ballast, shear strain magnitude is reduced, the pore pressure rises, and liquefaction recurs. The ballast then remains essentially stationary until the table has passed through its center position and has again exerted a large relative deformation upon the sand — causing dilation, reduction of pore pressure, and regain of strength. The reverse of the table motion then imparts a new impulse to the ballast through the resolidified soil, and the reverse portion of the loading cycle occurs. Thereafter the cycle is repeated.

Although various other types of apparatus are available for studying liquefaction, the foregoing explanations serve to illustrate the most pertinent characteristics of laboratory behavior.

PARAMETERS DIRECTLY ASSOCIATED WITH LIQUEFACTION

The above discussion dealt with some of the characteristics of liquefaction behavior. Some of the specific soil parameters involved will be considered individually.

14

(c) Measured relative displacement of ballast.

(b) Table displacement.

(a) Pore pressure.

$U_b + \sigma'_o$

U_b

U

t

t = Time

U_b = Back pressure

σ'_o = Initial effective pressure

Test 68-3, D_r = 68%
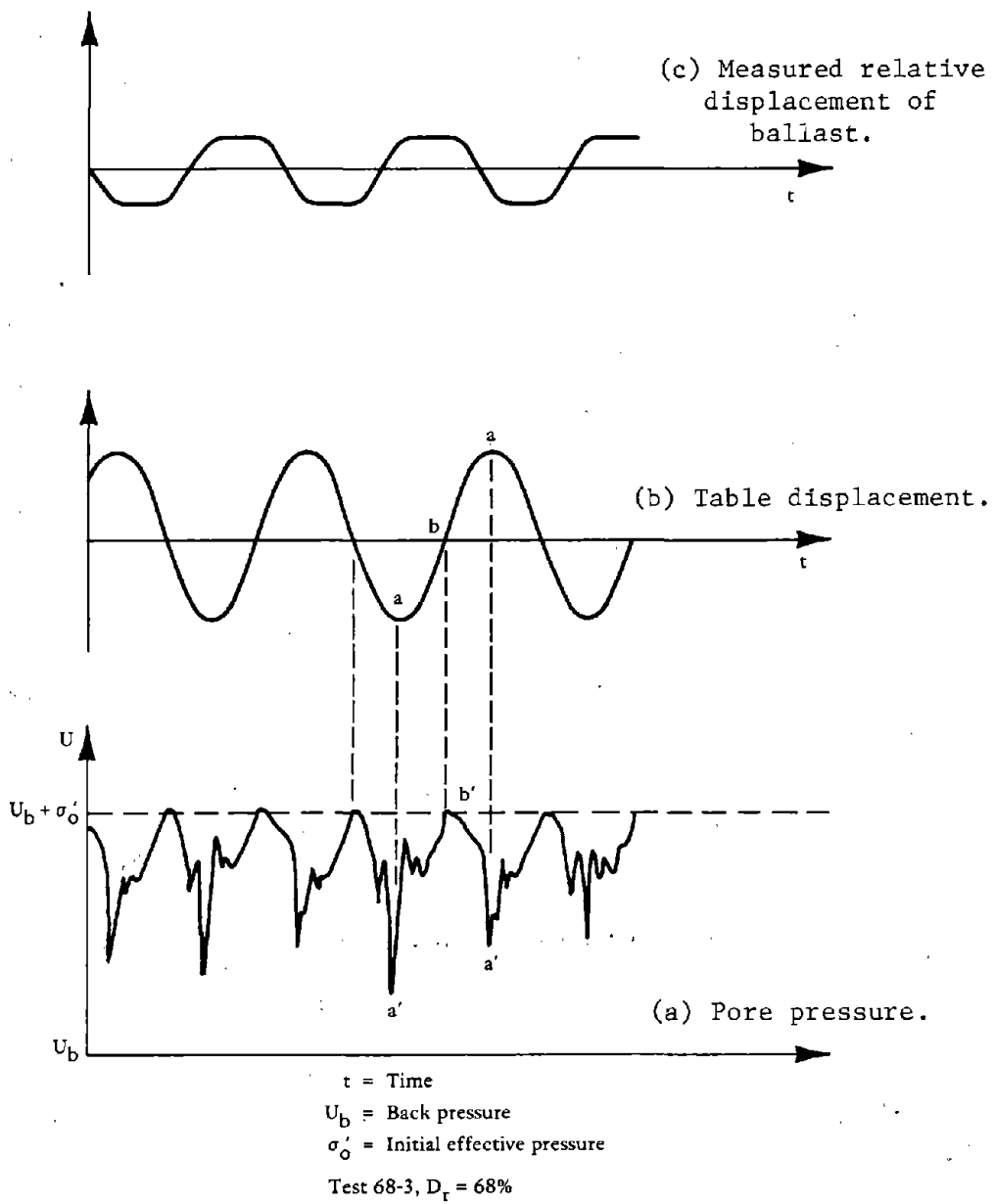
Figure 2-7. Specimen behavior after liquefaction (from DeAlba, Chan, and Seed, 1975).

The major factors associated with the liquefaction of saturated cohesionless soils appear to be: initial relative density, cyclic shear stress level, initial (static) shear stress level, initial effective confining pressure, drainage conditions, and number of cyclic shear stress applications, or duration of shaking. Of lesser importance are soil grain characteristics such as particle size, shape, and gradation. Soil structure, or fabric, as a result of previous history is known to be a significant parameter, but it is difficult to define or sometimes even recognize and, hence, its effects are difficult to quantify.

The foregoing factors reflect the physical properties of the soil, the initial stress conditions, stratigraphy in the ground, and the characteristics of the applied earthquake motions. Many of these items are difficult to control precisely in the laboratory and impossible to evaluate reliably in the field. A brief discussion follows on some of the more significant factors affecting liquefaction.

Dynamic Shear Stress Level

The fundamental concept of liquefaction is based upon the shear-strain/volumetric-strain coupling exhibited by soils. The process of pore pressure buildup, leading to liquefaction under cyclic loading, is dependent upon the volumetric strain response under applied shear stresses. The residual increment of pore water pressure generated by an applied dynamic shear stress cycle is, under undrained conditions, related to the shear strain which is, in turn, related to the magnitude of that stress cycle. In the field, the magnitude of dynamic shear stress may be ascertained from the acceleration levels, either by rough approximation or by more sophisticated computer analysis (see Volume I, Chapter 3).

In the laboratory, the applied shear stress levels are defined according to the type of test. In triaxial testing (see Volume I, Chapter 5) the applied shear stress is taken as one-half the maximum deviator stress excursion (when symmetric stress reversals are used). This is the maximum dynamic shear stress experienced by the specimen and is exerted upon planes oriented 45 degrees from the vertical axis. For the simple shear test described in Chapter 5, the applied shear stress is taken as that exerted on horizontal planes; this is not the maximum value of shear stress exerted upon the specimen. This situation is similar to that in other types of apparatus such as the hollow cylinder test. For shake table tests where shear stresses are applied by means of inertial forces, the horizontal shear stress varies slightly throughout the thickness of the specimen and usually is taken as the horizontal shear stress exerted at the bottom of the specimen.

Laboratory testing procedures generally simulate shaking in only one direction, whereas actual earthquake motions may have components in all three principal directions. The conclusion that the most critical stresses from a liquefaction viewpoint arise from vertically propagating horizontal shear waves appear to be relatively satisfactory. Vertical stress components are not considered significant since these are of a dilatational nature and completely absorbed by the pore water. For dynamic shear loading in a second horizontal direction, work by Pike, Chan and Seed (1974) have suggested that the allowable shear stress ratio should be reduced by 10%.

Characteristics of the Shear Stress Record

Earthquake ground motions generally consist of a number of randomly distributed peak stress cycles of varying shapes and magnitudes.

Difficulties involved in analyzing the various random earthquake ground motions have led to an attempt to express earthquake records in terms of an equivalent number of uniform stress cycles (Lee and Chan, 1972). The number of significant cycles in a particular earthquake record depends directly upon the frequency content and the duration of loading. These, in turn, are related to the magnitude of the earthquake, the distance to its epicenter, and the nature of the materials through which the stress waves must propagate.

It has been noted by Peacock and Seed (1968) and Yoshimi and Oh-Oka (1975) that the frequency of vibration, at least within 0.17 to 12 cps, which covers the range of earthquake motions, at least in overburden, is of secondary importance. Actual shape of the stress pulse used in laboratory test simulations has been found not to be critical; i.e., whether or not it is in the form of a sine wave, a saw tooth, or other form. It is common to present soil susceptibility to liquefaction in terms of number of uniform stress cycles causing liquefaction under a specified level of applied shear stress, as in Figures 2-8 and 2-9. As noted in these figures the number of stress cycles a specimen can withstand increases almost exponentially with a decrease in shear stress level for any constant confining stress level and relative density.

There are some weaknesses in simulating random earthquake motions in terms of uniform cycles. For example Martin, Finn and Seed (1975) note that the tendency for dry sands to undergo volume changes is a direct function of dynamic shear strain level. But dynamic shear strain level is a function of soil modulus of rigidity G, which in turn depends upon the effective confining stress level and, hence, the pore water pressure generated. Since the pore pressure level existing at the time of application of a specific peak is very important, the relative

17
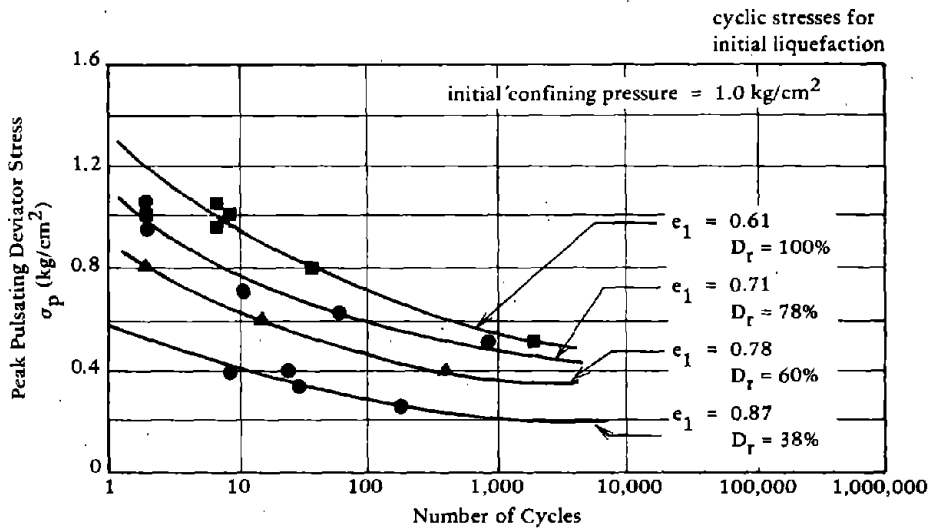
Figure 2-8. Effect of void ratio (from "Cyclic Stress Conditions
Causing Liquefaction of Sand," by K. L. Lee and H. B. Seed,
1967, in Journal of Soil Mechanics and Foundations,
ASCE, vol. 93, no. SM1, Jan 1967).
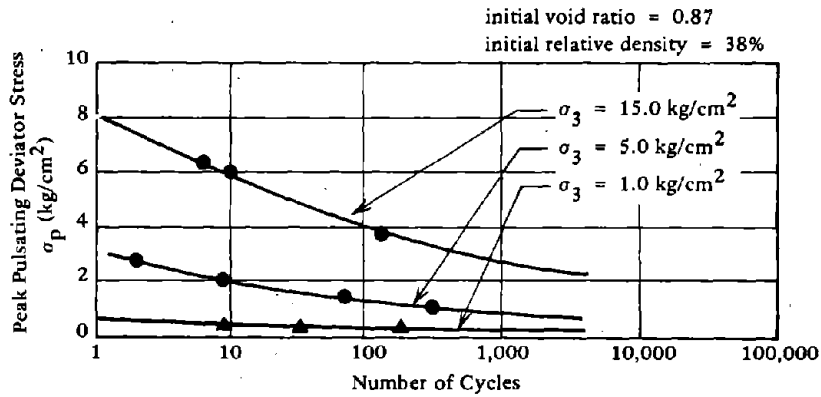
Figure 2-9. Effect of confining pressure (from "Cyclic Stress Conditions
Causing Liquefaction in Sand," by K. L. Lee and H. B. Seed,
1967, in Journal of Soil Mechanics and Foundations,
ASCE, vol. 93, no. SM1, Jan 1967).

18

position of any peak in a sequence of loading cycles is significant. The previous discussion on the effects of stress reversals also suggests that the peculiar characteristics of the loading history (i.e., the symmetry of the stress record, etc.) may be significant. Ishihara, Tatsuoka and Yasuda (1975) note that ground motion inputs in which the maximum peak occurs early are less critical than input records for which the peaks are more uniformly distributed (i.e., vibratory as opposed to shock loadings).

Relative Density

The relative density of a soil appears to be one of the major factors regarding liquefaction potential of cohesionless sands. Relative density is stressed here rather than absolute density since it is actually the pore volume of the soil compared to its minimum and maximum possible pore volumes that is of significance. The denser a soil, the lower is its tendency toward volume contraction during shearing; the lower is the pore pressure which will be generated; hence, the more unlikely to liquefy. This increased liquefaction resistance with increased density is illustrated in Figure 2-8.

Relative density can be controlled in the laboratory using reconstructed samples; however, in typical field situations with complex stratification, relative density may lose its meaning. (A factor such as relative density has meaning only in uniform soil conditions; actual experience shows that natural soil deposits are quite often very heterogeneous.)

It is also conceivable that there is an upper limit of relative density D_R, above which a soil under field behavior will either no longer tend to compress and generate pore pressures or will, immediately upon commencing yielding, undergo volume increases which prohibit liquefaction. Based on specific site data taken from the 1964 Niigata earthquake, Kishida (1969) concludes that these soils are not likely to liquefy at relative densities above 75%. Although cyclic mobility (temporary loss of strength) can occur at relative densities up to 100%, it is thought that negligible distortions occur in this range at least prior to any drainage or pore water redistribution (Castro and Poulos, 1976).

It is impossible to define an upper limit to D_r beyond which liquefaction will not occur; nevertheless, it appears realistic that for a value of D_r above about 80% could be considered less probable.

Initial Effective Confining Stress

The resistance of a soil to liquefaction under cyclic loading has been noted to be a function of the effective confining pressure, prior to application of shear (see Figure 2-9). Although larger confining stresses would seem to enhance volume decrease and, hence, liquefaction (at least under monotonic loading conditions), under cyclic loading this is apparently more than offset by other factors such as the increased level to which the pore pressure must be generated to achieve instability; i.e., the increased strength.

Perhaps, for this reason, field observations of liquefaction of level ground have generally been limited to relatively shallow depths, in few cases below 50 or 60 feet. This is in agreement with Kishida (1969) who observed in the 1964 Niigata earthquake that liquefaction did not occur where effective overburden stress exceeds 2 kg/cm^2 (27 psi). Although there is a trend toward reduced liquefaction potential at higher stresses, the observed field cases are very limited and cannot be expected to apply in all situations. Liquefaction evaluations must not omit regions simply because the effective pressure exceeds some empirical value.

In the isotropically unconsolidated triaxial test the effective confining stress prior to application of shear stress is the difference between the chamber pressure σ_3 and any back pressure applied to the pore fluid. For the simple shear test, the vertical effective pressure is generally used to represent the confining stress level. For the hollow cylinder tests, all components of the stress vector can, at least theoretically, be controlled so the effective confining stress level is often defined in terms of the effective volumetric stress, $1/3(\sigma_1' + \sigma_2' + \sigma_3')$.

Because of the difficulty of estimating lateral stress levels in the field, the vertical effective stress is used to define the level of confinement, but much work is available (Seed and Peacock, 1971) to indicate that the ratio of lateral to vertical stress K_o and, hence, the true degree of confinement actually existing in the field are of major importance.

The shear stress level required to cause liquefaction in remolded sand specimens at relative density less than 80% have been found to vary linearly with confining stress levels (Seed and Lee, 1966, and Peacock and Seed, 1968). Therefore it has been found convenient to normalize the effects of dynamic cyclic shear stress level with the value of initial effective confining stress. It is important to recognize that the use of this normalized ratio may not always be applicable to field conditons, particularly where strongly developed structure or cementation is present.

Thus, this simplification in treatment of liquefaction potential may not be valid in all circumstances. Soils near the ground surface, under very small degrees of confinement could have resistance to liquefaction in excess of that suggested from test results acquired at higher confining stress levels. This might be associated with material fabric or structure, or, in effect, equivalent to a previous stress history or over-consolidation pressure. That this exists for hydraulic fill sands has been suggested by Meehan (1976). For the above reasons, recovered soil samples as opposed to reconstituted specimens are preferred for cyclic shear testing, where possible. Where acquisition and testing of undisturbed samples are not possible, normalizing shear stress level with confining stress, based upon reconstituted samples is conservative in the surface layers and now forms a part of most simplified liquefaction treatments. This form of normalizing will be continued herein.

Drainage Conditions

The rate at which pore water pressure is permitted to dissipate from within a soil body has a major influence upon whether or not liquefaction can occur, particularly under cyclic loading (Wong, Seed, and Chan, 1974). Since the rate of pore pressure dissipation is known to be a function of the square of the longest drainage path, the detailed geometry of the soil profile is also important. A study of the interrelationships between different layer compressibilities and permeabilities on the occurrence of liquefaction has been presented by Yoshimi and Kuwabara (1973). This analytical study, based upon solutions to the Terzaghi one-dimensional consolidation problem, illustrates that liquefaction will propagate easily from a lower liquefied layer to an overlying one if the upper layer has a considerably lower compressibility or permeability than the initially liquefied striation.

A useful tool for investigating the influence of drainage on potentially liquefiable soil strata is discussed by Seed, Martin and Lysmer (1975). A computer code, APOLLO, discussed in Chapter 7 provides a numerical, one-dimensional solution of the diffusion equation with a pore-pressure-generating term included to represent the earthquake-generated pore pressure increases. With this code it is possible to investigate the influence of length of drainage path, stratification, water table and saturation level variations, different permeabilities, compressibilities, densities, and other conditions.

Grain Characteristics

Under normal triaxial test conditions, fine silty sands appear to be most susceptible to liquefaction (Lee and Fitton, 1969). That fine-grained soils, with cohesive strength, are less vulnerable to liquefaction, seems reasonable. With regard to coarser soils, however, this

observation is apparently influenced by system compliance. For example, coarser materials permit greater membrane indentation into the specimen under the influence of the confining pressure σ_3. Upon generation of pore pressure under cyclic loading, some of this membrane indentation is reduced, permitting, in effect, a degree of internal drainage. Work by Wong, Seed, and Chan (1974), which attempts to account for system compliance, shows that grain size is of little significance in the liquefaction of soils under undrained conditions. Thus, the fact that coarser materials perform much better even in the laboratory is probably due to membrane indentation permitting some internal drainage and, hence, pore pressure reduction (see also Martin, Finn, and Seed, 1975). Nevertheless, since coarser soils permit a much more rapid dissipation of excess pore pressure when drainage is possible in the field (due to their greater permeabilities), the potential for liquefaction is, in fact, reduced. This reduced permeability potential for coarser materials such as gravels was much in evidence during the Alaska earthquake of 1964 (Figure 2-10).

Alternatively, fine-grained materials such as cohesive soils get their strength primarily from intermolecular bonds rather than gravity forces; thus, liquefaction in the classical sense does not apply. Sensitive or highly structured clays can nevertheless undergo dramatic reductions in strength under cyclic loadings. Occasionally the percentage of fines is used to define limits beyond which liquefaction will not occur. For example, the Army Corps of Engineers has established the criterion — based upon the stability of point bar deposits in the Mississippi River — that those sands with more than 10% passing the 200 sieve are not apt to liquefy due to river fluctuations.

Grain shape does not appear to exert a significant influence upon liquefaction susceptibility within the narrow ranges of clean sands normally studied (Lee and Fitton, 1969; Rocker, 1968). However, Castro (1969) has reported sharp angular sands with higher liquefaction resistance than normally expected. Again, this might be somewhat due to the effect of membrane indentation as discussed in the previous paragraph in relation to the effects of grain size. Another variable closely associated with this might be surface texture of the grains, but this factor has been explored even less thoroughly.

The effects of soil gradation on liquefaction have not been studied to any extent, but it does not appear to be a significant variable. The gradation of critical soils shown on Figure 2-10 do not suggest any sensitivity to range of particle sizes. Although a well-graded soil exhibits frictional characteristics superior to those of a uniform soil, the graded soil can undergo a much broader range of volume changes than can uniform materials and is apt to be much less permeable. Thus, it is difficult to predict which material would be superior on an intuitive basis.
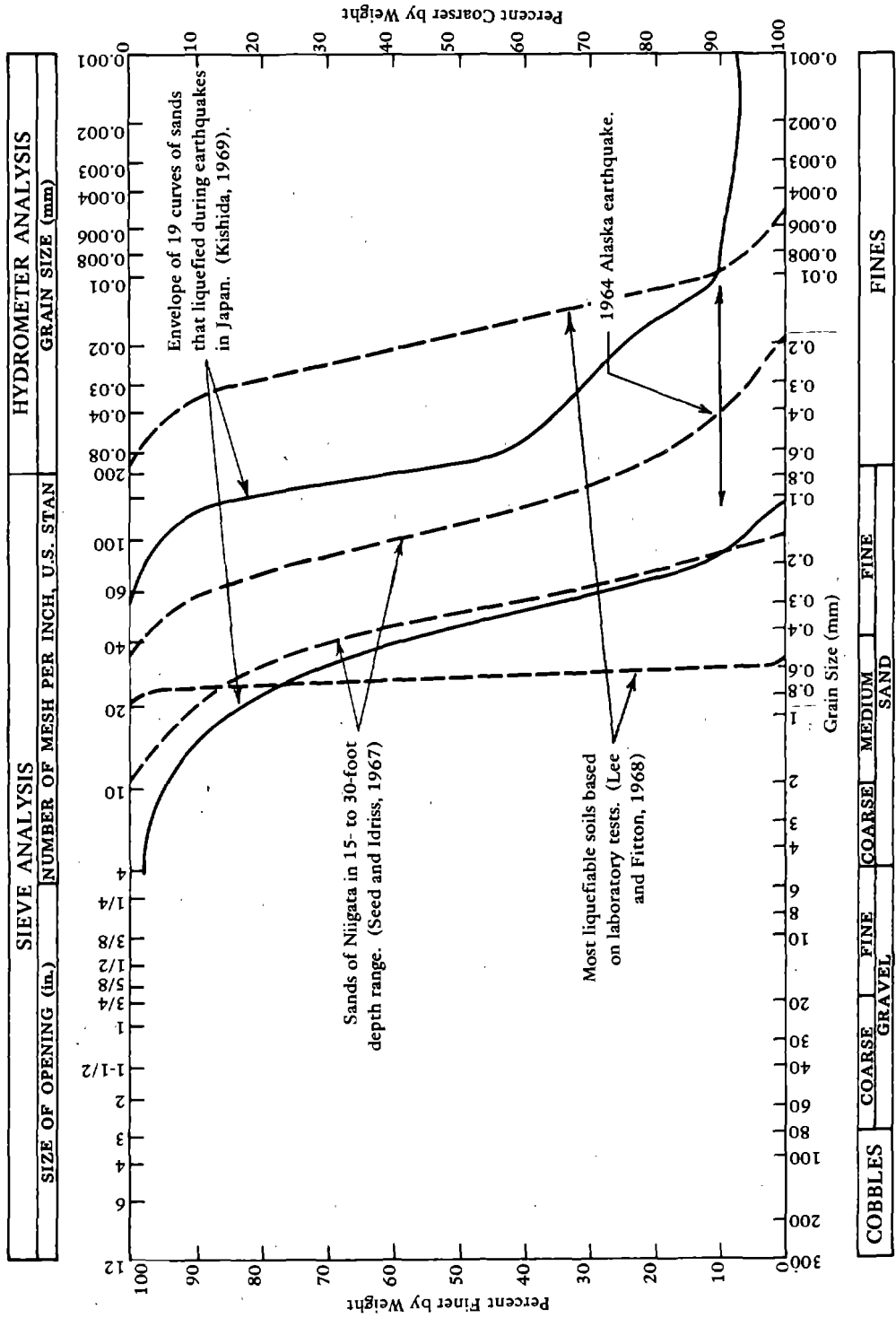
Figure 2-10. Soils susceptible to liquefaction (from "Evaluation of Soil Liquefaction Effects on Level Ground During Earthquake," by H. B. Seed, in a paper presented at the ASCE Annual Convention, Philadelphia, Pa., 27 Sep-1 Oct 1976).

23

Previous Stress History

The influence of previous stress history is of major interest in liquefaction studies. Finn, Bransby and Pickering (1970) present laboratory data showing that a sample, which has previously liquefied, is more susceptible to liquefaction. In Figure 2-11 data are shown on a specimen of sand at an initial relative density D_R of 50% and an initial effective isotropic confining pressure of 200 kN/m^2, which is subjected to cyclic loading with stress reversals. The specimen first underwent limited flow or cyclic mobility under the extensional portion of the 25th load cycle. This specimen then underwent several additional cycles wherein it reliquefied, flowed, and then restabilized (not shown in Figure 2-11). After a total of 29 load cycles, the specimen was permitted to drain, and was reconsolidated under an effective spherical pressure of 200 kN/m^2, which yielded a relative density D_R of 60%. Upon resumption of cyclic loading the specimen was noted as reliquefying during the extensional segment of its first loading cycle, in spite of its increased D_R value over that of the initial test sequence. Based on such information, it is possible that the number of loading cycles required to cause liquefaction is substantially reduced by previous episodes of liquefaction.

This conclusion, which would appear to contradict intuition, is discussed herein to illustrate that judgment is necessary in interpreting test data. The foregoing test data might be explained in terms of the sample disturbance and material redistributions that can take place in laboratory tests due to local stress variation.

During the stress cycles leading up to initial liquefaction, the specimen would have developed weak zones which remained susceptible to liquefaction during later load applications. Seed, Mori, and Chan (1975) have provided data indicating that previous shear stress history can increase the resistance of a soil specimen to cyclic mobility.

Others have noted increases of up to 10 cycles to failure between reconstituted and undisturbed samples. Standard penetration tests taken by Kishida (1970) in the vicinity of the Tokachi Oki earthquake showed decreased dynamic penetration resistances in hydraulic fills immediately following the earthquake (probably due to pore pressure generation) but increased penetration resistance after 3 weeks. The most important conclusion that can be made is that the susceptibility to future liquefaction depends primarily upon the condition of the soil resulting from the past liquefaction and the intensity of the subsequent shaking. Less dense areas will be more susceptible; more dense areas less susceptible.

24
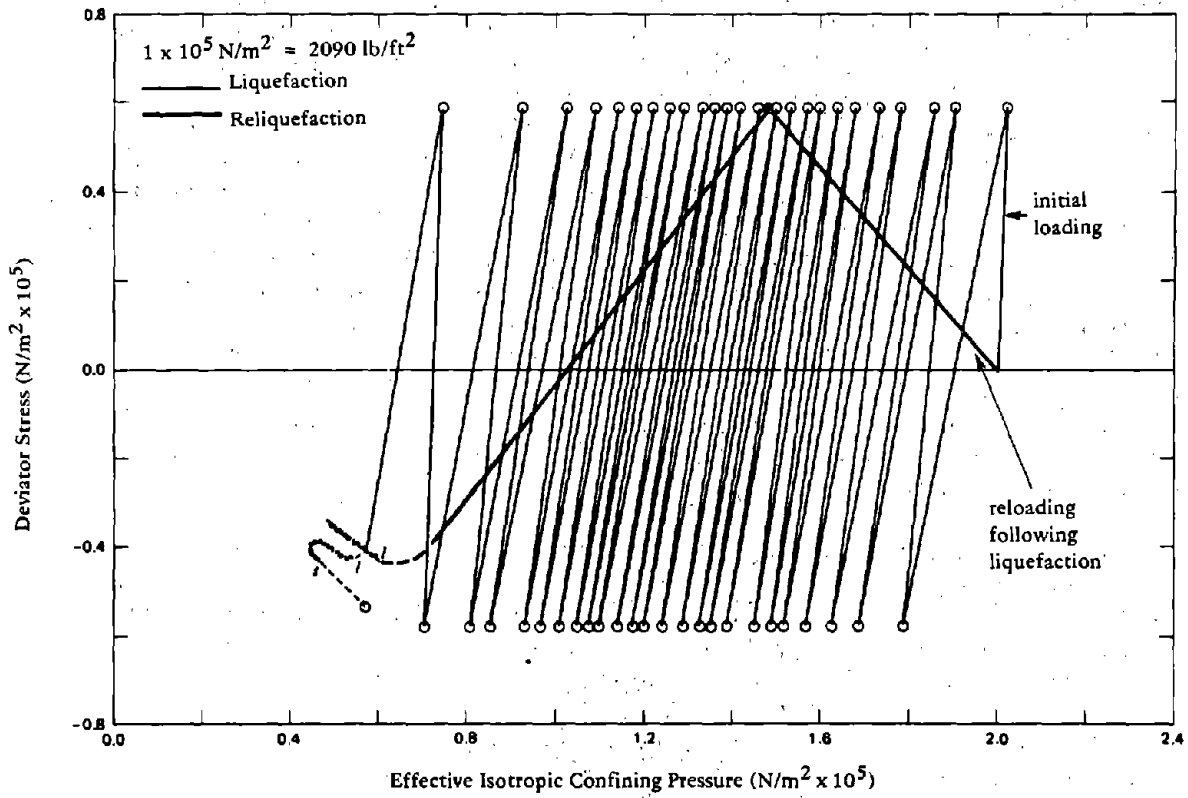
Figure 2-11. Stress paths from cyclically loaded liquefaction and
reliquefaction tests on Ottawa sand sample (sample underwent
liquefaction and limited flow in both tests)(from "Effect
of Strain History on Liquefaction of Sand," by W. D. L.
Finn et al. in Journal of Soil Mechanics and Foun-
dations, ASCE, vol. 96, no. SM6,
Figure 6, Jun 1970).

SUPERIMPOSED STATIC SHEAR LOADS

Current laboratory techniques for evaluating the liquefaction resistance of soils to earthquake loading (other than those directed toward specific dams) have considered only horizontal soil layers; i.e., situations where initial static shear stresses on the horizontal plane, due to any imposed loading, are minimal. Studies for evaluating the liquefaction potential of soils in dams have considered the effects of initial static shear stress. However, these studies are somewhat empirical, are site specific in nature, and involve extensive triaxial testing. Current laboratory techniques used for other liquefaction studies have considered it conservative and sufficiently accurate to neglect the effects of the initial static shear stresses caused by the foundation. Simple general methodologies for evaluating the effects of bridge foundations on liquefaction are not known to be in use.

Huang Win-Xi (1961) provides some insight into the behavior of sands during vibration by reporting pore water generation to be an inverse function of initial static principal stress ratio. This would suggest that at least for some levels of applied dynamic stress, an initial static stress ratio reduces the tendency for cyclic mobility to occur. Obviously this tendency can persist only within a narrow region. Otherwise, one is faced with the untenable conclusion that the greater the initial static shear stress level existing prior to application of cyclic shearing, the greater the resistance to cyclic mobility.

As long as one is interested only in the free field situation, where shake table or simple shear tests are directly applicable, standard test data, including empirical correction factors (Peacock and Seed, 1968; DeAlba, Chan, and Seed, 1975), is satisfactory for liquefaction analysis. However, should one desire insight into the liquefaction potential in regions of foundation load discontinuities, such as beneath footings or steep slopes, liquefaction criteria based more upon these latter situations are desirable. It is necessary that a general approach to defining liquefaction criteria be developed that can utilize the available body of triaxial and free field oriented experimental data, but that can still be applicable to the situation near foundations and structures, where static shear loads are acting. Any parameters selected for defining the liquefaction potential near load discontinuities should, if possible, be general enough to incorporate the bulk of experimental results that are available for the cases not involving concentrated loads.

The shear stress levels causing liquefaction in the triaxial test, simple shear and shake-table tests have generally been measured upon planes without any initial static shear stresses (principal planes). Thus, there has been no necessity to consider initial static shear

stresses. For triaxial tests in which cyclic stresses have been superimposed upon an initial static shear stress state, the stresses considered are those exerted on planes subjected to nonsymmetrical stress reversals. The influence of the degree of nonsymmetry of load application does not appear to have been addressed in any general manner, but rather the test data have been applied directly to specific cases.

Where initial static shear loads are acting on the plane of interest, prior to cyclic loading, questions arise such as: what is the significant shear stress to use for liquefaction evaluation (i.e., static plus dynamic, dynamic alone, etc.) and what is the influence of varying degrees of maximum stress reversal (Yoshimi and Oh-Oka, 1975). It is suggested herein that by considering the dynamic shear stress $\Delta\tau_I$ applied on the new major principal plane following application of any static shear stress increments, all the problems dealing with initial static shear load and unsymmetric stress reversals are avoided. Using this concept available experimental data is still applicable to areas of load discontinuity, such as beneath foundations or earth structures.

Consider for illustrative purposes the following stress sequences shown as a series of concentric Mohr circles in Figure 2-12. Let the Mohr's circle with radius r_o represent the initial effective stress conditions on a soil element (either in the ground or in a laboratory test) with horizontal effective stress $\sigma_h' = K_c\sigma_v$ and vertical effective stress σ_v'. Application of static shear stress $\Delta\tau_s$ to the horizontal plane results in the stress in the specimen now being represented by the larger Mohr circle with radius r_s. The use of a pure shear stress increment to the principal plane is merely for simplicity. It is not necessary for this development that the normal stresses be held constant. However, the application of a pure shear increment may be considered as either that applied in the simple shear device in the laboratory or that occurring in the field under a uniformly sloping ground surface. This shear stress increment $\Delta\tau_s$ causes a rotation of the principal plane (formerly the horizontal plane) through the angle ψ. Now, superposition of a dynamic (cyclic) shear stress increment $\Delta\tau_d$ upon the horizontal plane results in a new Mohr's circle of varying radius r_d. This causes dynamic shear stress increment $\Delta\tau_I$ applied to what was the major principal plane prior to application of $\Delta\tau_d$ (following τ_s). It may be seen from Figure 2-12 that:

$$\Delta\tau_I = r_d \sin \Theta$$

where

$$\Theta = \tan^{-1}\left(\frac{\Delta\tau_s + \tau_d}{r_o}\right) - 2\psi$$
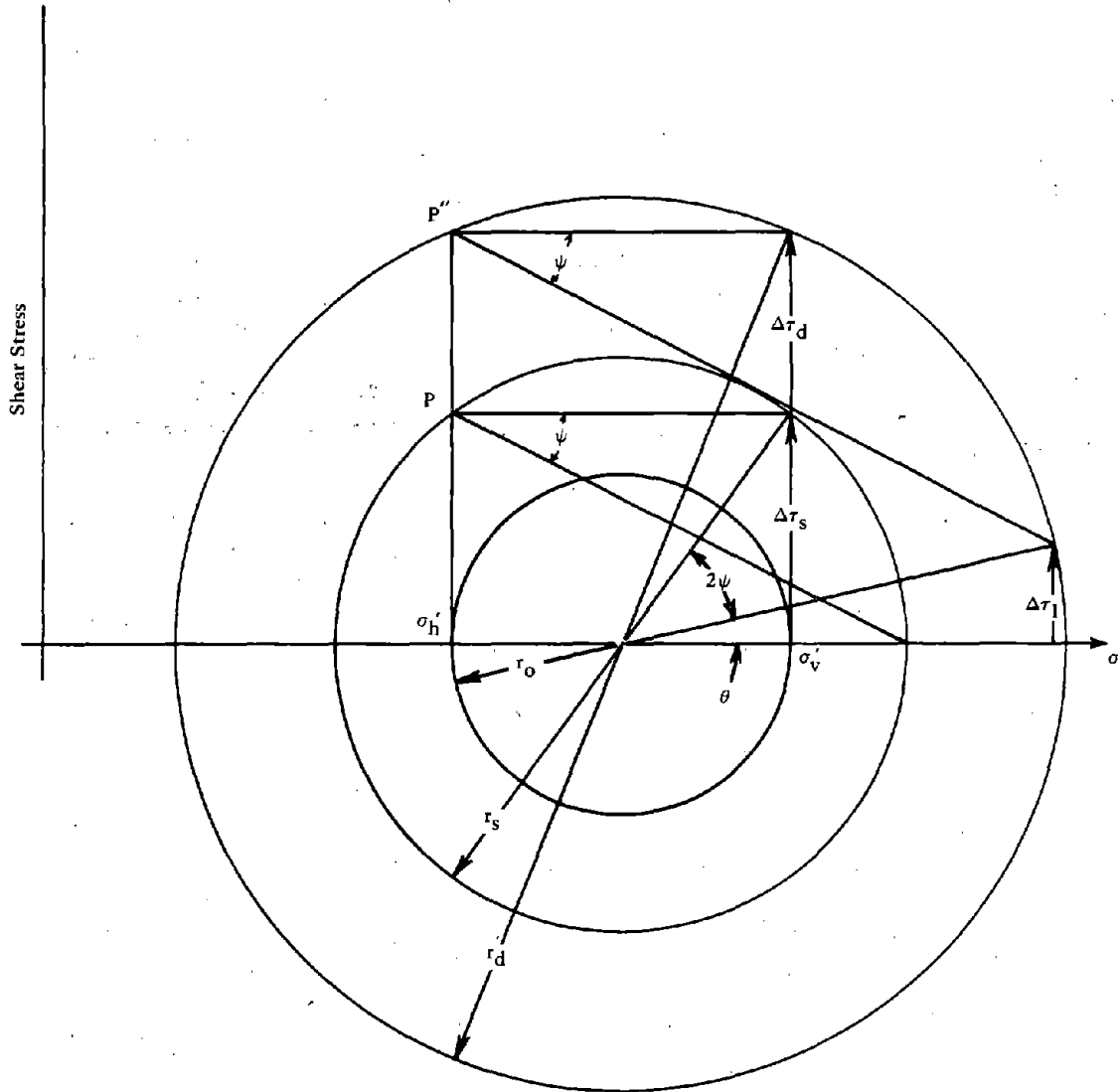
Figure 2-12. Illustration of critical shear stress $\Delta\tau_I$.

and

$$\psi \ = \ \tan^{-1}\left(\frac{\Delta\tau_s}{r_o + r_s}\right)$$

Here $\Delta\tau_I$ is defined for a dynamic stress increase $\Delta\tau_d$; however, it may be shown that for a dynamic stress decrease ($-\Delta\tau_d$ on the horizontal plane), the shear stress $\Delta\tau_I$ on the principal plane is of equal magnitude, but in the opposite direction.

The reference plane for measurement of cyclic shear stress (i.e., the major principal plane) is established prior to dynamic loading. Therefore, it is desirable to select the reference confining stress at this stage also. To this end the average or volumetric effective stress $\sigma_o' = (\sigma_1' + \sigma_2' + \sigma_1')/3$, acting prior to cyclic shearing, is selected. This is, incidentally, the reference confining stress used in calculating the stress ratio causing liquefaction in the isotropically confined tri-axial test. This confining stress remains constant irrespective of static shear stress increment where pure shear is involved, such as in either the simple shear or ring torsion apparatus. The drastic changes in effective stress taking place in undrained soils during cyclic loading make it desirable to select this reference stress prior to dynamic loading; i.e., when σ_o' is still well-defined.

EFFECTS OF PRINCIPAL STRESS RATIO

The use of average (effective) principal stress as the confining stress was previously suggested by Ishibashi and Sherif (1974) on the basis of torsional tests. Figure 2-13 shows best fit curves from results of cyclic ring-torsion shear tests (Ishibashi and Sherif, 1974) on Ottawa sand at a reported relative density of about 27%. This unusually low initial density appears to be a feature of the particular specimen preparation technique. It is noted that the plots of horizontal shear stress/volumetric stress, τ_d/σ_o' (shear stress on major principal plane/effective octahedral normal stress) ratio versus number of cycles to initial lique-faction are quite similar in spite of the different initial principal stress ratios (K_c). Ishibashi and Sherif (1974) compared many different ways of formulating stress ratios for defining liquefaction criteria, such as the maximum shear stress/octahedral stress, the horizontal shear stress/vertical stress, etc. The stress ratio presented in Figure 2-13 was the only one investigated for which the best fit curves of stress ratio versus number of cycles to failure for the three different initial principal stress ratios K_c were not significantly different.
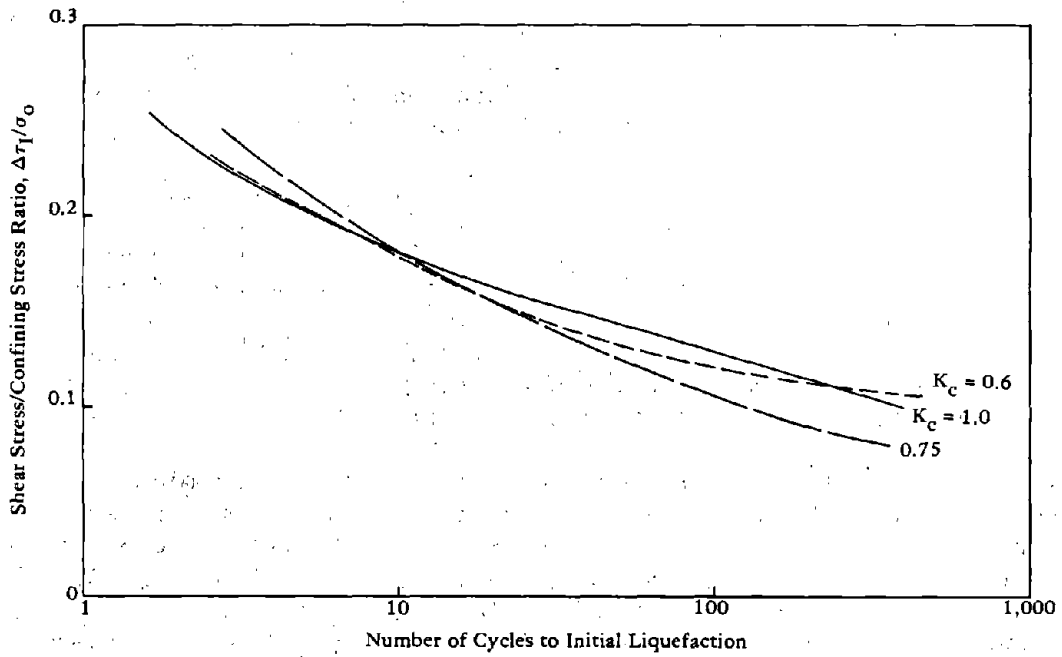
Figure 2-13. Results of ring-torsion shear tests on specimens having different initial principal stress.
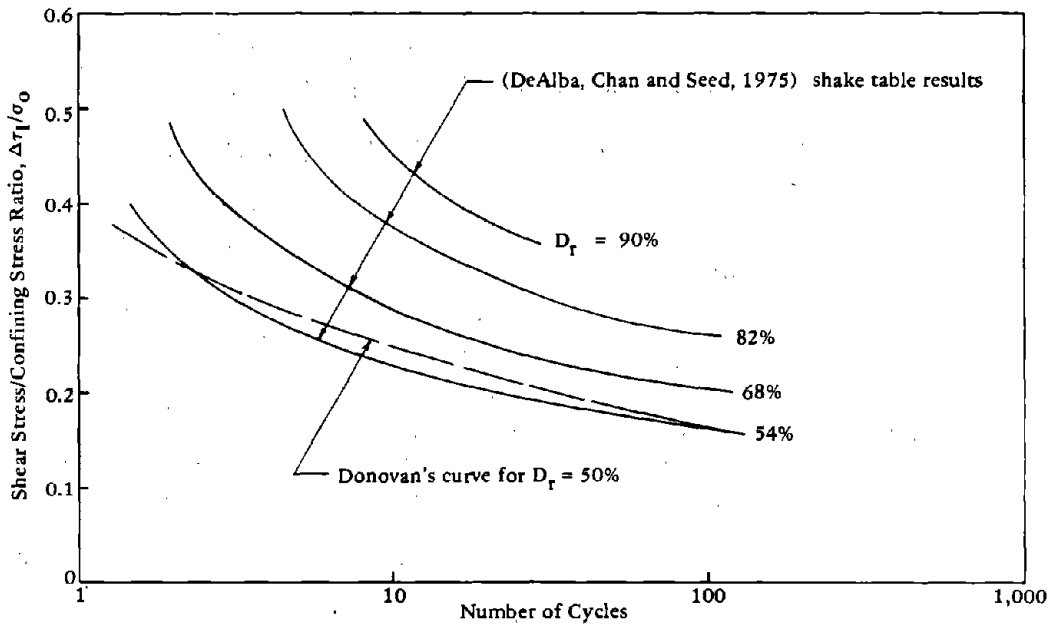
Figure 2-14. Comparison of stress ratios from triaxial and shake table testing.

In order to further investigate the general applicability of the foregoing method of defining liquefaction criteria, best-fit plots from extensive shake-table results (DeAlba, Chan and Seed, 1975) have been replotted in revised form in Figure 2-14 (assuming an at-rest coefficient of earth pressure K_c of 0.45). Also shown in Figure 2-14 is the best-fit line from the triaxial data from Donovan (1974) (see Figure 2-15) for a relative density of 50%. The sands used for the bulk of the data appeared to be similar in grain size and angularity to the Monterey sand used by DeAlba, Chan, and Seed (1975). Although the shapes of the different data summaries differ slightly, the differences in stress ratios when calculated in the proposed way are negligible compared with the correction factors required for converting triaxial test data to the horizontal-shear/vertical-stress ratio convention.

The foregoing liquefaction data were generated for application to the free-field situation and deal with coefficients of earth pressure K_c from typical at-rest values of about 0.45 up to 1.0. It would be of major interest to study earth pressure coefficients of less than 0.45; i.e., approaching maximum obliquity or the failure envelope for the soil. Such cases can occur where initial static shear loads are applied. Unfortunately, little test data are available where cyclic loading is applied following an initial static load increment. One such paper dealing with this problem has been presented by Yoshimi and Oh-Oka (1975). Specimens of fine sand at a relative density of about 37% were cyclically loaded in a torsional shear device. Three series of tests were conducted: the first without an initially applied static shear stress increment and the other two with static shear stress increments sufficient to permit (1) only partial shear stress reversal and (2) no shear stress reversal on the plane of applied shear stress. Because of the different stress situations between the three series, conventionally calculated shear-stress/confining-pressure ratios (ratios calculated using shear stress level on the plane initially subjected to static shear stress increment) gave markedly different stress ratio versus numbers of cycles to failure relationships.

The best-fit curves from these data, plotted in terms of the stress ratio recommended herein, versus number of cycles to initial liquefaction are shown in Figure 2-16. Initial liquefaction has been taken as the point at which a major change in rate of shear strain commences. It was assumed that prior to application of the static shear stress increment the coefficient of earth pressure K_c was 0.45.

Figure 2-15. Compilation of triaxial liquefaction data (after Donovan, 1974).

32
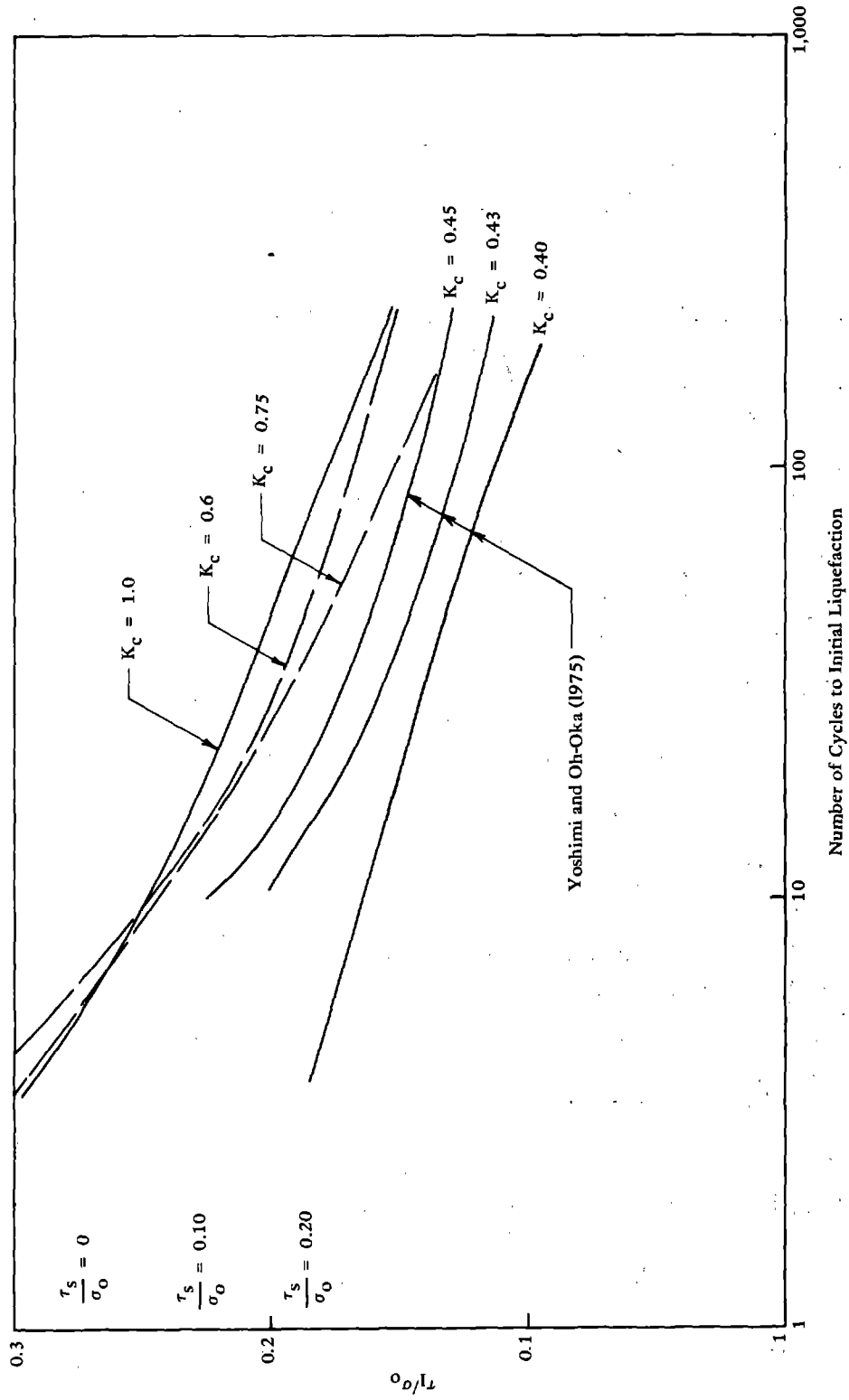
Figure 2-16. Liquefaction criteria applicable to regions with load discontinuities.

Following application of the static load increment it was assumed that the intermediate principal stress was unchanged but the minor principal stress was decreased by the same amount as the maximum principal stress was increased (Figure 2-12). This provided a reduction in the principal stress ratio K_c in the plane of maximum shear, and it is these revised values of K_c which are shown in Figure 2-16. Also shown on this figure are the curves from Figure 2-13 adjusted to the same relative density (D_r = 37%) as that of the Yoshimi and Oh-Oka (1975) data by multiplying the stress ratio by the factor 37/27. Although the plots on Figure 2-16 represent data on two different sands, both the reported gradations and the two testing devices appear quite similar.

The data in Figure 2-16 suggest that, for high K_c values, the use of the dimensionless coefficient recommended herein to define liquefaction provides an acceptable failure criterion for the various principal stress ratios. However, as the static K_c values fall below the normal free field situation (i.e., the Mohr circle representing the stress state approaches the yield envelope, as under a foundation), slightly reduced shear stress ratios may be required to cause liquefaction at a particular number of cycles. Yoshimi and Oh-Oka (1975) have noted that at the higher initial static stress levels, the number of cycles between initial liquefaction (marked increase in strain rate) and complete liquefaction (effective stress reduced to a negligible value) increases. Thus, the curves representing their data in Figure 2-16 would be in slightly better agreement with the Ishibashi and Sherif (1974) data were complete failure, rather than initial liquefaction, of concern. Actually, initial liquefaction by Ishibashi and Sherif (1974) appears to be closer to that defined as complete liquefaction by Yoshimi and Oh-Oka (1975).

Thus, liquefaction data can be presented in a format suitable to include the free field condition (away from concentrated loads) with horizontal soil layers, as has been generally considered, but also to include soil regions beneath load discontinuities. By plotting the ratio of dynamic shear stress generated on the major principal plane (prior to dynamic shearing) to average volumetric stress versus the number of stress cycles to liquefaction, cyclic triaxial tests can be used to provide an envelope of the liquefaction strength under foundation loads. By using the recommended format for plotting cyclic load data on specimens upon which initial static shear stresses are acting (K_c reduced to below a normal free field value of about 0.45), a more stringent criterion for liquefaction prediction may be identified for application beneath foundation loads.

The foregoing discussion attempted to provide insight into the liquefaction phenomenon. Various factors influencing the liquefaction potential were discussed with the aim of providing background to enable the engineer to use judgment in carrying out liquefaction hazard evaluations. The following portion of this chapter will deal with general

34

soil reponse characterizations. These latter soil properties are those
commonly used to define soil behavior from an engineering mechanics
point of view.

PARAMETERS INDIRECTLY AFFECTING LIQUEFACTION

There is a family of soil parameters which, while not related to
the liquefaction process directly, do influence the liquefaction poten-
tial. These are the response parameters which dictate how a soil will
respond to applied stress. For example, since volumetric changes and,
hence, liquefaction potential can be related to the distortional strain
levels which a soil undergoes (Martin, Finn, and Seed, 1975), the shear
stiffness or modulus of rigidity G of a soil under a specific load level
is of particular concern. Earthquake motions can be either amplified or
attenuated, depending upon characteristics of the soil profile (and its
interaction with the frequency content of the disturbing earthquake)
which, in turn, depends upon the values of the stiffness and damping
parameters involved.

Since many treatments of earthquake-induced liquefaction deal with
vertically transmitted horizontal shear waves, one approach to analysis
requires only a value for the shear modulus G, together with a damping
coefficient, to account for the energy absorption of the soil. Extensive
experimental work dealing with these two parameters has been carried out
by Seed and Idriss (1970), and Hardin and Drnevich (1970). These studies
permit characterizing the shear response parameters of soil in terms of
the basic soil index properties and the existing stress and strain
states. For example, the shear modulus value for clean granular soils
is related to void ratio, mean effective stress, maximum cyclic shear
strain amplitude, and number of loading cycles (some soils have an
additional dependency upon overconsolidation ratio, degree of saturation,
and plasticity index). Soil damping, particularly in cohesionless
soils, is at least partially due to relative movements between soil
particles and, hence, is hysteretic. The contribution by dry friction
to the damping ratio should be substantially independent of strain rate.
Nevertheless, for analytical expediency all damping is represented by an
equivalent viscous damping. Thus, selection of a damping coefficient
makes the damping ratio a function of frequency. As long as the ratio
of applied frequency to resonant frequency is not much greater than one,
this appears to be acceptable even though it is strictly true only at
resonance. For soils, damping is generally specified as a percentage of
critical damping, and measured in terms of specific damping capacity,
related to the ratio of the area within a hysteretic loop during a load
cycle and the maximum stored energy during the cycle. Seed and Idriss
(1970) have derived expressions for damping ratio as a function of
strain level, number of cycles, frequency, mean effective stress, and
the other index properties mentioned in reference to shear modulus G.

A number of investigations done on sandy soils have been summarized
in Table 2-1. Recent work on shear stiffness and damping, with particular
reference to sands, is being pursued by Silver and Park (1975) at the
University of Illinois.

In all of this work, shear modulus G is noted as increasing with
density and confining pressure and decreasing with shear strain amplitude.
Damping coefficients on the other hand increase with shear strain ampli-
tude and appear to decrease with confining stress and increased density.

Previous stress history is noted as increasing shear stiffness
value and decreasing damping. One application of the use of the foregoing
soil parameters to earthquake response analysis has been incorporated
into a computer program SHAKE (Schnabel, Lysmer and Seed, 1972) in which
the shear modulus of granular materials is treated as:

$$G = A K_2 (\sigma_n)^a$$

Where A and a are constants, normally having values of 1,000 and 0.5,
respectively, and K_2 is a function of the index properties of the soil
and is an inverse function of the shear strain amplitude.

Typical variation of K_2 for sands based upon the results of various
workers is presented in Figures 2-17 and 2-18, and a composite series of
relationships for various relative densities is shown in Figure 2-19
(Seed and Idriss, 1970). Shear modulus measurements at very low strain
levels are usually measured by shear wave velocity studies. For higher
strain amplitudes, resonant column and cyclic triaxial, simple shear and
hollow cylinder torsion tests are commonly employed, see Chapter 5 of
this volume.

It has been found (Seed and Idriss, 1970; Hardin and Drnevich,
1970) that shear modulus values at any strain level may be normalized in
terms of maximum shear modulus to permit a generalized relationship for
many soil materials to be collapsed into a single relationship. Such a
relationship is presented in Figure 2-20 (Seed and Idriss, 1970).

Damping ratios, as mentioned, were found to vary as functions of
soil index properties as well as the stress and strain states. Figure
2-21 shows the influence of friction angle, void ratio, coefficient of
lateral earth pressure, and degree of saturation on a clean sand under a
vertical effective stress of 1,000 psf (70 psi), based upon work by
Hardin and Drnevich (1970). The influence of effective confining pressure
is shown on Figure 2-22. Average values of damping ratio for an effective
vertical stress of about 1 to 1-1/2 kg/cm^2 have been presented in Figure
2-23.

36

Table 2-1. Summary of Laboratory Investigations of Shear Moduli and Damping Ratios for Sandy Soils (from H.B. Seed and I.M. Idriss, 1970)

Type of Test	Soil Tested	Range of Strain		Range of Confining Pressure (psf)
		Shear	Axial	
Forced Vibration: Longitudinal Vibration	Sand		$<5\times10^{-3}\%$	600 to 7,200
	Sand		$<5\times10^{-3}\%$	450 to 7,500
	Sand		$<5\times10^{-3}\%$	600 to 7,400
	Sand		$<5\times10^{-3}\%$	600 to 7,200
	Sand, silty sand and clayey sand		$<5\times10^{-3}\%$	1,000 to 3,500
Forced Vibration: Torsional Vibrations Solid Sample	Sand	$<10^{-2}\%$		600 to 7,200
	Sand	$<10^{-2}\%$		600 to 7,400
	Sand	$<10^{-2}\%$		450 to 7,500
	Sand	$<10^{-2}\%$		600 to 7,200
	Sand	$<10^{-2}\%$		600 to 8,500
Forced Vibration: Torsional Vibration Hollow Sample	Sand	10^{-3} to $6\times10^{-2}\%$		600 to 8,500
	Sand	10^{-3} to $6\times10^{-2}\%$		500 to 1,800
Free Vibration: Cylindrical Sample	Sand		10^{-3} to $10^{-4}\%$	400 to 6,400
Triaxial Compression	Sand and gravel, silt and sand		2×10^{-3} to $5\times10^{-3}\%$	400 to 1,800
	Sand, silty sand and clayey sand		5×10^{-3} to 0.1%	1,000 to 3,500
	Sand		10^{-1} to 1%	3,000 to 3,400
Simple Shear	Sand	3×10^{-2} to 0.5%		2,000
	Sand	10^{-2} to 0.5%		500 to 4,000

$$G = 1,000\,K_2(\sigma_m')^{1/2}\ \text{psf}$$

⊡	Weissman and Hart
△	Richart, Hall, and Lysmer
⊙	Drnevich, Hall, and Richart
●	Seed
▲	Silver and Seed
▼	Hardin and Drnevich
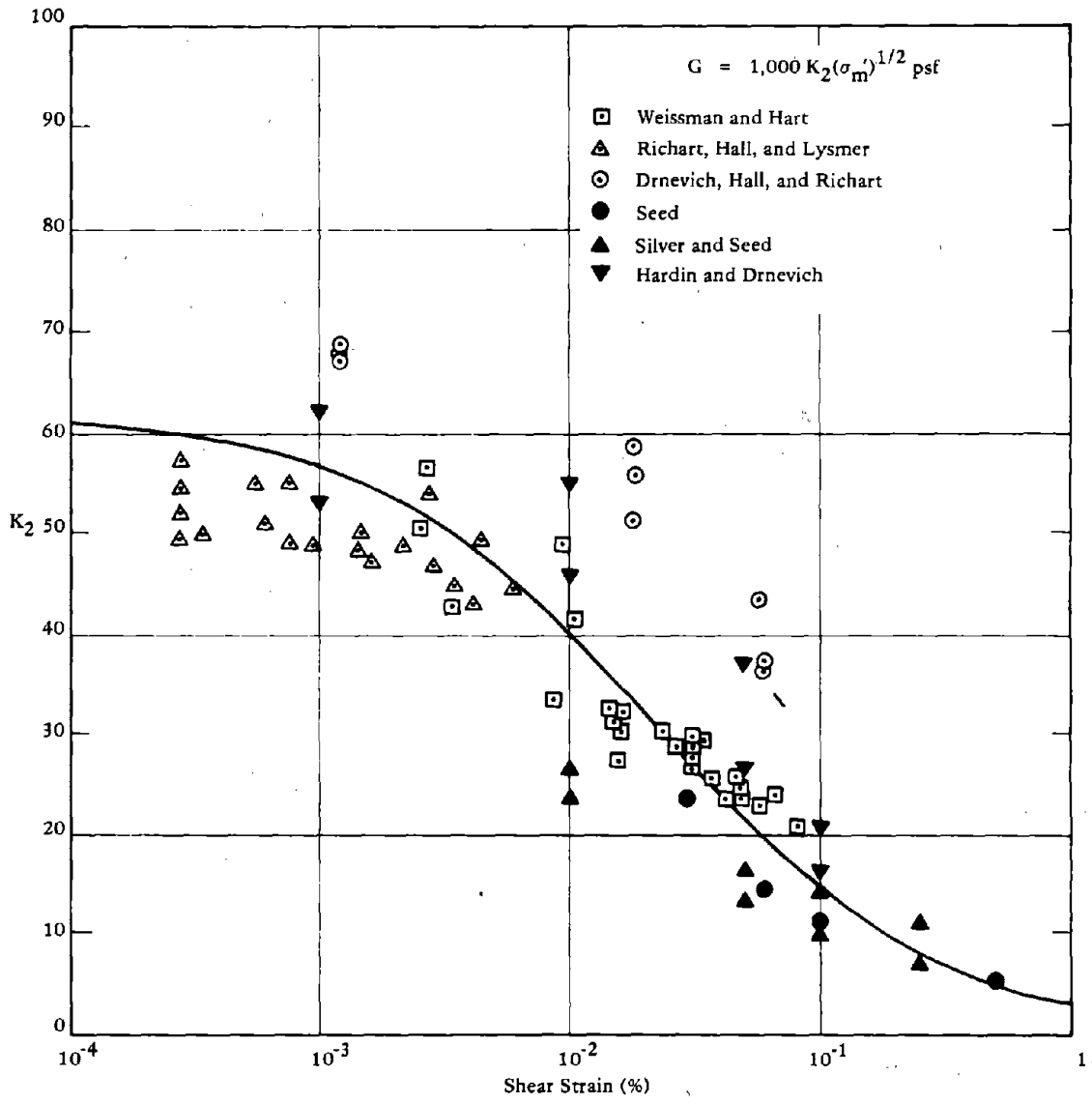
Figure 2-17.   Shear moduli of sands at relative density of about 75%
(from Seed and Idriss, 1970).

38
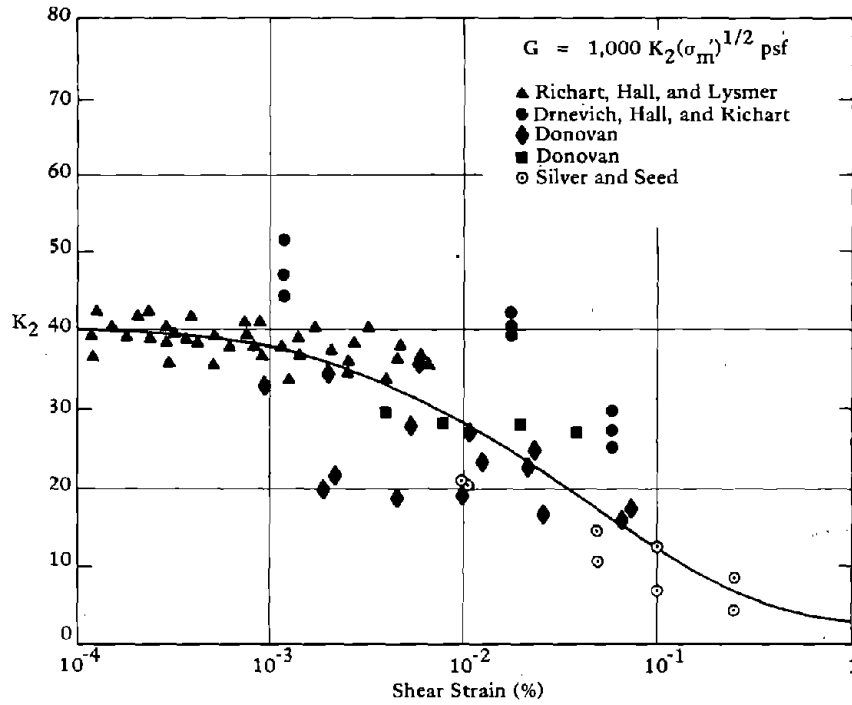
Figure 2-18. Shear moduli of sands at relative density of about 40% (from Seed and Idriss, 1970).
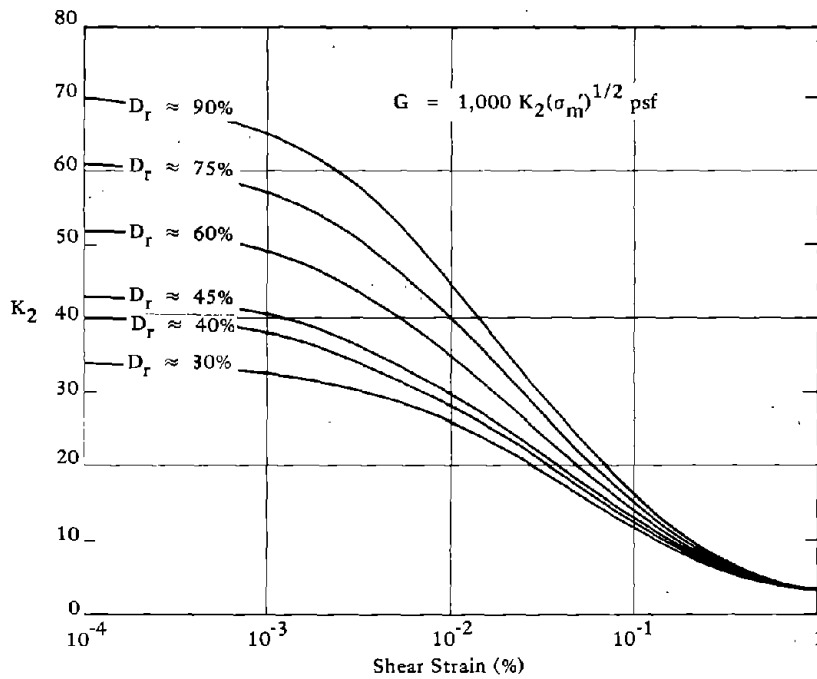
Figure 2-19. Shear moduli of sands at different relative densities (from Seed and Idriss, 1970).

39
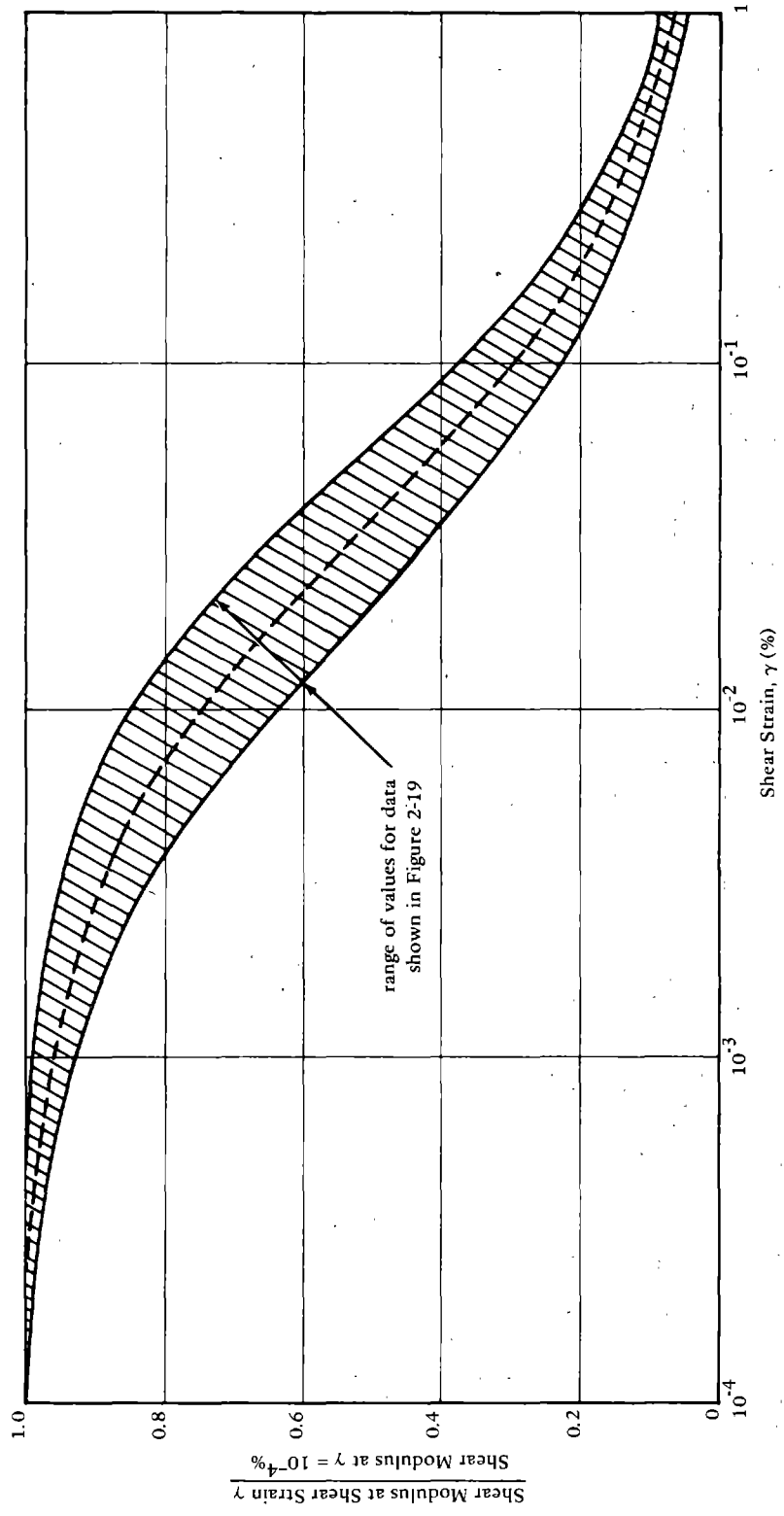
Figure 2-20. Variation of shear modulus with shear strain for sands. (from Seed and Idriss, 1970).

40
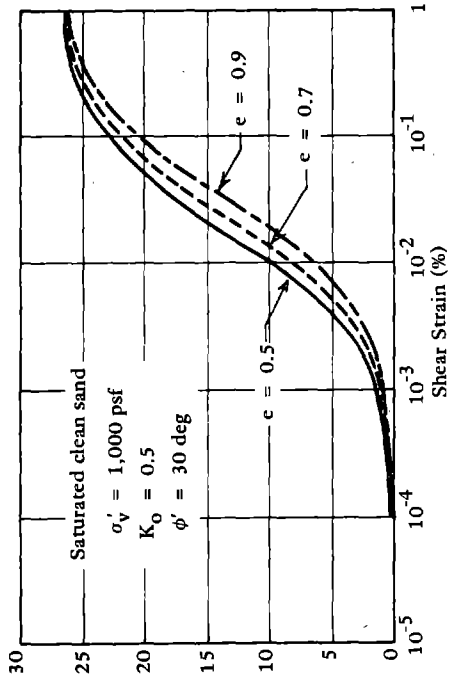
(a) Effect of angle of friction.

(b) Effect of void ratio.
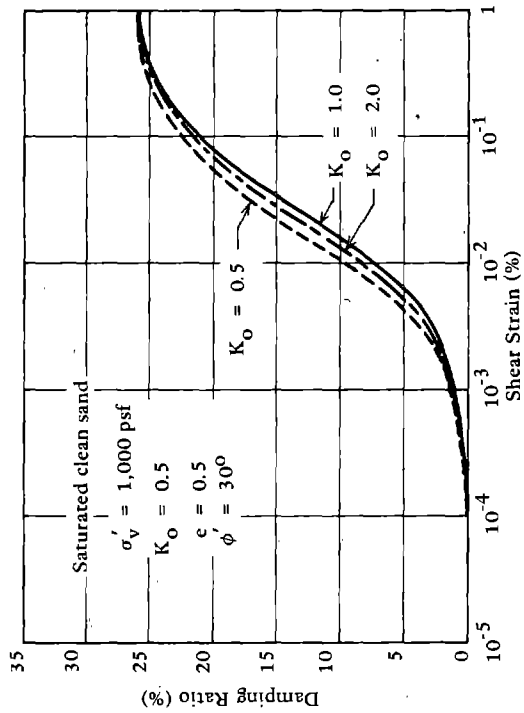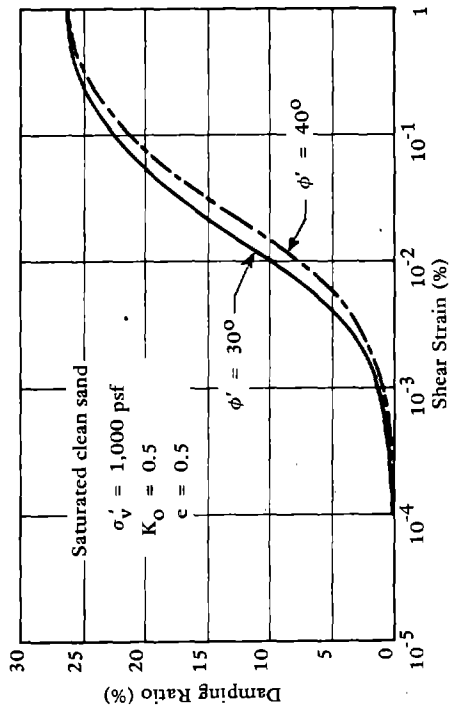
(c) Effect of K_o.

(d) Effect of saturation.
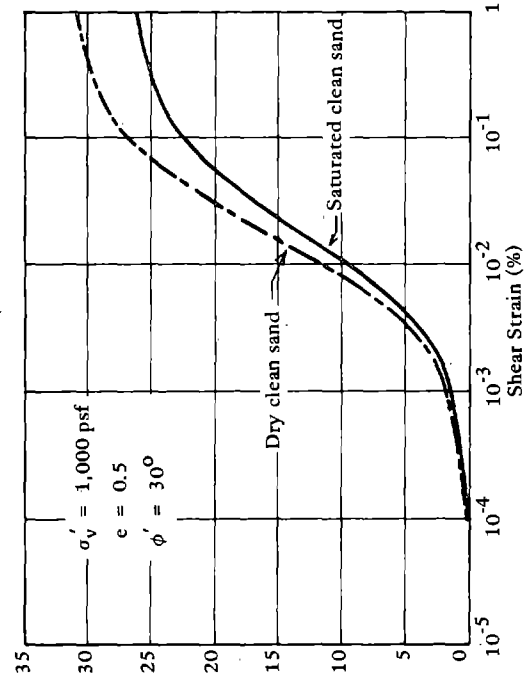
Figure 2-21. Influence of various factors on the damping ratios for sands (from Seed and Idriss, 1970; based on Hardin and Drnevich expressions).

41
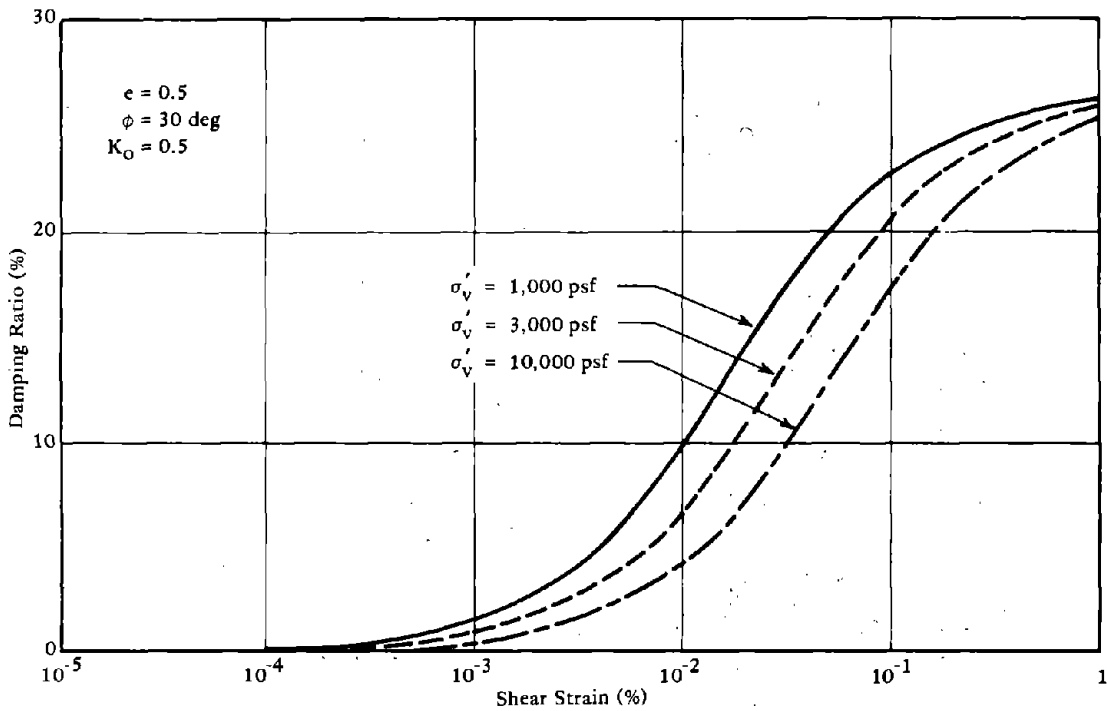
(a) Saturated sand (based on Hardin
and Drnevich expressions).
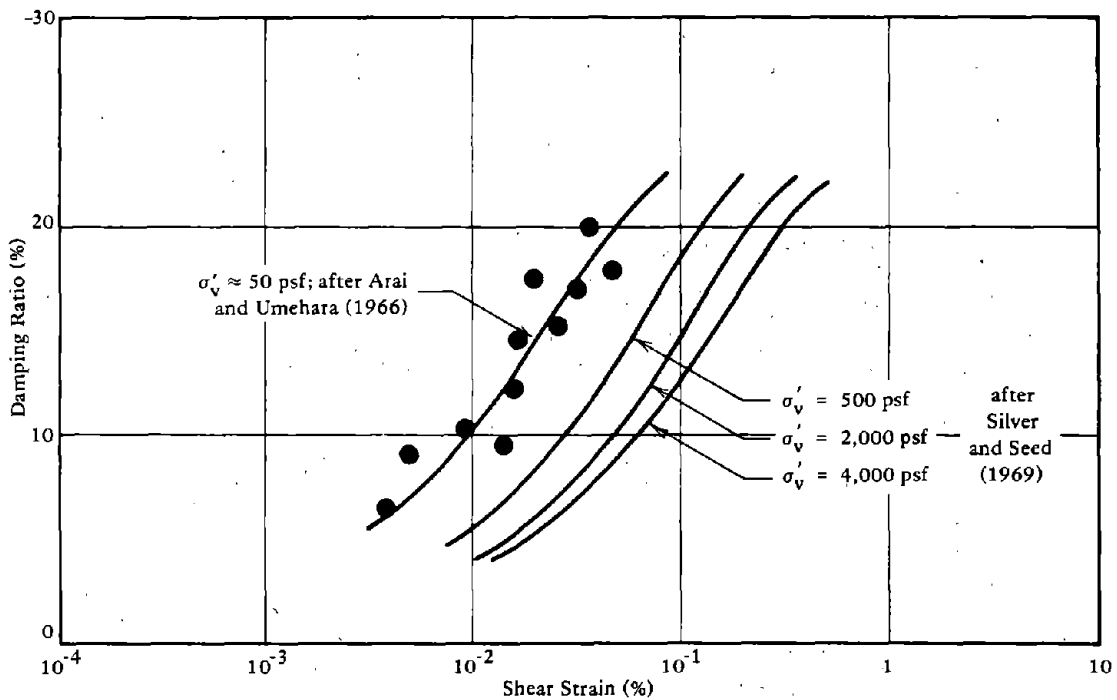
(b) Dry sand.

Figure 2-22. Influence of confining pressure on damping
ratio (from Seed and Idriss, 1970).

42
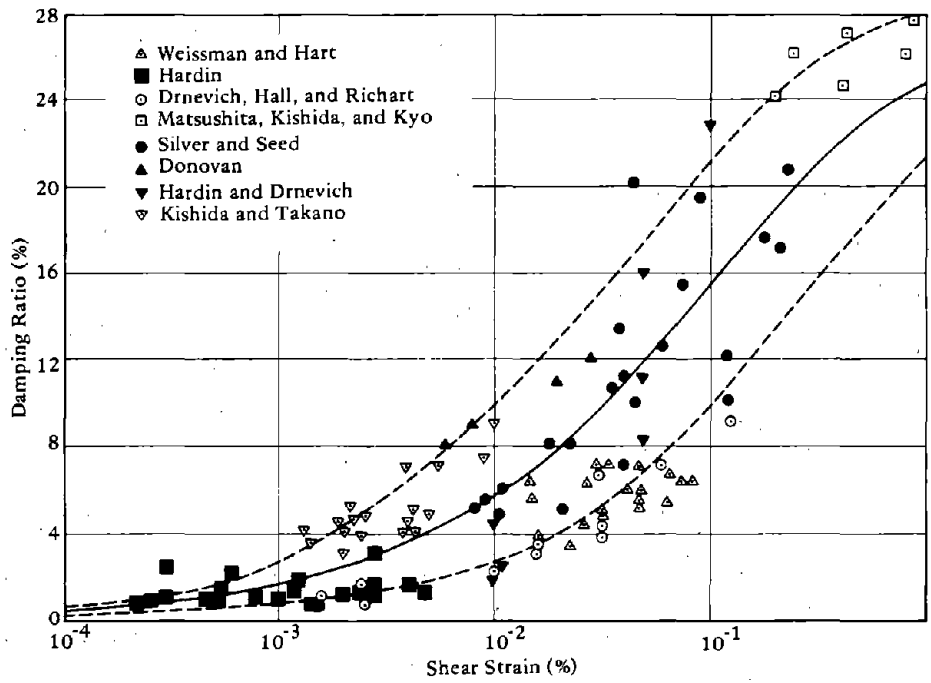
Figure 2-23. Damping ratios for sands (from Seed and Idriss, 1970).

The legend for the upper figure:
- △ Weissman and Hart
- ■ Hardin
- ⊙ Drnevich, Hall, and Richart
- ⊡ Matsushita, Kishida, and Kyo
- ● Silver and Seed
- ▲ Donovan
- ▼ Hardin and Drnevich
- ▽ Kishida and Takano

Axes: Damping Ratio (%) vs Shear Strain (%)
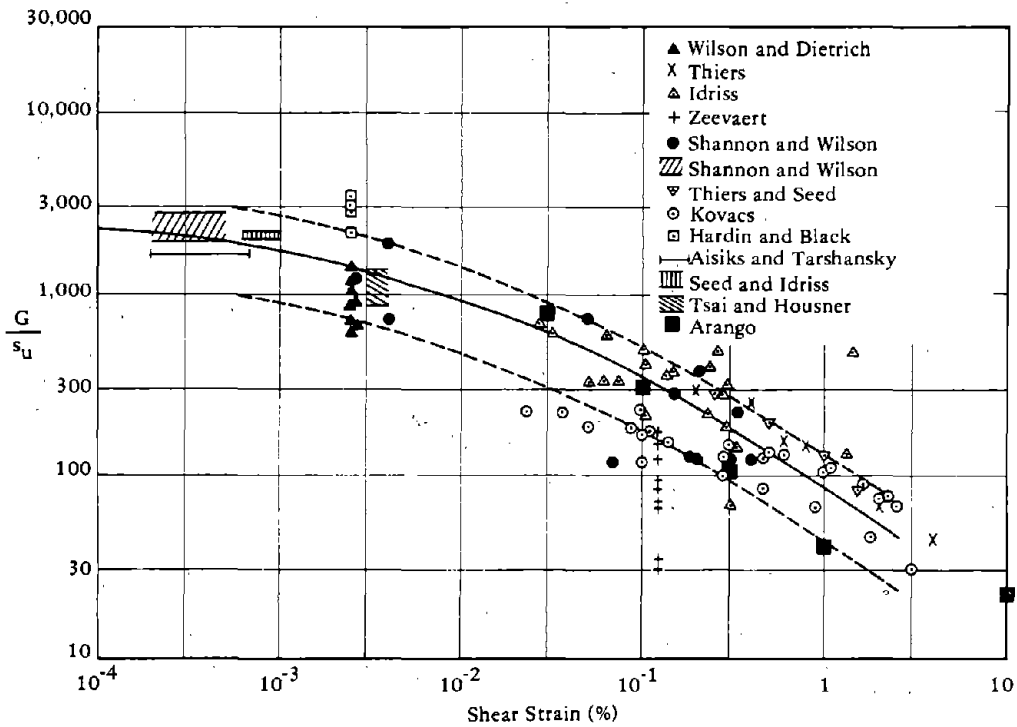
Figure 2-24. In situ shear moduli for saturated clays (from Seed and Idriss, 1970).

The legend for the lower figure:
- ▲ Wilson and Dietrich
- X Thiers
- △ Idriss
- + Zeevaert
- ● Shannon and Wilson
- ▨ Shannon and Wilson
- ▽ Thiers and Seed
- ⊙ Kovacs
- ⊡ Hardin and Black
- ⊢——⊣ Aisiks and Tarshansky
- ▥ Seed and Idriss
- ▧ Tsai and Housner
- ■ Arango

Axes: $\dfrac{G}{s_u}$ vs Shear Strain (%)

43

Although cohesive materials have been treated in the same format as granular materials, their soil models have not been found quite as satisfactory in this context. It is more expedient to normalize the shear modulus of clays in terms of the undrained shear strength S_u in the form of G/S_u versus shear strain amplitude. Data obtained by various investigations have been compiled in Table 2-2 and plotted in Figure 2-24. Again, it is possible to collapse the various shear modulus relationships into a single curve by normalizing them by the maximum value of shear modulus at infinitesimal strain (Figure 2-25). In this way, modulus values determined at very small strain levels, such as by measuring shear wave velocities in the field, can be used to predict the shear modulus under design loading conditions. Damping ratios for clays have been studied less extensively than for granular materials. However, a summary of the results of past studies is shown in Figure 2-26.

Little data is available for materials other than sands and clays, but available information indicates that coarser grained materials such as gravels may be expected to behave as sands (Seed and Idriss, 1970; Hardin and Drnevich, 1970). Figure 2-27 shows tentative modulus values for gravelly soils, but damping data is essentially nonexistent.

Peats are generally treated in the same format as clays. Available data on peats based upon field seismic wave velocities, laboratory studies, and earthquake ground response evaluations are shown in Figure 2-28.

One of the major weaknesses in selecting soil response parameters to use for liquefaction analysis is the difficulty of monitoring the changes that take place under applied load. Codes are available which consider the changes of the average values of the shear stiffness and damping parameters with maximum shear strain levels. However, the changes in effective confining pressure are generally lumped into an overall phenomenological approach. Following generation of the first increment of pore pressure the values of the soil parameters commence to undergo change.

In an attempt to consider the problem of loss of shear strength in a soil specimen due to liquefaction, Yen (1967) has attempted to develop a classical viscosity approach; his work suggests a straightforward procedure for determining what appears to be realistic viscosity values for saturated sands under cyclic loading. Unfortunately, the viscosity values developed for this approach are applicable only for the time preceding actual liquefaction. Table 2-3 shows typical viscosity values measured for Niigata sands. Figure 2-29 presents data for El Monte sand. Florin and Ivanov (1961) note that following liquefaction, the viscosity of sand inhibits flow failure. This viscous effect apparently increases with density. Thus, although liquefaction may result in surface settlement as a result of eventual drainage, actual flow failures may be limited.

Table 2-2. Summary of Laboratory Investigations of Shear Moduli and Damping
Ratios for Saturated Clays (from H.B. Seed and I.M. Idriss, 1970)

Type of Test	Soil Tested	Range of Strain		Range of Shear Strength (psf)	Data Correction Factor[a]
		Shear	Axial		
Field Tests					
Shear Wave Velocity	San Francisco Bay mud	$<10^{-3}$%		200 to 500	1.0
Compression Wave Velocity	Union Bay clay		$<10^{-3}$%		1.0
Laboratory Tests					
Free Vibration					
Longitudinal	Elkhorn Slough silty clay		3×10^{-2} to 2%	300 to 1,100	2.5
Shear	San Francisco Bay mud	2×10^{-2} to 0.5%		300	2.5
	Kaolinite/Bentonite mixture	5×10^{-2} to 2%		44 to 85	2.5
Forced Vibration					
Longitudinal	Cambridge clay		$\approx 2.5 \times 10^{-3}$%	1,080	2.5
	Mississippi gravels		$\approx 2.5 \times 10^{-3}$%	520	2.5
Torsional	Birch Bay clay	$\approx 2.5 \times 10^{-3}$%		1,000 to 2,420	2.5
	Montana clay	$\approx 2.5 \times 10^{-3}$%		6,000	2.5
Torsional (consolidated samples)	Whidbey Bay clay	$\approx 2.5 \times 10^{-3}$%		230 to 1,800	1.5[b]
	Silty clay	0.125%		800 to 1,500	1.0
	Edgar Plastic Kaolin	$\approx 2.5 \times 10^{-3}$%		1,400 to 1,800	1.0
Triaxial Compression	Ardmore clay		0.1 to 0.5%	—	—
	Ardmore clay		0.5 to 1%	—	—
	Union Bay clay		3×10^{-3} to 0.3%	200 to 880	2.5
	Silty clay		10^{-2} to 0.1%	—	—
	Webb Mark IV clay		0.2 to 1%	—	—
Torsional Shear	Georgia Kaolinite	3×10^{-2} to 0.2%		—	—
Simple Shear	San Francisco Bay mud	0.2 to 4%		300 to 400	2.5
	Kaolinite/Bentonite mixture	0.1 to 2.5%		44 to 85	2.5
	San Francisco Bay mud	0.1 to 3%		300	2.5

[a] Applied to modulus values to allow for sample disturbance.

[b] Sample disturbed slightly after consolidation.

45
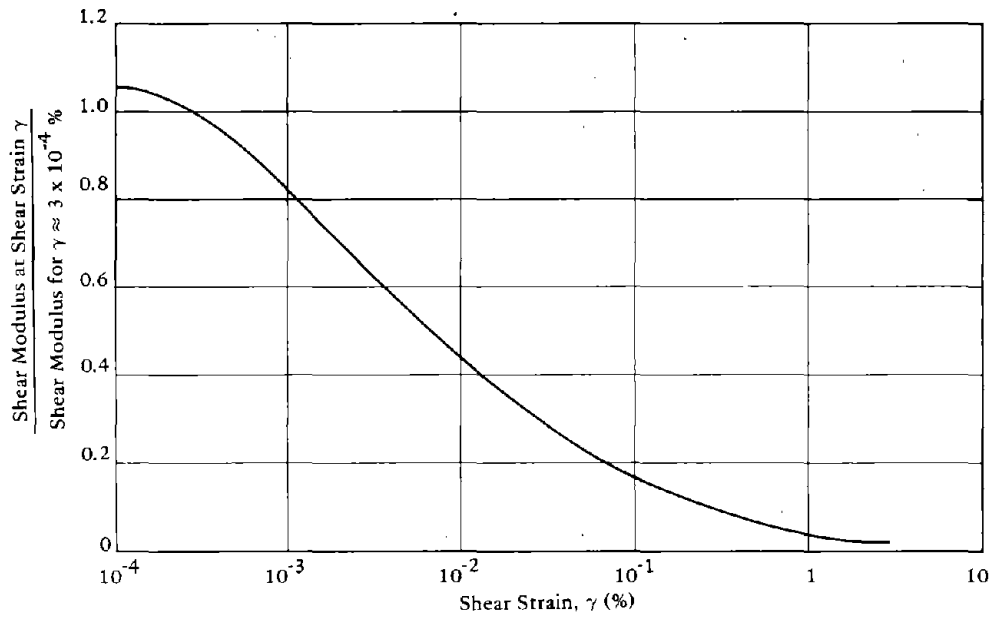
Figure 2-25. Typical reduction of shear modulus with shear
strain for saturated clays (from Seed and Idriss, 1970).
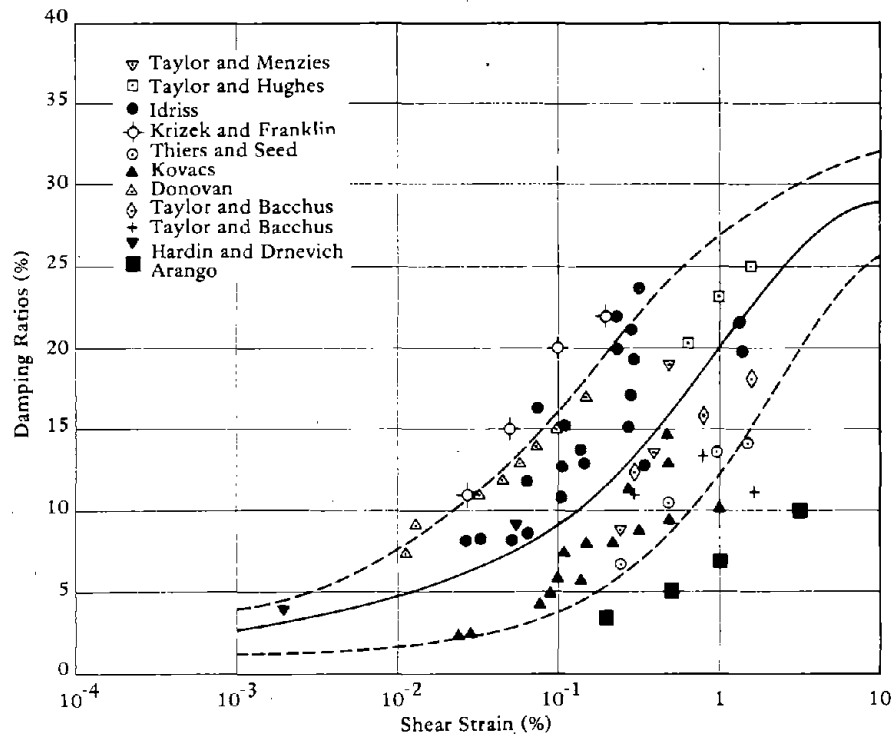
Figure 2-26. Damping ratios for saturated clays
(from Seed and Idriss, 1970).

46
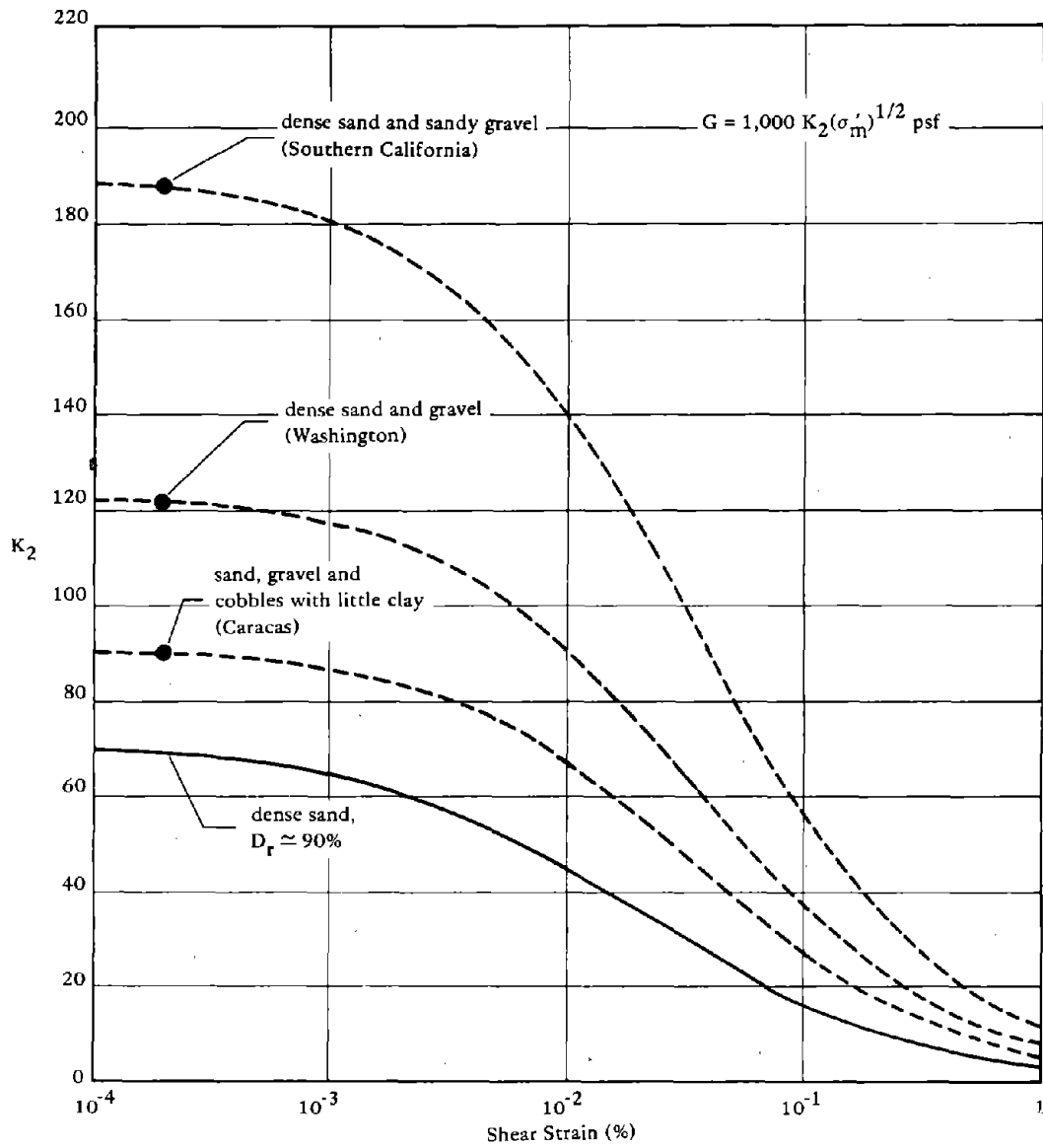
Figure 2-27. Modulus determinations for gravelly
soils (from Seed and Idriss, 1970).
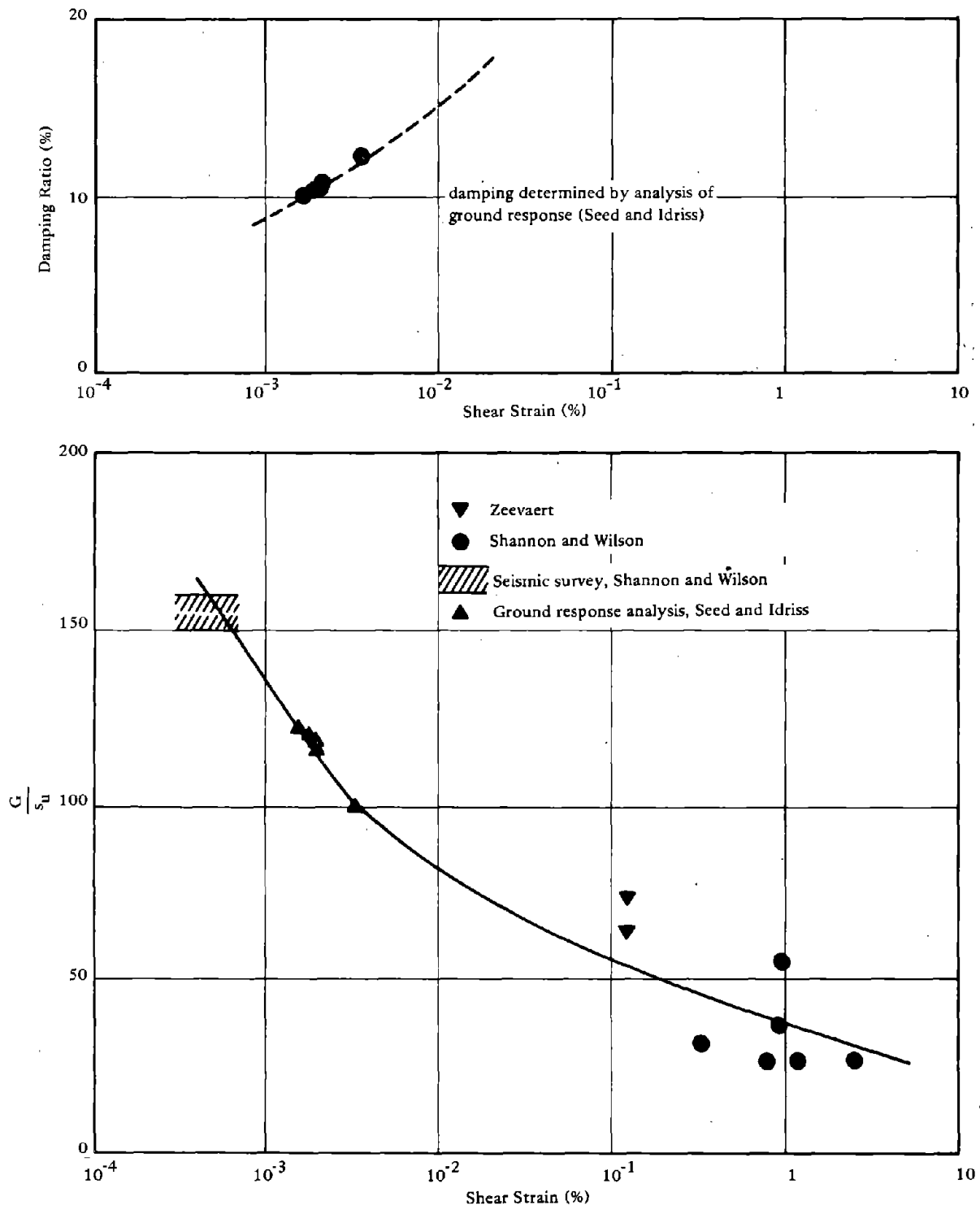
Figure 2-28. Moduli and damping determinations for
peats (from Seed and Idriss, 1970).

48

Table 2-3. Estimated Viscous Characteristics of Niigata
Sand During 1964 Earthquake

No. of Cycles	Apparent Coefficient of Viscosity (lb-sec/in.^{2})	Ratio of Viscosity to the Viscosity at Liquefaction	Strain (%)	Ratio of Strain at Liquefaction to Strain of Any Cycle
5	3,000	7.9	2$^+$	8.3
6	1,450	3.8	4	4.1
7	850	2.2	7.5	2.2
8	600	1.6	10	1.6
9	465	1.2	13.5	1.2
10^a	380	1.0	16.5	1.0

^{a}Liquefaction.
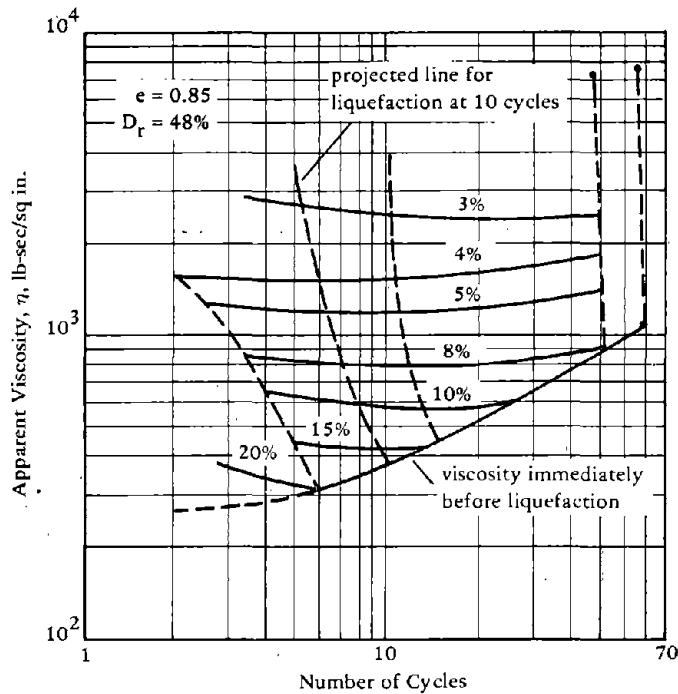
Figure 2-29. Effect of number of stress cycles and strain versus
viscosity in El Monte sand (from "Viscosity of Saturated
Sands Near Liquefaction," by B. C. Yen, copyrighted
by The University of New Mexico Press,
Albuquerque, N. M., 1967).

49

REFERENCES, CHAPTER 2

Castro, G. (1969) "Liquefaction in sands," Harvard Soil Mechanics
Series, no. 81, p. 112.

Castro, G. and Poulos, S. (1976) "Factors affecting liquefaction and
cyclic mobility," ASCE Preprint 2752 (Liquefaction Problems in Geotechni-
cal Engineering). American Society of Civil Engineers Annual Convention,
Philadelphia, Pa., 27 Sep — 1 Oct 1976.

DeAlba, P., Chan, C. K. and Seed, H. B. (1975) Determination of soil
liquefaction characteristics by large-scale laboratory test. University
of California, Earthquake Engineering Research Center, EERC Report No.
75-14. Berkeley, Calif., 1975.

Donovan, N. C. (1974) CUMLIQ: Evaluation of potential for liquefaction
of a soil deposit using random vibration procedures, University of Cali-
fornia, Earthquake Engineering Research Center, National Information
Service Earthquake Engineering. Berkeley, Calif., Jul 1974.

Finn, W. L. (1972) "Soil dynamics liquefaction of sands," in Proceedings
of International Conference on Microzonation for Safer Construction
Research and Application, 30 Oct — 2 Nov 1972. Seattle, Wash., 1972.

Finn, W. D. L., Bransby, P. L. and Pickering, D. J. (1970) "Effect of
strain history on liquefaction of sand," Journal of Soil Mechanics and
Foundation Division, ASCE, vol 96, no. SM6, Jun 1970, pp 1917-1934.

Florin, V. A. and Ivanov, P. L. (1961) "Liquefaction of saturated
sandy soils," in Proceedings of Fifth International Conference on Soil
Mechanics and Foundations, Paris, France. New York, N.Y., United Nations
Educational Scientific and Cultural Organization, Jul 1961.

Hardin, B. and Drnevich, V. (1970) Shear modulus and damping in soils,
University of Kentucky, College of Engineering, Technical Report UKY
26-70-CE2, Soil Mechanics Series. Lexington, Ky, Jul 1970.

Huang, W. (1961) "Investigations on stability of saturated sand
foundations and slopes against liquefaction," in Proceedings of Fifth
International Conference on Soil Mechanics Foundation Engineering,
Paris, France, vol 11, 1961, pp 629-632.

Ishibashi, I. and Sherif, M. A. (1974) "Soil liquefaction by torsional
simple shear device," Journal of the Geotechnical Division, ASCE, vol 100,
no. GT8, Aug 1974, pp 871-808.

Ishihara, K., Tatsuoka, F. and Yasuda, S. (1975) "Undrained deformation
and liquefaction of sand under cyclic stresses," Soils and Foundations
(Japan), vol 15, no. 1, Mar 1975.

Kishida, H. (1969) "Characteristics of liquefied sands during Mino-Owari, Tohnankai, and Kikui earthquakes," Soils and Foundations (Japan), vol 9, no. 1, Mar 1969.

Kishida, H. (1970) "Characteristics of liquefaction of level sandy ground during the Tokachioki earthquakes," Soils and Foundations (Japan), vol 10, no. 2, Jun 1970.

Lee, K. L. (1970) Triaxial compressive strength of saturated sands under seismic loading, Ph.D. thesis, University of California. Berkeley, Calif., Jun 1970.

Lee, K. L. and Chan, K. (1972) "Number of equivalent significant cycles in strong motion earthquakes," in Proceedings of the International Conference on Microzonation for Safer Construction Research and Application, 30 Oct — 2 Nov 1972, vol. II. Seattle, Wash., 1972, pp 609-627.

Lee, K. L. and Fitton, J. A. (1969) "Factors affecting the cyclic loading strength of soil," Symposium on Vibration Effects of Earthquakes on Soils and Foundations, Special Technical Publication No. 450, ASTM, pp 71-95.

Lee, K. L. and Seed, H. B. (1967) "Cyclic stress conditions causing liquefaction of sand," Journal of the Soil Mechanics and Foundations Division, ASCE, vol 93, no. SM1, Jan 1967, pp 47-70.

Martin, G., Finn, L. and Seed, H. (1975) "Fundamentals of liquefaction under cyclic loading," Journal of the Geotechnical Division, ASCE, no. GT5, May 1975.

Meehan, R. L. (1976) "Dynamic strength of hydraulic fill," Journal of the Geotechnical Division, ASCE, vol 102, no. GT6, Jun 1976.

Peacock, W. H. and Seed, H. B. (1968) "Sand liquefaction under cyclic loading simple shear conditions," Journal of the Soil Mechanics and Foundations Division, ASCE, vol 94, no. SM3, May 1968.

Pike, R., Chan, C. K. and Seed, H. B. (1974) Settlement and liquefaction of sands under multi-directional shaking, University of California, Earthquake Engineering Research Center, EERC Report No. 74-20. Berkeley, Calif., Feb 1974.

Rocker, K., Jr. (1968) The liquefaction behavior of sands subjected to cyclic loading; Progress Report no. 3, Repeated load and vibration tests upon sand, Massachusetts Institute of Technology, Department of Civil Engineering, Research Report R68-36, Soils Publ. no. 221. Cambridge, Mass., Jun 1968.

Schnabel, P. B., Lysmer, J. and Seed, H. B. (1972) SHAKE: a computer program for earthquake response analysis of horizontally layered sites, University of California, Earthquake Engineering Research Center, EERC Report No. 72-12. Berkeley, Calif., Nov 1972.

Seed, H. B. and Idriss, I. M. (1970) Soil moduli and damping factors for dynamic responses analysis, University of California, Earthquake Engineering Research Center, EERC Report no. 70-10. Berkeley, Calif., Nov 1970.

Seed, H. B. and Lee, K. L. (1966) "Liquefaction of saturated sands during cyclic loading," Journal of the Soil Mechanics and Foundations Division, ASCE, vol 92, no. SM6, Jun 1966.

Seed, H. B. and Lee, K. L. (1969) "Pore-water pressure in earth slopes under seismic loading conditions," in Proceedings of Fourth World Conference on Earthquake Engineering, Association Chilena de Sismologia e Ingenieria Anti-Sismica Impreso en Editorial Universelaria, Santiago, Chile, vol 3, 1969.

Seed, H. B., Martin, P. P. and Lysmer, J. (1975) The generation and dissipation of pore water pressures during soil liquefaction, University of California, College of Engineering, Earthquake Engineering Research Center, EERC Report No. 75-26. Berkeley, Calif., Aug 1975.

Seed, H. B., Mori, K. and Chan, C. K. (1975) Influence of seismic history on liquefaction characteristics of sands, University of California, Earthquake Engineering Research Center, EERC Report No. 75-25. Berkeley, Calif., 1975.

Seed, H. B. and Peacock, W. H. (1971) "Test procedures for measuring soil liquefaction characteristics," Journal of the Soil Mechanics and Foundations Division, ASCE, vol 97, no. SM8, Aug 1971.

Silver, M. L. and Park, T. K. (1975) "Testing procedure effects of dynamic soil behavior," Journal of the Geotechnical Division, ASCE, vol 101, no. GT11, Oct 1975.

Wong, T., Seed, H. B. and Chan, C. (1974) Liquefaction of gravelly soils under cyclic loading conditions, University of California, Earthquake Engineering Research Center, EERC Report No. 74-11. Berkeley, Calif., Nov 1974.

Yen, B. C. (1967) "Viscosity of saturated sand near liquefaction," in Proceedings of International Conference on Wave Propagation and Soil Mechanics, ASCE, University of New Mexico Press. Albuquerque, N.M., Aug 1967.

Yoshimi, Y. and Kuwabara, F. (1973) "Effect of subsurface liquefaction on the strength of surface soils," Soils and Foundations (Japan), vol 13, no. 2, Jun 1973.

Yoshimi, Y. and Oh-Oka, H. (1975) "Influence of degree of shear stress reversal on the liquefaction potential of saturated sand," Soils and Foundations (Japan), vol 15, no. 3, Sep 1975.

Youd, L. T. (1973) Liquefaction flow and associated ground failures, U.S. Geodetic Survey, National Center, Circular 688. Reston, Va., 1973.

Chapter 3

PROCEDURES FOR ANALYSIS OF LIQUEFACTION OF SOILS

GENERAL

Earthquake ground motions are capable of causing a loss of shear strength of loose deposits of sands below the water table. Field and laboratory tests have been performed to evaluate the liquefaction potential of soil deposits. This chapter will present field standard penetration test interpretation, a summary of the void ratio concept, Seed's (1976) simplified hand computation procedure, a simple computer analysis, a more complex computer analysis, finite element analysis techniques, and some interesting research in progress.

STANDARD PENETRATION TEST USED FOR LIQUEFACTION PREDICTION

Standard penetration tests are also discussed in Chapter 4 and can be used directly to give an *in situ* evaluation of soil deposit. Seed (1976) presents Figure 3-1 which is an evaluation of the Niigata, Japan 1964 earthquake. Several lines in an early evaluation divide regions of light damage (no liquefaction) from heavy damage (liquefaction). Such a correlation is applicable only to the Niigata soil and earthquake; however, the methodology may be extended. Castro (1975) has compiled earthquake field observations of liquefaction in terms of an effective shear stress ratio

$$\tau_e / \sigma_v'$$

where τ_e is defined* as

$$\tau_e = 0.7 \times A_{max} \times \sigma_v$$

* This will be discussed in more detail in the section entitled SIMPLE HAND COMPUTATION.

54

and

$$\sigma_v' \quad = \quad \text{effective overburden pressure}$$

$$A_{max} \quad = \quad \text{maximum horizontal acceleration, g's}$$

$$\sigma_v \quad = \quad \text{total overburden pressure}$$

and a corrected blow count N' defined as

$$N' \quad = \quad \frac{50N}{\sigma_v' + 10}$$

where   N = standard penetration resistance measured in
        the field

The relationship is shown in Figure 3-2.

Christian and Swiger (1975) utilized discriminant analysis techniques to analyze the data from 39 earthquakes. They define a parameter A as

$$A \quad = \quad \frac{a\,\sigma_v}{\sigma_v'}$$

where   a = site surface accelerations

The parameter A is a measure of the stress-strength ratio τ/σ_v'. Relative density is determined by use of the Gibbs and Holtz (1957) relation from standard penetration tests (Chapter 4). This value is not used as an absolute but rather as an intermediate correlation. Figure 3-3 shows the results of their analysis. The probability numbers are the confidence indicators that the line shown is the dividing line separating liquefiable from non-liquefiable cases. Thus, a P = 0.10 means that the location of the line is associated with a 90% confidence that all liquefiable cases are above the line. (Note: it is not to be confused with the probability of occurrence of liquefaction.) These curves give estimates of the standard penetration resistance required at a site to preclude liquefaction for a given confidence level.
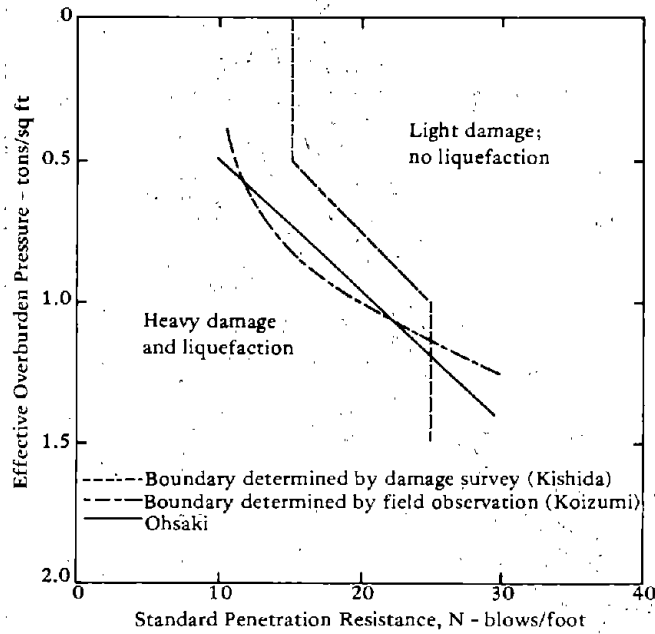
Figure 3-1. Analysis of liquefaction potential at Niigata for earthquake
of June 16, 1964 (from "Liquefaction and Cyclic Mobility of
Saturated Sands," by G. Castro in ASCE Geotechnical
Journal, GT6, Jun 1975).
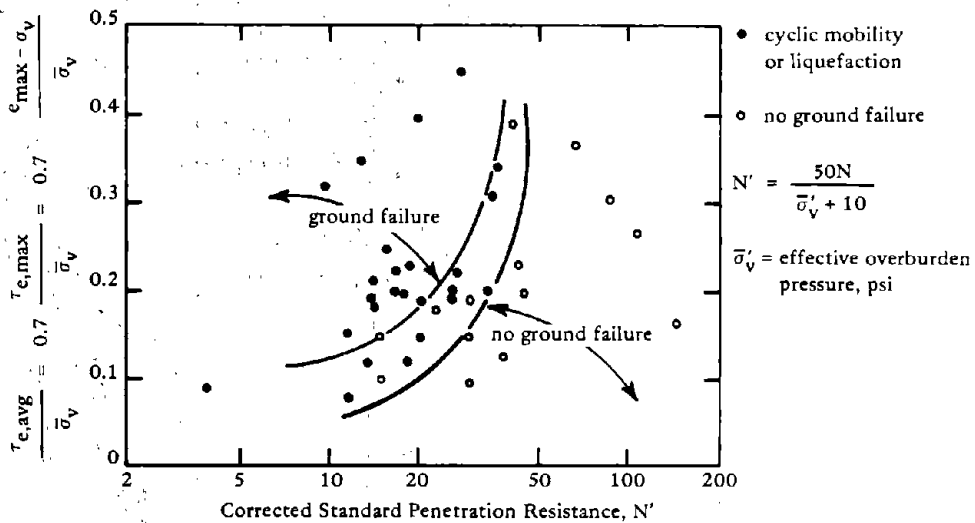
Figure 3-2. Performance of saturated sands at earthquake sites
(from "Liquefaction and Cyclic Mobility of Saturated Sands,"
by G. Castro in Journal of the Geotechnical Division,
ASCE vol. 101, no. GT6, Jun 1975).
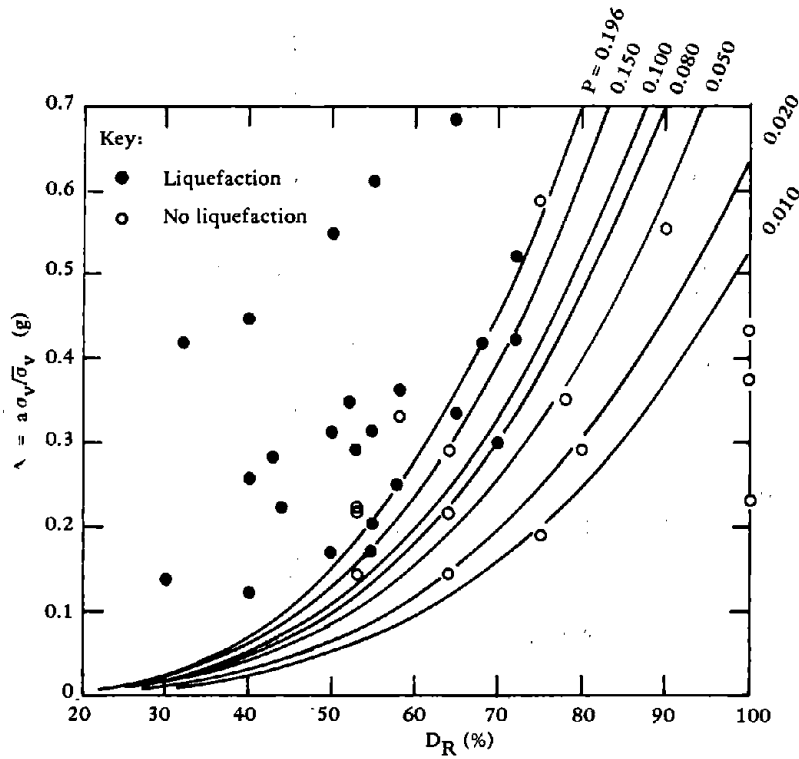
(a) Arithmetic scales.
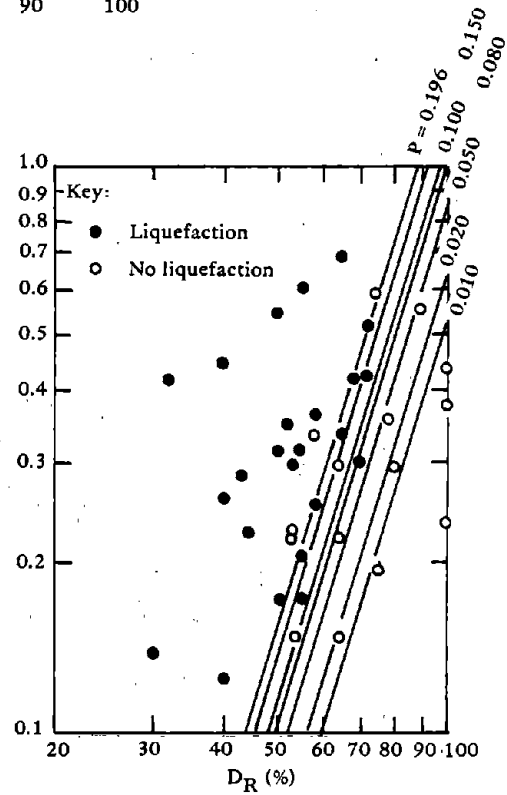
(b) Logarithmic scales.

Figure 3-3. Historical observations of liquefaction and discriminant curves (from "Statistics of Liquefaction and SPT Results," by J. T. Christian and W. F. Swiger in Journal of the Geotechnical Division, ASCE, vol. 101, no. GT11, Nov 1975 and discussion, vol. 102, no. GT12, Dec 1976).

Seed (1976) gives the results of a detailed study on penetration resistance in Figure 3-4. To use the information presented in Figure 3-4, the value of the standard penetration resistance should be corrected to an effective overburden pressure of 1 ton/ft^2 by means of the following expression

$$N_1 = C_N N$$

where C_N is taken from Figure 3-4c and

N_1 = corrected penetration resistance

N = standard penetration resistance as measured at the depth under consideration

σ_o' = effective overburden pressure in ton/ft^2 (where the penetration resistance has the value N)

σ_1' = 1 ton/ft^2

Liquefaction studies in mainland China conducted independently but along similar lines to those developed in this country have also led to a correlation between earthquake shaking conditions causing liquefaction and the standard penetration resistance of sands. In this correlation, the critical value of the standard penetration resistance, N_{crit}, separating liquefiable from nonliquefiable conditions is determined by the following expression

$$N_{crit} = \bar{N}\{1 + 0.125 (d_s - 3) - 0.05 (d_w - 20)\}$$

where d_s = depth to sand layer under consideration in meters

d_w = depth of water table below ground surface in meters

$\bar{N}$ = a function of the shaking intensity as follows:

Modified Mercelli Intensity	$\bar{N}$ (blows/ft)
≈ 7	6
≈ 8	10
≈ 9	16

This correlation was found by Seed (1976) to agree with data in Figure 3-4.

(

58
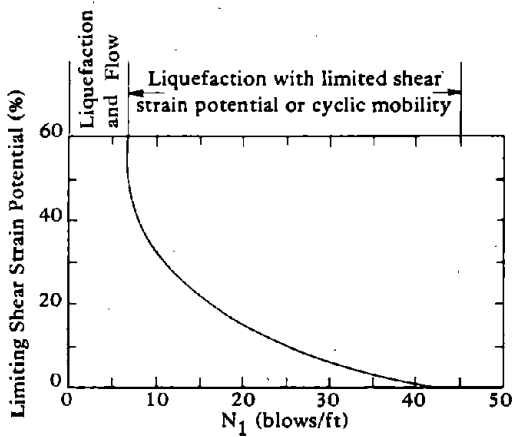
(a) Strain potential.
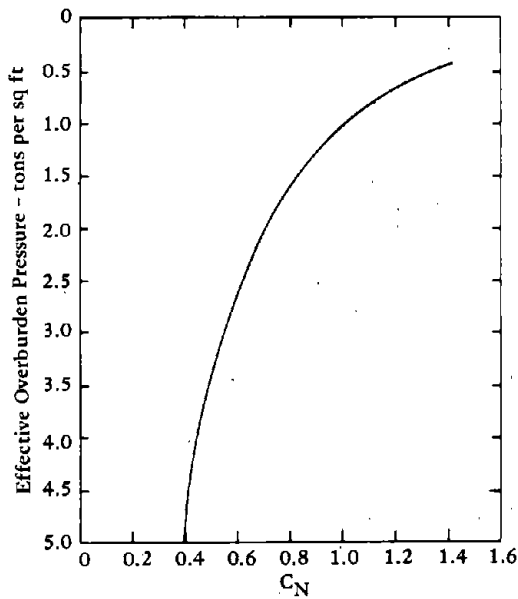
(b) Stress ratio.
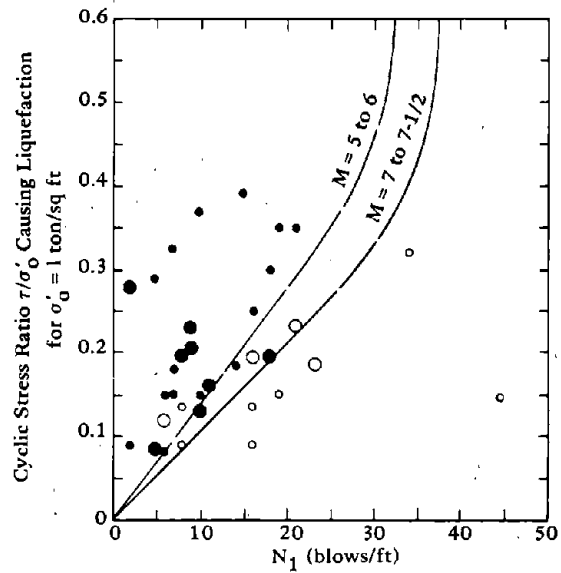
(c) Relationship between C_N and effective overburden pressure.

Figure 3-4. Use of standard penetration for liquefaction evaluation (from "Evaluation of Soil liquefaction Effects on Level Ground During Earthquake," by H. B. Seed, in a paper presented at the ASCE Annual Convention, Philadelphia, 27 Sep-1 Oct 1976).

(a) Stress — axial strain.

(b) Volume change — axial strain.

(c) Volume change — void ratio.

(d) Volume change — confinement.

(e) Volume change — confining stress.
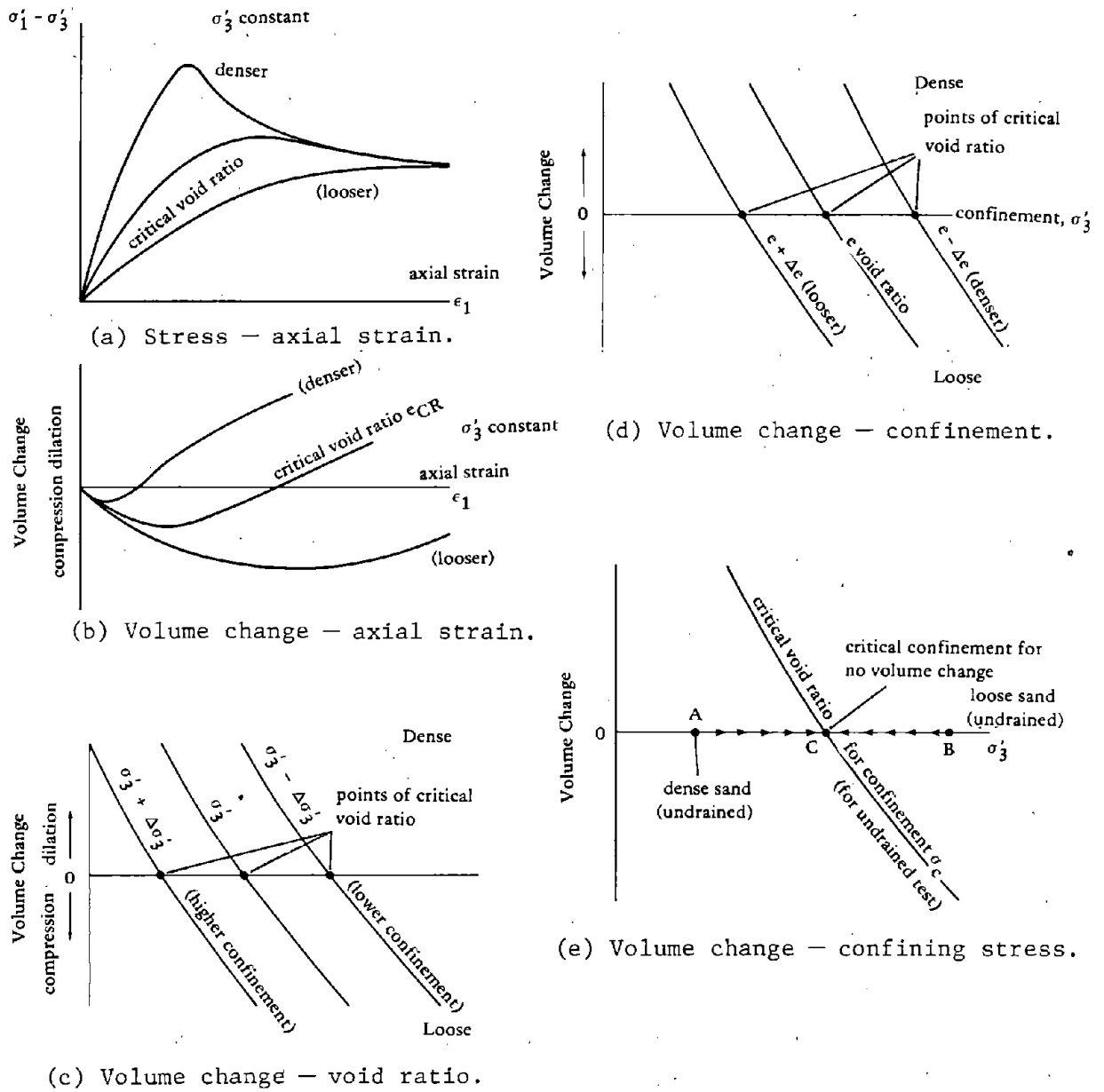
Figure 3-5. Drained
triaxial test data.

The data presented in this section can be used to give an approximate estimate of the liquefaction potential at a site. Clearly the number of observations is limited, making the scatter in the data large. This method is well-suited for preliminary evaluation of alternative sites when detailed tests are not possible.

CRITICAL VOID RATIO CONCEPT

Castro (1975) differentiates between liquefaction (occurring as a result of loss of shear resistance under monotonic loading) and cyclic mobility, which he defines as progressive softening of a saturated sand under cyclic load. Castro (1975) questions the belief that cyclic mobility can occur in dilative sands *in situ* during earthquakes, at least to the same degree as has been observed in the laboratory. He presents data to suggest that the large strains exhibited in laboratory cyclic tests are due to redistribution of void ratios.

In order to better understand this approach, it is of interest to briefly review typical monotonic triaxial test data for cohesionless material. Figure 3-5a and b shows drained triaxial test results for a loose sand, a dense sand, and a sand at critical void ratio. Here, critical void ratio is defined as that value of initial void ratio that corresponds to the void ratio that would be reached at the maximum shear stress level for a specific soil under a particular confining stress level. As can be seen at failure, the net volumetric strain of a specimen at critical void ratio is zero at maximum shear loading. Loose and dense may be determined in relation to this. Figure 3-5c and d shows this more clearly for another series of tests at different initial void ratios and confinements. In Figure 3-5c volume change at maximum shear stress level is plotted versus initial void ratio for three series of triaxial tests under three different confining stresses. Figure 3-5d shows volume change versus confining pressure for three series of tests at different initial void ratios.

Information from the foregoing tests may be applied to undrained triaxial tests to predict their behavior. Since drainage is not allowed, volume change — and, thus, void ratio — is essentially unchanged. Figure 3-5e shows a plot of volume change versus initial confining pressure for drained triaxial tests on sand, similar to Figure 3-5d. Also shown are state paths for both a dense sand (point A) and a loose sand (point B) undergoing shear under undrained conditions.

Since drainage is not permitted, the dense sand trying to dilate reduces pore pressure, thereby increasing effective confinement under monotonic loading. The opposite is noted for the loose soil which increases pore pressure as it tends to try to compress. Figure 3-6

61
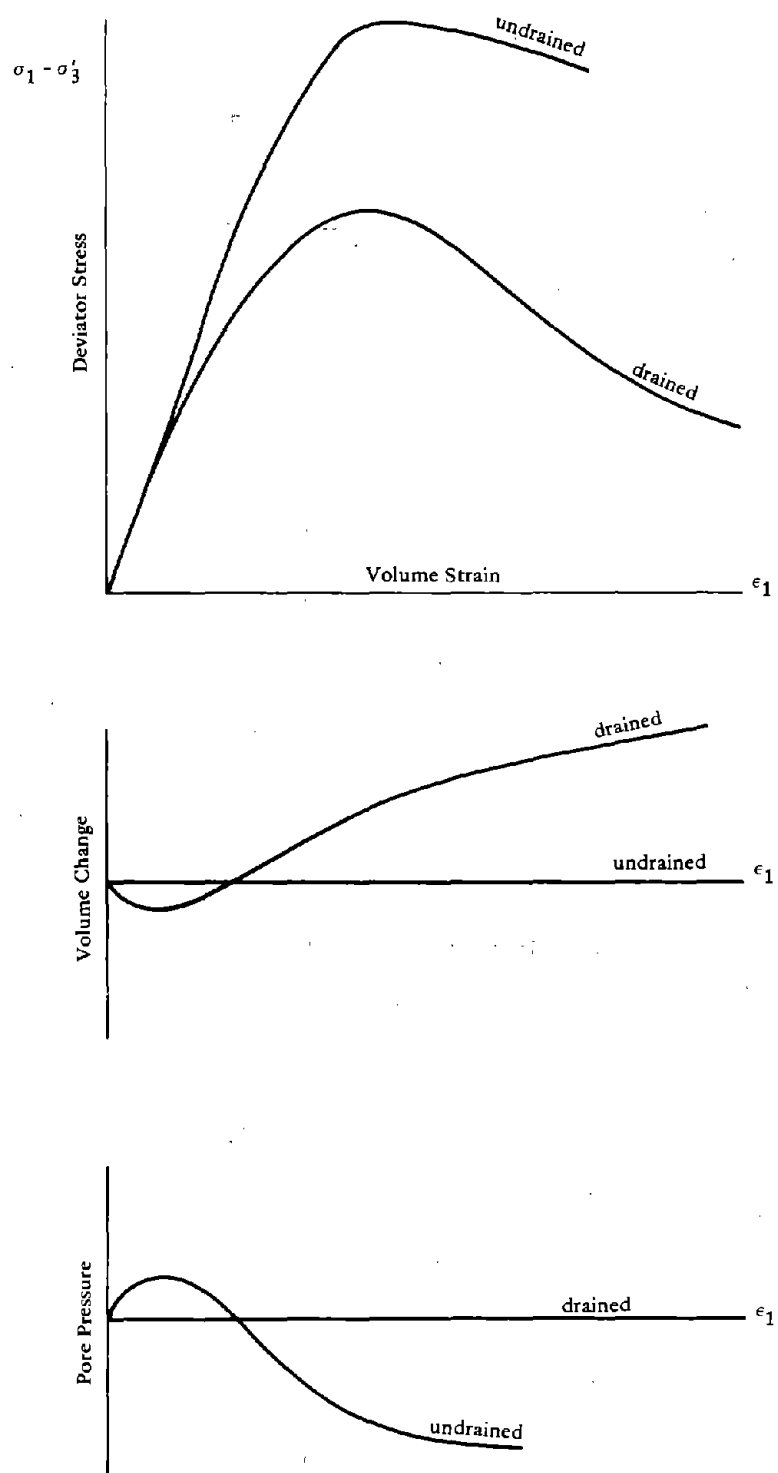
Figure 3-6. Comparison of drained and undrained triaxial test data.

compares drained and undrained triaxial test data for a dense sand. It should be noted that although the dense sand does tend to dilate at failure strains, it initially undergoes compression at lower strain levels. These strain levels, although lower than failure, may be within the strain level noted in some earthquakes. Thus, pore pressure might build up even in dense undrained sands.

Castro (1975) in Figure 3-7 makes use of a state diagram to explain liquefaction under monotonic or cyclic loading. Under loading, a loose soil responds by an increase in pore pressure (reducing confinement) moving from point C toward point A. At point A, unlimited flow occurs at some small residual stress level.
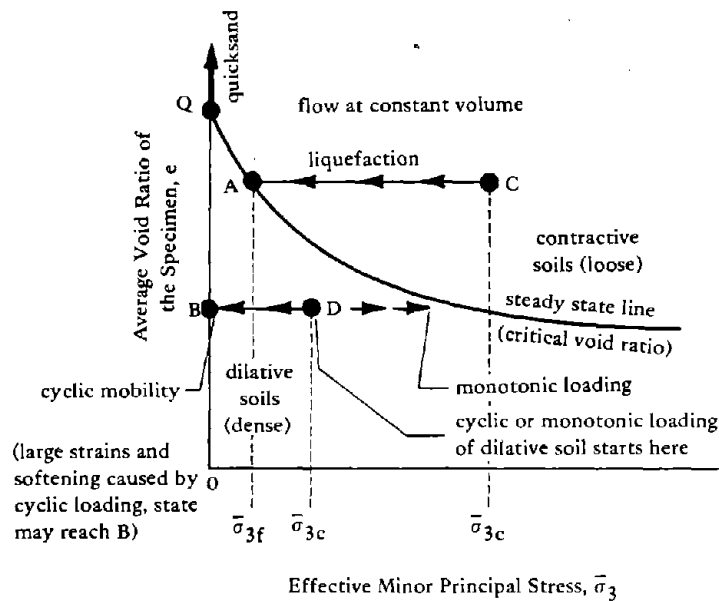
Figure 3-7. Undrained tests on fully saturated sands depicted on state
diagram (from "Liquefaction and Cyclic Mobility of Saturated Sands,"
by G. Castro in ASCE Journal of the Geotechnical Division,
vol. 101, no. GT6, Jun 1975).

In order to have a quicksand condition, defined by Castro (1975) as complete loss of strength, the soil would require a void ratio greater than Q. Dense sands may also respond by increase in pore pressure moving from point D toward point B. Should the cyclic load repetitions be vigorous enough, the sand state reaches point B, where the effective confining stress becomes zero. However, upon shearing, the specimen

commences to deform, thereby dilates, and the state of the sand moves toward point D. With further loading the sand state continues to move to the right until, presumably with high enough loading, it meets the steady-state line and commences to deform at constant shear stress level.

This state diagram is used to define a liquefaction potential

$$L_p = \frac{\overline{\sigma}_{3c} - \overline{\sigma}_{3f}}{\overline{\sigma}_{3f}} \quad \text{(after Casagrande)}$$

where $\overline{\sigma}_{3c}$ = the initial effective minor principal stress

$\overline{\sigma}_{3f}$ = the effective minor principal stress at yielding

Since it is assumed that the friction angle of the sand is fully mobilized at steady-state yielding, the liquefaction potential may be defined by using Mohr-Coulomb theory as:

$$L_p = \frac{\overline{\sigma}_{3c} - \overline{\sigma}_{3f}}{\overline{\sigma}_{3f}} = \frac{\Delta u}{\sigma_{3f}} = \frac{\Delta u}{\sigma_{df} \frac{1 - \sin \phi}{2 \sin \phi}}$$

where Δu = the pore pressure generated in reaching the critical state line

σ_{df} = the deviator stress existing at this state

The pore pressure Δu can be related to deviator stress σ_{df} by means of Skempton's parameter A_f

$$L_p = A_f \times \frac{2 \sin \phi}{1 - \sin \phi}$$

Although Castro (1975) applies this liquefaction potential value qualitatively (i.e., higher L_p's suggest higher liquefaction tendency), no quantitative criteria are given. Further, a sand classified as dense by this approach would have a negative L_p. Although the implication is that this would not liquefy, no specific statements to this effect are made.

64

Castro (1975) also shows state diagrams for various sands which show the steady-state lines to be functions of very subtle changes in particle shape, size, and gradation. In some cases these latter parameters are noted to exert an influence on the liquefaction potential as great, for example, as that of relative density.

The foregoing work also states that soils with initial static shear loading may exhibit greater resistance to cyclic mobility. This is explained in terms of the reduced load reversals resulting in reduced void ratio redistribution on laboratory samples.

Castro (1975) points out that tests on undisturbed samples are more realistic than tests on remolded samples; he feels the use of average density specimens to represent stratified sands may introduce large errors. Relative density is not applicable to these types of deposits, and there is no equivalent basis for comparing unit weights of remolded sand with that of the *in situ* sand.

SIMPLE HAND COMPUTATION

Seed and Idriss (1970a) have proposed a simplified hand computation procedure for evaluating liquefaction. They assume that the liquefaction producing shear stresses developed in a soil deposit are caused by upward propagating shear waves. The depth to the soil region under liquefaction investigation is defined as h. The soil column within a depth h is assumed to behave as shown in Figure 3-8. The maximum shear stress at a depth h is related to the ground acceleration by equilibrium

$$\tau_{max} = \frac{\gamma h}{g} (A_{max}) \, r_d$$

where γ = total unit weight of soil

   h = depth to region where liquefaction is expected

   A_{max} = maximum surface acceleration

   r_d = acceleration correction factor
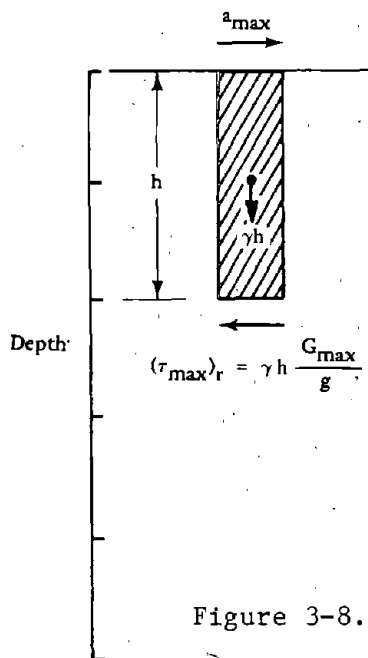
Figure 3-8. Approximate equilibrium representation.

The factor r_d is used to reduce the surface acceleration for depth since the soil is a deformable body rather than a rigid one. Figure 3-9 gives a range of values for r_d with depth. The actual time history of motion will have an irregular form (Figure 3-10), and an equivalent average stress is taken as 65% of the maximum which corresponds to an equivalent number of uniform cycles. Thus, the average stress τ_{av} is

$$\tau_{av} = 0.65 \left(\frac{\gamma h}{g}\right) A_{max} \, r_d$$

Evaluation of earthquake data has provided information on the equivalent number of significant stress cycles that can be expected as a function of earthquake magnitude, which will be presented later in this chapter.

Having the number of cycles, the average applied shear stress and the effective confining stress (σ_v', vertical stress), a simple procedure can be used to determine the liquefaction factor of safety. The number of cycles causing liquefaction can be determined by a laboratory test program using cyclic loading triaxial compression tests. Correction factors have been developed by DeAlba, Chan, and Seed (1975) (Figure 3-11a) to relate triaxial tests to (free-field) field observation.

66
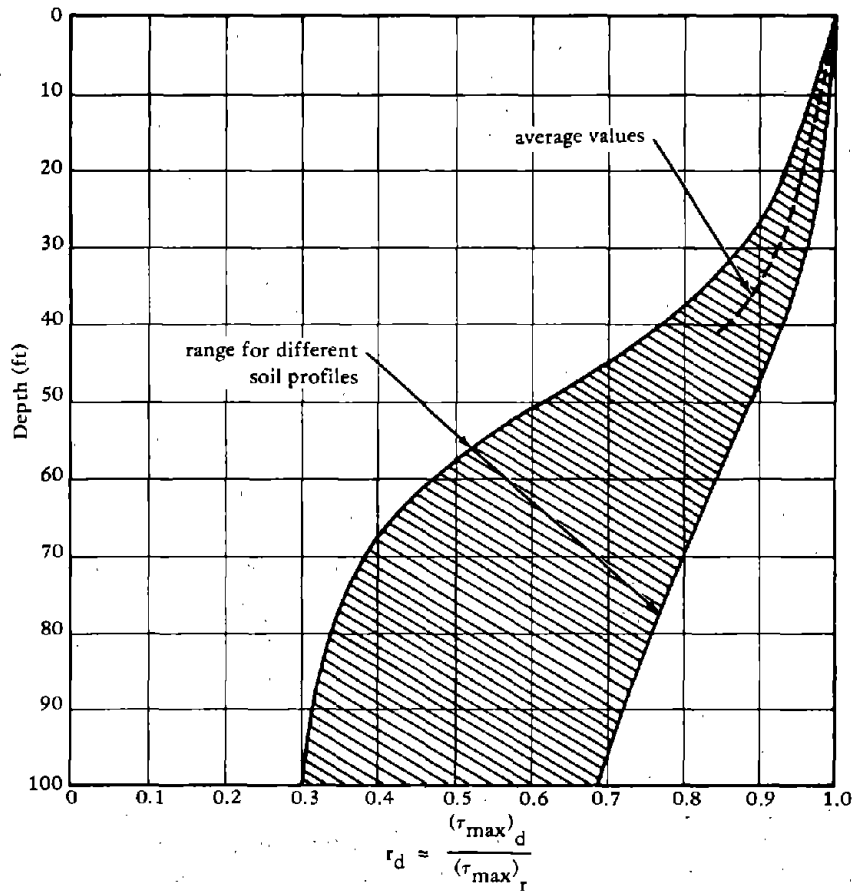
Figure 3-9. Range of value of r_d for different soil profiles.
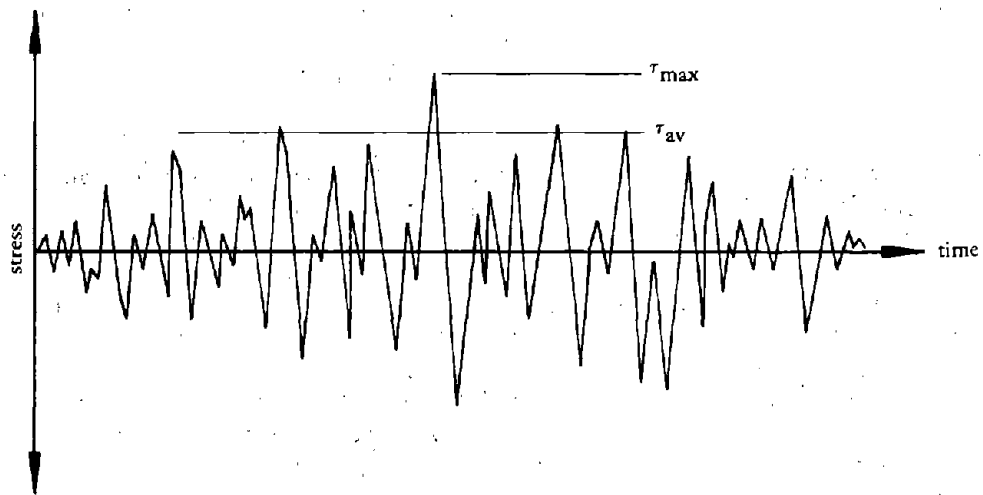
Figure 3-10. Time history of shear stresses during earthquake.

67
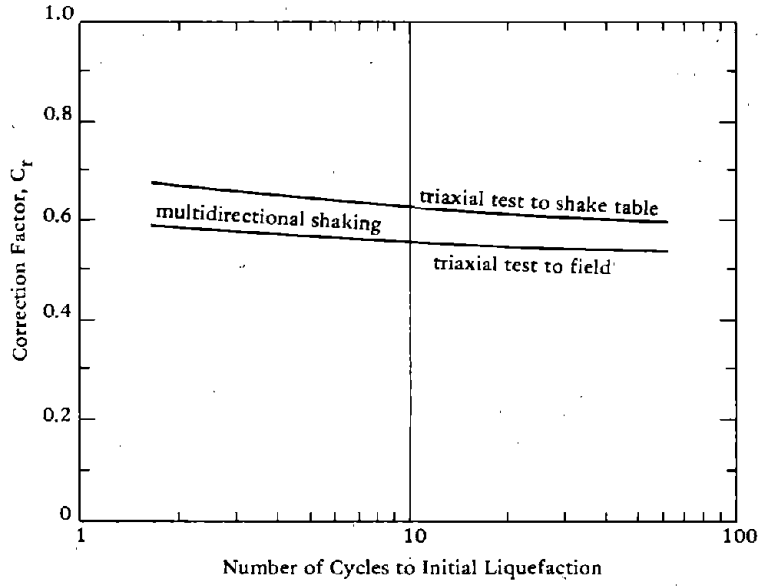
(a) $K_O = 4$.
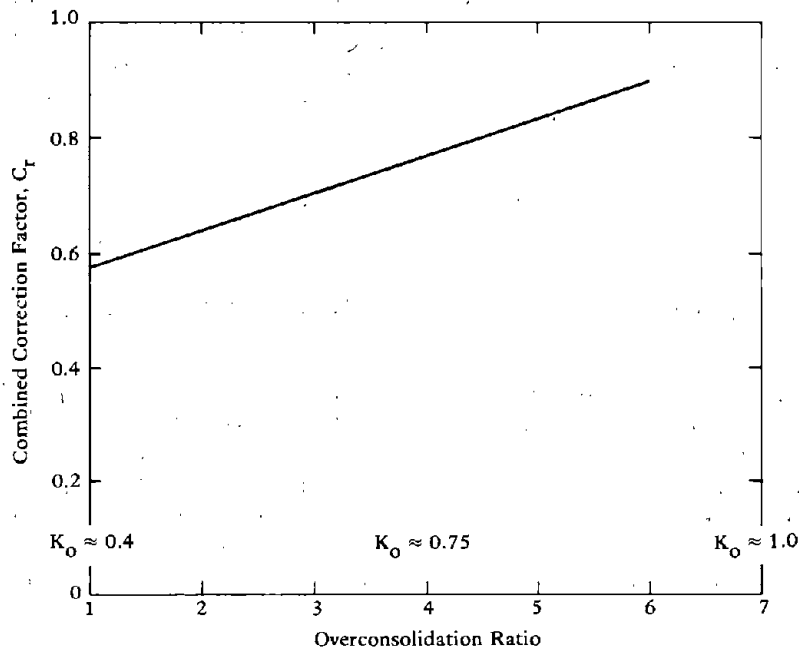
(b) Combined correction factor for cyclic triaxial compression
tests accounting for multidirectional shaking
and overconsolidation.

Figure 3-11. Correction factors for triaxial test results
(from P. DeAlba, C. K. Chan, and H. B. Seed, 1975).

68

Additional correction factors for multidirectional shaking (Pyke, Chan and Seed, 1974) and soil *in situ* overconsolidation (Mulilis, Chan, and Seed, 1975) are also given (Figure 3-11a and b). Laboratory tests on undisturbed samples should be performed to determine the number of uniform cycles of shear causing liquefaction as a function of τ_{av}/σ_v. The factor of safety is defined as the ratio of resisting shear stress capacity (determined from corrected triaxial test) to applied shear stress (τ_{av} calculated above) for the number of equivalent uniform earthquake cycles expected.

Figure 3-12 is a summary of triaxial test data compiled by Donovan (1974). The data is normalized in terms of stress ratio divided by relative density and is limited to D_r less than 75%. The value of σ_3 is used as the effective confining stress. The mean value of the data in Figure 3-12 appears to be a fairly good representation for uniform sands and could be used when undisturbed samples are not available for testing. Since this curve represents triaxial test results, the stress ratio must be corrected for application to the field.

There are 34 cases of observed liquefaction where data of ground motion and site profile were estimated (Seed and Peacock, 1970). This data was used to plot the points shown in Figure 3-13 correcting field data to triaxial conditions. As can be seen there are no cases in which liquefaction was observed which extend below the mean minus one standard deviation and no cases in which liquefaction was not observed which extend above the mean plus one standard deviation. Thus additional validity is provided for Figure 3-12.

APPLICATION OF SIMPLE HAND COMPUTATION IN DEVELOPING CHARTS

To evaluate the liquefaction potential of a deposit it is necessary to determine whether the shear stress induced at any depth by the earthquake τ_{av} is large enough to cause liquefaction at that depth as indicated by corrected data from Figure 3-12 or by laboratory tests. For deposits in which the water table is at a depth of 0 to 10 feet, the critical depth will often be about 20 feet. Thus, the evaluation can often be made simply for a representative element at one of these depths.

Consider for example, a deposit of sand for which the water table is 5 feet below the ground surface and which is subjected to 10 cycles of ground shaking. The average shear stress induced will be:

$$\tau_{av} = 0.65 \left(\frac{\sigma_v}{g} \right) (A_{max}) \, r_d$$

69
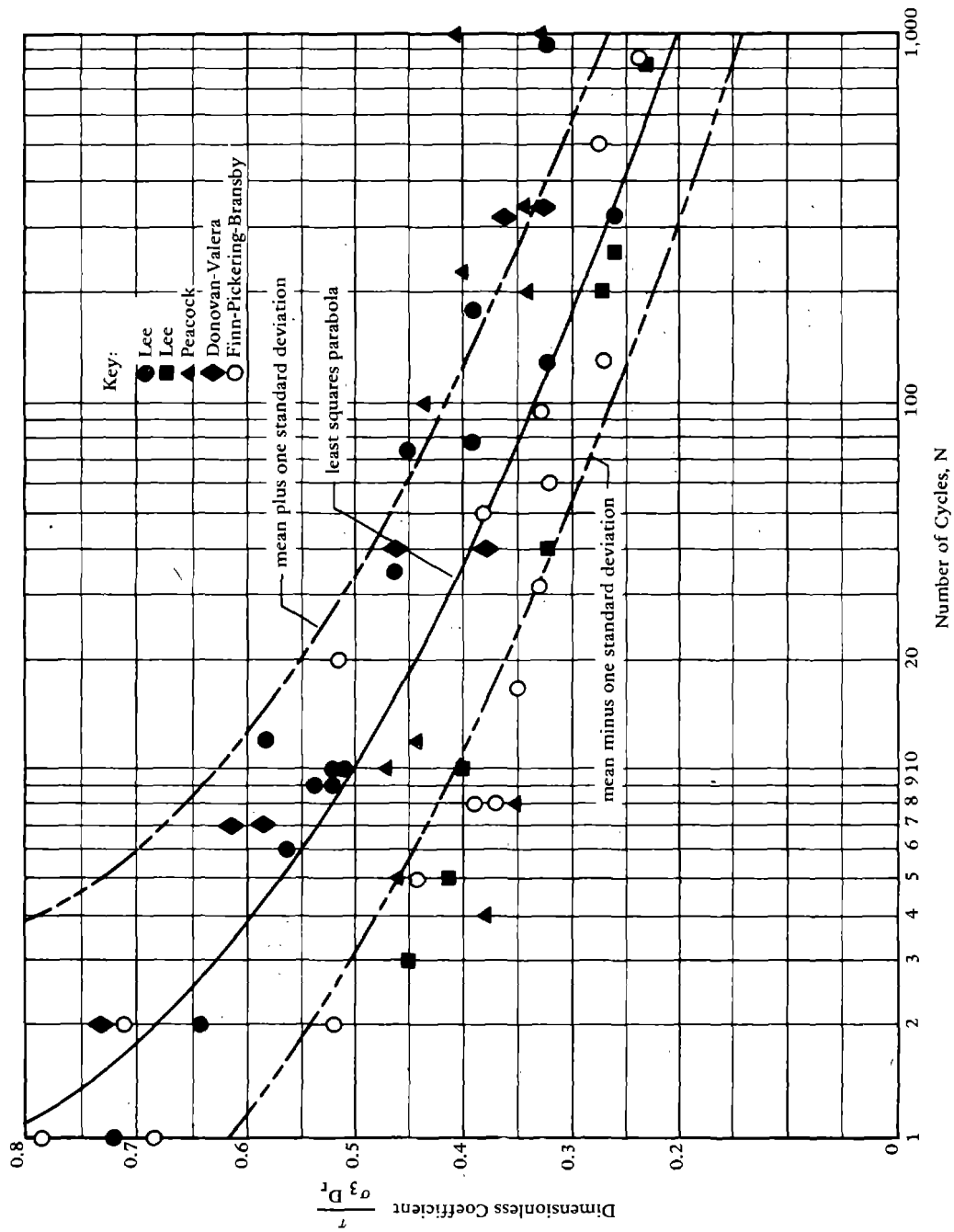
Figure 3-12. Soil strength for initial liquefaction (triaxial test data) (from Donovan, 1974).

70
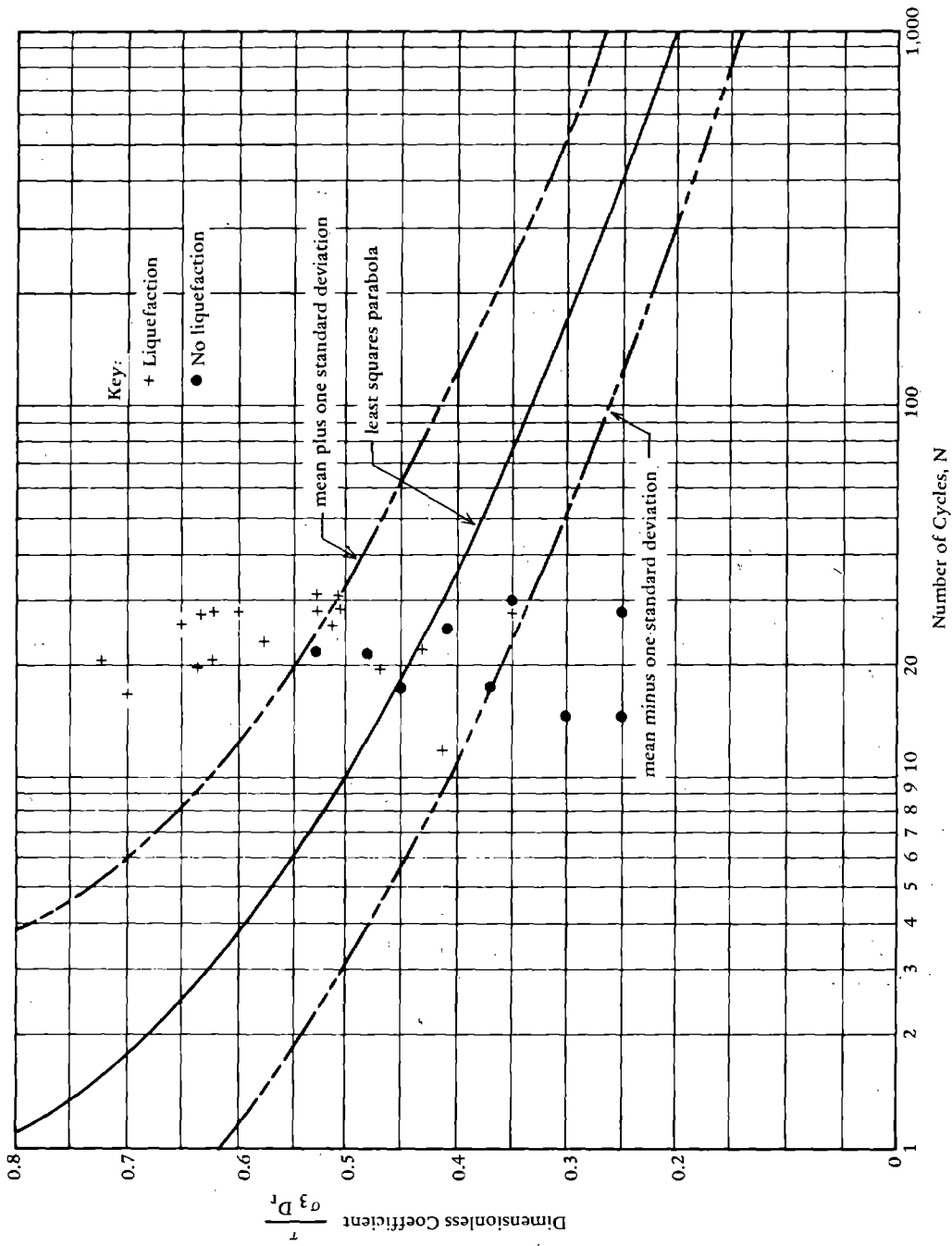
Figure 3-13. Field observations corrected to triaxial conditions (from Donovan, 1974).

71

At a depth of 20 feet, $r_d = 0.95$ (see Figure 3-9) giving

$$\tau_{av} = 0.65 \times 0.95 \times \frac{\sigma_v}{g} A_{max}$$

From Figure 3-12 the shear stress required to cause initial liquefaction for 10 cycles is

$$\tau/(\sigma_3' D_r) = 0.5$$

and

$$\tau_{av}/\sigma_v' = \frac{\tau C_r}{\sigma_3'}$$

Thus,

$$\tau_{av} = 0.5 \, \sigma_v' \, C_r \, D_r$$

where D_r is expressed as a decimal value and C_r is obtained from Figure 3-11.

Equating the applied τ_{av} with τ_{av} to give initial liquefaction gives

$$0.65 \times 0.95 \left(\frac{\sigma_v}{g}\right) A_{max} = 0.5 \, \sigma_v' \, C_r \, D_r$$

$$\frac{A_{max}}{g} = 0.81 \frac{\sigma_v'}{\sigma_v} C_r \, D_r$$

where $\sigma_v = \gamma h$

Assume a total saturated density of 132 lb/cu ft, a total density above the water table of 117 lb/cu ft, and a buoyant density of 69 lb/cu ft. This reduces to

$$\frac{A_{max}}{g} = 0.81 \times \frac{1620}{2565} \times C_r \, D_r$$

$$\frac{A_{max}}{g} = 0.512 \, C_r \, D_r$$

For 10 cycles, $C_r = 0.57$

$$\frac{A_{max}}{g} = 0.29 \, D_r$$

Thus, the following can be determined:

D_r	A_{max}/g*
0.40	0.116
0.50	0.145
0.60	0.174
0.70	0.203

The above values give the acceleration required to cause initial lique-faction at a depth of 20 feet with the water table at 5 feet, subject to 10 cycles of ground shaking.

Observed cases of liquefaction from Seed and Peacock (1970) are summarized in Figure 3-14 from which the following may be stated:

---

* Causing liquefaction in 10 cycles.

73
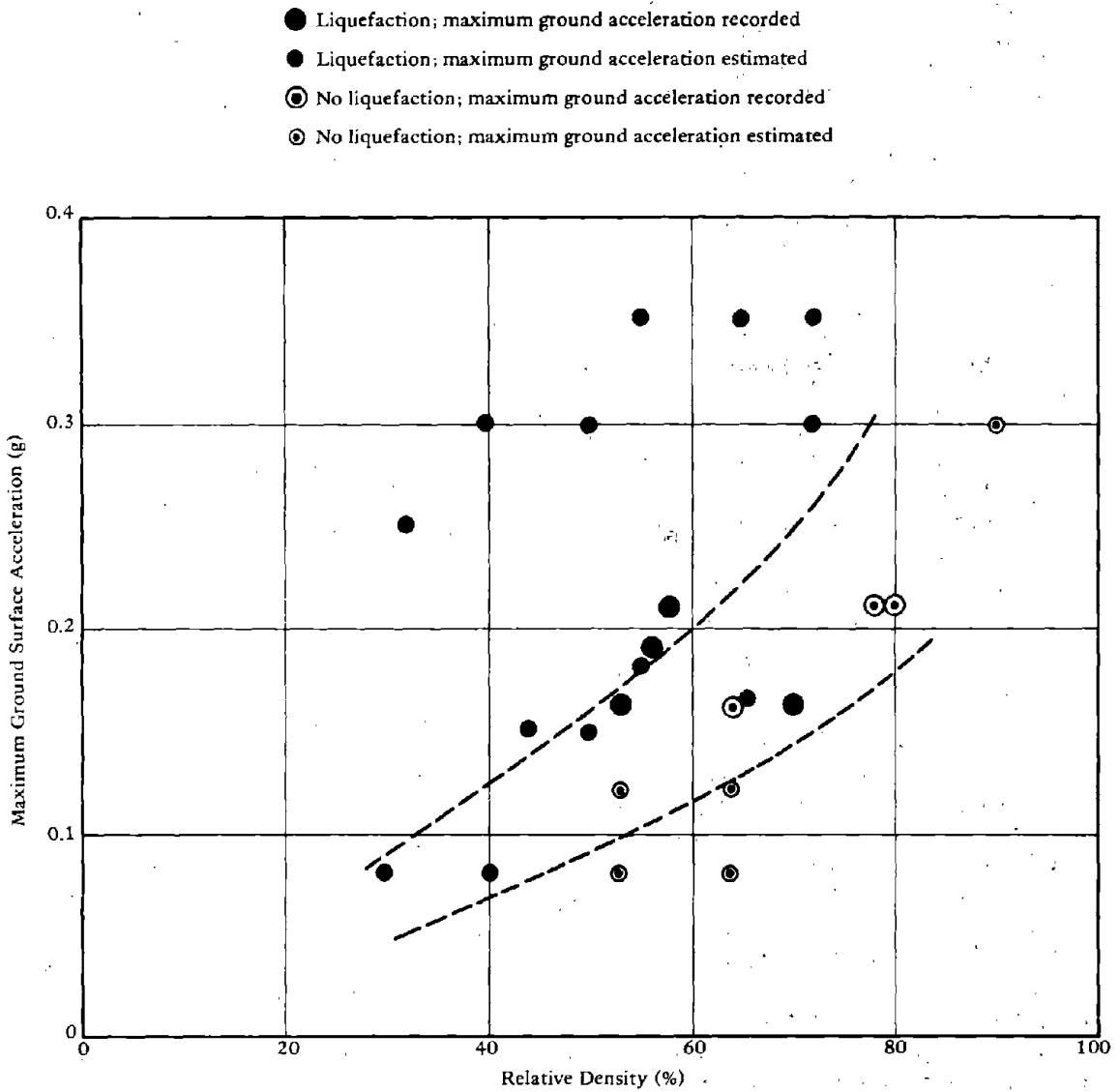
Figure 3-14. Evaluation of liquefaction potential for sands (water table
5 feet below ground surface) ("Evaluation of Soil Liquefaction Effects
on Level Ground During Earthquakes," by H. B. Seed, in ASCE Preprint
2752 of Liquefaction Problems in Geotechnical Engineering, ASCE
Annual Convention, Philadelphia, Pa., 27 Sep-1 Oct 1976).

Maximum Ground Surface Acceleration	Liquefaction Very Likely	Liquefaction Potential Depends on Soil Type and Earthquake Magnitude	Liquefaction Very Unlikely
0.10 g	$D_r < 33$	$33 < D_r < 54$	$D_r > 54$
0.15 g	$D_r < 48$	$48 < D_r < 73$	$D_r > 73$
0.20 g	$D_r < 60$	$60 < D_r < 85$	$D_r > 85$
0.25 g	$D_r < 70$	$70 < D_r < 92$	$D_r > 92$

The data from Seed and Peacock may also be plotted to give Figure 3-15.

The values of relative density may be converted to values of standard penetration as a function of depth (see Chapter 4). Charts have been prepared by Seed and Idriss (1970a) giving the range of penetration resistance values in which liquefaction might be expected, Figures 3-16a and b.

SIMPLE COMPUTER ANALYSIS

Donovan (1974) has developed a computer program based in part on the simple soil model described in the previous section. The earthquake record is represented in terms of the peak acceleration, duration, and predominant frequency. The number of cycles at various acceleration levels is determined by a Rayleigh distribution. Miner's Linear Damage criteria are used to convert the different stress levels to an average stress for computation of a factor of safety. Donovan (1974) has compiled various triaxial test data, Figure 3-12. This data is used in the program as a measure of the soil shear strength. The input to the program requires a soil profile, limited knowledge of soil material and limited knowledge of the earthquake. The input to the program is simple and straightforward, consisting of the following:

1. Relative density of the soil layer of interest

2. Depth to center of the layer

3. Correction factor for triaxial test data (Figure 3-11)

4. Pressure produced by total weight of material above center of layer

5. Effective stress at center of layer
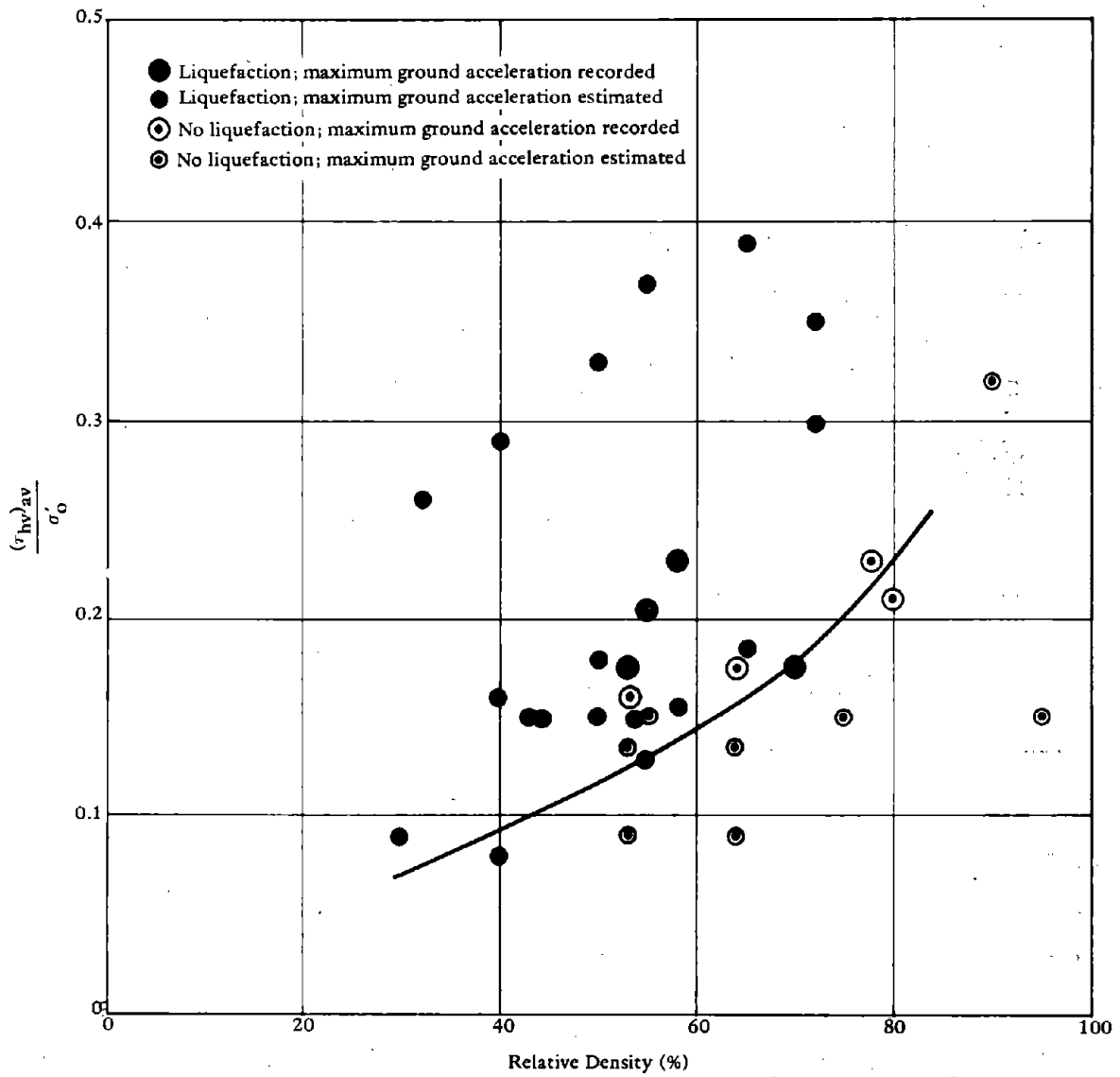
Figure 3-15. Relationship between $(\tau_{hv})_{av}/\sigma_0'$ and relative density for known cases of liquefaction and nonliquefaction (from Report No. EERC 70-8 by H. B. Seed and W. H. Peacock, Nov 1970).
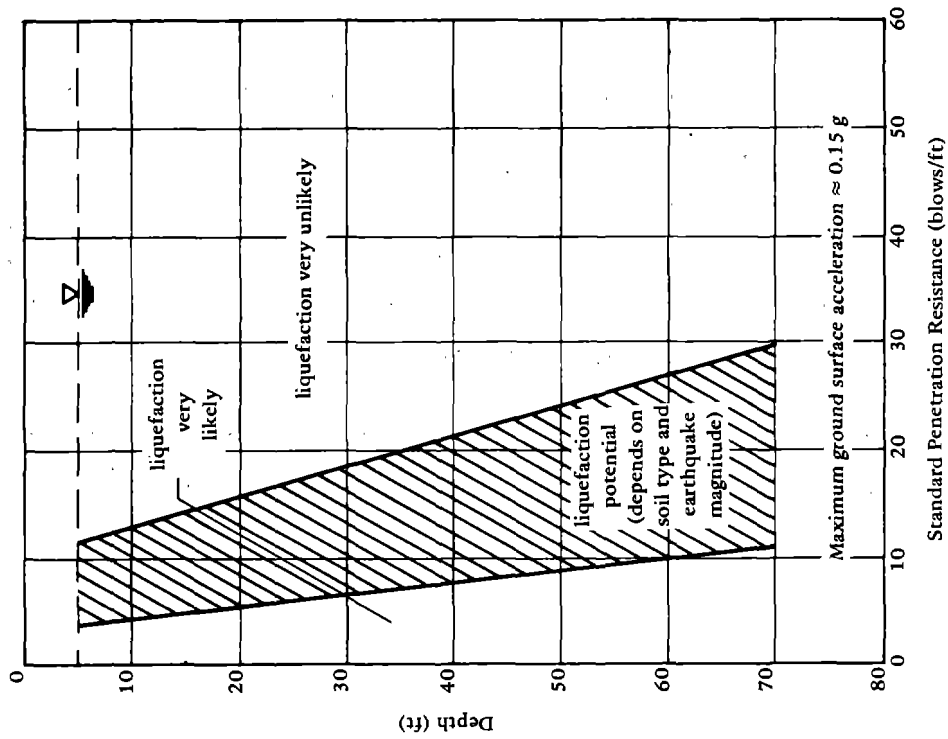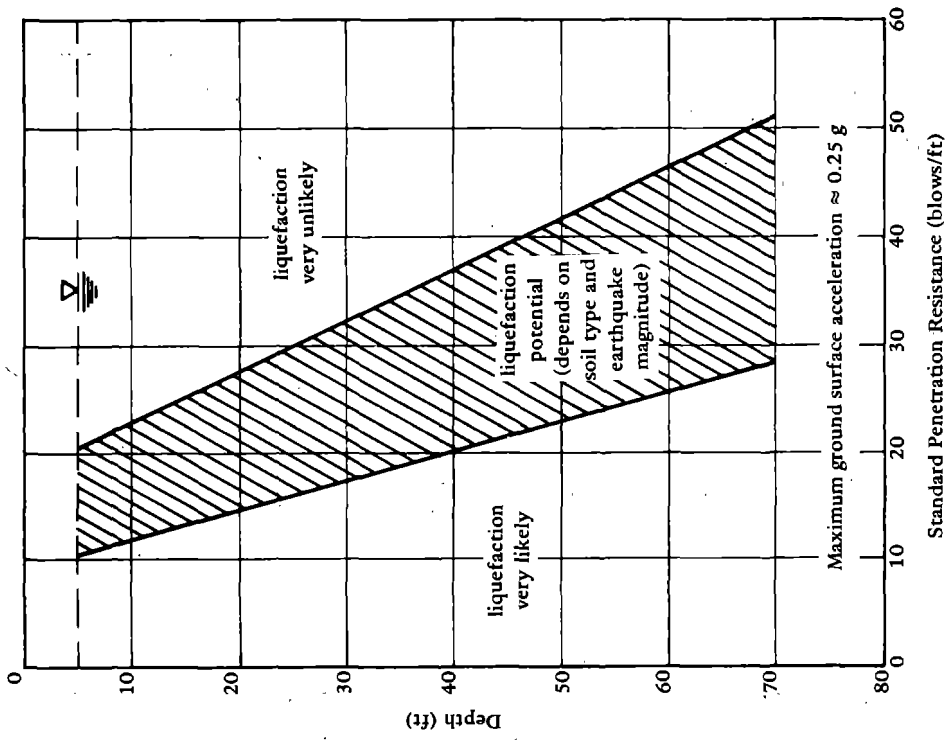
Figure 3-16. Liquefaction potential evaluation charts for sands (from Report No. EERC 70-8 by H. B. Seed and W. H. Peacock, Nov 1970).

(a) Water table at a depth of about 5 feet.
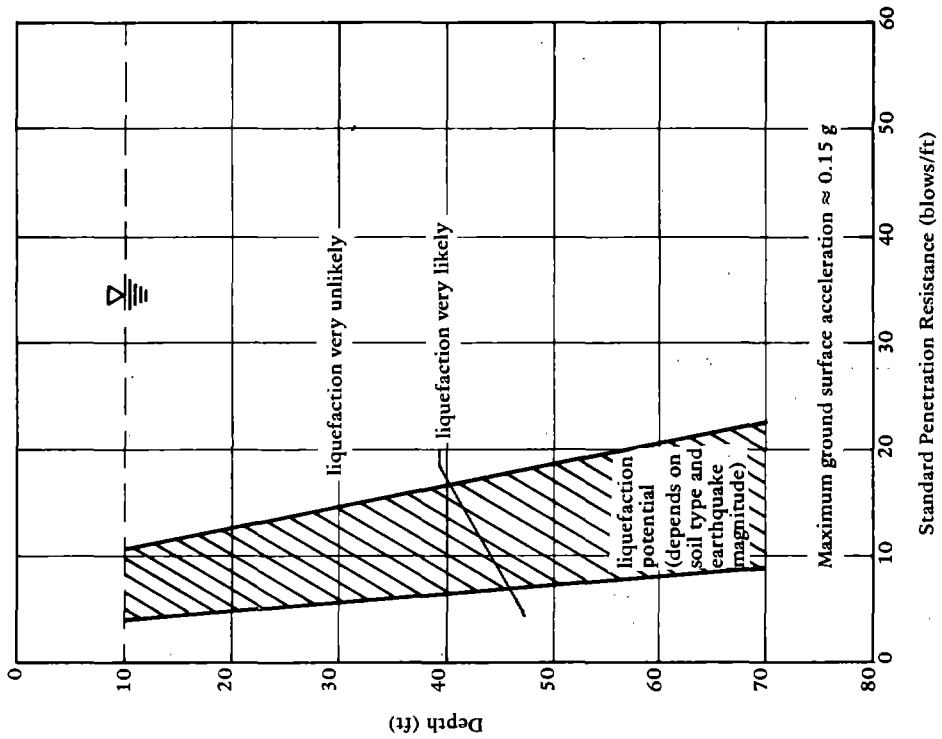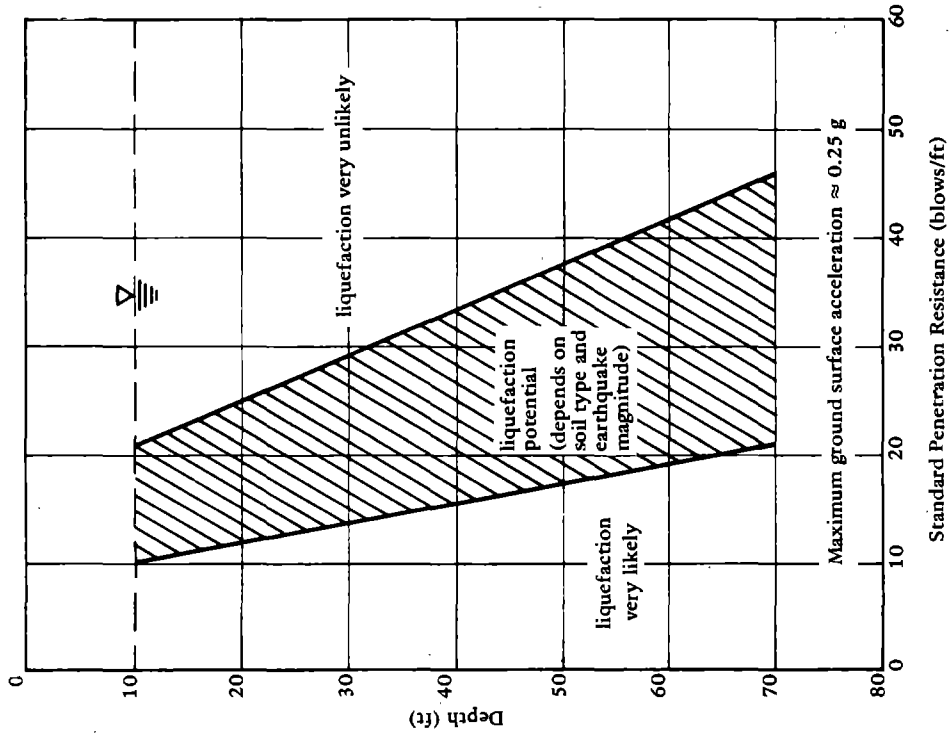
(b) Water table at a depth of about 10 feet.

Figure 3-16. Continued.

78

6. Factor relating peak stress to root-mean-square value (3.5 to 4.5 is used) (see Donovan, 1974)

7. Reduction of stress for depth (usually 0.9 to 1.0)

8. Maximum surface acceleration

9. Duration of earthquake

10. Fundamental period of soil deposit

11. Data pairs defining the τ_{av}/σ_v' ratio versus the number of cycles (Figure 3-12)

The fundamental period of a soil deposit given as item 10 above is equal to the fundamental period of the soil overlying rock-like formations when subject to vertically propagating shear waves. For this usage, a rock-like formation is defined to be any material in which the shear wave velocity at small strains is about 2,500 ft/s or greater. The limit to depth is taken to be 500 feet. Based on this, the natural period will vary from less than 1.0 second to 2.5 seconds. The value 0.5 second is usually used as a minimum natural period. Firm sites, where only dense granular soils overlie bedrock and the depth to bedrock is less than 30 feet or where very dense cemented granular soils overlie bedrock and the depth of bedrock is 70 feet or less, may be considered to have a natural period of 0.5 second. For soils where the shear wave velocity of the soil does not decrease markedly with depth, the characteristic site period may be computed by:

$$T = \frac{4\ H}{R\ V_s}$$

where   H = the depth of soil overlying bedrock

   V_s = average shear wave velocity of soil as measured in the field

   R = correction factor to V_s for higher strain levels as follows:

R	Earthquake Magnitude	Peak Acceleration
0.9	6	0.1 g
0.8	6	0.2 g
0.67	7	0.3 g
0.67	7	0.4 g

79

The program computes the number of cycles by dividing the duration of the earthquake by the period of the soil deposit.

An example problem is given in Figure 3-17.

COMPLEX COMPUTER ANALYSIS, ONE-DIMENSIONAL MODELS

A soil profile may be analyzed as a one-dimensional shear wave problem assuming the stress wave to be only a vertically propagating shear wave. The differential equations of motion can be solved in closed form for linear elastic soil properties. This has been done by Seed and Idriss (1969) and Kanai (1961) to provide a one-dimensional analysis of sites of simple geometry. However, the stress-strain characteristics of a site are highly nonlinear, hysteretic, and strain-dependent as shown in Chapter 2.

Streeter, et al. (1974) developed a computer program using the method of characteristics for calculating one-dimensional dynamic behavior of soils. A soil profile is divided into layers down to bedrock. Dynamic excitation of the soil is introduced at the rock-soil interface. The response of the soil can be evaluated on the basis of elastic, viscoelastic, or nonlinear (Ramberg-Osgood) soil behavior. The program determines shear, velocity, and displacement information.

An analytical technique for analyzing the response of horizontal soil profiles to earthquake motion is described by Seed and Idriss (1969, 1970b) and Idriss and Seed (1968, 1970). The soil profile is idealized by a series of discrete masses and springs with linear viscous dampers. The nonlinear and hysteretic stress-strain characteristics of the soil are introduced by using an equivalent shear modulus and an equivalent viscous damping factor which can vary with each layer of soil profile and with the strain level within the layer. The equivalent shear modulus for a given strain level is taken as the slope of the diagonal line (average slope) drawn through the hysteresis loop, which is shown in Figure 3-18 for a cyclically loaded laboratory specimen. The average equivalent viscous damping coefficient is proportional to the ratio of area of the hysteretic loop, as shown in the figure, to the maximum stored energy during the cycle.

An iterative procedure is used to obtain strain compatible values of shear modulus and damping. The response of the soil profile modeled as discrete masses is computed, and strains are determined.

```
EXAMPLE DATA SET FOR LIQUEFACTION BY STOCHASTIC PROCEDURES:  NCD  6-74
EL CENTRO EARTHQUAKE OF 1940.  LIQUEFACTION IN BRAWLEY, CALIF. (M=7.0)

LIQUEFACTION EVALUATION BY DONOVAN≠S STOCHASTIC PROCESS FOR LAYER
NUMBER 1 AT DEPTH OF 15.0 FEET,    NARROW BANDWIDTH USING ASSUMED
RAYLEIGH DISTRIBUTION

LIQUEFACTION POTENTIAL ESTIMATION BASED ON INTERPOLATION OF A
SERIES OF POINTS ON A (TAU/SIGMA) VS LOG10(NUMBER OF CYCLES)
RELATIONSHIP.  DATA FOR A RELATIVE DENSITY OF  55 PERCENT

          TAU/SIGMA  NUMBER OF CYCLES

   1        .421         1.00
   2        .359         3.00
   3        .332         5.00
   4        .297        10.00
   5        .265        20.00
   6        .225        50.00
   7        .198       100.00
   8        .173       200.00

   AVERAGE MAXIMUM SHEAR STRESS      =     180.0 PSF
   PEAK VALUE SIGMA LEVEL            =       4.0
   SIMPLE SHEAR CORRECTION FACTOR    =        .59
   DEPTH EFFECT REDUCTION FACTOR     =      1.00
   PEAK SURFACE ACCELERATION         =       .100 G
   EFFECTIVE NORMAL STRESS           =    1800.0 PSF
   FUNDAMENTAL PERIOD                =        .50 SECONDS
   DURATION OF STRONG SHAKING        =      30.0 SECONDS
   MOST PROBABLE NUMBER OF CYCLES    =      60
   RELATIVE DENSITY                  =      55.000

     ALL STRESS VALUES REPRESENT THE  4.00 TIMES SIGMA LEVEL

       LIQUEFACTION WILL NOT OCCUR AT A RELATIVE DENSITY OF 55.000


   ITERATION NUMBER       =  1
   PEAK SHEARING STRESS   =  180.00 PSF

        STRESS      CUMULATIVE
          PSF         DAMAGE

        180.00    15.154E-03


   ITERATION NUMBER       = 17
   PEAK SHEARING STRESS   =  487.69 PSF
   FACTOR OF SAFETY       =   2.709

        STRESS      CUMULATIVE
          PSF         DAMAGE

        487.69    99.977E-02
```

Figure 3-17. Example problem using simple computer program.

$$(\lambda_{eqh})_{\gamma_1} = \frac{\text{Area of hysteresis loop}}{4\pi \times \text{Area OAB}} \qquad (\lambda_{eqh})_{\gamma_2} = \frac{\text{Area of hysteresis loop}}{4\pi \times \text{Area OCD}}$$
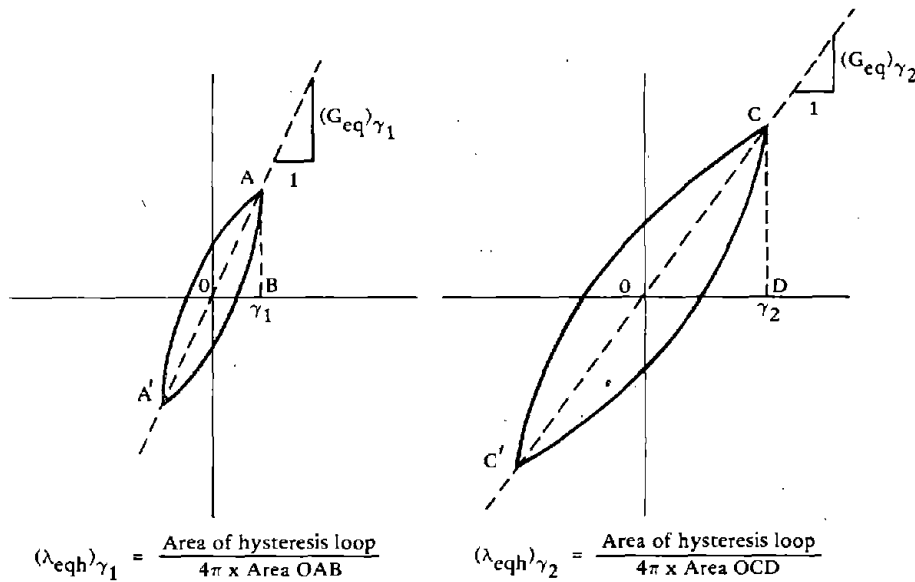
Figure 3-18. Equivalent linear shear moduli and damping used in discrete mass model (from H. B. Seed and I. M. Idriss, Jan 1969).

Another automated-analysis technique, more widely used today for treating horizontal soil layers, has been developed by Schnabel, Lysmer, and Seed (1972), based on the one-dimensional wave propagation method. This program, SHAKE, can compute the responses for a given horizontal earthquake acceleration specified anywhere in the system. The analysis incorporates nonlinear soil behavior, the effect of the elasticity of the base rock, and variable damping. It computes the responses in a system of homogeneous viscoelastic layers of infinite horizontal extent, subject to vertically traveling shear waves. The program is based on the continuous solution of the wave-equation adapted for use with transient motions through the Fast Fourier Transform algorithm. Equivalent linear soil properties are obtained by an iterative procedure for values of modulus and damping compatible with the effective strains in each layer. The following assumptions are made:

1. The soil layers extend infinitely in the horizontal direction.

2. The layers are completely defined by shear modulus, critical-damping ratio, density and thickness.

3. The soil values are independent of frequency.

4. Only vertically propagating, horizontal shear waves are considered.

The soil model is similar to that developed by Seed and Idriss (1970c), using data based on Hardin and Drnevich (1970) as discussed earlier (Chapter 2). The absolute range of soil parameter variation may be stipulated by merely in-putting factors whose numerical values may be derived from simple soil strength properties. These strength properties may be the undrained shear strength of a clay or the relative density for sands as shown in Chapter 2. The program requires the definition of the soil profile down to bedrock (assumed as seismic velocity 2,500 ft/s) as well as an earthquake time history record in digital form.

The motion used as a basis for the analysis can be given in any layer in the system, and new motions can be computed in any other layer. Maximum stresses and strains, as well as time histories, may be obtained in the middle of each layer. Response spectra may be obtained and amplification spectra determined.

For liquefaction analysis of a soil profile the stress history of the various layers is compared to their susceptibility to liquefaction.

The calculated shear stress history is used to determine a number of equivalent cycles of load at an average stress level from which τ_{av}/σ_v' is determined. The liquefaction susceptibility may be measured directly by cyclic loading test or estimated on the basis of Figure 3-12.

For laboratory cyclic load tests, soil specimens are prepared to represent the *in situ* conditions and are subjected to stress cycles of various magnitudes to determine the number of actual cycles necessary to cause liquefaction. The triaxial test information corrected to field conditions is used to estimate the shear stress level to cause liquefaction for the number of cycles determined in the computer analysis. The factor of safety is the ratio of the resisting shear strength from the triaxial test data to the applied shear stress level from the computer analysis.

Lee and Chan (1972) have developed a procedure for computing the equivalent number of cycles. The term equivalent number of significant cycles N_{eq} refers to that number of uniform cycles of stress intensity τ_{av} which, if applied to an element of soil, would have the same effect in terms of the soil strength or deformation as if the actual train of irregular cyclic shear stresses were applied (see Figure 3-19). The value of τ_{av} is usually taken to be equal to 0.65 τ maximum. To convert the actual stress time history into an equivalent number of uniform cycles, divide the stress range (0 to τ maximum) into a convenient number of levels and note the stress within each level or increment, τ_i, as shown in Figure 3-20. The actual number with peaks in the computed stress history which fall within each of these levels is counted $n_{\tau i}$. Since the actual time history is not symmetric about the zero stress

(a) Computed Actual Response   (b) Equivalent Response
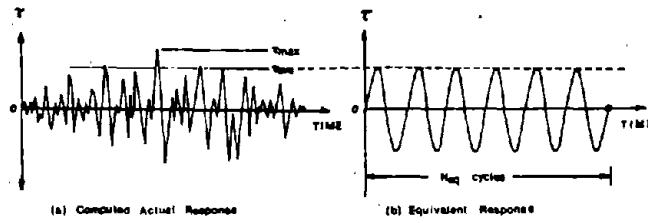
Figure 3-19. Actual and equivalent
earthquake stress history.
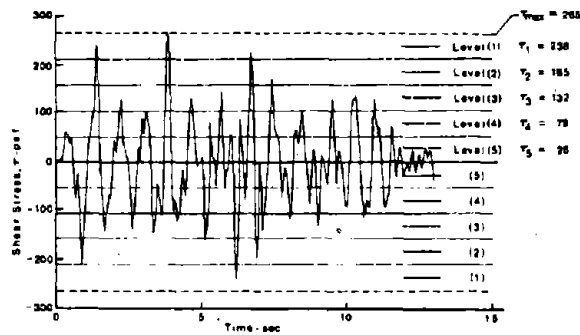
Figure 3-20. Steps in calculating N_{eq} from seismic stress history.

84

axis, the number of peaks on both sides are counted, and two peaks are equivalent to one cycle. A shear strength curve from laboratory tests or Figure 3-12 is corrected to field conditions. This curve represents a factor of safety of 1.0; theoretically the values on the curve should be divided by the estimated factor of safety to correctly show the true relationship for the soil under the specific earthquake.

The number of cycles N_{τ_i} and $N_{\tau_{av}}$ corresponding to the incremental stress levels and τ_{av} level are obtained. The ratio of the number of cycles at the τ_{av} stress level to cause liquefaction $N_{\tau_{av}}$ to the number of cycles at the incremental stress levels to cause liquefaction N_{τ_i} is used to multiply the actual number of counted cycles at that incremental stress level n_{τ_i}. These ratios are summed for all n increments of stress from 0 to τ_{max}

$$N_{eq} = \sum_{i=1}^{n} \left(\frac{N_{\tau_{av}}}{N_{\tau_i}} \text{ from test data or Figure 3-12} \right) \left(n_{\tau_i} \begin{array}{l} \text{actual} \\ \text{SHAKE} \\ \text{data} \end{array} \right)$$

If the estimated factor of safety is correct, N_{eq} determined from the summation would equal $N_{\tau_{av}}$ from the laboratory test data or Figure 3-12 at the average stress level. If it does not, revise the estimate of the factor of safety and repeat. In practice it has been found that it is not necessary to multiply the strength curve by the estimated factor of safety. In this case the factor of safety would then be the ratio of τ at N_{eq} from test data divided by τ_{av}.

Seed, et al. (1975) have proposed Figure 3-21 as an average shape representation of the relationship between stress ratio and number of cycles to liquefaction. Using Figure 3-21, Figure 3-22 is generated; a factor of safety of 1.5 is applied to produce the lower curve. From this curve, Table 3-1 is obtained which gives conversion factors for equivalent stress levels. An example is given in Figure 3-23. Seed, et al. (1975) have also evaluated the equivalent number of uniform stress cycles based on strong motion data (Figure 3-24).

EFFECTS OF SOIL AND SITE PARAMETERS

Frequently, the parameters needed in the response studies are poorly defined at a given location. Often, the values of these parameters must be assumed in order to perform the ground response analyses. Experience has shown that variations in the value of any one of the parameters may affect the solution differently from site to site, and no general rules may be formulated at this time to establish the influence of the variables.
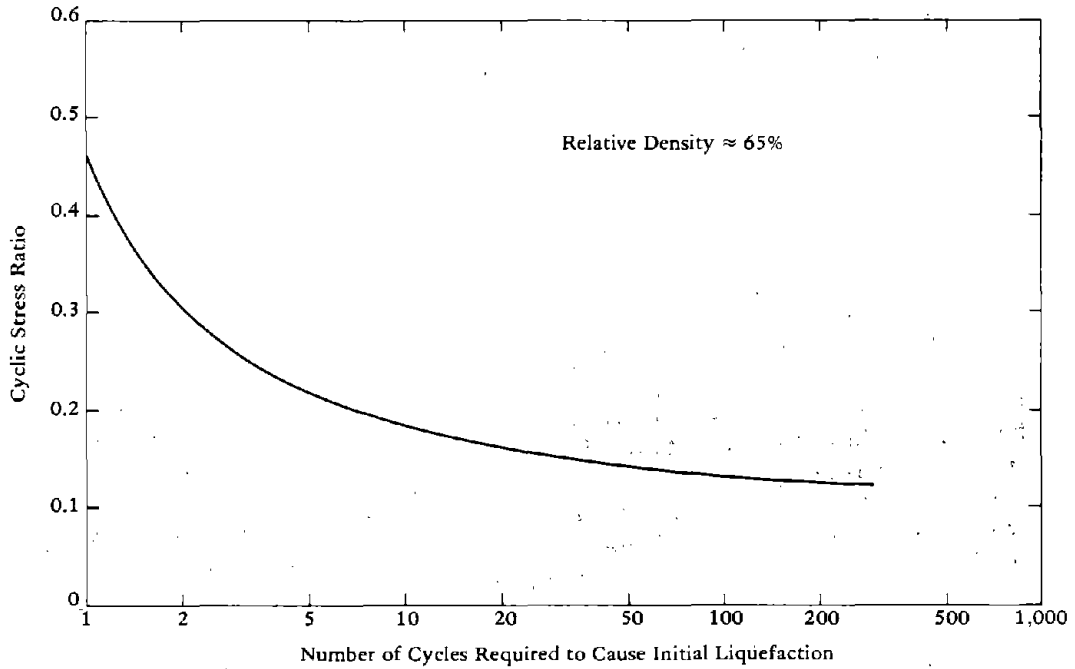
Figure 3-21.   Representative curve for relationship between cyclic
stress ratio and number of cycles to liquefaction
(from H. B. Seed, 1976).
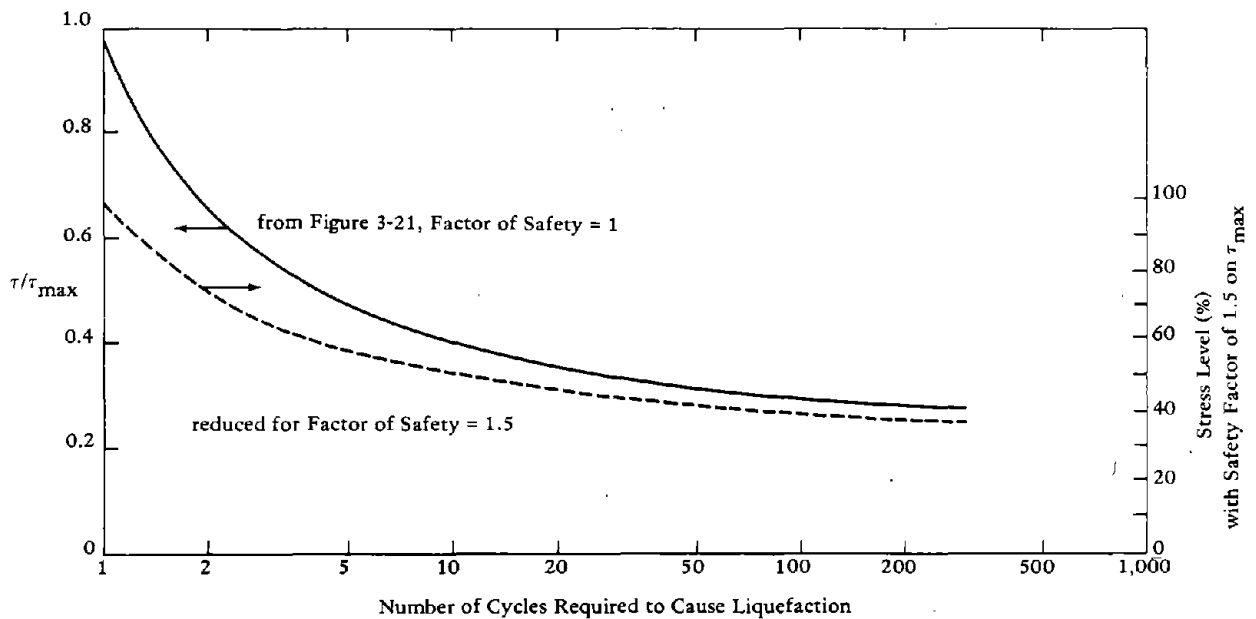
Figure 3-22.   Representative relationship between τ/τ_{max} and
number of cycles required to cause liquefaction
(from H. B. Seed, 1976).

86

Table 3-1. Equivalent Stress Levels Based on Figure 3-17

Single Cycle at the Following Stress Levels (τ_{max})	Equivalent Number of Cycles at 0.65 τ_{max}
1.0	3
0.95	2.7
0.9	2.4
0.85	2.05
0.8	1.7
0.75	1.4
0.7	1.2
0.65	1.0
0.6	0.7
0.55	0.4
0.5	0.2
0.45	0.1
0.4	0.04
0.35	0.02

ORION BLVD RECORD, E-W COMP, SAN FERNANDO EARTHQUAKE, 1971

Acceleration (g)

0.1320
0.1056
0:0792
0.0528
0.0261
0
-0.0261
-0.0528
-0.0792
-0.1056
-0.1320

0 2 4 6 8 10 12 14 16 18 20 22 24 26

Time (s)
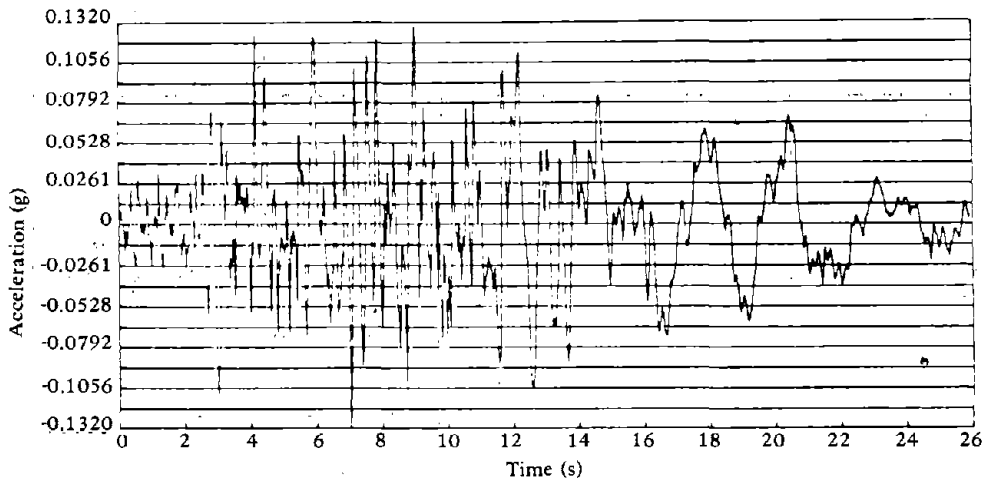
Stress Level: Fraction of τ_{max}	ABOVE HORIZONTAL AXIS			BELOW HORIZONTAL AXIS		
	Number of Stress Cycles	Conversion Factor	Equivalent No. of Cycles at $0.65\,\tau_{max}$	Number of Stress Cycles	Conversion Factor	Equivalent No. of Cycles at $0.65\,\tau_{max}$
τ_{max}	—	—	—	I	3.00	3.00
0.95 "	3	2.70	8.10	—	—	—
0.90 "	I	2.40	2.40	—	—	—
0.85 "	2	2.05	4.10	I	2.05	2.05
0.80 "	—	—	—	2	1.70	3.40
0.75 "	3	1.40	4.20	—	—	—
0.70 "	—	—	—	2	1.20	2.40
0.65 "	I	1.00	1.00	I	1.00	1.00
0.60 "	2	0.70	1.40	I	0.70	0.70
0.55 "	3	0.40	1.20	3	0.40	1.20
0.50 "	I	0.20	0.20	5	0.20	1.00
0.45 "	3	0.10	0.30	5	0.10	0.50
0.40 "	3	0.04	0.12	—	—	—
0.35 "	5	0.02	0.10	7	0.02	0.14
0.30 "	—	—	—	—	—	—
		Total	23.12		Total	15.39
Average number of cycles at $0.65\,\tau_{max}$ = 19.30						

Figure 3-23.   Evaluation of equivalent uniform cyclic stress
series, Orion Boulevard record, east-west component
(from H. B. Seed, 1976).
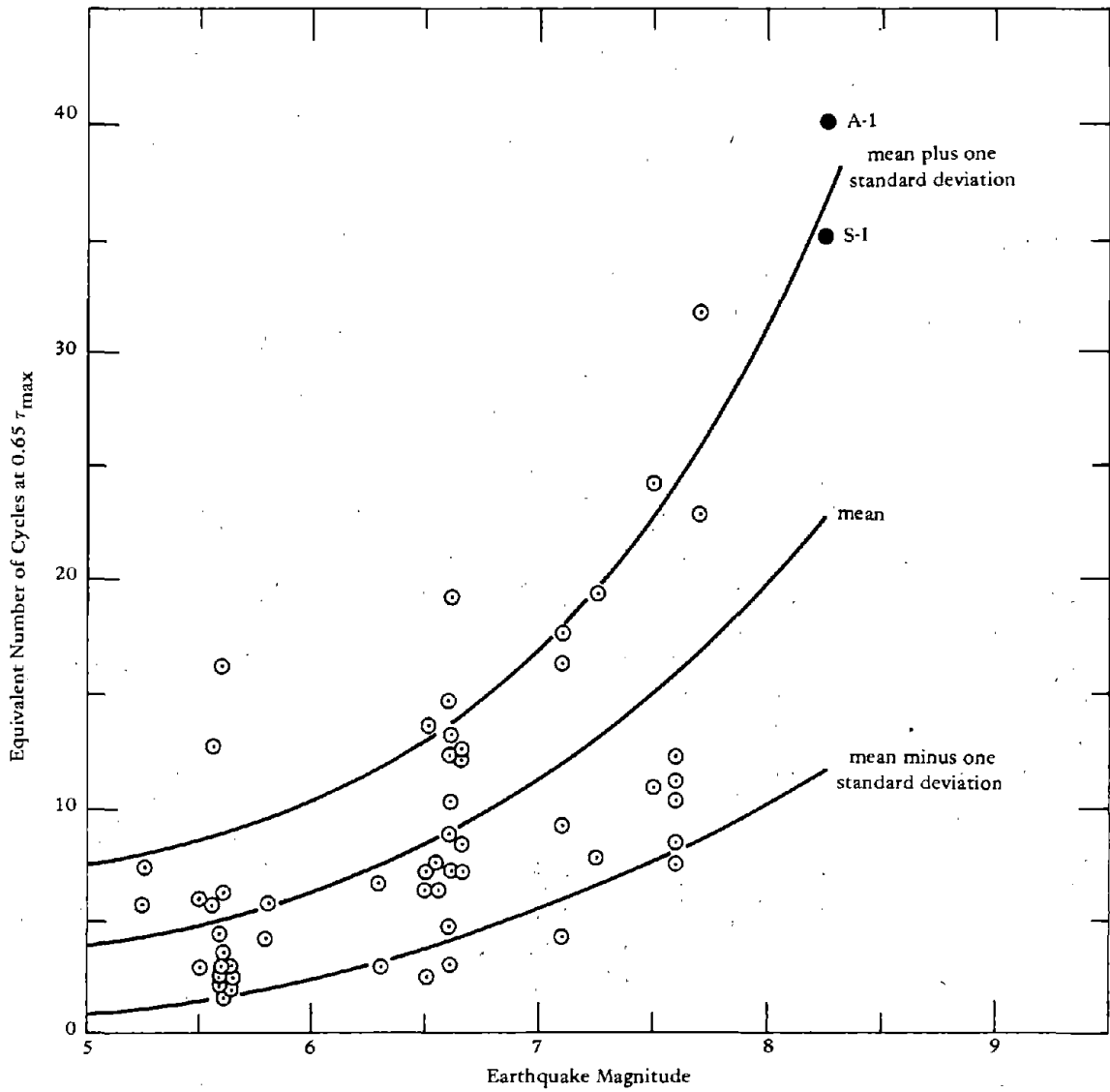
Figure 3-24. Equivalent numbers of uniform stress cycles
based on all components of ground motion
(from H. B. Seed, 1976).

Earthquake motions are produced by a stress wave, which is transmitted more rapidly and with less energy loss through the bedrock than through the overlying soils. When the bedrock has a horizontal surface of great extent and the overlying soil layers are also horizontal, it is frequently assumed that the earthquake motion within the soil is produced essentially by horizontal shear waves which propagate upward through the soil from the bedrock surface. This assumption greatly simplifies the analysis since the problem can be reduced to a one-dimensional shear wave problem. This is a simplification, since vertical components of the earthquake motion are always present and the wave transmission problem may be more complex than can be simulated in a one-dimensional model.

When the bedrock or soil layers are inclined, a one-dimensional shear wave assumption is questionable, and a two-dimensional model may be required to account for the more complex geometry and wave motion.

Lysmer, Seed, and Schnabel (1970) have shown that under identical boundary conditions, the lumped mass solution and the wave propagation solution are basically the same. Arango and Dietrich (1972) have investigated the variation of parameters for the two methods. They note close agreement in peak levels of motion with some differences in computed time histories.

Depth to Bedrock

In many cases the depth to bedrock is not well-defined. A preliminary analysis may be required to assess the influence of depth to bedrock on the ground response. Dezfulian and Seed (1969) have shown that an increase in thickness of the deposit may or may not cause a substantial change in surface motion. Their studies show that for shallow deposits, an increase in thickness of medium sand from 38 feet (12 meters) to 50 feet (15.6 meters) reduced the response significantly. Increasing the thickness to 80 feet (25 meters) reduced the response still more, but a further increase from 80 to 100 feet (31.2 meters) did not produce any additional reduction in the response.

For much deeper deposits, 1,000 feet (330 meters), Kiefer, et al. (1970) analyzing the conditions at Osaka, found that the response was not very sensitive to the range of depths investigated.

Arango and Dietrich (1972) studied the variation for depths to bedrock equal to 600, 800, and 900 feet. The values of the maximum acceleration and the velocity and acceleration spectra are shown in Figure 3-25. The acceleration spectra for two depths to bedrock at Study Site A are also shown in Figure 3-25.
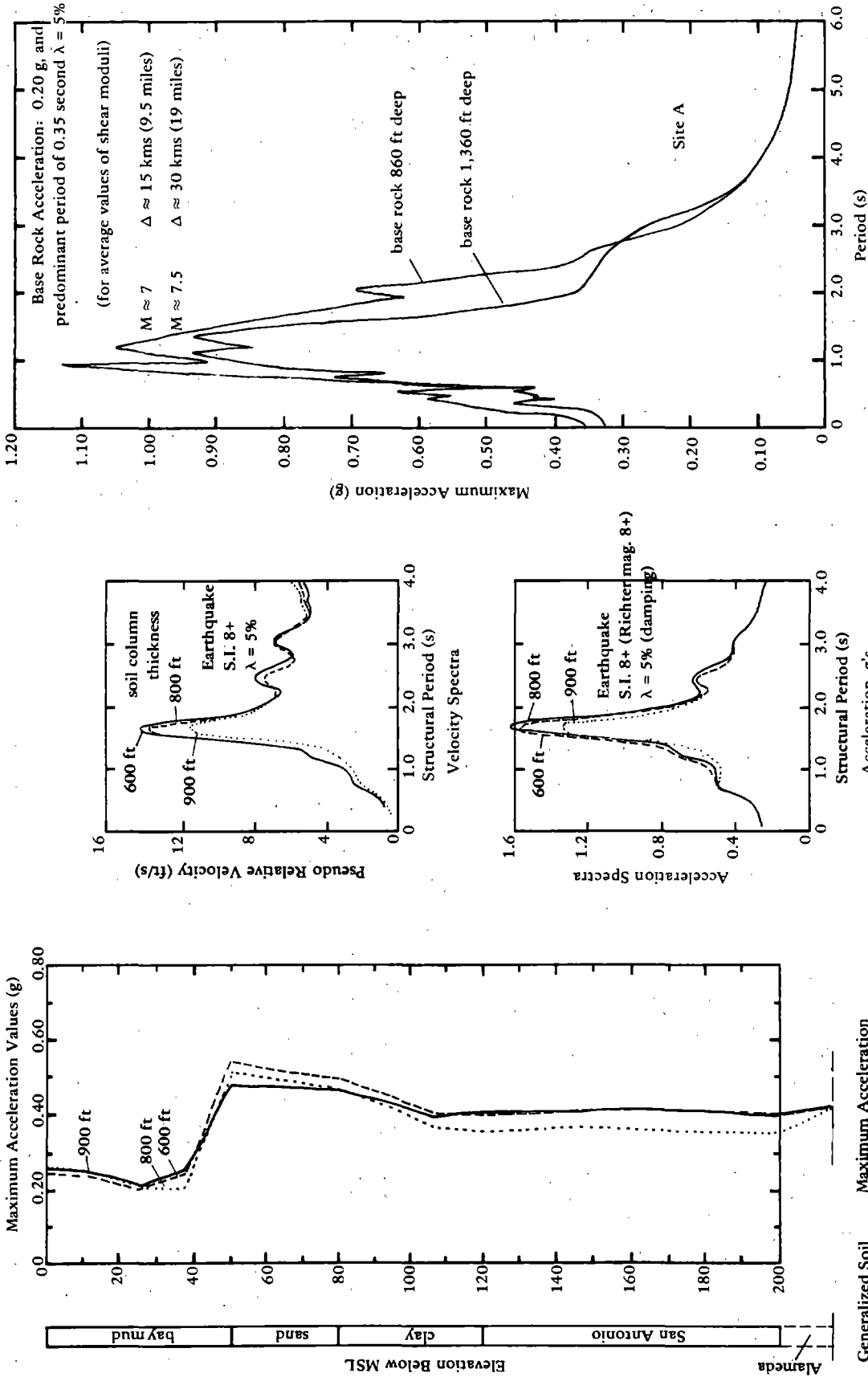
(b) Effect of depth to rock on the acceleration response spectra.

(a) Influence of depth to bedrock.

Figure 3-25. Response spectra and maximum surface accelerations (from "Soil and Earthquake Uncertainties on Site Response Studies," by I. Arango and R. J. Dietrich, in Proceedings of the International Conference on Microzonation for Safer Construction Research and Application, 30 Oct-3 Nov 1972).

The above examples show that for shallow soil deposits, the depth to bedrock may or may not significantly affect the response. Deep soil deposits are in general less sensitive. Preliminary studies using a reasonable range of depth to bedrock should precede any ground response calculation when uncertainties regarding the actual depth are present.

Influence of Soil Profile

The frequency characteristics of the ground motions and the form of the ground response spectra may be influenced by the nature of the soil conditions underlying the sites. This is illustrated by the studies by Arango and Dietrich (1972). Different soil profiles were used in the response analysis as shown in Figure 3-26. The values of the maximum acceleration and displacement obtained are shown in Figure 3-27. The corresponding response spectra are shown in Figure 3-28. Significant changes in response can result from variation in soil profile, and great care must be placed on the correct site stratigraphic representations. The importance of the time history of the ground motion on the response values is also apparent by comparing the spectra from Figure 3-28a to that of Figure 3-28b.

Soil Rigidity

Since the stiffness of the soil deposits can only be approximated, it is often desirable to run preliminary response analyses using the most reasonable values of the shear moduli for the various soils and values (say 50% to 100%) greater than those judged to be the most reasonable. Arango and Dietrich (1972) calculated the maximum ground surface acceleration, ground displacement, the fundamental period of the soil column, and the response spectra by using the average values of the shear moduli and values 50% higher. The results of the calculations are shown in Figure 3-29. In some cases, errors in the estimated shear moduli cause minor differences in the calculated ground response which have no practical significance for engineering purposes. In other cases, however, it has been found that great differences may occur as a consequence of varying the values of the shear moduli.

Amplitude of Rock Acceleration

Schnabel and Seed (1972) have indicated that spectral acceleration values are often not significantly influenced by substantial reductions in maximum acceleration levels in rock. It was found that generally a reduction of 15% to 25% in maximum rock acceleration values will affect the spectral acceleration by less than 10%.

92

Model 1

Layer Classification	Layer Thickness (ft)	Unit Weight γT pcf	Strength Su (psf) or K_2*	Shear Modulus $g \times 10^6$ (psf)	Shear Wave Velocity, Vs fps
Bay Mud	21 / 21	110 / 110	200 / 250	0.4 / 0.5	340 / 380
Sand	15 / 15	125 / 125	$K_2 = 80$ / $K_2 = 80$	3.0 / 3.6	880 / 960
Clay	40	130	2,000	4.0	1,020
San Antonio	80	130	2,900	5.8	1,200
Alameda	100	130	12,000 clay	4.0	2,400
	100	130	$K_2 = 115$ gravel	12.8	1,800
	100	130	12,000 clay	24.0	2,440
	100	130	12,000 clay	24.0	2,440

*Shear modulus = $1,000 \, K_2 (\sigma'm)^{1/2}$
where $\sigma'm$ = mean effective stress.

(a) Model 1   C = 12,000 psf.

Model 2

Layer Classification	Layer Thickness (ft)	Unit Weight γT pcf	Strength Su (psf) or K_2*	Shear Modulus $g \times 10^6$ (psf)	Shear Wave Velocity, Vs fps
Bay Mud	21 / 21	110 / 110	200 / 250	0.4 / 0.5	340 / 380
Sand	15 / 15	125 / 125	$K_2 = 80$ / $K_2 = 80$	3.0 / 3.6	880 / 960
Clay	40	125	2,000	4.0	1,020
San Antonio	80	130	2,900	5.8	1,200
	100	130	3,700 clay	7.4	1,350
Alameda	100	130	$K_2 = 115$ gravel	12.8	1,800
	100	130	7,300 clay	14.6	1,900
	100	130	9,000 clay	18.0	2,100

C = Su = Undrained clay strength.
P = Effective overburden pressure.

(b) Model 2   C/P = 1/4.

Figure 3-26. Four soil profile representations of same site (from "Soil and Earthquake Uncertainties on Site Response Studies," by I. Arango and R. J. Dietrich, in Proceedings of the International Conference on Microzonation for Safer Construction Research and Application, 30 Oct-3 Nov 1972).

(d) Model 4 · C/P = 1/3.

Layer Classification	Layer Thickness (ft)	Unit Weight γT pcf	Strength Su (psf) or K_2*	Shear Modulus g x 10^6 (psf)	Shear Wave Velocity, Vs fps
Bay Mud	21 / 21	110 / 110	200 / 250	0.4 / 0.5	340 / 380
Sand	15 / 15	125 / 125	$K_2 = 80$ / $K_2 = 80$	3.0 / 3.6	880 / 960
Clay	40	130	2,000	4.0	1,020
San Antonio	80	130	2,900	5.8	1,200
Alameda	100	130	4,950 clay	9.9	1,560
	100	130	7,240 clay	14.5	1,900
	100	130	9,500 clay	19.0	2,170
	100	130	10,750 clay	21.5	2,320

(c) Model 3 · intermediate properties.***

Layer Classification	Layer Thickness (ft)	Unit Weight γT pcf	Strength Su (psf) or K_2*	Shear Modulus g x 10^6 (psf)	Shear Wave Velocity, Vs fps
Bay Mud	21 / 21	110 / 110	200 / 250	0.4 / 0.5	340 / 380
Sand	15 / 15	125 / 125	$K_2 = 80$ / $K_2 = 80$	3.0 / 3.6	880 / 960
Clay	40	130	2,000	4.0	1,020
San Antonia	80	130	2,900	5.8	1,200
Alameda	100	130	6,000 clay	12.0	1,730
	100	130	$K_2 = 115$ gravel	12.8	1,780
	100	130	10,000 clay	20.0	2,240
	100	130	10,000 clay	20.0	2,240

***Strength between Models 1 and 2.

Figure 3-26. Continued.

(a) El Centro earthquake.
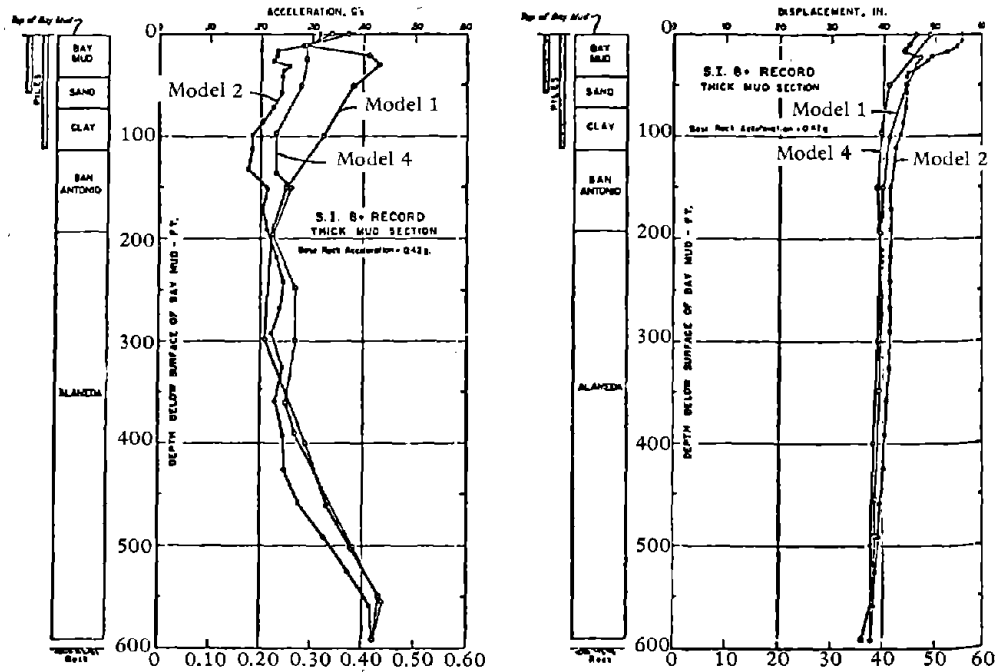
(b) Site intensity = 8+ earthquake.

Figure 3-27.   Response of soil models (from "Soil and Earth-
quake Uncertainties on Site Response Studies," by I. Arango
and R. J. Dietrich, in Proceedings of the International
Conference on Microzonation for Safer Construction
Research and Application, 30 Oct-3 Nov 1972).
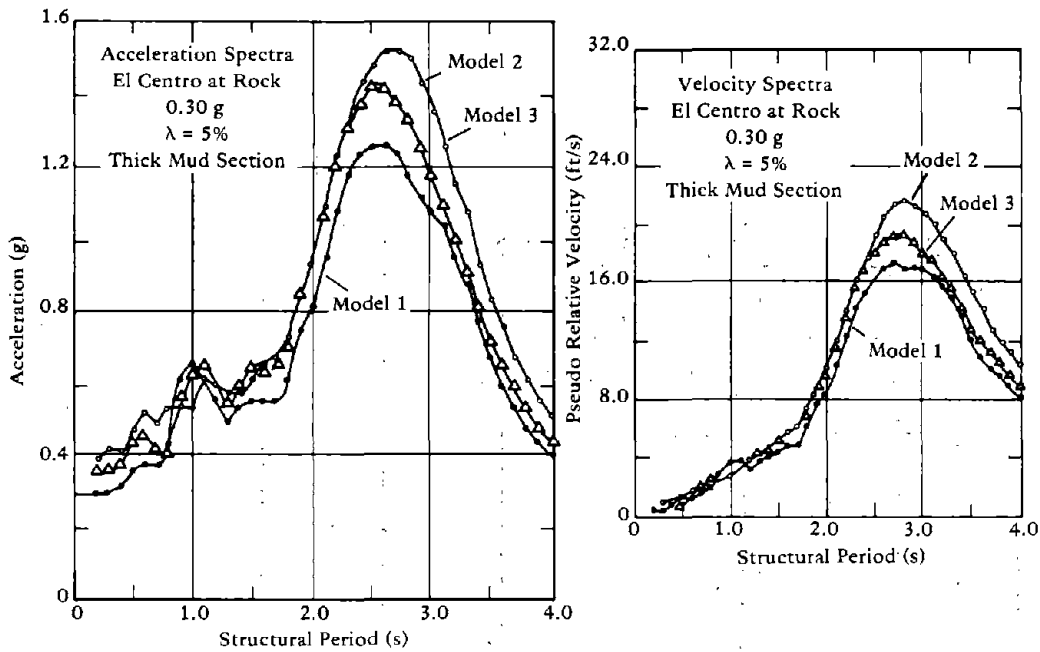
(a) El Centro earthquake.
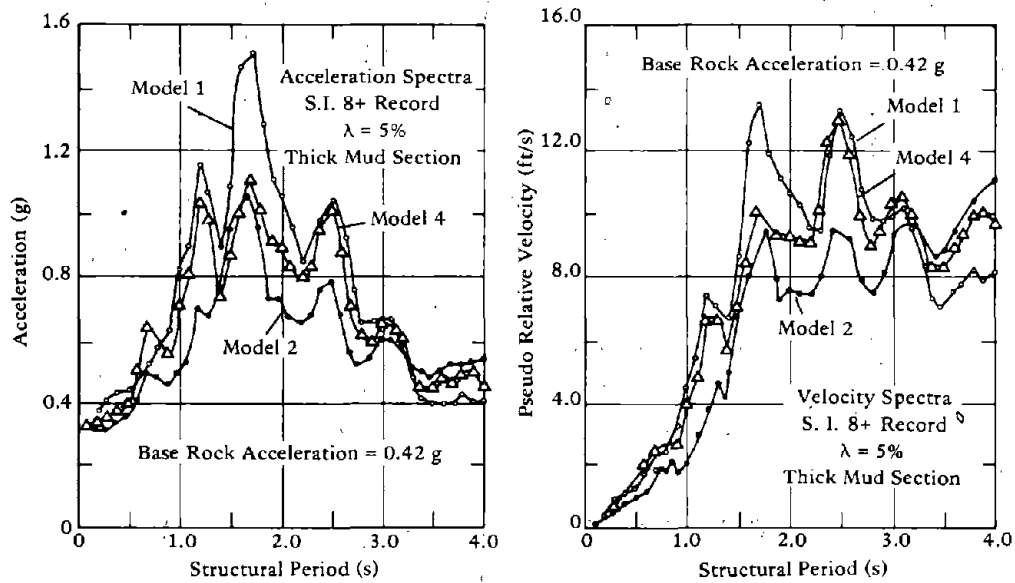
(b) S.I. 8+ earthquake.

Figure 3-28. Response spectra (from "Soil and Earthquake Uncertainties on Site Response Studies," by I. Arango and R. J. Dietrich, in Proceedings of the International Conference on Microzonation for Safer Construction Research and Application, 30 Oct-3 Nov 1972).

96.

	γ_T (pcf)	Strength (psf)	Relative Density (%)
Loose Silt	95		30
Peat and Silt	95	600	
Silt to Clayey Silt	100	2,000	
Sand and Gravel (Recessional Outwash)	130		100
Till	140		100
Hard Clays	135	20,000	
Rock			
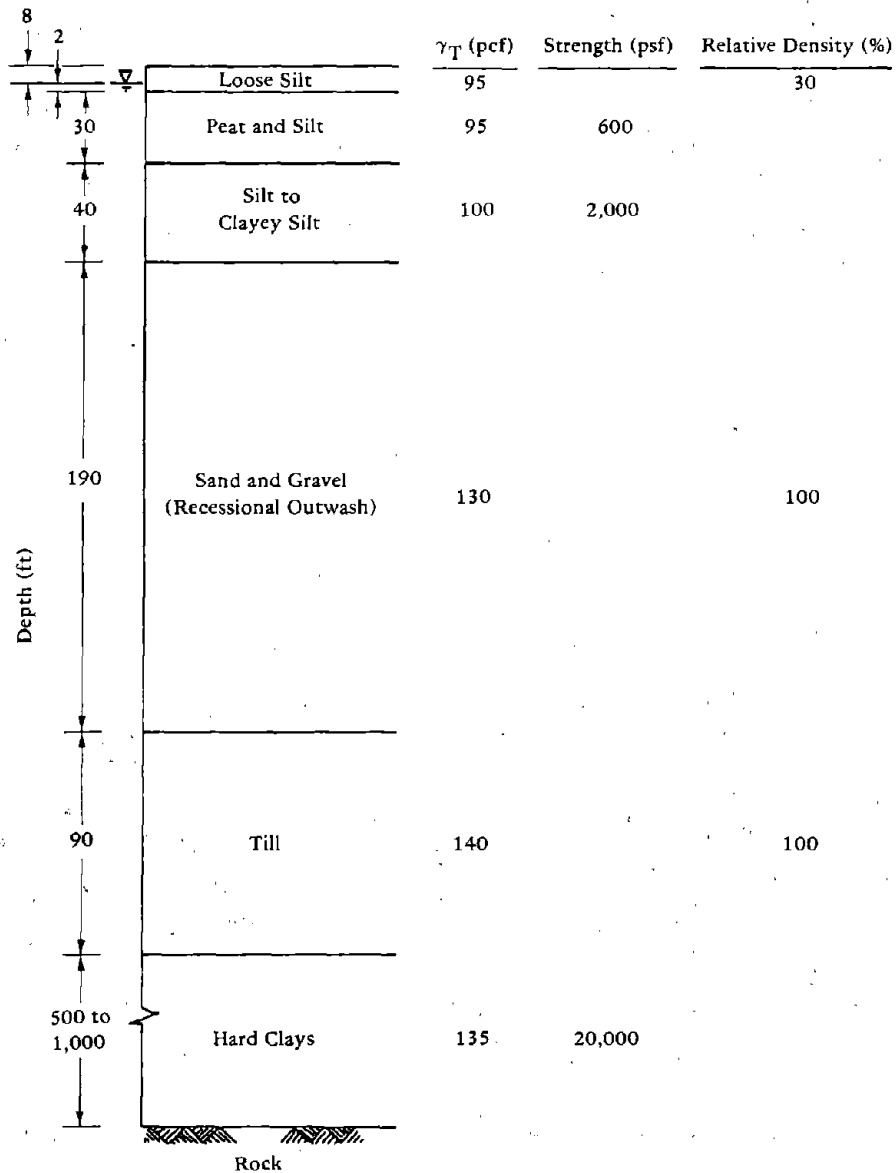
(a) Generalized soil profile.

Figure 3-29. Effect of variation of material properties (from "Soil and Earthquake Uncertainties on Site Response Studies," by I. Arango and R. J. Dietrich, in Proceedings of the International Conference on Microzonation for Safer Construction Research and Application, 30 Oct-3 Nov 1972).

97
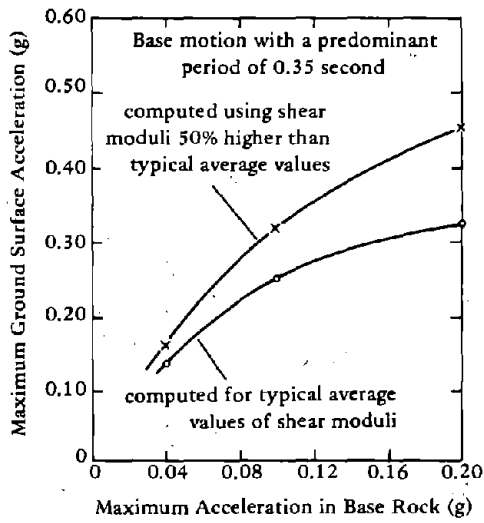
(b) Relationship between maximum ground surface displacement and maximum base rock acceleration.
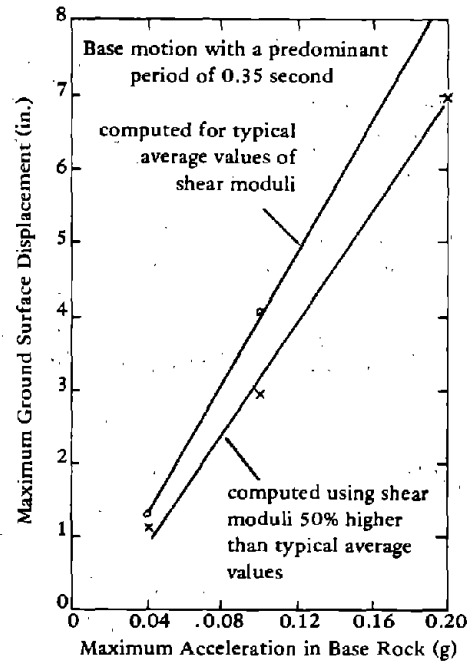
(c) Relationship between maximum ground surface displacement and maximum base rock acceleration.
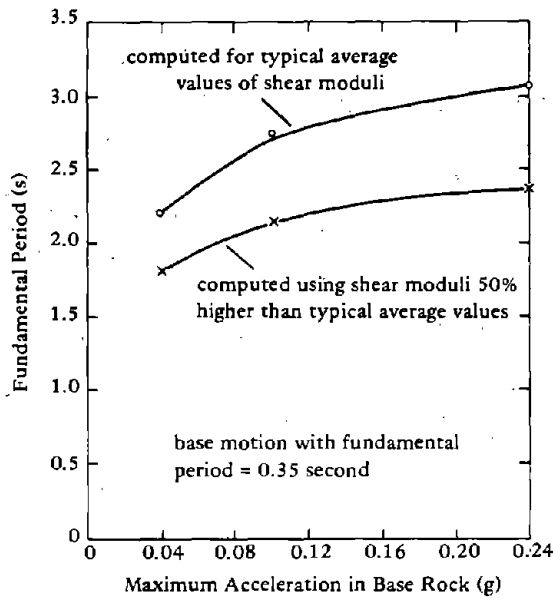
(d) Fundamental period of soil deposit.
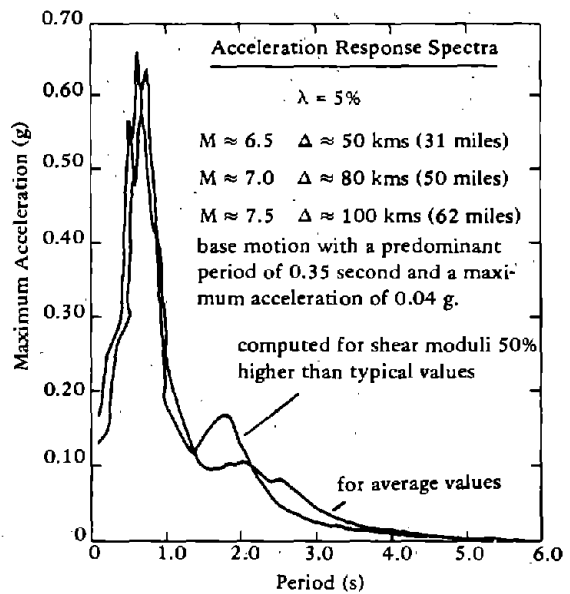
(e) Effect of soil moduli on the acceleration response spectra.

Figure 3-29. Continued

Frequency Content of the Rock Motions

The form and frequency characteristics of the base input may have a very significant influence on the response of soils. Arango and Dietrich (1972) studied a site under two different earthquakes (Figure 3-30). As shown at the right side of Figure 3-30, the two acceleration histories applied to the outcrop rock had the same peak acceleration and the spectra were similar. However, the small differences in frequency caused the motion to be amplified differently in the three soil columns. Therefore, two or more histories of acceleration should be considered in any given response study in order to define the relative magnitude of the ground response at any given location.

COMPLEX COMPUTER ANALYSIS, TWO-DIMENSIONAL MODELS

As pointed out earlier, when the ground surface or the soil layers are inclined, one-dimensional wave assumptions may not be valid and a two-dimensional model may be required to represent the more complex geometry. Although two-dimensional liquefaction analyses are not in routine soil practice, the same procedures for evaluation of a stress history can be utilized. Finite element representations have been used to study dams and embankments.

Idriss, et al. (1973) have developed a two-dimensional finite element program — QUAD-4 — for the evaluation of seismic response of soil deposits. This program allows for variable damping in each element using a Rayleigh damping expression for that element. The damping matrix for the entire assemblage of elements is obtained by appropriate addition of the damping submatrices of all the elements.

The response is evaluated by the solution of the equations of motion using direct numerical integration methods with a time increment small enough to provide stability. The program uses plane strain quadrilateral and triangular elements. An iteration procedure is used to determine the strain-dependent modulus and damping for each element, based on the average strain developed in that element. The relation of modulus and damping is based on Seed and Idriss (1970c). The solution is obtained using the modulus and damping for each element which is compatible with the average strain. The developers of the program report that comparison with one-dimensional methods shows that the finite element solution values of shear stress are about 10% greater. The response spectra of one- and two-dimensional methods are of similar shape. Major differences on response spectra occur only when the input motion has large amounts of high frequency components or when the finite element model is very coarse. The addition of variable damping makes the response calculation results in better agreement with recorded data.

99

(a) Response spectra.

(b) Maximum surface accelerations.

(c) Generalized longitudinal soil profile.
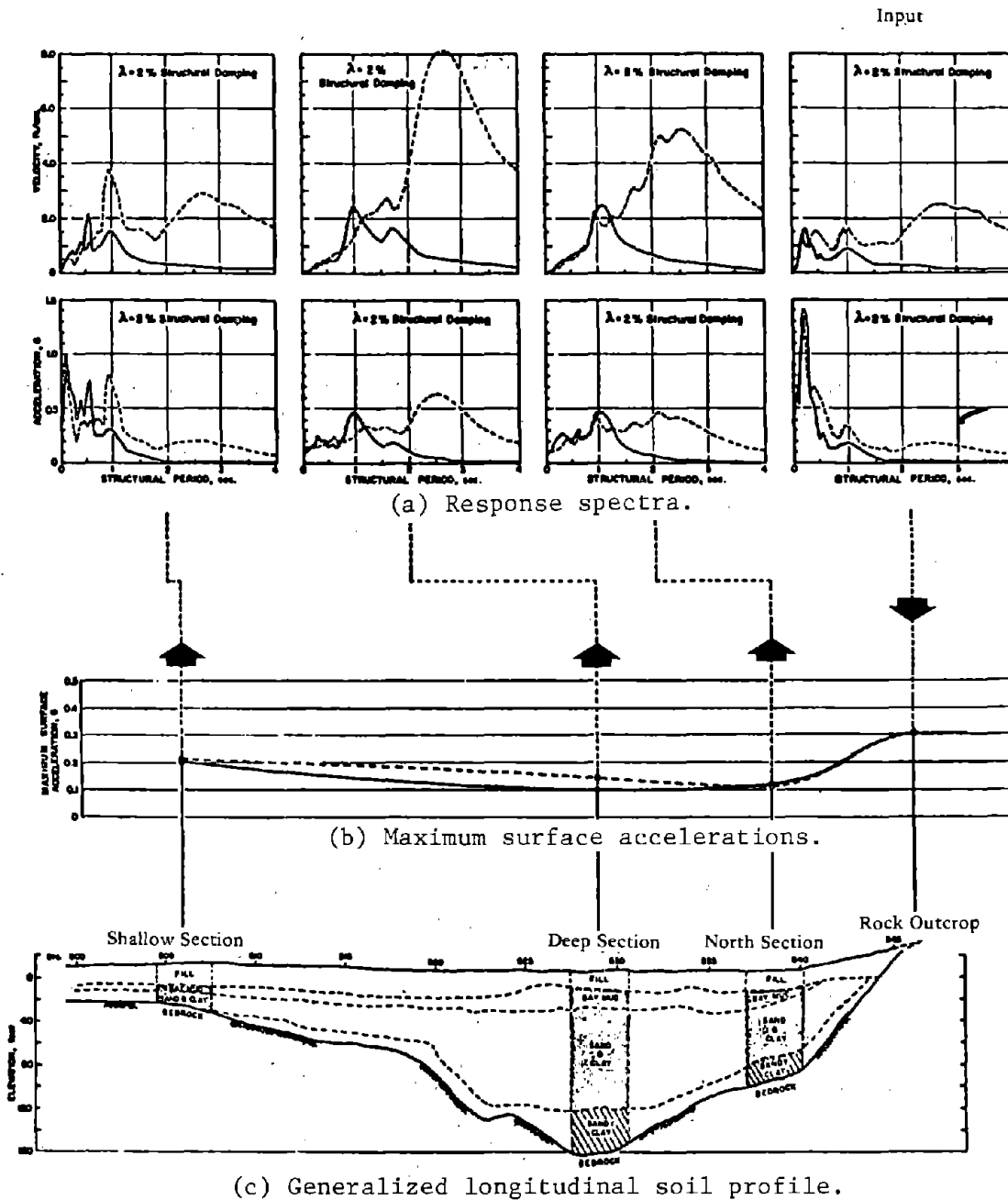
Figure 3-30. Response spectra and maximum surface accelerations
(from "Evaluation of Soil Liquefaction Effects on Level Ground
During Earthquake," by H. B. Seed in ASCE Preprint 2752,
Liquefaction Problems in Geotechnical Engineering,
ASCE Annual Convention, Philadelphia, Pa.,
27 Sep-1 Oct 1976).

Lysmer, Udaka, Seed, and Hwang (1974) have developed a two-dimensional finite element program, LUSH (revised version called FLUSH), which solves the transient response problem in soil sites by complex frequency response. It can calculate the response of sloping soil layers and can include the soil-structure interaction effect. The program accounts for the nonlinear effects which occur in soil masses by a combination of the equivalent linear method described in the section on one-dimensional analyses (Seed and Idriss, 1969) and the method of complex response with complex moduli allowing for different damping properties in all elements.

The model consists of plane quadrilateral or triangular elements. Three different material types are provided for: nonlinear clays and sands, elastic solids, and rigid solids. Typical relationships between stiffness, damping, and effective shear strains for sand and clay are provided within the program. These are similar to the curves used in SHAKE. Viscous damping is introduced by using complex moduli in the formation of the stiffness matrix which lends to the same amplitude response as nodal analysis with a uniform fraction of critical damping. The initial soil properties are specified at low strain level ($\gamma = 10^{-4}\%$ strain) and the program iterates to find material properties at strain levels compatible with the specified motion.

The mesh size of elements in the model should be small compared with the wave length of shear waves propagating through the model. A suggested maximum height element is

$$ h = (1/5) \lambda = 1/5 \left(\frac{V_s}{w} \right) $$

where
h = element height

λ = wavelength of shortest shear wave

V_s = velocity of shear wave at strain level of earthquake

w = highest frequency of the analysis

The existing methods for liquefaction evaluation discussed above, including finite element programs, do not compute the pore pressure change with loading directly from the material properties and the actual shear strain produced by the actual time-dependent load. The process of liquefaction transforms an element of soil from a saturated granular solid to a viscous fluid. As a result of this change of material state, the soil in a liquefied zone has reduced shear strength and can undergo

large displacements. The actual *in situ* pore water pressure determination under dynamic field loading conditions is of theoretical interest in the analysis of the liquefaction potentiality of a soil. The following paragraphs present some current research in progress.

Ghaboussi, et al. (1974) have proposed a method for determination of pore pressures and intergranular stresses by considering the soil as a two-phase medium. In the two-phase representation of saturated soils the granular solid skeleton and the fluid are treated as independent materials with individual material properties. The coupling between the volume changes of fluid and solid skeleton is taken into account through an additional material parameter. The flow of fluid with respect to the solid is assumed to be governed by a generalized form of Darcy's flow law, for which the material's parameter is the coefficient of permeability. The bulk modulus of the fluid, the coupling material parameter, and the coefficient of permeability can be reasonably assumed to remain constant in the present dynamic analysis. The solid granular skeleton, in contrast, is a highly nonlinear material. A realistic constitutive relation for the solid skeleton of saturated granular soils must be capable of simulating the important nonlinear features such as dilatancy, compaction, shear failure and load reversal effects. Stress compaction, being a factor in the pore pressure buildup, is of special importance in liquefaction analysis.

The onset of liquefaction in an element of saturated soil is to be determined by a "liquefaction criterion" defined as reduction of the mean intergranular pressure. The initiation of liquefaction in any analysis, as determined by satisfying the liquefaction criterion, marks the boundary between two behavior conditions for an element of soil. In the pre-liquefaction state the soil is treated as a two-phase, fluid-saturated, porous solid. The important characteristics of a potentially liquefying soil at this stage is the increase of the pore pressures accompanied by the decrease of the mean intergranular pressure. After the initiation of liquefaction the behavior of an element of soil changes from a fluid-saturated granular material to a viscous material of limited shear strength.

The analysis in the pre-liquefaction stage will lead to determination of the potentiality of liquefaction. If the extent of the development of the liquefaction and the associated stress and pore pressure distribution are of interest, then the analysis should be carried into the post-liquefaction stage. Doing so requires accounting for the change in behavior from the fluid-saturated granular material to a viscous material in an element of soil which has satisfied the liquefaction criterion.

The key to the success of the liquefaction analysis of the type proposed by Ghaboussi, et al. (1974) in this work lies in the appropriate mathematical modeling of the important features of the constitutive

102

response of the granular solid skeleton of the soil. Loose sands are susceptible to liquefaction under seismic loading conditions since they tend to compact under shear deformation. This reduction of the volume in loose sands causes the pore pressure buildup and consequent reduction of the mean intergranular pressure, leading to liquefaction. Appropriate representation of the properties of granular soils requires special attention in a liquefaction analysis. Nonlinear material models are required to model the plastic behavior of the soil. This pre-liquefaction is under investigation using a soil model developed by Ishihara et al. (1975). Much work is required to validate this model. Present results by Ghaboussi et al. (1974) are given in Appendix A.

Ishihara et al. (1975) have presented a model for liquefaction based upon studies of the cyclic deformation of undrained sands. This model permits assessing pore pressures, shear strains, and the occurrence of liquefaction in undrained horizontal soil layers. This model, originally based on triaxial data, has been revised to fit torsion test results and incorporated into a computer code by Ishihara et al. (1976). The applied stress history for the *in situ* soil profile may be calculated by some of the foregoing computer programs, such as SHAKE (Schnabel, Lysmer and Seed, 1972). This stress history is then applied to the soil model to predict pore pressures and shear distortions.

Test data on undrained sands illustrate that for shearing loads below a particular shear stress/effective stress ratio, q/p', reloading always retraces the unloading path. Plastic yielding, associated with the original application of shear stress, results in a buildup of residual pore pressure (and thus reduction in effective stress). Thus, it is possible to define for any particular soil density, a so-called virgin state, defined by a relationship such as that of Figure 3-31, in terms of shear stress, q versus effective mean principal stress p'. A series of such planes forms a vector surface in p' - q - e space (where e is void ratio or a measure of initial density). This "state" surface specifies the route or path in p' - q - e space along which stresses must be changed in order for deformations to be plastic. Plastic yielding occurs only when stresses are changed along paths lying on the state surface, and all other paths away from it are associated merely with elastic deformations. For undrained shearing of saturated sand, the stress paths can be defined for a specific state by a single slice or plane through the p' - q - e surface, such as Figure 3-32 (for a loose sand). This figure shows yield lines, or "equi-γ lines," which are curves in p' - q space at which yielding occurs whenever stress paths cross them. For stress paths within previously approached yield loci the deformations are assumed to be elastic, and no change in effective stress occurs.

With increase in the q/p' ratio, shear strains are generated with magnitudes equal to those values shown on the equi-γ lines in Figure 3-32.
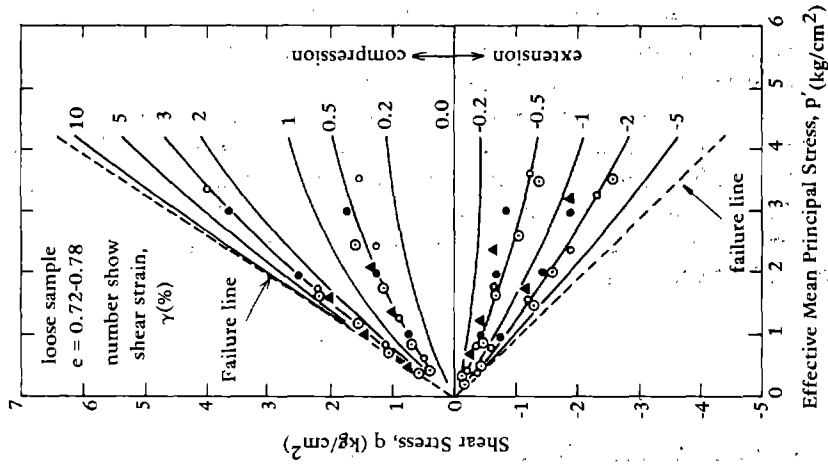
Figure 3-32. Equi-γ lines for loose samples (Fuji River sand) (from K. Ishihara, 1975).
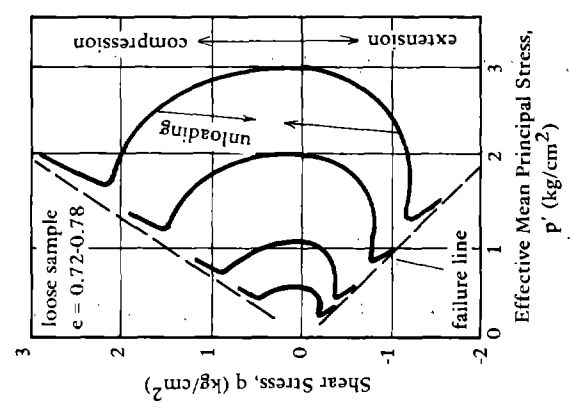
Figure 3-31. Typical undrained stress paths for loose samples (Fuji River Sand) (from K. Ishihara, 1975).

104

Experimental results on saturated sands show that the shear in one direction below some limiting stress ratio does not influence the virgin state response for shearing in the opposite direction. However, beyond a certain q/p' ratio, the pore pressure commences to increase drastically during any unloading (and increases even more dramatically during loading in the opposite direction). This defines a threshold stress value which, if not exceeded, permits elastic response during unloading and provides plastic work-hardening response during any load increase. The angle defined by the threshold stress value is called the angle-of-phase transformation and is slightly flatter than the failure envelope as shown in Figure 3-32. It is assumed that initial liquefaction occurs where the stress ratio crosses this angle-of-phase transformation. This model is based on the following postulates.

Postulate 1

The tendency for volume change in saturated sand samples is expressed in development of residual pore pressures. State surfaces such as Figure 3-31 contain a series of concentric curves which represent the changing stress state of any specimen undergoing undrained deformation. Any loading path at stress ratios below the angle-of-phase transformation follows the curved state line passing through its point of initiation. Unloading (from stress values beneath the angle-of-phase transformation) is considered elastic; i.e., no change in effective stress with reduction in shear stress.

Postulate 2

The undrained shear strain levels are defined by the equi-γ lines.

Postulate 3

These equi-γ lines may be approximated by straight lines passing through the p' - q origin. (Changes in state caused by the very small volume changes associated with change in effective pressure are neglected.)

Postulate 4

The yield conditions for loading in one direction are independent of the stress history of loading in the opposite direction.

105

Postulate 5

Instability of the saturated sand occurs when q/p' reaches the angle-of-phase transformation $\theta*$ (a state of initial liquefaction is assumed). It is noted that this model does not provide a reliable means of predicting response once the liquefaction state is reached.

In order to adapt the model for numerical computations, the stress paths in $p' - q$ space must be expressed in terms of a mathematical function. These stress paths selected for virgin loading below the angle-of-phase transformation may be represented by circles with centers at $p*$ along the p-axis which intersect this axis at p_0', the initial consolidation pressure. It is noted that the curvature for dense sands is less than for loose sands (the radius is greater).

To attempt to model the sand behavior beyond initial liquefaction — i.e., between initial and complete liquefaction (effective stresses are reduced to zero) — it is assumed that the loading stress path in the $p' - q$ plane follows the angle-of-phase transformation $\theta*$. Upon load release, the developed pore pressure has been found to be proportional to the ratio of the shear stress level prior to unloading q_r, divided by that at initial liquefaction q_θ, or

$$\frac{p_r'}{p_0'} = K_r \frac{q_o}{q_r}$$

where p_r' = the effective pressure following unloading

  p_o' = the effective pressure at initial liquefaction

  K_r = a new material constant

This model, for undrained sand using only three parameters — $\theta*$, p_0' and K_r — may be used to determine pore-pressure buildup and shear strain for any prescribed stress path.

SELECTION OF METHODS FOR BRIDGE SITES

Various methods for prediction of liquefaction have been reviewed. Figure 3-4 may be used for preliminary analysis when data is limited. For the simple geometry of essentially horizontal ground, the simple hand computation procedure should be adequate. Figure 3-33 gives a comparison of the Simple Hand Method, the Simple Computer Program, and
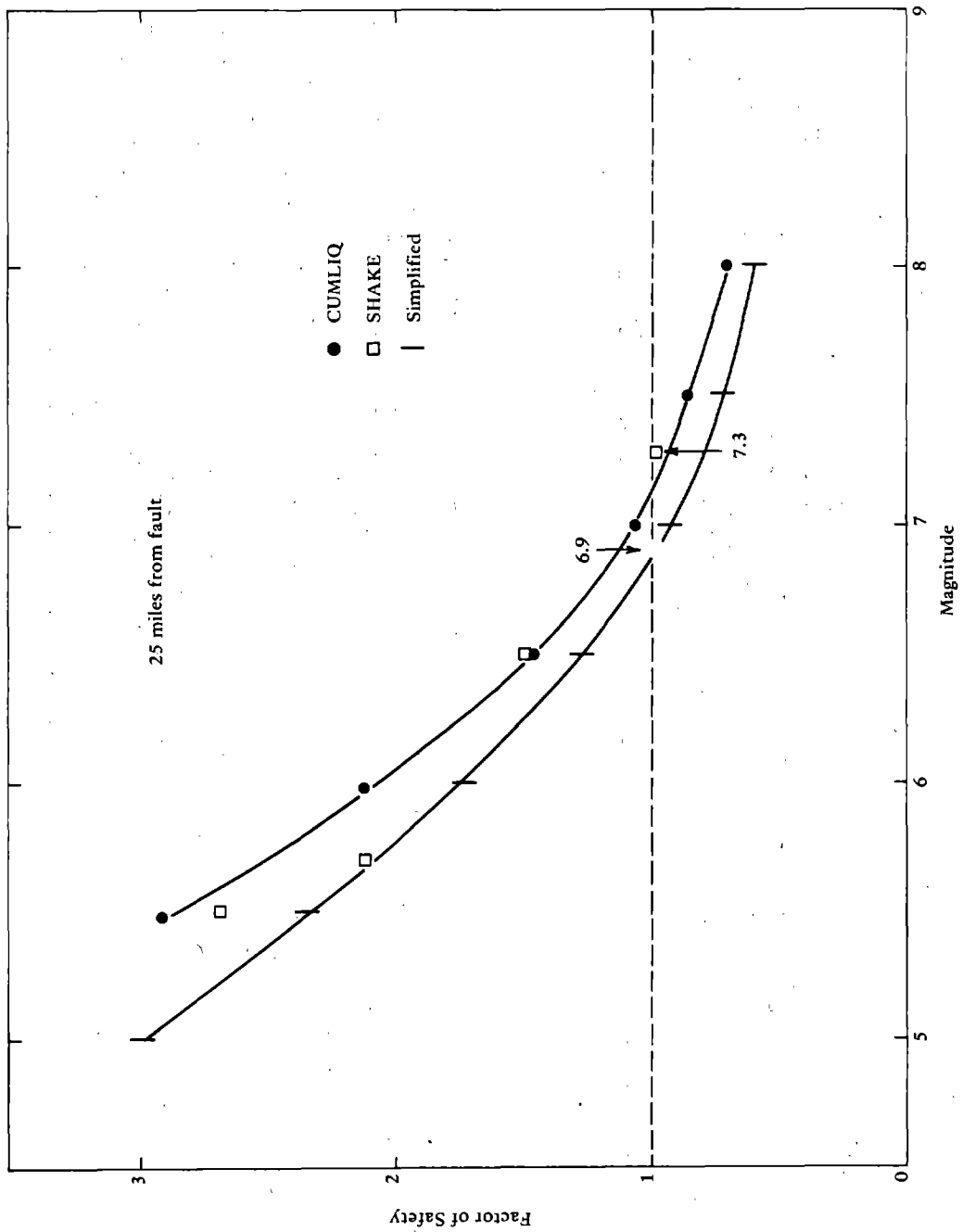
Figure 3-33. Comparison of prediction procedures.

107

SHAKE. For the profile used, the simple hand computation procedure provides a conservative estimate of the factor of safety when compared with the other procedures presently in use. This makes liquefaction analysis for simple sites possible without the use of a computer. Figures 3-11, 3-12, and 3-24 can be used as a guide to give the strength of the soil and the number of earthquake cycles. The τ/σ ratio used for soil strength should be reduced by 10% to account for multidirectional shaking and overconsolidation.

REFERENCES, CHAPTER 3

Arango, I. and Dietrich, R. J. (1972) "Soil and earthquake uncertainties on site response studies," in Proceedings of the International Conference on Microzonation for Safer Construction Research and Application, 30 Oct - 3 Nov 1972. Seattle, Wash., National Science Foundation.

Castro, G. (1975) "Liquefaction and cyclic mobility of saturated sands," Journal of the Geotechnical Division, ASCE, vol 101, no. GT6, Jun 1975, p. 55.

Christian, J. T. and Swiger, W. F. (1975) "Statistics of liquefaction and SPT results," Journal of the Geotechnical Division, ASCE, vol 101, no. GT11, Nov 1975.

DeAlba, P., Chan, C. K. and Seed, H. B. (1975) Determination of soil liquefaction characteristics by large-scale laboratory tests, University of California, Earthquake Engineering Research Center, EERC Report No. 75-14. Berkeley, Calif., May 1975.

Dezfulian, H. and Seed, H. B. (1969) Seismic response on soil deposits underlain by sloping rock boundaries, University of California, Earthquake Engineering Research Center, EERC Report No. 69-9. Berkeley, Calif., Jul 1969.

Donovan, N. C. (1974) CUMLIQ: Evaluation of potential for liquefaction of a soil deposit using random vibration procedures, University of California, Earthquake Engineering Research Center, National Information Service on Earthquake Engineering. Berkeley, Calif., Jul 1974.

Ghaboussi, I. and Wilson, E. L. (1974) "Liquefaction analysis of saturated granular soils," in Proceedings of Fifth World Conference on Earthquake Engineering, Rome, Italy, Jun 1973. Rome, Italy, International Association for Earthquake Engineering, Apr 1974, p. 380.

Gibbs, H. J. and Holtz, W. G. (1957) "Research on determining the density of sand by spoon penetrator test," in Proceedings of Fourth International Conference on Soil Mechanics and Foundations Engineering, vol 1, London, England, 1957.

Hardin, B. and Drnevich, V. (1970) Shear modulus and damping in soils, University of Kentucky, College of Engineering, Soil Mechanics Series Technical Report UKY 26-70-CE2. Lexington, Ky., Jul 1970.

Idriss, I. M., et al. (1973) QUAD 4: A computer program for evaluating the seismic response of soil structures by variable damping finite element procedures, University of California, Earthquake Engineering Research Center, EERC Report No. 73-16. Berkeley, Calif., Jul 1973.

Idriss, I. M. and Seed, H. B. (1968) "Seismic response of horizontal soil layers," Journal of the Soil Mechanics and Foundations Division, ASCE, vol 94, no. SM4, Jul 1968, pp 103-1031.

Idriss, I. M. and Seed, H. B. (1970) "Seismic response of soil deposits," Journal of the Soil Mechanics and Foundations Division, ASCE, vol 96, no. SM2, Mar 1970, pp 631-638.

Ishihara, K., et al. (1975) "Undrained deformation and liquefaction of sand under cyclic stresses," Soils and Foundations (Japan), vol 15, no. 1, Mar 1975.

Ishihara, K., et al. (1976) "Prediction of liquefaction in sand deposits during earthquakes," Soils and Foundations (Japan), vol 16, no. 1, Mar 1976.

Kanai, K. (1961) "An empirical formula for the spectrum of strong earthquake motions," Bulletin, Tokyo University Earthquake Research Institute, vol 39, 1961.

Kiefer, F. W., Seed, H. B. and Idriss, I. M. (1970) "Analysis of earthquake ground motions at Japanese sites," Bulletin of the Seismological Society of America, vol 60, no. 6, Dec 1970, pp 2057-2070.

Lee, K. L. and Chan, K. (1972) "Number of equivalent significant cycles on strong motion earthquakes," in Proceedings of the International Conference on Microzonation for Safer Construction Research and Application, 30 Oct - 3 Nov 1972. Seattle, Wash., National Science Foundation, 1972.

Lysmer, J., et al. (1974) LUSH: A computer program for complex response analysis of soil structure systems, University of California, Earthquake Engineering Research Center, EERC Report No. 74-4. Berkeley, Calif., Apr 1974.

Lysmer, J., Seed, H. B. and Schnabel, P. B. (1970) Influence of base rock characteristics on ground reponse, University of California, Earthquake Engineering Research Center, EERC Report No. 70-7. Berkeley, Calif., Nov 1970.

Mulilis, J. P., Chan, C. K. and Seed, H. B. (1975) The effects of method of sample preparation on the cyclic stress-strain behavior of sands, University of California, College of Engineering, Earthquake Engineering Research Center, EERC Report No. 75-18. Berkeley, Calif., Jul 1975.

Pyke, R., Chan, C. K. and Seed, H. B. (1974) Settlement and liquefaction of sands under multi-directional shaking, University of California, College of Engineering, Earthquake Engineering Research Center, EERC Report No. 74-2. Berkeley, Calif., Feb 1974.

Schnabel, P. B., Lysmer, J. and Seed, H. B. (1972) SHAKE: A computer program for earthquake response analysis of horizontally layered sites, University of California, Earthquake Engineering Research Center, EERC Report No. 72-12. Berkeley, Calif., Dec 1972.

Schnabel, P. B. and Seed, H. B. (1972) Accelerations in rock for earthquakes in the western United States, Unversity of California, College of Engineering, Earthquake Engineering Research Center, EERC Report No. 72-2. Berkeley, Calif., Feb 1972.

Seed, H. B. (1976) "Evaluation of soil liquefaction effects on level ground during earthquakes," ASCE Preprint 2752 (Liquefaction Problems in Geotechnical Engineering), American Society for Civil Engineers Annual Convention and Exposition, Philadelphia, Pa., 27 Sep - 1 Oct 1976.

Seed, H. B., et al. (1975) Representation of irregular stress time histories by equivalent uniform stress series in liquefaction analysis, University of California, College of Engineering, Earthquake Engineering Research Center, EERC Report No. 75-29. Berkeley, Calif., Oct 1975.

Seed, H. B. and Idriss, I. M. (1969) "Influence of soil conditions on ground motions during earthquakes," Journal of the Soil Mechanics and Foundations Division, ASCE, vol 95, no. SM1, Jan 1969, pp 99-137.

Seed, H. B. and Idriss, I. M. (1970a) A simplified procedure for evaluating soil liquefaction potential, University of California, Earthquake Engineering Research Center, EERC Report No. 70-9. Berkeley, Calif., Nov 1970.

Seed, H. B. and Idriss, I. M. (1970b) "Analysis of ground motions at Union Bay, Seattle, during earthquakes and distant nuclear blasts," Bulletin of the Seismological Society of America, vol 60, no. 1, Feb 1970, pp 125-136.

Seed, H. B. and Idriss, I. M. (1970c) Soil moduli and damping factors for dynamic response analysis, University of California, Earthquake Engineering Research Center, EERC Report No. 70-10. Berkeley, Calif., Dec 1970.

Seed, H. B. and Peacock, W. H. (1970) Applicability of laboratory test procedures for measuring soil liquefaction characteristics under cyclic loading, University of California, Earthquake Engineering Research Center, EERC Report No. 70-8. Berkeley, Calif., Nov 1970.

Streeter, V. L., Wylie, E. G. and Richart, F. E. (1974) "Soil motion computations by characteristics method," Journal of the Geotechnical Division, ASCE, vol 100, no. GT3, Mar 1974, pp 247-263.

Chapter 4

FIELD DETERMINATON OF SITE AND SOIL CONDITIONS

GENERAL

As pointed out in Chapter 3, various types of information about the
soil at a bridge site are required depending upon the method of analysis
used. Location of ground water table and definition of soil layers,
in situ relative density, and unit weight are usually necessary. This
chapter will briefly review the field methods used in site evaluation.
It is not the intent to cover these topics in any detail but rather to
give the reader an indication of how the data used in a liquefaction
analysis is normally obtained.

Most field exploration methods may be divided into two broad groups:
direct physical methods such as drilling and sampling in borings and
indirect or nondestructive techniques such as geophysical explorations.
Some of these methods can provide subsurface data to depths of thousands
of feet, if necessary.

Drilling and recovery of samples provide the most direct method
for evaluating a site. The number and depth of borings depend on the
site conditions and the characteristics of the bridge foundation.

Geophysical exploration consisting of seismic refraction velocity
measurements are useful to determine the depth of bedrock and define, in
general, the overburden strata. Seismic reflection studies are used for
greater depths. The most common type of seismic refraction measures the
propagation velocity of a compression wave from an explosive source to a
geophone. The distance versus travel time is plotted, and the slope
gives the average velocity of the compression wave. A change in the
slope indicates that the wave has passed into a layer with different
soil properties. Other seismic techniques such as the cross-hole method
measure transit time of either shear or dilatational waves. Unfortunately,
the geophysical exploration methods do not provide a detailed physical
description of the underlying soil.

For a liquefaction analysis it is necessary to determine, as a minimum, the type and *in situ* relative density of soils at a site, the thickness of soil layers, the location of the ground water, and the depth of bedrock.

SOIL PROFILE

The determination of the soil profile and thickness and composition of soil layers can be accomplished by standard drilling and sampling techniques. For the upper 50 feet, sampling intervals should be small enough to define any material changes and the thickness of the layers. Is is particularly important in liquefaction investigations that layers of looser materials be accurately located. When penetrating weak or loose zones, continuous sampling of a nature in keeping with the detail of information required by the analysis should be used. It is important to note that when materials are interbedded in relatively thin layers, average material properties (such as density) obtained by mixing the layers together can provide test data very much in error. Preliminary investigations can determine the extent of borings required.

IN SITU RELATIVE DENSITY

The relative density is a significant liquefaction parameter for granular soils but perhaps one of the most difficult to obtain reliably. The determination of the density of loose cohesionless material below the water table is very difficult. Furthermore, a 10% error in absolute density measurements either in the field or in determination of maximum or minimum densities in the laboratory could mean a 30% error in relative density. Unfortunately, a 30% range in relative density can cover a range of liquefaction probability from "not probable" to "very probable."

The only direct method for determining field relative density at depths is through undisturbed samples. Data from Shannon-Wilson and Agbabian Associates (1972) (Figure 4-1a) show relative density of samples obtained by piston samples to have a scatter of 30% to 40%. This is considered typical of that obtained using the best sampling procedures. Relative density measured in the laboratory on undisturbed specimens should be used only to establish average trends rather than relying on individual measurements.

Penetration resistance tests are also used to determine *in situ* soil properties indirectly through experimental correlations. These tests are relatively simple and inexpensive. The resistance to penetration is generally measured using either static or dynamic cone penetrometers or drive sample spoons. The standard penetration test (ASTM Test
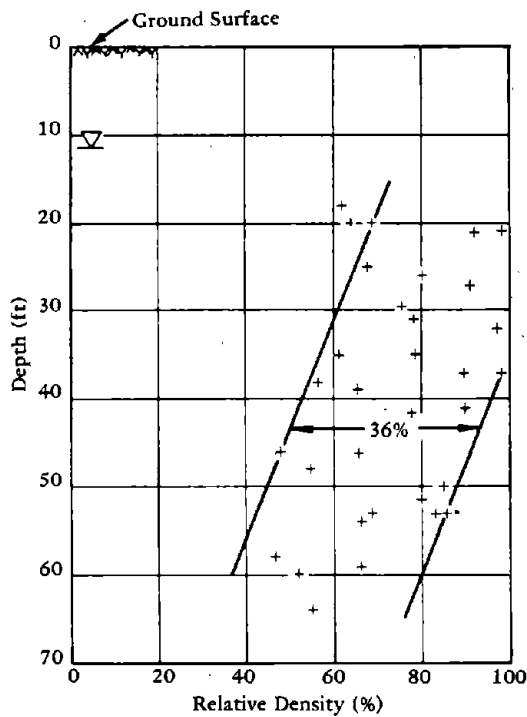
(a) Laboratory-determined relative density.
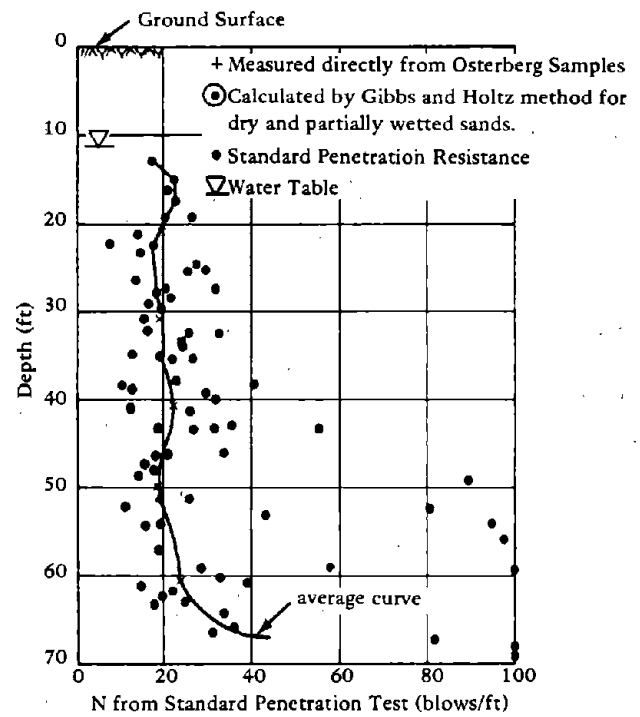
(b) Field standard penetration data.
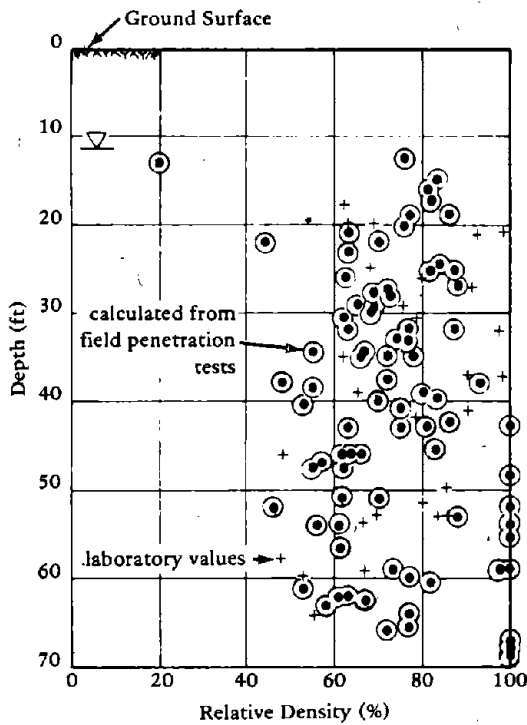
(c) Comparison of measured relative density with that based on the blow count.
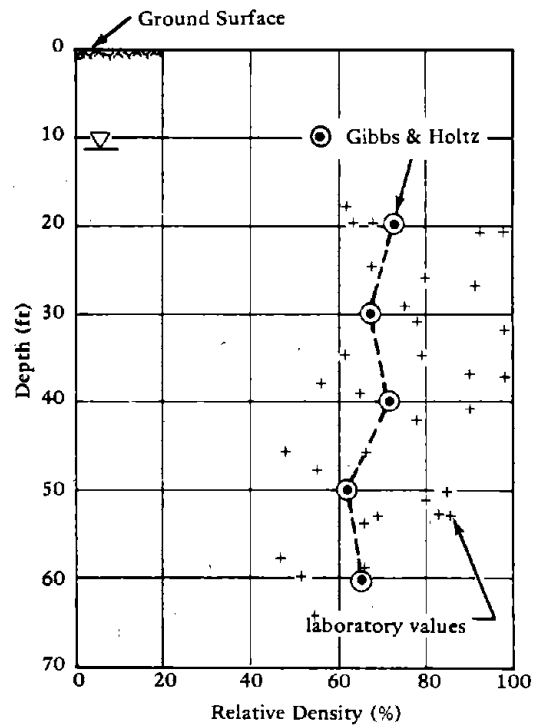
(d) Comparison of average penetration criteria and actual measured data.

Figure 4-1. Relative densities from field penetration tests and laboratory measurements (natural saturated deposit of medium dense, gray, fine to medium sand) (from Shannon-Wilson and Agbabian Associates, 1972).

114

D1586-70) is the most widely used on this continent. It consists of
determining the number of blows of a 140-pound hammer falling 30 inches
that are necessary to drive a 2-inch-diameter split spoon in a sample a
distance of 12 inches.

The most popular type of penetration test in Europe is the friction
cone test. This test, although not widely used in North America has
distinct advantages in that it not only gives an indication of the soil
resistance to point penetration, but also, by measuring the side friction
on a standard sleeve located above the cone, provides a method of distin-
guishing the soil type (for example, friction ratios of 0% to 2% indicate
gravel or clean sand while values over 5% indicate clay). The friction
cone has a cross-sectional area of 10 cm^2 and is inserted into the ground
at a constant velocity of 2 cm/s. The friction cone is sometimes corre-
lated with the standard penetration test by the relationship:

$$N = \frac{Q_c}{a}$$

where Q_c = static cone penetration resistance, kg/cm^2

      a = constant, varying from 2.5 to 8

      N = standard penetration value in blows per foot

The standard penetration test has also been correlated to dynamic cone
penetration (2-inch-diameter, 60-degree cone) by the relationship:

$$N = \frac{N_c}{b}$$

where N_c = dynamic cone penetration in blows per foot

      b = constant, usually 2.0

Gibbs and Holtz (1957) and others have developed correlations
between standard penetration resistance and relative density. Unfortu-
nately, there is only fair agreement between the various correlations;
however, the Gibbs and Holtz (1957) correlations are the most widely
accepted relationships (see Figure 4-2). Figure 4-1b from Shannon-
Wilson and Agbabian Associates (1972) shows standard penetration resis-
tance values for the same site as Figure 4-1a. The standard penetration
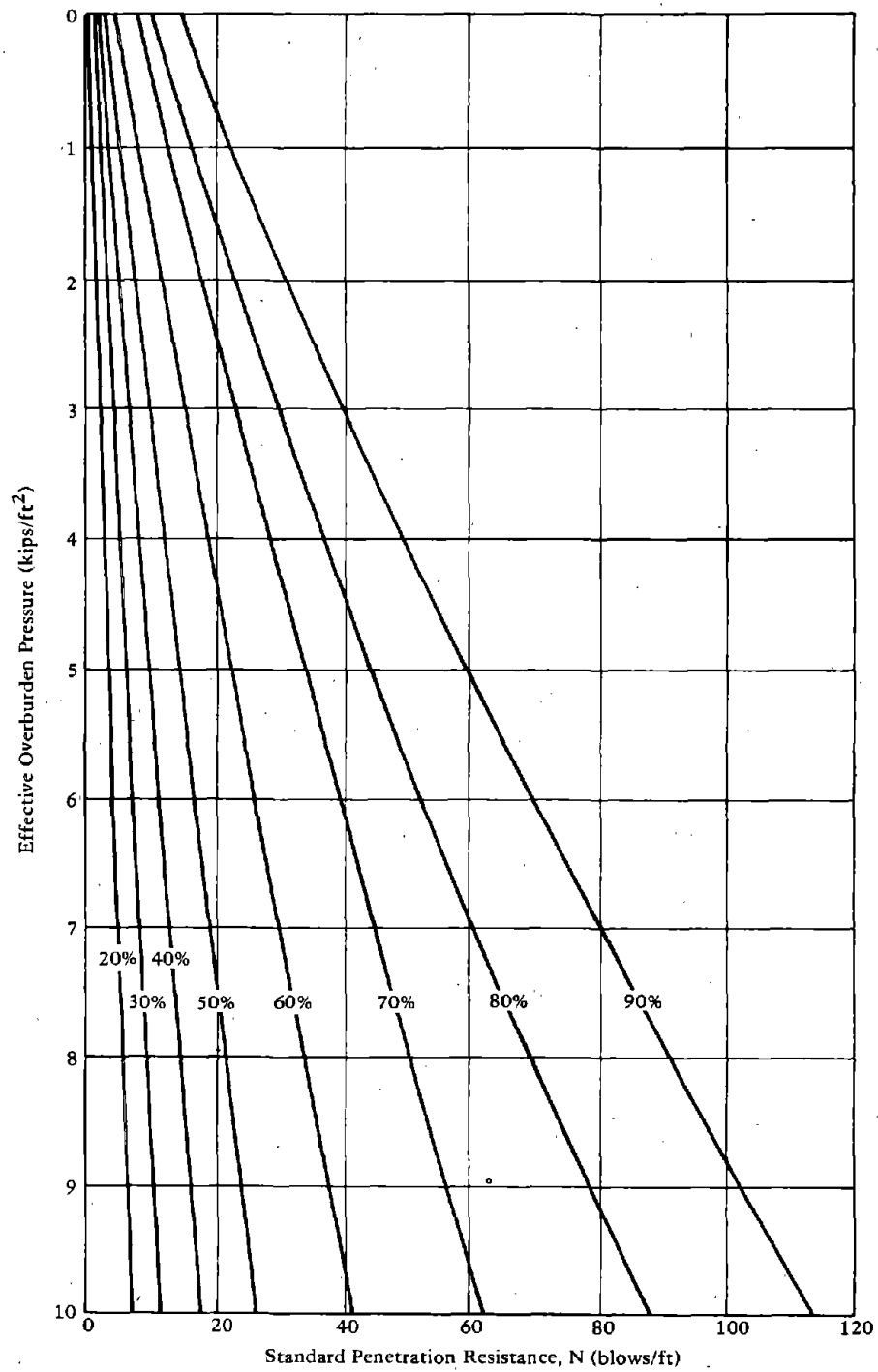
Figure 4-2. Relationship of standard penetration resistance, relative density and effective overburden pressure (from Shannon-Wilson and Agbabian Associates, 1972).

116

data of Figure 4-1b is converted to relative density using Figure 4-2 and is shown in 4-1c. Figure 4-1d shows a comparison between laboratory data and field data. The Gibbs and Holtz (1957) correlations produce average values slightly lower (more conservative) than the measured laboratory values. Recent work accomplished by Marcuson and Bieganowsky (1976) suggests use of the following:

$$D_r = 8.6 + 0.83 \left[\frac{N + 10.4 - 3.2 \ (OCR) - 0.25 \ (\sigma_v)}{0.0045} \right]^{1/2}$$

where   N   =   SPT N-value blow per foot

OCR   =   over consolidation ratio

σ_v =   vertical effective stress psi

D_r =   relative density percent

The overconsolidation ratio is meant to account for such items as structure, or partial orientation, etc. It may be estimated from site historical development. When no information is available the value of 1.00 should be used.

As pointed out previously, D_r has been used throughout this report to include factors other than density, such as structure, particle shape, and orientation, etc. which in turn, are largely influenced by past overconsolidation ratio.

Static cone penetrometer tests provide values of both point resistance and the resistance from side friction along a standard sleeve at increments of 20 cm.* Based on the ratio of side friction to point resistance, the type of material encountered can be estimated. Forrest and Ferritto (1976) have qualitatively found good agreement between the standard penetration test and the cone penetration test for several soil types.

GROUNDWATER LEVEL

The groundwater level enters into liquefaction analysis in two ways. The presence of ground water is required for development of pore pressures and the depth of the water table determines the effective

---

* A later development, known as the electric cone, is capable of giving continuous readings.

confining stress level (which influences the shear strength and the soil modulus and damping parameters). Sites which are susceptible to liquefaction typically have ground water tables within 10 feet of the surface. The level of the water table may be determined either from boring holes or by nondestructive test methods.

DEPTH OF BEDROCK

The depth of bedrock is of interest to liquefaction analysis since it affects response calculations, as shown in Chapter 3. The depth of bedrock affects the fundamental period of the overlying soil profile. Geophysical refraction surveys and nearby water or oil well drilling logs, if available, can be used to determine the depth to bedrock. For response analysis, bedrock is assumed when shear wave velocities exceed 2,500 ft/s.

SHEAR MODULUS

As discussed in Chapters 2 and 3, the shear modulus is required for the complex computer analysis methods to determine site response. Geophysical tests, surface vibrator tests, and plate bearing tests are also used and will be discussed in Chapter 5. A brief discussion of field methods used to determine values of shear modulus are presented here.

Geophysical Tests

This method consists of propagating low energy waves through a soil and measuring the wave velocity. Assuming an elastic medium, the elastic modulus can be related to the compression velocity and the shear modulus to the shear wave velocity. To determine a value of shear modulus by dilatational waves a value for Poisson's ratio must be assumed. The strain levels in the range of 10^{-4}% used in the geophysical methods are lower than the strain levels found in earthquakes.

Geophysical tests utilize a series of geophones and an energy source. Some combinations that are popular for determining shear wave velocity are: (1) cross hole technique in which an energy source is located in a drill hole and geophones located in other drill holes; (2) up-hole technique in which the energy source is in a drill hole, but the geophones are on the ground surface; and (3) down-hole techniques in which the geophones are in drill holes, and an energy source is at the

surface. The time of arrival of the shear wave traveling through the soil media from the energy source to the geophones is measured and the shear wave velocity determined. The more homogeneous and less stratified the soil deposit, the easier it is to delineate shear waves from compression waves.

Surface Vibrator Tests

A surface vibrator can be used to generate (surface) Rayleigh waves which, for small strains, have a velocity close to shear waves. Geophones on the ground surface are used to measure the wave length and compute the wave velocity. It is believed that the depth of soil through which the shear wave is propagating is approximately equal to $\lambda/2$ where λ is the measured wave length. By varying frequency, it is theoretically possible to investigate different depths of soil.

Plate Bearing Tests

The soil modulus can be determined by plate load tests by either measuring load deflection information or by resonant frequency of a small vibrator. This procedure, which requires estimation of Poisson's ratio, is not a practical test for liquefaction investigation in which the modulus at depth is required.

DAMPING

The damping value is also used in computer response calculations. Although it is theoretically possible to measure the damping in the field by observing the attenuation of wave motion, or the decay of vibration level, this has not proved practical. Laboratory tests as described in Chapter 5 currently provide the basis for damping estimates.

LATERAL K_o VALUE

It is extremely difficult to determine the lateral earth pressure in an *in situ* soil deposit; nevertheless this factor can exert a major influence on liquefaction potential (see Chapter 2).

One of several methods is that by Tahara, Takata, and Fukuoka (1960) who invented a device to measure the lateral K_o value in a drill hole. The device consists of a rubber tube which is inserted in the

hole and connected by pipe to pressure tanks with associated compressors. Water, under pressure, is increased in steps to the rubber tube in the hole and the pressure and volume change noted. Both static and dynamic K_0 values may be measured.

EXPLOSIVE TESTS

One of the attempts to study dynamic pore water pressures directly in the field was made by Kummeneje and Eide (1961), who conducted a series of blasting tests in marine deposits of sands and silts in Norway in order to estimate the probable danger of a flow slide occurring. Before blasting, a number of piezometers were installed at various depths in the ground at different distances from the explosive charge. Pore water pressures as high as 80% of the effective overburden pressure were recorded at a distance of 5.5 meters from the point of detonation.

Prakash and Gupta (1970) reported on the results of blast tests carried out in loose sand deposits in the bed of the Damodar River, India, where the stability of a 55-meter-high earthdam was in question. A piezometer embedded at a depth of 6 meters, 3 meters from the detonation point, registered a pore pressure equal to 80% of the effective overburden pressure.

The recordings of pore pressures in the above tests were not primary measurements but, rather, secondary measurements to monitor the amount of densification occurring due to the detonation. The pore pressures developed during blasting tests are hardly a good indicator of the liquefaction potential of a site during earthquakes because the duration of the vibrations caused by an explosion is very short compared to the duration of an earthquake. Another disadvantage of the blasting technique is that it cannot be performed in congested areas.

Yamamura and Koga (1974) conducted a series of tests in which dynamite was detonated in a borehole 4 to 8 meters deep. Accelerometers and pore pressure gauges were installed in boreholes in the surrounding ground. All the boreholes made for monitoring were back-filled with sand. The magnitude of settlement of wooden piles installed in the ground surface was measured before and after each explosion by use of a level. Estimation of ground liquefaction potential was made by noting the relation between shock pore water pressure and residual pore water pressure and the ground settlement rate.

REFERENCES, CHAPTER 4

Forrest, J. B. and Ferritto, J. M. (1976) An earthquake analysis of
the liquefaction potential at the Naval Air Station, North Island. Civil
Engineering Laboratory, Technical Report R-847. Port Hueneme, Calif.,
Sep 1976.

Gibbs, H. J. and Holtz, W. G. (1957) "Research on determining the
density of sand by spoon penetrator test," in Proceedings of Fourth
International Conference on Soil Mechanics and Foundations Engineering,
London, England, vol 1, 1957.

Kummeneje, O. and Eide, O. (1961) "Investigation of loose sand deposits
by blasting," in Proceedings of Fifth International Conference on Soil
Mechanics and Foundation Engineering, vol 1, 1961, pp 491-497.

Marcuson, W. and Bieganowsky, W. (1976) Laboratory standard penetration
tests on fine sands, ASCE Preprint 2752 (Liquefaction Problems in Geotech-
nical Engineering), American Society of Civil Engineers Annual Convention
and Exposition, Philadelphia, Pa., 27 Sep - 1 Oct 1976.

Prakash, S. and Gupta, M. K. (1970) "Blast tests at Tenughat Dam site,"
Journal of the Southeast Asian Society of Soil Engineering, vol 1, no. 1,
Jan 1970, pp 41-50.

Shannon-Wilson and Agbabian Associates (1972) Soil behavior under
earthquake loading conditions state-of-the-art evaluation of soil charac-
teristics for seismic response analysis. Seattle, Wash., Jan 1972.

Tahara, Y., Takata, T. and Fukuoka, M. (1960) "Some experimental
studies on the earthquake proof design of the foundation of bridge pier
in soft ground," in Proceedings of Second World Conference on Earthquake
Engineering, Tokyo and Kyoto, Japan, vol 1, 1960, pp 197-209.

Yamamura, K. and Koga, Y. (1974) "Estimation of liquefaction potential
by means of explosion test," in Proceedings of the Sixth Joint Meeting
of United States-Japan Panel on the Wind and Seismic Effect. Washington,
D. C., May 1974.

Chapter 5

LABORATORY INVESTIGATIONS

GENERAL

During the past three decades, considerable development has occurred in dynamic testing procedures for soils. The motivation for this was partly generated by the Department of Defense's necessity to design against the threat of nuclear weapons and was furthered by the requirement for more detailed soil characterizations for input into advanced computer code analysis. Following an increased awareness of the earthquake liquefaction hazard, largely as a result of the Niigata and Alaska earthquakes of 1964, dynamic testing procedures were applied to the specific evaluation of soil liquefaction under cyclic loads.

Laboratory investigations for evaluating the liquefaction potential existing in a particular field situation may fall within a broad range of complexity. Testing may be limited to simple index tests on disturbed samples of soil to confirm the type and broad nature of the *in situ* soils, or it may include dynamic or vibratory testing upon either reconstituted or carefully obtained field samples. It should be noted here that, where cohesionless soils particularly those beneath the water table (which is the case in liquefaction studies) are concerned, there is no such thing as a truly undisturbed sample, even when techniques such as *in situ* freezing are used. The term "undisturbed" is commonly applied where efforts are made to avoid severe agitation or "washing" of the soil samples such as by wash boring, etc. The term undisturbed is really applicable only to such cases as those involving hand trimmed samples of cohesive soils.

SOIL CLASSIFICATION AND INDEX PROPERTIES

Since liquefaction in the classic sense is limited to saturated cohesionless soils, index tests of major significance are as follows: Determination of plasticity to decide if liquefaction considerations are necessary (Atterberg Limits, ASTM D-423-66 and ASTM D-424-59), grain size analysis (ASTM D-422-63), and sensitivity. Structure or degree of cementation should be noted, at least in qualitative terms.

In situations where other than cohesionless materials are located, laboratory testing of all other soil types involved may be required for dynamic analysis of the geologic profile.

Assuming cohesionless soils are present, the most critical index property from a liquefaction standpoint is the *in situ* relative density. Thus, density determinations must be obtained, preferably from undisturbed samples if reasonably undisturbed samples have been obtained. In addition, values of maximum and minimum density must be determined for the soil material (ASTM D-2049-69; ASTM D-208-64T) in order that relative density may be calculated. Relative density is considered more significant than absolute density since it is a better indicator of the potential changes in volume that can occur under applied stresses and, hence, is a better measure of potential level of pore pressure generation and, therefore, liquefaction.

Having maximum, minimum, and in-place densities (or void ratios), the relative density may be computed from the following equation:

$$D_r \; (\%) \; = \; \frac{e_{max} - e}{e_{max} - e_{min}} \; \times \; 100 \; = \; \frac{\gamma_{max}(\gamma - \gamma_{min})}{\gamma(\gamma_{max} - \gamma_{min})} \; \times \; 100$$

In which,

D_r = relative density

γ_{max} and γ_{min} = maximum and minimum dry density

e_{max} and e_{min} = maximum and minimum void ratio

γ and e = natural (*in situ*) dry unit weight and void ratio

Although the influence of relative density on the liquefaction potential of homogeneous cohesionless soils has been very clearly established in the laboratory, this parameter is not readily applicable to the complex stratification generally encountered in the field. Typical field profiles consist not only of interbedded strata of different densities, but also of different grain sizes and soil types. What samples should be selected as representative of the profile being considered can pose a very difficult decision. Also, it is possible that the growth of liquefaction is related to interdrainage between zones of soil having different characteristics (Castro, 1975). Hence, a layer of average relative density could not be expected to simulate one made up of a series of varying layers. Even where uniform homogeneous materials are encountered, errors in determining the maximum and minimum density values for the soil can lead to amplified errors in calculations of relative density, in some cases up to 25% or more.

123

The ability of laboratory tests on saturated sands to provide the liquefaction potential *in situ* is based on the premise that (field) samples are representative of soil elements in the field as long as they are of the same relative density. Obviously, such factors as seismic history and fabric are important but are generally unknown or very difficult to evaluate in the field. Thus, the measurement of relative density is very important to proper evaluation of liquefaction. Tavenas (1971) has noted the following:

(1) The absolute error on the relative density due solely to the influence of the efforts on the minimum and maximum unit weights, as measured according to ASTM test procedures, varies between ±1.5% and ±4.5%. If different experimental procedures are used, the error may range from ±5% to ±20%.

(2) The minimum absolute error on the relative density determined under ideal conditions (say, on a triaxial test sample in the laboratory) ranges from ±4% to ±7%.

(3) The average absolute error on the relative density measured in the field by any convenient method is of the order of ±14%. This means that a relative density measured at 70% may actually be equal to anything between 56% and 85%.

Finn (1972) noted that errors of similar magnitude occur when the relative density is evaluated by correlation with standard penetration N-values. The standard deviation in any group of N-values has been evaluated at ±25%. As an example, if an average index N = 25 has been determined at a depth corresponding to an overburden pressure of 20 psi the use of the Gibbs and Holtz correlation would give D_r = 73%. If the standard deviation of both the correlation curve for 20 psi and the value of N are taken into account, D_r is given by 56% < D_r < 86%; this is not an extreme case. Tavenas (1971) concludes that:

(1) The strict use of the known correlations may be misleading and will probably give a wrong estimate of the *in situ* relative density.

(2) The correct use of these correlations, taking into account all sources of error, leads to a wide range of possible values of the relative density.

(3) The definition and use of the relative density concept should be thoroughly re-appraised to eliminate the significant absolute error affecting each measured value of this parameter.

(4) The use of the relative density in its actual form should be largely restricted to cases where no alternative is already available; i.e., where "undisturbed" samples are not available or cyclic testing is beyond the scope of the project investigation.

Where sophisticated analysis incorporating generation and dissipation of pore pressures are being considered, permeability measurements may be warranted, for use with such analytical tools as Apollo, see Chapter 7. Otherwise, a satisfactory estimate of permeability can generally be based upon the grain size analysis. Various other index property tests might be desirable for more detailed definition of the *in situ* soil, but these are not specifically associated with liquefaction analysis and will not be covered further herein.

DYNAMIC LOAD RESPONSE

Traditionally, soil reponse has been considered within two different contexts: the quasi-static stress-strain response in the volumetric mode (consolidation and settlement) and strength in the shearing mode (collapse or failure). As in the earlier work, where shear strength was considered the major criterion in soil performance, shear response has received the most attention in recent dynamic developments.

Volumetric response in the dynamic regime is generally accounted for merely by assuming some constant value of Poisson's ratio μ (although bulk modulus is sometimes used). For this reason, the parameters most commonly investigated for defining soil response under earthquake-type loadings have been the shear modulus, or modulus of rigidity G, and a damping factor λ to account for the energy dissipation and dispersion that takes place under dynamic loads. Since the induced-earthquake motions considered most significant to soil profile response are those caused by upward propagating horizontal shear waves, the dynamic testing procedures considered most pertinent concentrate upon techniques incorporating shear stress reversals.

The more complex computer analysis procedures for liquefaction evaluation presented in Chapter 3 require relationships to characterize stiffness and damping. Simple stiffness models may be elastic or strain-dependent elastic representations. More complex models for use with finite element computer programs may be nonlinear representations. For use in ground reponse calculations like SHAKE, which should be sufficient for almost all bridge investigations, the shear modulus and damping as shown in Figure 5-1 are required. The effective shear modulus of the soil is expressed as the equivalent secant modulus determined by the slope of a line passing through the end of the hysteresis cycle at the peak stress and strain after each cycle of load. This definition, rather than the tangent modulus, is used to be consistent with normal linear viscoelastic systems allowing for normal use of the damping rates.

vertical stress

$+\Delta\sigma_v$

$-\Delta\sigma_v$

compression

vertical strain

$B + \epsilon_v$

A

E

O

$-\epsilon_v$

B'

A'

tension

Damping ratio

$\lambda = \dfrac{1}{2\pi} \quad \dfrac{\text{Area of Hysteresis Loop}}{\text{Area of Triangle OAB \& OA'B'}}$

(b) Equivalent hysteretic stress–strain properties.

$\sigma_v + \Delta\sigma_v$

ϵ_v

σ_H

σ_v

σ_H

$\sigma_v - \Delta\sigma_v$

ϵ_v

ϵ_v and $\Delta\sigma_v$ can be measured
from triaxial test.
Then from theory of elasticity

$E = \Delta\sigma_v/\epsilon_v$

$G = E/2(1 + \mu)$

$\gamma = \epsilon_v(1 + \mu)$

(a) Triaxial test conditions.

Figure 5-1. State of stress for the triaxial properties test and the definition of equivalent linear modulus and hysteretic damping.

126

Assuming equivalent viscous damping, the damping ratio becomes:

$$\lambda = \frac{A_L}{4\pi A_T}$$

where A_T is the maximum energy stored under the stress-strain curve at maximum amplitude and A_L is the area enclosed by the hysteretic loop. As is apparent from Figure 5-1, values of shear modulus and damping are strongly dependent upon maximum dynamic shear strain amplitude (and to a lesser degree, load cycle number).

Various techniques are utilized to evaluate the dynamic response parameters of soils over a range of deformation magnitudes. Figure 5-2 shows the different strain levels investigated by various testing procedures and their relation to the strain levels experienced during earthquakes. The geophysical region in Figure 5-2a also applies to laboratory testing techniques in which dilatational and shear stress wave velocities are measured in test specimens.

SHEAR MODULUS

There are several test methods available to determine the dynamic shear modulus in the laboratory:

1. Cyclic triaxial

2. Cyclic simple shear

3. Cyclic torsional shear

4. Resonant column

5. Shake table

The triaxial test is one of the most widely used types of test for determining soil stiffness of strength properties while the others are usually found only in research laboratories. A major limitation of all laboratory testing is that truly undisturbed samples are difficult to obtain. In general, the greater the degree of sample disturbance, the lower the shear modulus and the higher the apparent damping that will be measured.
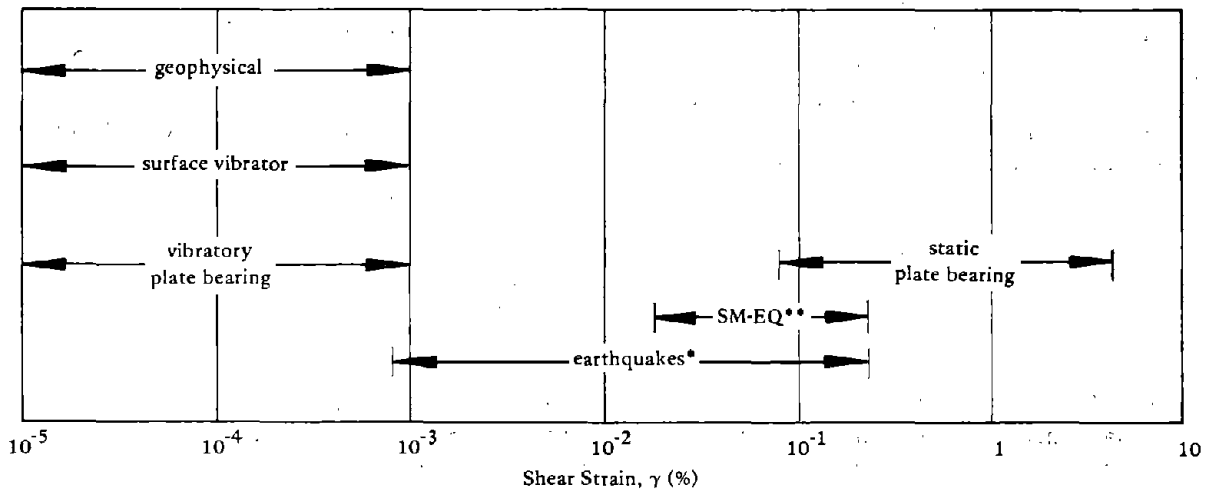
(a) Field tests.
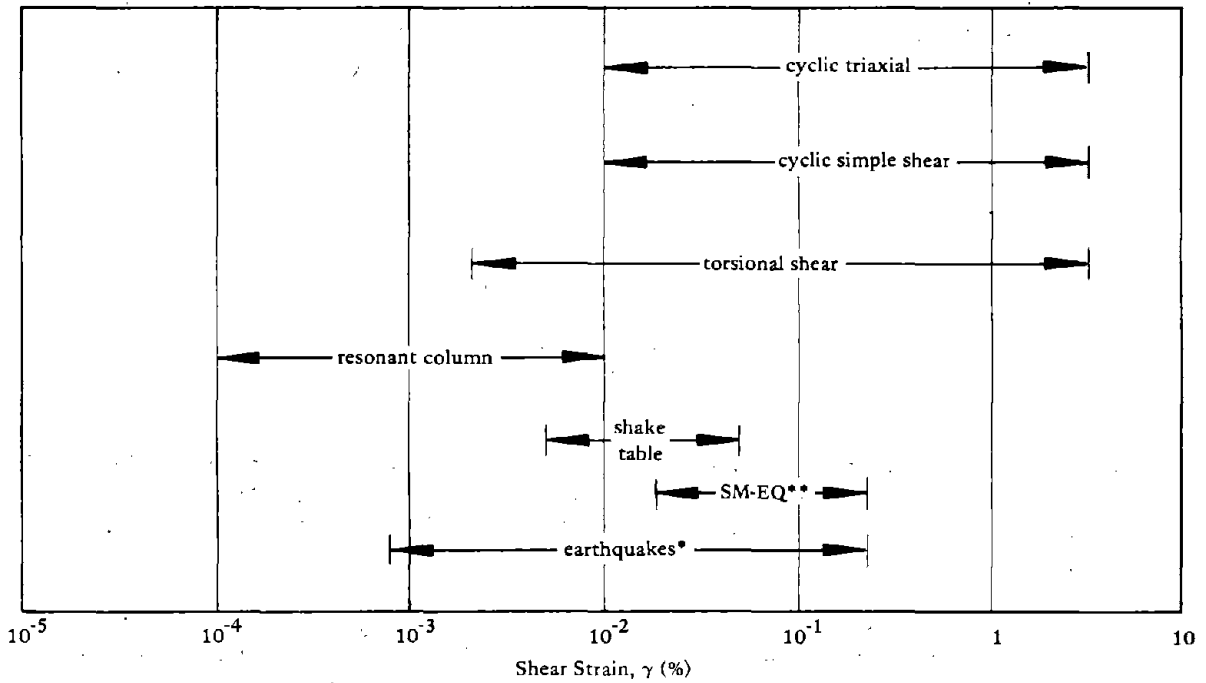
(b) Laboratory tests.

*Represents an extreme range for most earthquakes.

**Strong motion earthquakes.

Figure 5-2. Tests showing approximate strain ranges of test procedures (from Shannon-Wilson and Agbabian Associates, 1972).

The cyclic triaxial test may be conducted in a standard triaxial compression cylinder with a modified connection between the loading piston and the specimen loading cap to permit alternating tensile and compressive deviator vertical stress applications (see Seed and Lee, 1966). For values of shear modulus, the lateral strain amplitude may be measured, and the shear modulus calculated by the expression:

$$G = \frac{\Delta(\sigma_1 - \sigma_3)}{2[\Delta(\epsilon_1 - \epsilon_3)]}$$

where $\Delta(\sigma_1 - \sigma_3)$ is the alternating deviator stress (equal to one-half the maximum applied shear stress) and $\Delta(\epsilon_1 - \epsilon_3)$ is the maximum principal strain difference (maximum shear strain by elasticity theory).

Measurement of dynamic radial strain requires specialized equipment, such as strain gaged-cantilever sensors or radially oriented linear variable differential transformers (LVDTS). As a result, such techniques are not really suitable to liquefaction studies.

The value of Poisson's ratio, μ, may be assumed, and the secant shear modulus calculated by the elasticity formula:

$$G = \frac{E}{2(1 + \mu)}$$

where

$$E = \frac{\Delta(\sigma_1 - \sigma_3)}{\Delta\epsilon_1}$$

where $\Delta\epsilon$ is the alternating axial strain experienced by the soil specimen under the vertical deviator stress $\Delta(\sigma_1 - \sigma_3)$. The hysteretic curve in compression is generally used to calculate the damping coefficient as explained in Chapter 2.

When initially conceived, a change in confining stress (σ_3) with change in deviator stress was considered in the cyclic triaxial test to keep the average degree of confinement (total hydrostatic stress) constant. However, with saturated specimens this refinement contributes nothing since the applied total stresses are modified by the pore pressures generated. The triaxial test maintains its symmetry of applied shear stresses only by testing a specimen which is confined under isotropic confining stress. Upon each reversal of the direction of the deviator stress pulse, the shear stresses upon the planes of maximum shear stress (oriented at an angle of 45 degrees with the vertical axis) undergo a reversal in sign. The principal stresses undergo a 90-degree rotation

during a complete load cycle, and the intermediate principal stress (σ_2) alternates between the value of the minor principal stress during compression to the value of the major principal stress during an extension.

The foregoing does not represent the situation existing within the field, where the principal stress undergoes rotations that are generally less than 90 degrees and where the soil is initially under anistropic confining stresses. The degree of anisotropy is (with level ground) defined by the existing value of the coefficient of lateral earth pressure K_o.

Additional shortcomings of the triaxial test are those which apply also to most basic soils testing and include such items as sample end restraint, membrane indentation, disturbance, etc. The cyclic triaxial test in spite of its shortcomings is perhaps the most versatile and expedient test used in dynamic soil reponse evaluations.

Using the same equipment, the damping characteristics may be determined from the hysteretic stress-strain data. (The triaxial test may also be used to measure the bulk modulus of soils.)

The simple shear test was first developed by the Swedish Geotechnical Institute (Kjellman, 1951) to provide for a more realistic evaluation of the shear response of soil than that offered by either the direct shear test or triaxial testing procedures. This simple shear test was adapted by Peacock and Seed (1968), and Thiers and Seed (1968) to provide direct evaluation of dynamic shearing parameters for soil. In this test, the specimen is generally forced by means of rigid sidewalls to undergo uniform strain in simple shear throughout the height of the specimen. The specimen can be prepared under the anistropic stress conditions thought to represent actual *in situ* conditions and may be subjected to horizontal shear stresses or strains simulating those expected to occur in the actual soil strata under the design earthquake. Unfortunately, this type of apparatus also introduces stress and, consequently, strain irregularities (particularly near the corners of the specimen) that may lead to premature yielding.

Torsional shear testing techniques have been developed in order to reduce these stress concentration problems. With the use of hollow cylinder specimens it is at least theoretically possible to subject a specimen to a relatively uniformly distributed shear stress field while maintaining control over the normal stresses in three perpendicular directions. Relatively refined torsional test equipment has been developed by Hardin and Drnevich (1970). More recent developments of this nature have been reported by Ishibashi and Sherif (1974). The major disadvantage of this type of test is that hollow cylinder specimens are very difficult to obtain by undisturbed sampling techniques, and it is generally necessary to use reconstituted or remolded specimens.

130

In an attempt to avoid some of the boundary and size effects associated with testing small specimens, shake table experiments have been carried out (Maslov, 1957; Tanomoto, 1967; Yoshimi, 1967; Whitman, 1970; Kovacs, Seed and Chan, 1971; DeAlba, Chan and Seed, 1975). Initial procedures used free vibration techniques, but later test methods attempted to evaluate actual free field response to applied impulses. Although recent efforts have been made to provide realistic levels of confining pressure and sample drainage, one major problem remaining is that of providing sufficiently high inertia forces to the relatively small masses undergoing shaking.

Free and forced vibration testing techniques, based upon resonant column procedures, vibration attenuation rate, etc., were once very prominent types of dynamic testing for determining soil modulus and damping factors in particular. These tests, borrowed from other fields of mechanics such as mechanical vibrations, are less popular in the field of soil mechanics today. Procedures such as cyclic triaxial and simple shear tests are much more desirable in that they are capable of investigating strain levels of interest in the field. In addition, the soil parameters can be measured directly in the cyclic techniques rather than calculated, based upon theoretical assumptions regarding the influence of specimen geometry and energy attenuation. These vibration methods appear to provide higher stiffness and lower damping parameter values than cyclic tests, probably due to the smaller strain levels encountered.

LABORATORY TESTS TO EVALUATE LIQUEFACTION POTENTIAL

There are four types of laboratory tests available for measuring the liquefaction potential of a sand:

1. Cyclic triaxial

2. Cyclic simple shear

3. Cyclic torsional shear

4. Shake table

The stress ratio τ/σ_0' is commonly used to represent the combined effect of both static and cyclic stresses on liquefaction potential. The effective confining pressure in the field is taken as the vertical stress for purposes of expediency, since it can usually be determined with reasonable accuracy. The cyclic shear stress τ, to cause liquefaction in a given number of cycles N_L, has been noted to increase approximately linearly with the confining pressure. Thus, an undrained saturated

sand subjected to a specific stress ratio, $R = \tau/\sigma_o'$, should liquefy in cyclic loading tests in the same number of cycles N_L, irrespective of the initial confining stress values (at least within the range of interest for liquefaction studies).

The cyclic triaxial test was developed by Seed and Lee to study the factors controlling the liquefaction of a saturated sand under cyclic loading conditions. Because of its relative simplicity and the wide availability of the necessary equipment, it is still the most commonly used test. In this test a saturated cylindrical sample of sand is consolidated under an effective ambient pressure σ_3. All drainage is prevented, and the sample is then subjected to cycles of axial stress change $\pm\Delta\sigma_d$.

This loading procedure creates stress conditions on a plane at 45 degrees through the sample (these conditions are meant to correspond to those on horizontal planes under a level ground surface during an earthquake).

Data recorded by Finn (1972) during a typical stress-controlled cyclic triaxial test has been shown in Figure 2-5 (note that the pore water pressure increases during each cycle of loading). In the initial stages the rise in water pressure is fairly uniform but toward the end of the test the rate of development of pore water pressure increases rapidly. The final significant increase to values associated with liquefaction occurs over a few cycles of stress. A steady rise in pore water pressure together with pressure fluctuations in phase with the cyclic loading are noted.

The shear strains become appreciable only when the pore water pressure reaches about 60% of the effective overburden pressure. After this point they increase rapidly with continuing cyclic loading.

There are several theoretical objections to the suitability of a triaxial test for evaluating liquefaction potential in the field (DeAlba, Chan and Seed, 1975; Peacock and Seed, 1968; Finn, Pickering and Bransby, 1971).

1. To preserve symmetry of shearing, the ratio between vertical and horizontal principal stresses after consolidation must be kept at unity; $K_o = 1$, instead of a value of about 0.4, which is more typical of field conditions.

2. Deformations do not occur in plane strain, and the intermediate principal stress alternates between the maximum and minimum stress values.

132

3. The principal stresses rotate 90% during testing rather than the much smaller 30- to 40-degree range considered typical of field conditions (where the failure plane is generally considered to be the horizontal plane).

In spite of these shortcomings, cyclic loading triaxial test data can provide a useful basis for identifying those conditions in the field in which sands will liquefy during a given earthquake. The triaxial test can overestimate the shear strength as applied to field conditions and correction factors or modifications in interpretation, as discussed in Chapter 3, must be applied.

One problem in evaluating laboratory data is the difficulty in defining what degree of distress corresponds to failure in the field. With liquefaction testing, various criteria are used. These may be the number of cycles at which the pore pressure reaches the level of the confining pressure, even instantaneously (initial liquefaction), or some arbitrary degree of strain. It is important in specifying what constitutes failure to adopt a consistent criterion. With loose specimens, the number of cycles between initial distress and almost complete loss of strength may be very small but with stiffer soils, resistance to applied load may exist long after initial signs of increased strain level are observed. In these cases, whether one signifies failure as one-half the double strain amplitude or as maximum strain excursion from the base line, etc., can become very important here.

Various workers have performed dynamic triaxial shear tests on a saturated sand using loadings with various kinds of irregular time history resembling the histories which actually occur during an earthquake. In work reported by Ishihara and Yasuda (1974) the maximum stress required to cause liquefaction was compared with the similar amplitude determined from tests in which the sand was subjected to 20 cycles of uniform amplitude loading. It was found that for the case of shock loading, defined as a loading in which the maximum stress builds up in a few cycles, the corresponding 20-cycle failure amplitude ranges between 47% and 61% of the maximum stress of the irregular load. The corresponding ratio for the case when the stress builds up more slowly is in the range of 56% to 65%. This work shows the differences between conventional constant amplitude cyclical tests usually performed and the irregular dynamic loadings expected in an earthquake.

TRIAXIAL TEST PROCEDURE FOR LIQUEFACTION EVALUATION

As stated above, triaxial test equipment is the most commonly used equipment for evaluating dynamic soil properties. Since most soil laboratories utilize this type of test, it is probably the most appropriate for bridge site liquefaction evaluations discussed herein.

133

The test may be either stress-controlled or strain-controlled. Stress-controlled cyclic triaxial tests have been used to evaluate liquefaction by applying a constant peak cyclic deviator stress and noting the number of cycles to cause liquefaction. Ratios of shear stress to confining stress may be determined and plotted against the number of cycles to some degree of distortion or to either response level.

Dynamic cyclic strain-controlled tests, in which the specimen's vertical deformation is controlled rather than the deviator stress, may also be used. For this type of test, it is the reduction in stress at constant strain amplitude rather than the increase in strain at constant stress level that is of interest. This type of cyclic triaxial test is frequently used to determine stress-strain properties. The constant strain hysteretic loading cycle may be used to determine equivalent linear modulus and damping. In a strain-controlled cyclic test, the rate of pore water pressure developed is dependent on the magnitude of the strain amplitude, as it is dependent on the magnitude of stress in a stress-controlled test. However, in strain-controlled tests, the cyclic load levels drop off as the sample undergoes increased cycles. Silver and Park (1975) have developed a procedure extending strain-controlled tests for dynamic stress-strain properties to predict liquefaction potential at the same time, thus providing a more complete picture of dynamic soil behavior. They indicate little difference between strain-controlled tests and stress-controlled tests. Fresh specimens should be used at each strain level because of the effects of previous history.

Silver and Park (1975) conducted a series of tests using two types of sands at a relative density of 60% and a confining stress of 2,000 psf. All of the tests were done on remolded specimens. Two methods of specimen preparation were used: (1) dry vibration in which a preweighed amount of dry sand was poured in layers into a membrane-lined mold and (2) wet rodding in which a preweighed amount of moist sand was placed in layers in a membrane-lined mold and compacted by hand-tamping.

Stress-controlled test results (Figure 5-3) showed that samples prepared using different methods exhibit significantly different resistance to liquefaction in dynamic triaxial strength tests (much more information along these lines is presented by Mulilis, Chan and Seed, 1975). It may also be noted that only a few cycles separate the initial liquefaction and 10% strain. The pore pressure in a stress-controlled test increases uniformly until the pore water pressure ratio equals about 0.5. Thereafter, the excess pore water pressure increases rapidly in only a few cycles until the point of initial liquefaction.
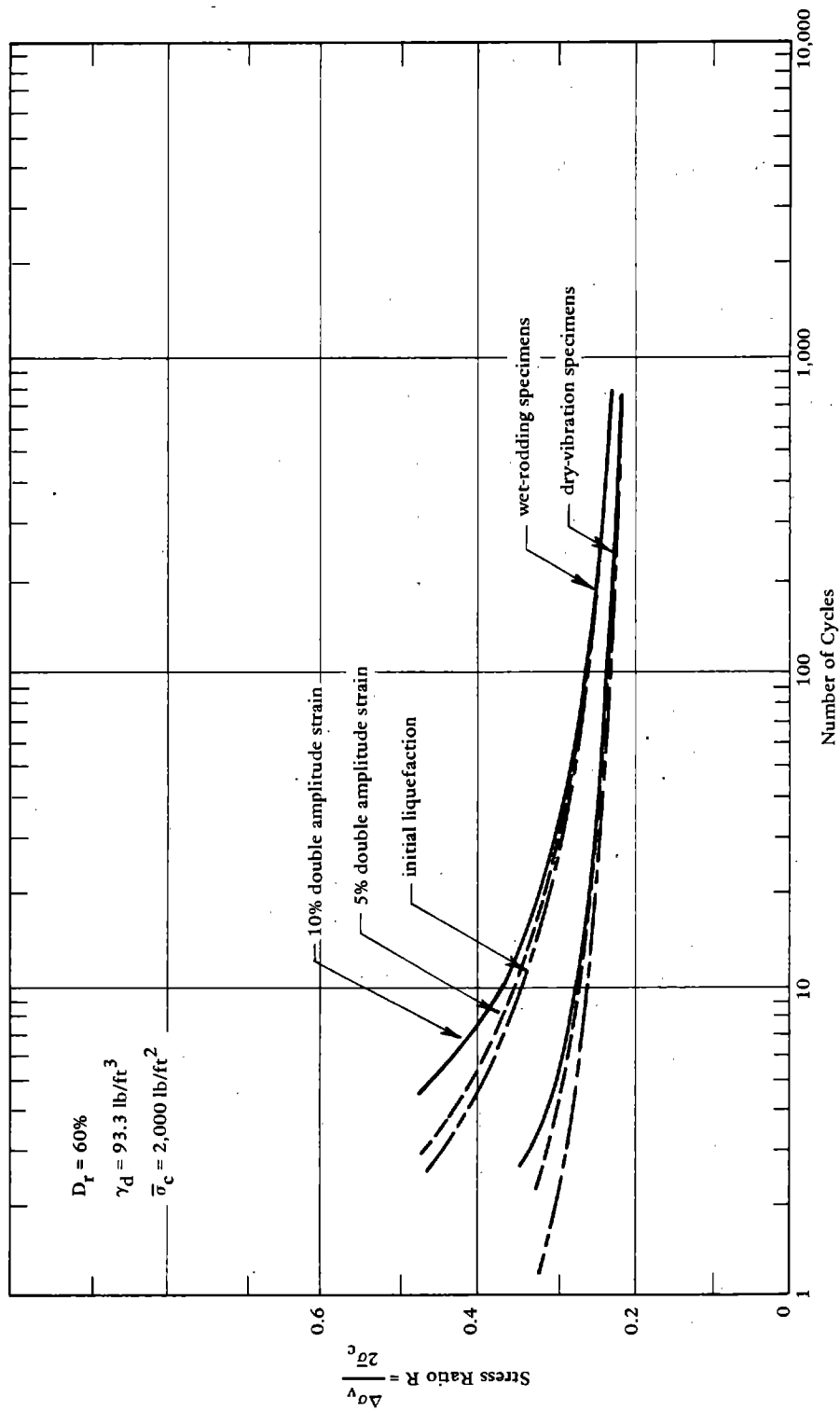
134

Figure 5-3. Summary and comparison of the triaxial liquefaction potential of medium-dense sand specimens prepared by wet-rodding and dry-vibration methods (from "Liquefaction Potential Evaluated from Cyclic Strain-Controlled Properties Tests on Sands," by M. L. Silver and T. K. Park, in Journal of the Geotechnical Engineering Division, ASCE, vol. 101., no. GT10, Oct 1975).

135

A series of strain-controlled tests was also performed by Silver and Park (1975) from which it was noted that the shear modulus values for wet-rodded specimens were much greater than the values for the dry vibration prepared specimens. This is consistent with the cyclic strength difference in Figure 5-3. This demonstrates the need for controlling specimen preparation techniques. There was no significant difference between damping values for samples prepared by either method. In strain-controlled tests the hysteresis loops showed the stress-strain relationship for the saturated sand became progressively flatter with increasing numbers of cycles. It was also noted that the pore water generated more rapidly as the strain levels increased. The excess pore water pressures were generated more rapidly in specimens prepared by dry vibration than in wet-rodded specimens. In stress-controlled tests, it was noted that the pore water pressure increased rather rapidly immediately prior to failure. In strain-controlled tests, the applied stress state is considerably different and the pore water pressure was noted to increase gradually and uniformly. The stress-controlled liquefaction test load form causes the weakened specimen to rapidly deform, inducing high pore water pressures, while the strain-controlled displacement loading induces a fall-off in generated load as the soil weakens. Silver and Park (1975) reasoned that the pore pressure response in both strain- and stress-controlled tests is similar up to a pore pressure ratio of 0.5 and since, for loose to medium-dense sands, large strains occur only a few cycles after the 0.5 pore pressure ratio is reached, it should be possible to use induced pore pressure in strain-controlled tests to predict liquefaction. Values of the cyclic vertical stress were plotted in terms of the stress ratio R versus the constant cyclic vertical strain (Figures 5-4 and 5-5). It may be noted that soil resistance to load reaches a maximum value for a given number of cycles and falls off with increased strain. This behavior implies that the specimen may be weakened critically when subject to the high pore water pressure generated by straining to high amplitude. Figures 5-4 and 5-5 also show the relationship between stress ratio and normalized pore water pressure. It is significant to note that when the stress ratio reaches its maximum value at some strain amplitude for any given number of strain cycles, the peak pore pressure ratio always approaches a value of about 0.5. For example, in Figure 5-4a for cycle 10, the maximum stress ratio is 0.35 at a strain of 0.09% which corresponds to a peak pressure ratio of 0.5 from Figure 5-4b. Each maximum value of stress ratio will determine the dynamic strength of the soil in a given number of cycles. Silver and Park (1975) compared the values of stress ratio from strain-controlled tests and have found good agreement. Thus, the soil strength determined by the peak stress ratio for a given number of cycles during strain-controlled tests gives a good measure of initial liquefaction for loose to medium-dense cohesionless soils. In Table 5-1 Silver and Park present a guide for selecting the number of cycles to be added to the number of cycles for initial liquefaction to determine the number of cycles to 5% and 10% double-amplitude strain.

136
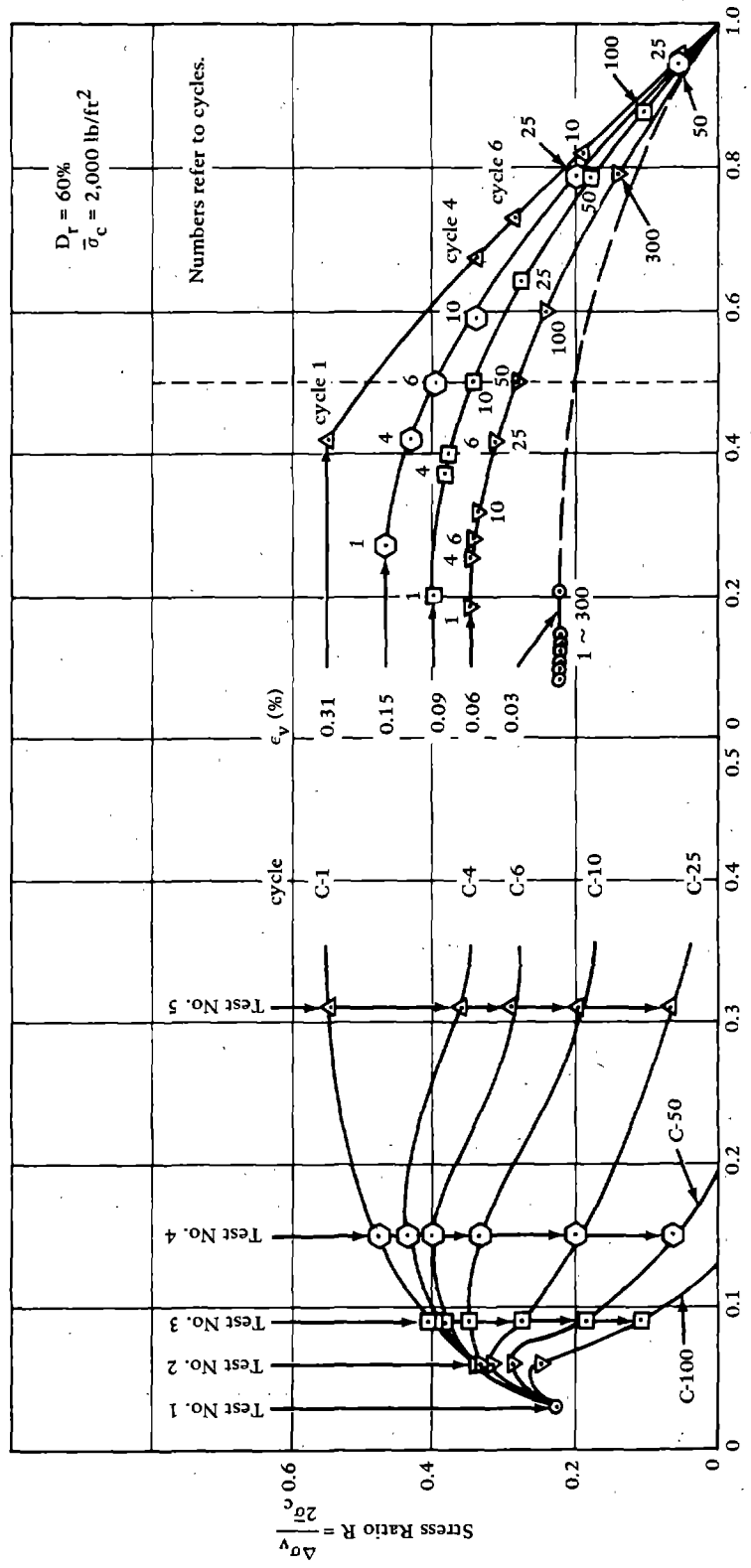
(a) Single amplitude vertical strain ϵ_v.

(b) Normalized pore water pressure $\dfrac{\Delta U}{\bar{\sigma}_c}$.

Figure 5-4. Cyclic vertical stress-strain relationship and cyclic vertical stress-excess pore water pressure relationship for samples prepared using the wet-rodding method (from "Liquefaction Potential Evaluated from Cyclic Strain-Controlled Properties Tests on Sands," by M. L. Silver and T. K. Park, in Journal of the Geotechnical Engineering Division, ASCE, vol. 101, no. GT10, Oct 1975).

137
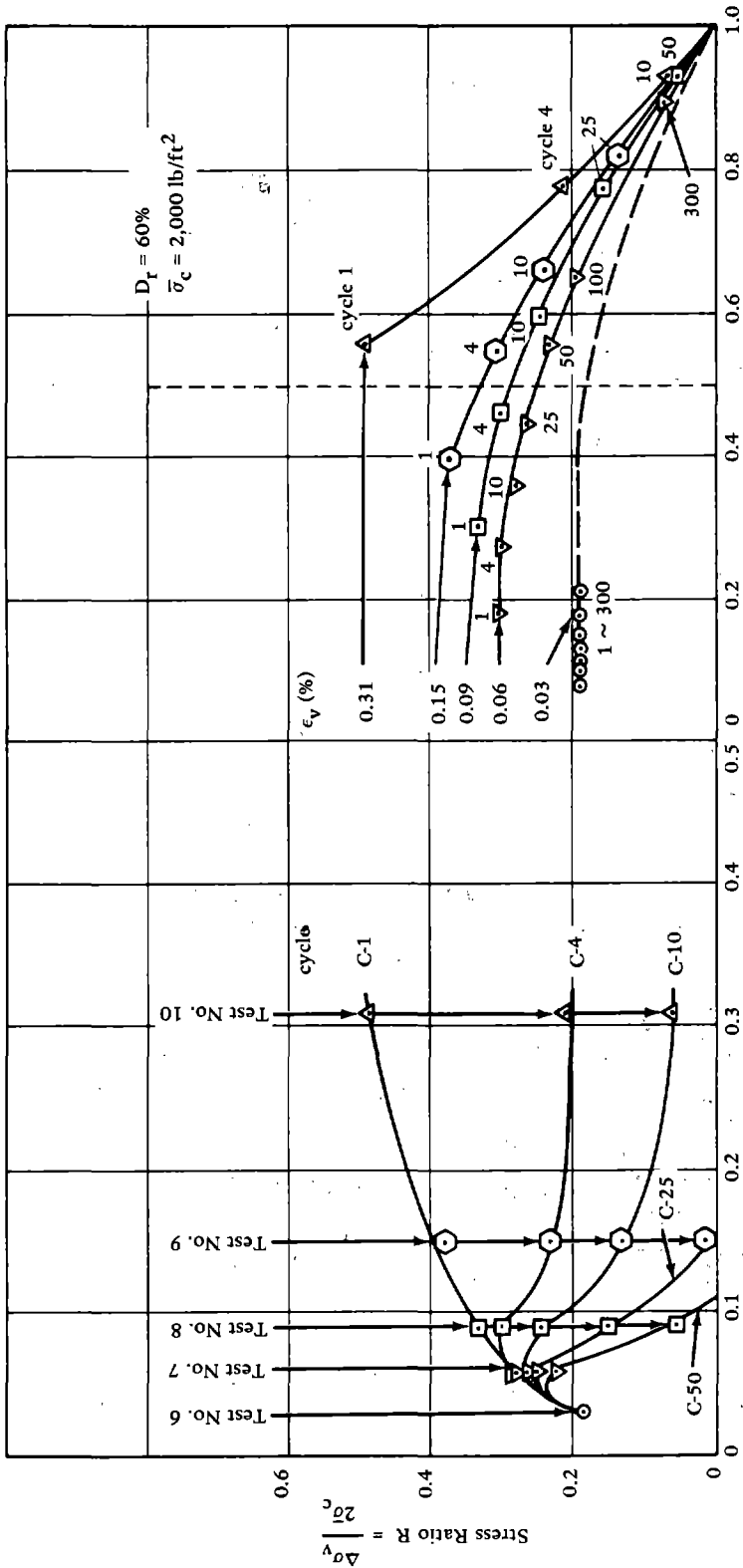
(a) Simple amplitude vertical strain.　　(b) Normalized pore water pressure.

Figure 5-5.　Cyclic vertical stress-strain relationship and cyclic vertical stress-excess pore water pressure relationship for samples prepared using the dry vibration method (from "Liquefaction Potential Evaluated from Cyclic Strain-Controlled Properties Tests on Sands," by M. L. Silver and T. K. Park, in Journal of the Geotechnical Engineering Division, ASCE, vol. 101, no. GT10, Oct 1975).

Table 5-1. Typical Relationship Between the Number of Cycles
to Initial Liquefaction and 5% and 10% Double Amplitude
Strain for Loose to Medium-Dense Sand

(From "Liquefaction Potential Evaluated From Cyclic Strain-
Controlled Properties Tests on Sands," by M. L. Silver and
T. K. Park, in Journal of the Geotechnical Engineering
Division, ASCE, vol 101, no. GT10, Oct 1975.)

| Sand Description | Relative Density (%) | Additional Cycles After Initial Liquefaction | |
		To 5% Double-Amplitude Strain	To 10% Double-Amplitude Strain
Loose	15 to 35	1 to 2	1 to 3
Medium Medium-dense	35 to 65 65 to 75	1 to 3	2 to 5

Silver and Park (1975) propose the following procedure to evaluate liquefaction potential from strain-controlled dynamic triaxial tests:

1. Perform a series of strain-controlled cyclic triaxial tests. Use fresh specimens for each test when strains are greater than about 0.1%.

2. Construct a stress-strain diagram in terms of the initial stress ratio and the vertical strain. Draw curves connecting values of stress ratio for the same number of cycles measured in each different test (Figures 5-4 and 5-5).

3. Obtain the maximum stress ratio value from this diagram for each given number of cycles.

4. Define the initial liquefaction curve by plotting values of the maximum stress ratio versus the corresponding numbers of cycles from Step 3.

5. Estimate the number of cycles to 5% and 10% double-amplitude strain from Table 5-1.

Since the maximum value of stress ratio developed at some strain level in strain-controlled tests for any given number of cycles is the same stress ratio and the same number of cycles developed when the peak pore pressure ratio reaches 0.5 during the test, the following simplified procedure for evaluating initial liquefaction potential from strain-controlled tests is suggested:

1. Perform a series of strain-controlled cyclic triaxial tests. Use fresh samples for each test at strain levels greater than about 0.1%.

2. Determine the number of cycles required for the excess pore water pressure to reach half of the effective confining pressure for each test.

3. Measure the vertical cyclic load and calculate the stress ratio developed at the cycle number obtained in Step 2 for each test.

4. Define the initial liquefaction strength curve by plotting values of stress ratio versus the corresponding numbers of cycles obtained in Step 3.

5. Estimate the number of cycles to 5% and 10% double amplitude strain from Table 5-1.

It should be noted that strain-controlled tests are not normally conducted for liquefaction studies. This procedure has been treated in some detail above because it combines the capability of combining a testing technique for soil parameter evaluation with liquefaction determinations.

OTHER TESTS FOR LIQUEFACTION

The remaining tests — the simple shear test, the torsional shear test and the shake table test — are generally limited to research at the present time because of the unavailability of the equipment except at a few laboratories. Hence, their present application to bridge site liquefaction analysis is limited. Finn (1972) describes and compares the tests in more detail.

Simple Shear Test

The cyclic simple shear test as developed by Peacock and Seed (1968) use samples of rectangular cross sections which are consolidated under an effective vertical pressure. Lateral deformation is prevented

during consolidation. A cyclic horizontal shear stress is then applied to the sample. This test appears to duplicate field stress conditions more closely than the triaxial test. Differences in estimates of liquefaction potential that exist depend on the type and stiffness of the side walls of the apparatus. Sample preparation is of major importance.

Torsional Shear Test

A triaxial torsion shear apparatus has been used by Ishihara and Li (1972) which permits cylindrical sand specimens to be consolidated at various values of K_c and sheared by cyclic torsional shear stress.

Shake Table Test

Shake tables provide a direct method for creating liquefaction under simple shear loading. However, a number of factors complicate the procedure, such as sample placement, sample confinement, realistic overburden and shear stress levels, and the deformation characteristics of the container. The number and location of a sufficient number of pressure and displacement instruments is important to provide an understanding of the test results.

REFERENCES, CHAPTER 5

Castro, G. (1975) "Liquefaction and cyclic mobility of saturated sands," Journal of the Geotechnical Division, ASCE, vol 101, no. GT6, Jun 1975.

DeAlba, P., Chan, C. K. and Seed, H. B. (1975) Determination of soil liquefaction characteristics by large-scale laboratory tests, University of California, Earthquake Engineering Research Center, EERC Report No. 75-14. Berkeley, Calif., May 1975.

Finn, W. D. L. (1972) "Soil dynamics liquefaction of sands," in Proceedings of the International Conference on Microzonation for Safer Construction Research and Application, Seattle, Wash., 30 Oct - 3 Nov 1972. Seattle, Wash., National Science Foundation, 1972.

Finn, W. D. L., et al. (1971) "Sand liquefaction in triaxial and simple shear tests," Journal of the Soil Mechanics and Foundations Division, ASCE, vol 97, no. SM4, Apr 1971. (Proceedings Paper 8039)

Hardin, B. O. and Drnevich, V. P. (1970) Shear modulus and damping in soils, University of Kentucky, College of Engineering, Technical Report 26-70-CE-2 (Soil Mechanics Series no. 2). Lexington, Ky., Jul 1970.

Ishibashi, I. and Sherif, M. A. (1974) "Soil liquefaction by torsional simple shear device," Journal of the Geotechnical Engineering Division, ASCE, vol 100, no. GT8, Aug 1974. (Proceedings Paper 10752)

Ishihara, K. and Li, S. (1972) "Liquefaction of saturated sand in triaxial torsion shear test," Soils and Foundations (Japan), vol 12, No. 3, Jun 1972, pp 19-30.

Ishihara, K. and Yasuda, S. (1974) "Sand liquefaction under random earthquake loading condition," in Proceedings of Fifth World Conference on Earthquake Engineering, Rome, Italy, Jun 1973. Rome, Italy, International Association for Earthquake Engineering, Apr 1974.

Kjellman, R. (1951) "Testing the shear strength of clay in Sweden" Geotechnique, vol 2, no. 3, Jun 1951, pp 225-235.

Kovacs, W. D., Seed, H. B. and Chan, C. K. (1971) "Dynamic moduli and damping ratios for a soft clay," Journal of the Soil Mechanics and Foundations Division, ASCE, vol 97, no. SM1, Jan 1971, pp 59-75.

Maslov, N. M. (1958) "Questions of seismic stability of submerged sandy foundations and structures," in Proceedings of Fourth International Conference of Soil Mechanics and Foundation Engineering, vol 1, London, England, 1957. London, England, Butterworths Scientific Publications, 1958, pp 368-373.

Mulilis, J. P., Chan, C. K. and Seed, H. B. (1975) The effects of method of sample preparation on the cyclic stress-strain behavior of sands, University of California, Earthquake Engineering Research Center, EERC Report No. 75-18. Berkeley, Calif., July 1975.

Peacock, W. H. and Seed, H. B. (1968) "Sand liquefaction under cyclic loading simple shear conditions," Journal of the Soil Mechanics and Foundation Division, ASCE, vol 94, no. SM3, May 1968, pp 689-708.

Seed, H. B. and Lee, K. L. (1966) "Liquefaction of saturated sands under seismic loading," Journal of Soil Mechanics and Foundations Division, ASCE, vol 92, no. SM5, Sep 1966, pp 1199-1218.

Shannon-Wilson and Agbabian-Jacobsen Associates (1972) Soil behavior under earthquake loading conditions. Seattle, Wash., Jan 1972.

Silver, M. L. and Park, T. K. (1975) "Liquefaction potential evaluated from cyclic strain-controlled properties tests on sands," Journal of the Geotechnical Engineering Division, ASCE, vol 101, no. GT10, Oct 1975.

Tanomoto, K. (1967) "Liquefaction of sand layer subjected to shock and vibratory loads," in Proceedings of Third Asian Regional Conference on Soil Mechanics and Foundation Engineering, vol 1, Haifa, Israel, Sep 1967. Haifa, Israel, Israel Society of Soil Mechanics and Foundation Engineering, Jerusalem Academic Press, 1968, pp 362-365.

Tavenas, F. A. (1971) "Discussion of 'The standard penetration test,' by Victor F. B. DeMello," in Proceedings of Fourth Pan American Conference on Soil Mechanics and Foundation Engineering, San Juan, Puerto Rico, vol 3. New York, N.Y., ASCE, 1971, pp 64-69.

Thiers, G. R. and Seed, H. B. (1968) "Cyclic stress-strain characteristics of clay," Journal of the Soil Mechanics and Foundations Division, ASCE, vol 94, no. SM2, Mar 1968, pp 555-569.

Whitman, R. V. (1970) Summary of results from shaking table tests at University of Chile, using medium sands; Progress report no. 9: Effect of local soil conditions under earthquake damage, Massachusetts Institute of Technology, Department of Civil Engineering, Research Report R70-25, Soils Publication No. 258. Cambridge, Mass., May 1970.

Yoshimi, Y. (1967) "An experimental study of liquefaction of saturated sands," Soils and Foundations (Japan), vol 7, no. 2, Mar 1967, pp 20-32.

Chapter 6

SEISMIC MOTION AND DESIGN EARTHQUAKE

GENERAL

Chapter 3 described various methods of analysis of the liquefaction potential of a site. All methods require expected ground motion at the site, which may be characterized by peak acceleration, duration, and predominant period. A time history of motion is required for the complex computer analysis procedure. A variety of procedures exist to evaluate ground motion; unfortunately, it has not been clearly demonstrated that any one method is better than the rest. This chapter will present a discussion of the earthquake motion and of the methods for determining site acceleration values.

GEOLOGIC FAULTS AND EARTHQUAKES

Since the San Francisco earthquake of 1906 and the subsequent pioneering work on the elastic rebound theory of earthquakes, there has been general agreement on the close relationship between earthquakes and geologic faults. Most tectonic earthquakes of the type that cause major structural damage are associated with fracture on a fault. Earthquakes are assumed to occur when the strength of the rock can no longer withstand stress that has built up, which is attributed to plate motion. Fault plane solutions and earthquake mechanism studies have contributed to a consistent picture of the earthquake generation process which satisfactorily explains most of the observed facts.

Some misunderstandings have occurred — and perhaps some significant differences of opinion — about the direct relationship between geologic faults and the earthquake hazard. Experience dating from 1906 has shown that ground shaking is not necessarily at a maximum in the immediate vicinity of the causative fault (Hudson, 1972). More often than not, the maximum ground shaking is observed to be some miles from the fault, as can be explained by a number of the features of the generation and propagation of seismic waves. Classical photographs of the 1906 major

movements along the San Andreas fault, for example, show horizontal surface displacements of as much as 15 feet passing several feet from a small wood-frame house that received no significant damage. Similarly, during the San Fernando earthquake of February 9, 1971, a 5-foot vertical fault scarp passed directly through a wooden barn just a few hundred feet from a single-story residence. The barn was severely damaged, but no significant structural damage to the house was noted (Hudson, 1972). The San Fernando earthquake also furnished numerous examples of surface faulting passing through heavily populated areas. Although severe structural deformation, with a resulting economic loss, occurred in numerous cases, catastrophic collapses leading to loss of life and serious injury were not directly associated with these surface breaks. Hazardous collapses were in all cases the consequence of severe ground shaking, which is pervasive over a large area and is not limited to the vicinity of faults.

The focus or hypocenter is the point within the earth's crust where the initial rupture occurs and from which the first waves are released. The projection of this point to the ground surface is the epicenter. The epicenter and hypocenter do not necessarily indicate the center of total energy release of the earthquake but rather the point where the seismic energy waves were first created. For small earthquakes the center of total energy release and the epicenter cannot be far apart because the fault break length is short; however, this is not the case for large earthquakes. The majority of earthquakes in the United States have had relatively shallow focal depths (10 to 40 km). In California, earthquakes have occurred in regions where surface fault patterns were clearly visible. However, in the Puget Sound area and in many parts of the eastern United States earthquakes are focused at deeper locations within the earth's crust so that a surface rupture is not observable (Bolt, 1970; Newmark and Rosenblueth, 1971). Figure 6-1 shows common surface fault types.

Surface faults can be identified and the recurrence of faulting determined by the geologic age of the soil layers displaced. Displaced Pleistocene age deposits would indicate that movement has taken place in the last 10,000 years to 3 million years. Displacements of Holocene age deposits would indicate more recent movement.

A fault undergoing tectonic creep or one with abrupt displacement causes changes in the terrain it crosses. Very distinctive patterns are produced where active faults cross streams, such as landslides. The ongoing geologic process causes scarps, trenches, sag ponds and stream offsets. Figure 6-2 shows a landform with an active fault (Wesson, et al., 1975).
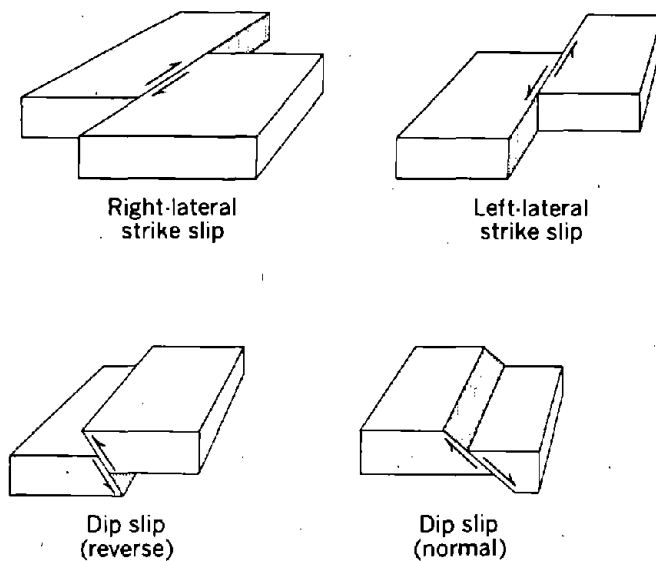
Figure 6-1. Four types of fault movement (after
U. S. Geological Survey).

Estimates of the maximum size and frequency of earthquakes on a
fault are based on (1) the geologically determined slip rate and the
historic record of ground deformation, (2) the seismic history of the
fault and surrounding tectonic region, (3) a geological evaluation of
the tectonic setting, and (4) empirically derived relationships between
earthquake magnitude and fault length.

GEOLOGICAL, SEISMOLOGICAL, AND SOILS INVESTIGATIONS

The objective of the geological investigation is to establish the
lithology, stratigraphy, structure, and history of the general region.
Tectonic structures underlying the region must be identified, and any
evidence of fault activity determined. The seismological investigation
complies a listing of all earthquakes of record which may have affected
the general area of the site. The magnitude of the earthquakes, epicenter
locations, dynamic characteristics, and durations of the resulting
ground motion are determined. Epicenters within about 200 miles of the
proposed site are of particular significance. Geological fault structures
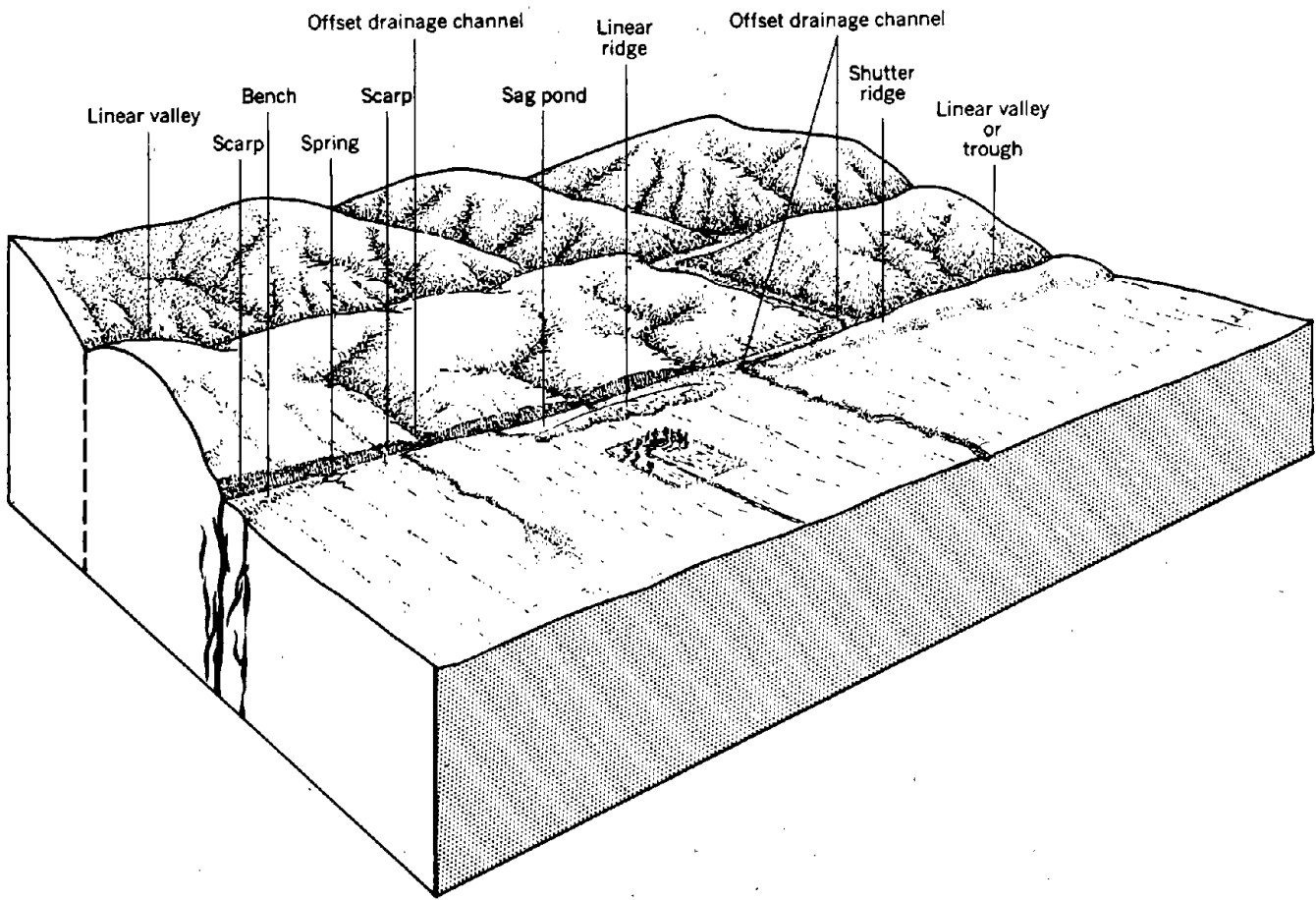within this approximate radius should be studied.

Figure 6-2. Landforms developed along recently active
strike-slip faults (after U. S. Geological Survey).

The information required includes identification and delineation of those faults that are active; that is, capable of generating earthquakes. Information about recency of faulting is useful in designating particular faults as active for specific land uses. Designation of a fault as active can be based on the assumption that the more recent the faulting the more likely that the fault will undergo intermittent displacement in the geologically near future. Movement is presumed less likely to occur along faults that have progressively longer periods of demonstrated quiescence. Because of the apparent great range in frequency of movement, there is no agreement at present on the length of geologic time pertinent to evaluation of the near-future behavior of faults. Selection of the timespan used to designate faults as active from age of latest movement has been influenced by the potential consequence of seismic shaking of surface faulting on the specific structure. The greater the risk to be incurred, the longer the timspan that must be considered. Displacement during Holocene time (the past 11,000 years) is a generally accepted criterion of activity for many land uses. This timespan is probably inadequate, however, to assure recognition of all active faults. Historic offsets have occurred along faults, such as the White Wolf fault in southern California, that had no previously recognized evidence of Holocene faulting. Wentworth and Yerkes (1971) state that evidence of displacement during late Quaternary time (the past several hundred thousand years) should be considered evidence that a fault is probably active for low seismicity regions.

The Nuclear Regulatory Commission requires that faults with movements during the past 500,000 years be considered active for siting and design of nuclear power facilities (Shannon-Wilson and Agbabian Associates, 1975). The summary of present opinion indicates at least the past hundred thousand years are important for assessing present activity of a fault. The last two earthquakes producing damage in southern California (Arvin-Tehachapi, 1952, and San Fernando, 1971) occurred on faults lacking historic activity. With the exception of the San Jacinto fault system, every event greater than magnitude 6 in southern California occurred on a fault without prior historic activity.

Several researchers have developed empirical expressions relating magnitude of earthquake, fault length, and offset displacements. Although these relationships can serve as guides, they have inherent weaknesses due to uncertainties involved in their development.

PREDICTION OF EARTHQUAKE MAGNITUDE

Seismologists may define a design earthquake for a site by predicting the earthquake magnitude M and the strength of ground motion. Factors which influence these are the length of geologic fault structures, their

relationship to the regional tectonic structures, the geologic history of displacement along the structure and the seismic history of the region.

The design earthquake in engineering terms is a specification of the ground motion that the project is required to survive successfully with an avoidance of loss of life and acceptable damage and loss of service. A design earthquake on a statistical basis considers the probability of the recurrence of a historical event.

Earthquake magnitudes may be specified in terms of a design level earthquake which can reasonably be expected to occur during the life of the structure. As such, this represents a service load which the structure must withstand without significant structural damage or interruption of required operation. A second level of earthquake magnitude is a maximum credible event for which the structure must not collapse; however, significant structural damage may occur. The inelastic behavior of the structure must be limited to insure the prevention of collapse and catastrophic loss of life.

The selection of a magnitude level may be based on

1. Known design level and maximum credible earthquake magnitudes associated with a fault of known seismicity

2. Specification of probability of occurrence for a given life of the structure such as having a 10% chance of being exceeded in 25 years

3. Specification of required level of ground motion as in a code provision

4. Fault length

Earthquake magnitude can be related to length of fault for shallow depth earthquakes. Data have been plotted by Seed et al. (1969), Krimitzsky (1974), Housner (1965), and by Tocher (1958) to provide the curves indicated (see Figure 6-3). It is important to note that in some regions, correlations of these types are of little value since many of the important geologic features may be deeply buried by weathered materials.

All historical events within about 200 miles of the site can be tabulated to evaluate the seismicity. This gives a measure of the earthquake proneness of a geographic area and is usually discussed in terms of an earthquake recurrence equation of the form
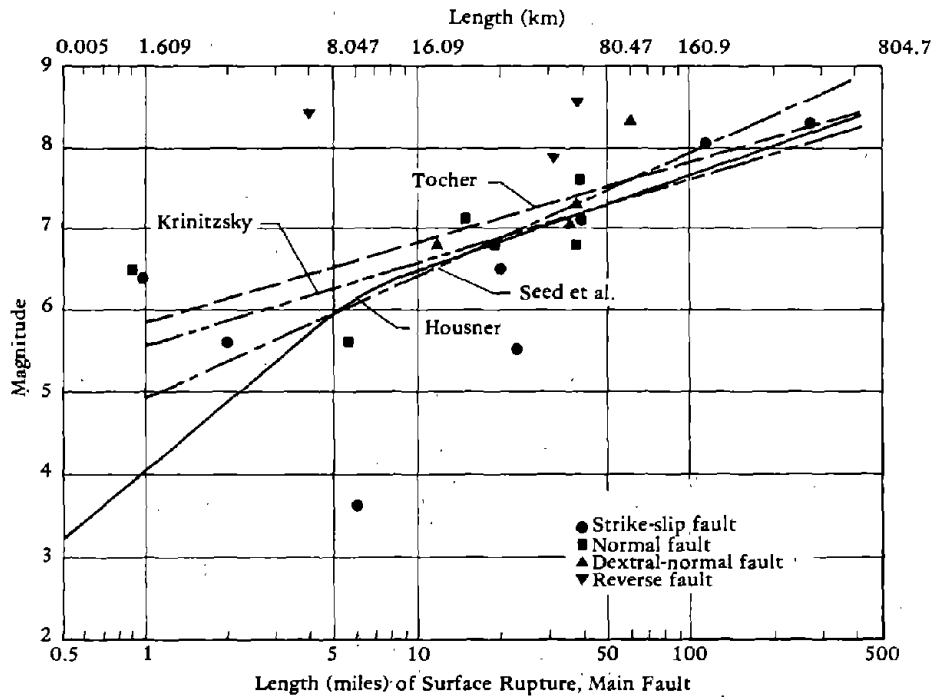
$$Log_{10} N = A - bM$$

149

Figure 6-3. Relationship between earthquake magnitude and length of surface rupture (after Krinitzsky, 1974).
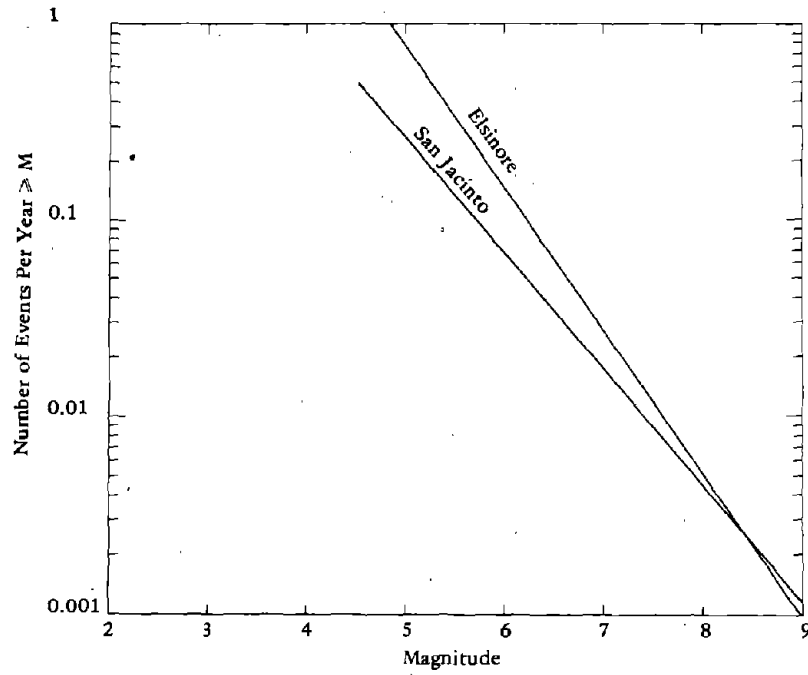

Figure 6-4. Recurrence data.

where N = number of earthquakes per year exceeding a magni-
            tude M

       A = seismicity constant for an area

       b = constant for an area

The tabulated historical data may be arranged according to magnitude,
normalized to 1 year by dividing by the timespan covered, and the number
of events greater than a magnitude M plotted against M. This graph,
plotted on semilog graph paper, can be used to evaluate the coefficients
A and b.

Some recurrence plots for major faults having historic activity are
available in the literature. A typical recurrence curve for the southern
California Elsinore fault and San Jacinto faults is shown in Figure 6-4
(San Diego Seismic Safety Element). Having this data it is possible to
develop probability of occurrence data for selection of a design and
collapse-level earthquake magnitude. The distance of the site to the
fault is important in determining the site motion as will be shown
later. Recurrence data has been developed based on slip observed in
geologic time and the fault length which may be very useful in areas of
low seismicity where historic data is limited and may not provide statis-
tical confidence (Lamar et al., 1973).

Nuttli (1974) has compiled recurrence information for the central
United States. The recurrence equation for the region of his study
covering the states of Illinois, Indiana, Kentucky, Tennessee, Mississippi,
Arkansas, and Missouri is

$$\text{Log } N \ = \ 3.55 \ - \ 0.87 \ (\pm 0.11) \ M$$

where N is the number of earthquakes per year occurring in the magnitude
range M ±0.2. This indicates a return period of 6.3 years for a magni-
tude 5 earthquake, 47 years for a magnitude 6 earthquake, and 347 years
for a magnitude 7 earthquake.

The National Bureau of Standards (Culver, et al., 1975) has published
a guide for the evaluation of earthquake hazards. This guide contains
tables which contain the coefficients A and b and an effective site
distance for 1/2-degree squares of the entire United States. This data
was developed considering the seismicity of each sector and averages the
results of the sector. When specific recurrence data is available for a
specific fault within 200 miles of the site, the actual fault data and
distance to the site should be used. However, since recurrence data for
most areas is not available the National Bureau of Standards information
is of help in evaluating the seismicity and risk of a given area.

A probability distribution is applied to the recurrence data to determine the probability of occurrence of a specified magnitude event in a number of years. The Poisson model is the most common. Cornel (1974), Estana (1968), and Milne and Davenport (1969) have established the general basis for this analysis. The probability of occurrence of an event M in time t is

$$P(t) = 1 - e^{-\lambda(M)t}$$

where $\lambda(M)$ is the rate of occurrence for magnitude M determined from the recurrence plots. In some regions of the world and at least for main shocks, the above authors have verified the Poisson model favorably; however, Knopoff (1964) reports after testing different regions in the world the Poisson model is inadequate to explain the time distribution of low magnitude shocks. Small magnitude earthquakes may contribute heavily to the general seismic risk, rendering the Poisson model inadequate. A more refined model of generation should then be used. In seismic risk analysis the Poisson model is generally an acceptable approach except when working with return periods of several thousand years or in analyzing one structure that has just been damaged (Oliveira, 1975). The Poisson distribution is intended to be used with National Bureau of Standards Tables. The main deficiency of the simple Poisson model is that it ignores the tendency of earthquakes to come in groups which are often triggered by a large main shock; magnitude is treated as a separate independent phenomenon. The Poisson is thought to be adequate for a liquefaction analysis.

An example of the use of the Poisson model is shown in Figures 6-5 and 6-6.

An improvement over the Poisson distribution is the Weibull distribution suggested by Chou and Fisher (1975)

$$P(t) = 1 - e^{ut^{\gamma}}$$

where u and γ are scale and shape parameters, respectively. Several methods are available to estimate the parameters. The maximum-likelihood method is recommended because it utilizes the available information in the most appropriate manner. The shape factor γ is estimated by solving the general equation:

152

$$\frac{n}{\gamma} + \sum_{i=1}^{n} (\ln t_i) - n \frac{\sum\limits_{i=1}^{n} (t_i^{\gamma} \ln t_i)}{\sum\limits_{i=1}^{n} (t_i^{\gamma})} = 0$$

and the scale parameter μ is obtained by equating:

$$\mu = \frac{n}{\sum\limits_{i=1}^{n} (t_i^{\gamma})}$$

where n is the size of the sample and t_i is the time interval involved.

A graphical method of plotting historic earthquake data is very useful and widely used in practice. A new random variable is introduced as $Z = \ln(\mu t^{\gamma})$, and

$$F(Z) = 1 - e^{-e^{Z}}$$

The list of earthquake occurrence data is arranged in groups of intensity or magnitude ranges. Within each group of earthquake events of the same magnitude range the data is ordered by time intervals between occurrences, the most frequent first. The plotting position of any data point within a group is $[t_i, F(i)]$ where t_i is the ith longest time interval and

$$F(i) = \frac{i}{n+1}$$

where i = position on the list; i.e., first, second, etc.

n_ = total number of events in the group

The parameters μ and γ are determined by the intercept and slope, respectively, of the plotted data following the relationship:
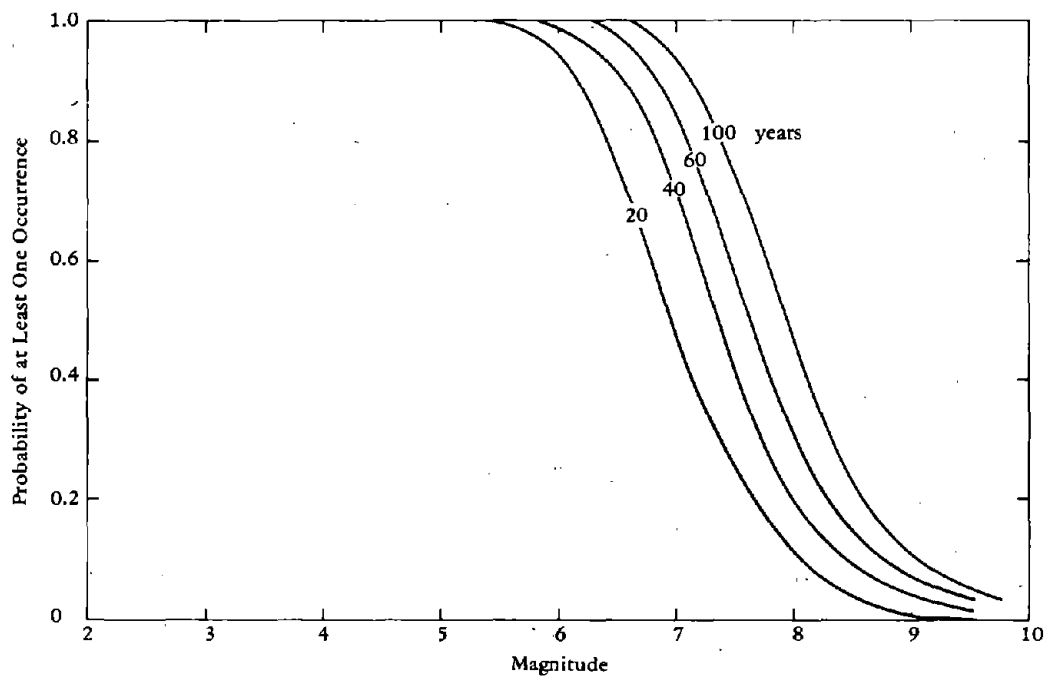
153
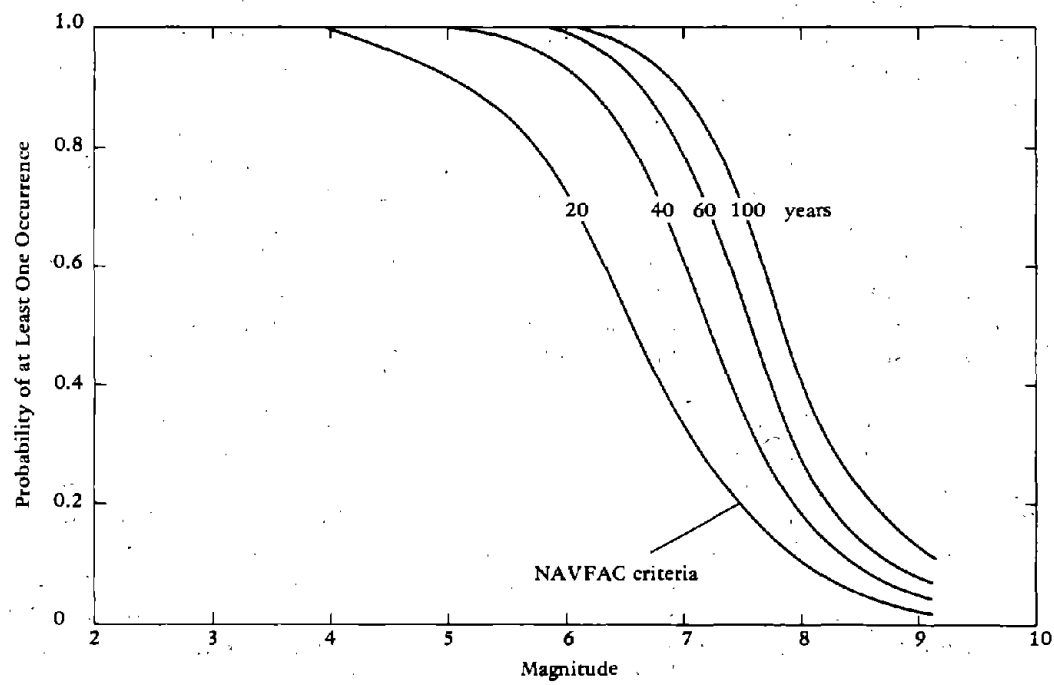
Figure 6-5. Probability of occurrence for Elsinore fault.

Figure 6-6. Probability of occurrence for San Jacinto fault.

154

$$Z_i = \ln \mu + \gamma \ln t_i$$

where t_i is the ith longest time interval and Z_i is given by

$$\ln\ln \left[\frac{1}{1 - F(Z)}\right]$$

or

$$\ln\ln \left(\frac{n + 1}{n - i + 1}\right)$$

A sample is shown in Figure 6-7. When $\gamma = 1$ the Weibull distribution is equivalent to the Poisson distribution.

EARTHQUAKE INDUCED GROUND MOTION LEVELS

The rupture of a fault generates body waves propagating within the earth and surface waves propagating on the surface. The body waves are composed of dilational, longitudinal, compressional waves and distortional, transverse, shear waves, both vertical and horizontal. The surface waves are waves which involve a surface layer in horizontal transverse vibration and Rayleigh waves comprising vibration in retrograde orbit. Each of these types of waves propagates at its own velocity and arrives at specific locations at different times. Body waves travel fastest through the higher velocity mediums at depth (bedrock). The waves tend to be refracted toward the vertical as they propagate upward through increasingly softer materials near the surface. (This follows from Snell's law because shallower layers generally have lower wave velocities.)

Thus, shear waves tend to approach the surface traveling in the vertical direction and vibrating in a horizontal plane. Most structures are well designed for vertical loads by use of standard safety factors. However, horizontal shear waves induce motions and load in the structure in the horizontal plane. Strong motion accelerograms show that vertical accelerations are often about two-thirds as large as horizontal vibrations. For this reason, vertically propagating, horizontal motions are considered of greatest importance and most work has centered on understanding them.

Rock motions beneath a particular site will depend upon the energy released along the fault (characterized by the magnitude of the earthquake and type of fault and the distance of the site from the zone of energy release).
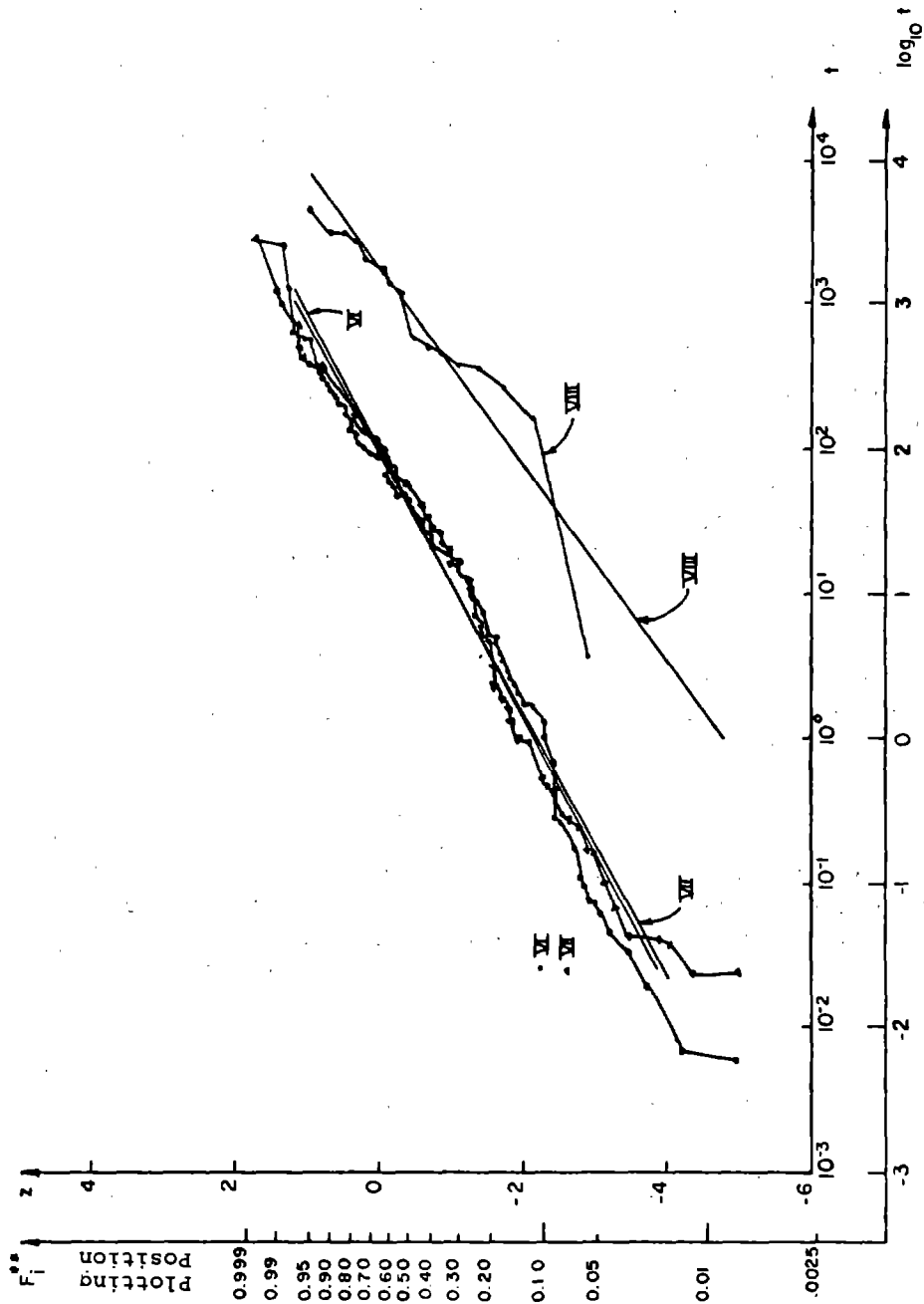
155

Figure 6-7. Presentation of data for Weibull distribution (after Chou and Fisher, 1975).

Having the estimated magnitude of a seismic event and its distance from the site of interest, it is then possible to predict ground motions.

In order to understand the response of any point on the surface, it is necessary to determine the surface topography and the underlying rock configurations. The types of soils and their characteristics determine their response under dynamic loading. It is important to understand bedrock motion underlying the soil deposits and the transfer mechanisms to the surface. (For earthquake engineering purposes, bedrock may be loosely defined as a material exhibiting a shear wave velocity of 2,500 ft/s or greater.)

WESTERN UNITED STATES

Several correlations are available to relate earthquake magnitude, distance from causative fault, and peak acceleration. An early correlation by Housner (1965) estimated peak acceleration for seismic motions experienced at the ground surface. At that time the influence of overlying soils on the peak accelerations could not be evaluated. Peak accelerations represented by these curves are not, therefore, directly applicable to the bedrock level.

A study by Schnabel and Seed (1972) evaluated the peak rock outcrop motions. The curves given in Figure 6-8 resulted from this study and relate peak rock acceleration with earthquake magnitude and distance from causative fault.

Seed et al. (1975) show that for the range from 20 to 250 km all measured accelerogram peak data from 6.5 magnitude earthquakes tends to lie within a band of two standard deviations (Figure 6-9). Prediction at closer distances is based on extrapolation. Figures 6-10 and 6-11 show similar data for stiff soil conditions and deep cohesionless sites. Figure 6-12 compares acceleration in rock to acceleration in various soil profiles.

Trifunac and Brady (1975a) suggest that peaks of ground motion may be scaled by the following, where A_{max} is in./s^2

$$\log_{10} [A_{max}] = M + \log_{10} A_o (R) + \log_{10} [A_o(M)]$$

157
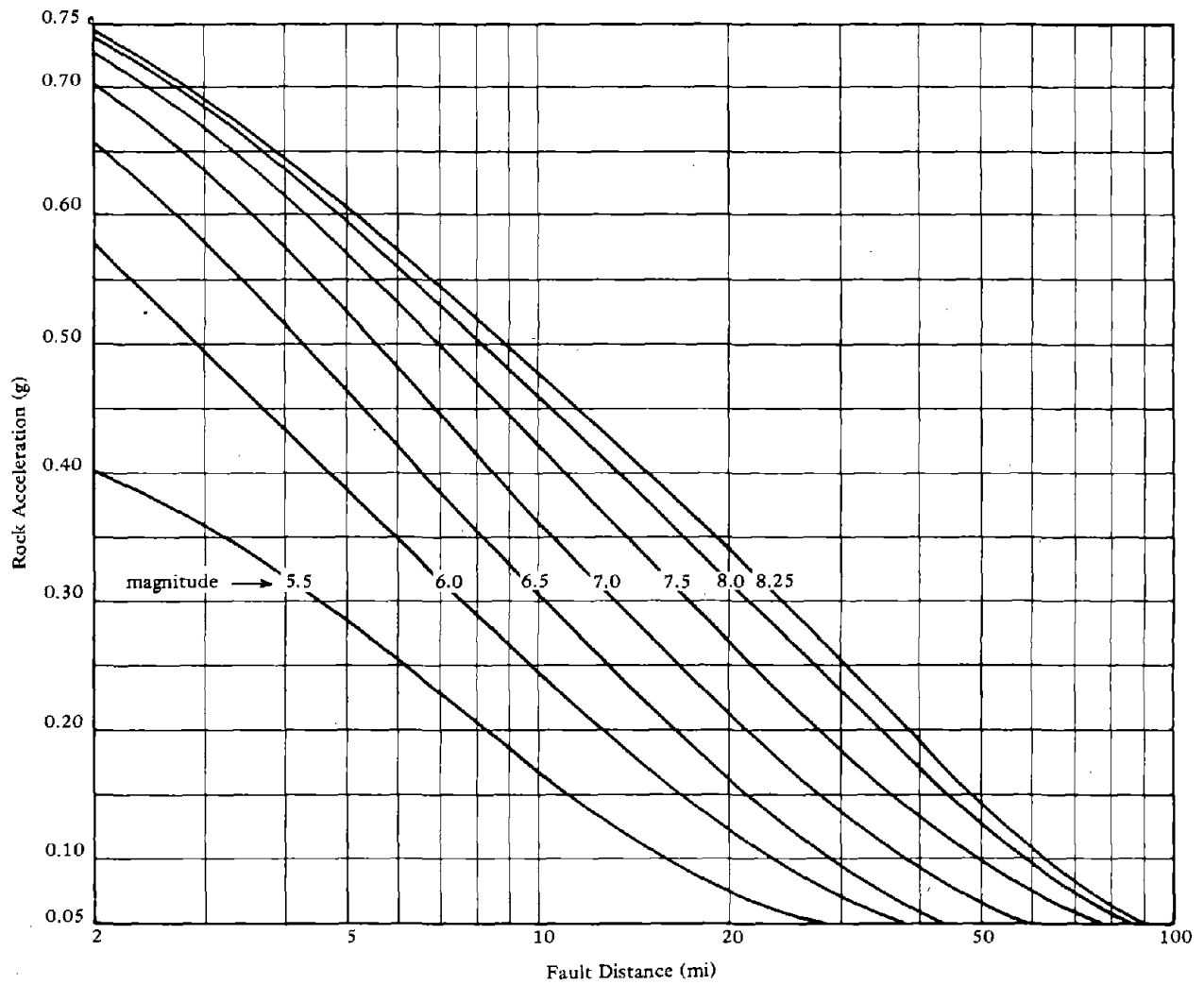
Figure 6-8. Rock acceleration versus fault distance and earthquake magnitude (after P. B. Schnabel and H. B. Seed, 1972).

Figure 6-10. Relationship between maximum ground
acceleration and distance from zone of energy
release for stiff soil conditions (from
H. B. Seed et al., 1975).

Figure 6-9. Relationship between maximum ground
acceleration and distance from zone of energy
release for rock sites (from H. B. Seed
et al., 1975).

159
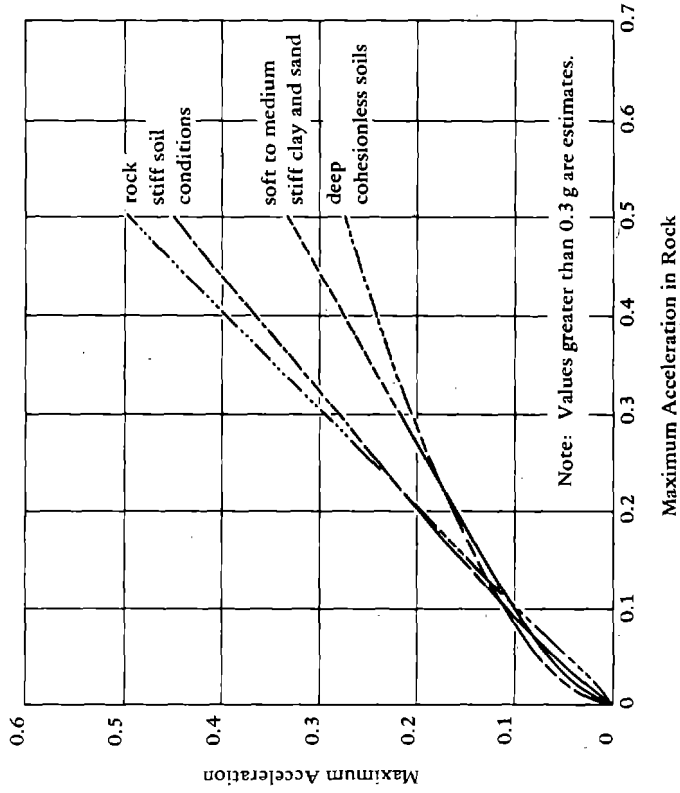
Figure 6-12. Approximate relationships between maximum accelerations on rock and other local site conditions (from Seed et al., 1975).
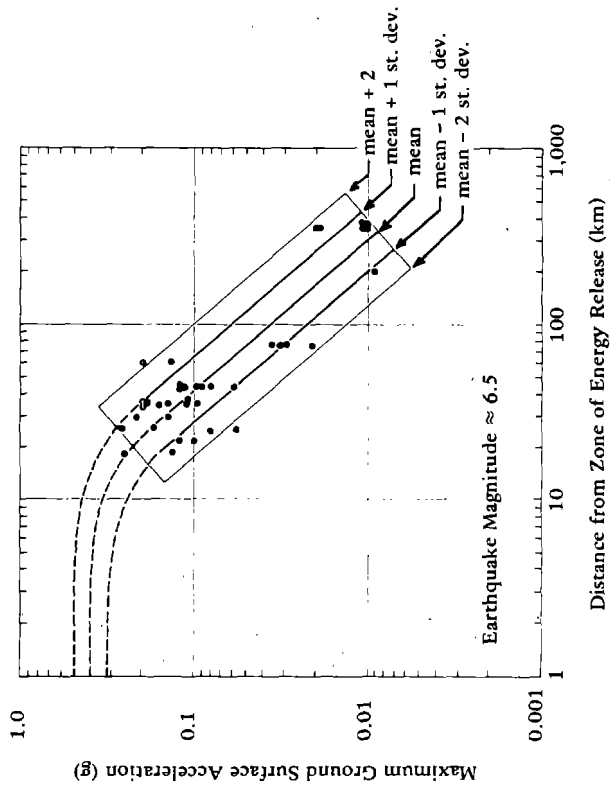
Figure 6-11. Relationship between maximum ground acceleration and distance from zone of energy release for deep cohesionless soil conditions (from Seed et al., 1975).

160

They characterize site conditions s as

$$0 = \text{alluvium}$$
$$1 = \text{intermediate}$$
$$2 = \text{basement rock}$$

Tables 6-1 and 6-2 give values of $\log_{10} A_o(R)$ and $\log_{10} A_o(M)$. They extend the applicability of the equation to include confidence level p, site condition s, and component direction $v(v = 0$ for horizontal, $v = 1$ for vertical) as follows

$$\log_{10} [A_o(M, p, s, v)] = ap + bM + c + ds + dv + fM^2$$

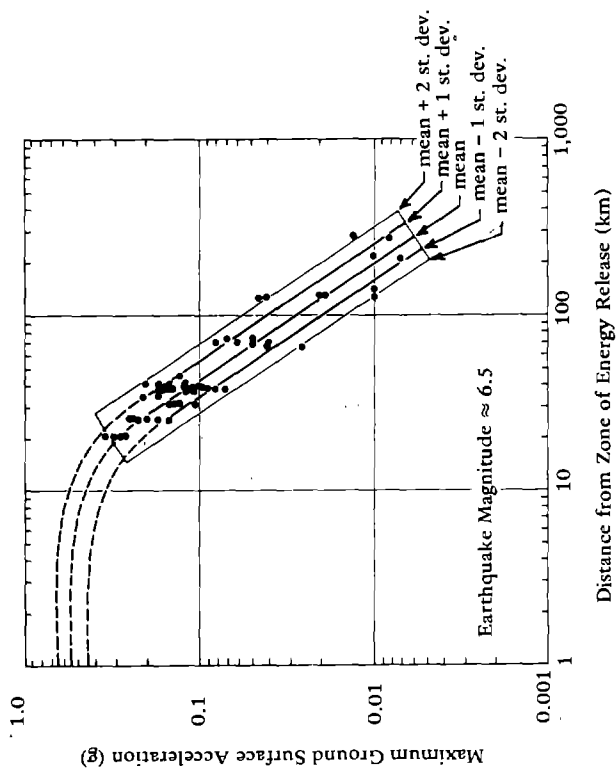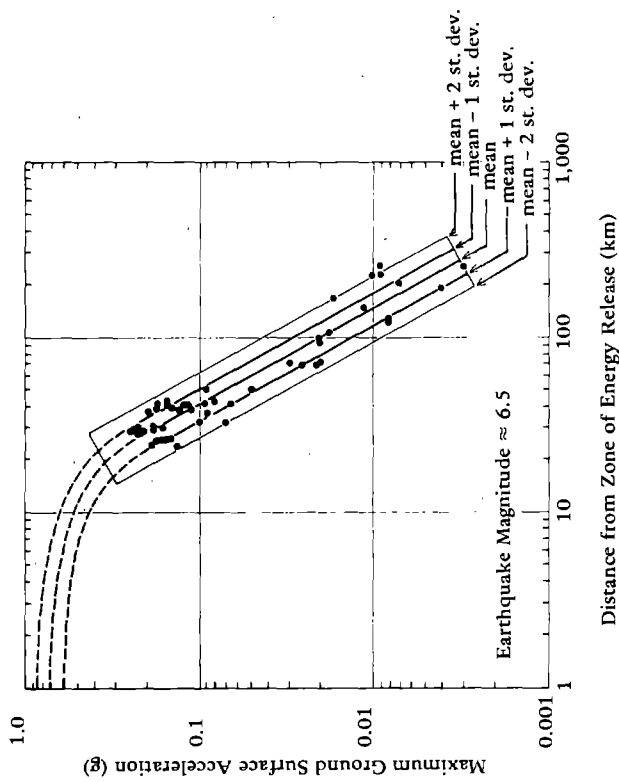The following coefficients in the expression are results of a least-squares fit to available strong motion data.

$$\log_{10} [a_o(M, p, s, v)] = \begin{cases} ap + bM + c + ds + ev + fM^2 - f(M - M_{max})^2 & M \geq M_{max} \\ ap + bM + c + ds + ev + fM^2 & M_{max} \geq M \geq M_{min} \\ ap + bM_{min} + c + ds + ev + fM_{min}^2 & M \leq M_{min} \end{cases}$$

where

$$a = -0.898$$
$$b = -1.789$$
$$c = 6.217$$
$$d = 0.060$$
$$e = 0.331$$
$$f = 0.186$$
$$\text{Total N Data} = 227$$
$$M_{min} = 4.80$$
$$M_{max} = 7.5$$

The Trifunac and Brady (1975b) equation results in ground motions near the fault much greater than Seed's estimates (see Volume II for numerical data).

Table 6-1. $\log_{10} A_o(R)$ Versus Epicentral Distance R

R (km)	$-\log_{10} A_o(R)$	R (km)	$-\log_{10} A_o(R)$	R (km)	$-\log_{10} A_o(R)$	R (km)	$-\log_{10} A_o(R)$
0	1.400	120	3.135	330	4.164	540	4.817
5	1.500	130	3.182	340	4.209	550	4.835
10	1.605	140	3.230	350	4.253	560	4.853
15	1.716	150	3.279	360	4.295	570	4.869
20	1.833	160	3.328	370	4.336	580	4.885
25	1.955	170	3.378	380	4.376	590	4.900
30	2.078	180	3.429	390	4.414		
35	2.199	190	3.480	400	4.451		
40	2.314	200	3.530	410	4.485		
45	2.421	210	3.581	420	4.518		
50	2.517	220	3.631	430	4.549		
55	2.603	230	3.680	440	4.579		
60	2.679	240	3.729	450	4.607		
65	2.746	250	3.779	460	4.634		
70	2.805	260	3.827	470	4.660		
80	2.920	270	3.877	480	4.685		
85	2.958	280	3.926	490	4.709		
90	2.989	290	3.975	500	4.732		
95	3.020	300	4.024	510	4.755		
100	3.044	310	4.072	520	4.776		
110	3.089	320	4.119	530	4.797		

Table 6-2. Means and Standard Deviations of the Logarithm of the
Magnitude-Dependent Scaling Function A_o (M)

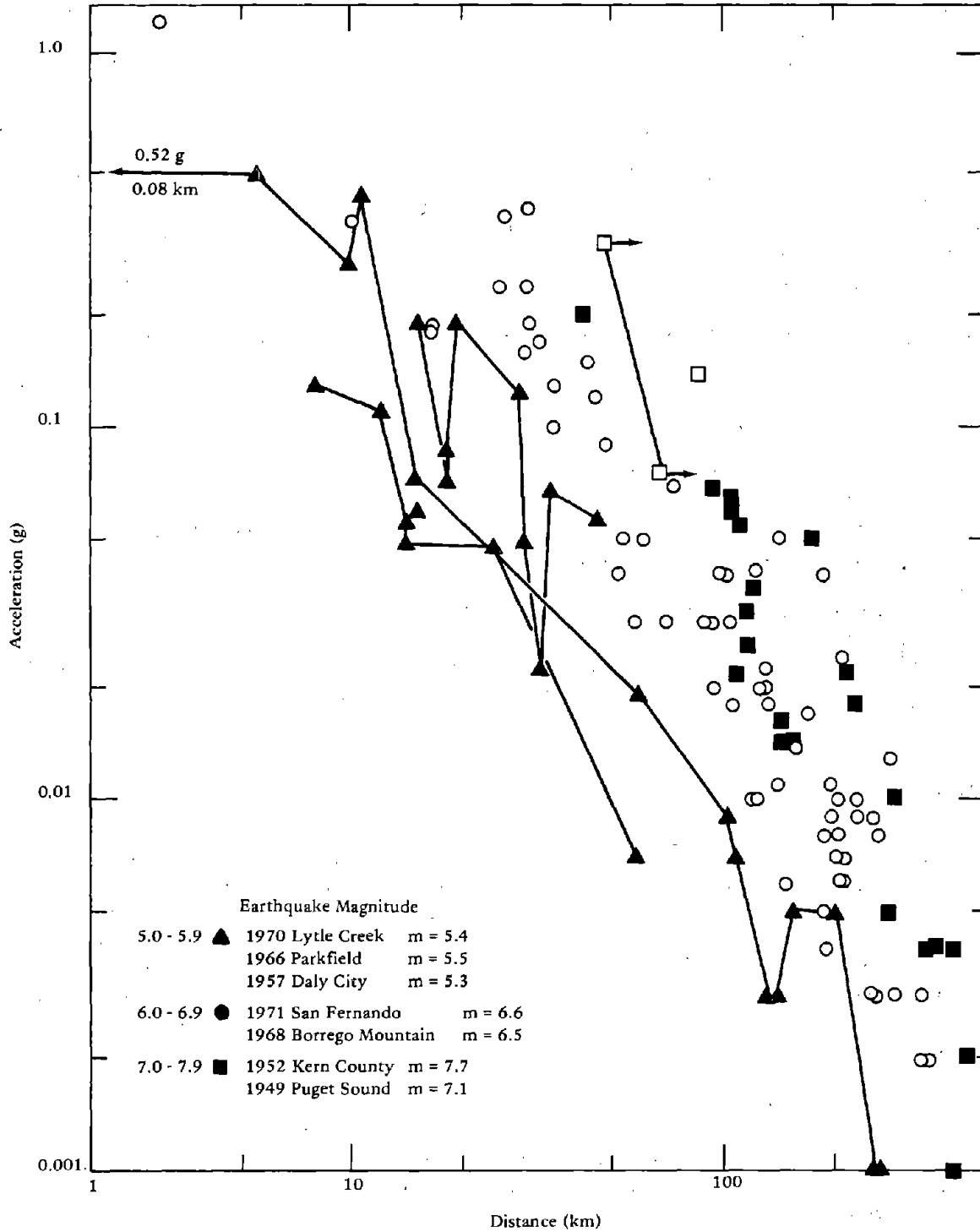| Magnitude	Site Classification	Vertical Acceleration (cm/s^2)		Horizontal Acceleration (cm/s^2)		No. of Data Used	
		log A_o	σ	log A_o	σ	Vertical	Horizontal
4.0 – 4.9	0	1.80	0.036	1.38	0.309	3	6
	1	1.39	0.519	1.07	0.368	2	4
	2	–	–	–	–		
5.0 – 5.9	0	1.83	0.494	1.56	0.503	24	47
	1	1.94	0.253	1.54	0.313	15	30
	2	1.60	0.213	1.41	0.390	2	4
6.0 – 6.9	0	2.21	0.270	1.94	0.278	82	164
	1	2.25	0.253	1.94	0.205	34	68
	2	2.25	0.332	2.05	0.331	12	24
7.0 – 7.9	0	3.21	0.107	2.87	0.163	7	14
	1	–	–	–	–		
	2	–	–	–	–		

Figure 6-13. Peak horizontal acceleration versus distance to slipped fault as a function of magnitude.

164

Page et al. (1975) reviewed ground motion records where the distance to fault was accurately known. They found that peak acceleration attenuates with distance r at a rate in the range $r^{-1.5}$ to $r^{-2.0}$ at distances beyond 10 km for magnitude 5, about 20 km for magnitude 6, and 40 km for magnitude 7 (Figure 6-13). For distances less than 10 km there are no strong motion data for shocks larger than magnitude 6. They estimate the near fault, free-field, horizontal ground motion in Table 6-3. The free-field peak acceleration values close to the fault are higher than those estimated by Seed. This table reflects the analysis of the 6.6-magnitude 1971 San Fernando earthquake's Pacoima Dam record. Motions for magnitudes greater than this were extrapolated considering that peak acceleration increased with magnitude and that near-fault peak acceleration is proportional to the effective stress causing slippage.

Table 6-4 (after Donovan, 1974) summarizes other different attenuation equations developed for ground motions. Figure 6-14 compares the attenuation equations for a magnitude 6.5 earthquake with measured data for the 1971 San Fernando earthquake. Although site conditions are not defined, other than as soil or rock, it is clear that there is a range in predictions of motion at a given distance. Thus, the estimation of ground motion is still an imperfect procedure with upper and lower bounds differing as much as 100% from mean predictions. Since no single relationship has been shown to give more reliable results than any other, it is recommended that the data presented in this section be reviewed to select the methodology most compatible with the intended usage, site characteristics and importance of the structure.

CENTRAL AND EASTERN UNITED STATES

Insofar as its effects on landform are concerned, the most destructive earthquakes in North America, since its settlement by Europeans, occurred in the New Madrid fault zone between December 1811 and February 1812 (Nuttli and Zellweg, 1974; Nuttli, 1973a, b, c, and 1974). This area includes southeast Missouri, northeast Arkansas, western Tennessee, western Kentucky and southern Illinois. However, in this region the occurrence of earthquakes is very infrequent. The historical data is limited to less than 200 years. Thus, it is possible that there are regions in the United States that have not experienced a destructive earthquake in the past 200 years but might suffer one in the next 100 years. There is a significant lack in strong motion records in the eastern and central United States. Since most of the recorded data for the United States have come from California, the characteristics of the accelerograms reflect seismologic and geologic conditions which are different from the east and central parts of the country. The tectonic forces in California are dominated by the San Andreas fault system, a strike-slip fault more than 600 miles long. No comparable fault system

Table 6-3. Near-Fault Horizontal Ground Motion

Magnitude	Acceleration (g) Peak Absolute Values				Velocity (cm/s) Peak Absolute Values			Displacement (cm)	Duration^a (s)
	1st Peak	2nd Peak	5th Peak	10th Peak	1st Peak	2nd Peak	3rd Peak		
8.5	1.25	1.15	1.00	0.75	150	130	110	100	90
8.0	1.20	1.10	0.95	0.70	145	125	105	85	60
7.5	1.15	1.00	0.85	0.65	135	115	100	70	40
7.0	1.05	0.90	0.75	0.55	120	100	85	55	25
6.5	*0.90^b*	*0.75*	*0.60*	*0.45*	*100*	*80*	*70*	*40*	*17*
5.5	*0.45*	*0.30*	*0.20*	*0.15*	*50*	*40*	*30*	*15*	*10*

a Time interval between first and last peaks of absolute acceleration equal to or greater than 0.05 g.

b Italic values are based on instrumental data.

Notes —

1. The values in this table are for a single horizontal component of motion at a distance of a few (3-5) km of the causative fault; are for sites at which ground motion is not strongly altered by extreme contrasts in the elastic properties within the local geologic section or by the presence of structures; and contain no factor relating to the nature or importance of the structure being designed.

2. The values of acceleration may be exceeded if there is appreciable high-frequency (higher than 8 Hz) energy.

3. The values of displacement are for dynamic ground displacements from which spectral components with periods greater than 10 to 15 seconds are removed.

166

exists elsewhere in the United States. Nuttli has compiled a list of
earthquakes in the central United States since 1843. He concludes that
the attenuation rate of motion with distance is less in the central
United States, and consequently a given magnitude earthquake is felt
over a larger area. Nuttli defines geographic regions (Figure 6-15) and
associates maximum credible earthquakes of 7.2 with region 1, 6.2 with
region 2, and 5.7 with region 3. He further adds however, that there is
no place in the central United States that can be considered completely
aseismic.

For region 1 the maximum credible earthquake is equal to that of
the three largest earthquakes of the 1811-1812 New Madrid sequence.
Since the attenuation with distance is less in the central United States,
the earthquakes can be expected to be more destructive. Earthquake
surface waves are dispersed which result in an increase in the time
duration of the wave motion with an increase in epicentral distance.
This is not a problem in California because strong attenuation of wave
energy with distance reduces the motion to low levels at distances at
which dispersion becomes important. The weak attenuation in the central
United States produces prolonged shaking of as much as 1 or 2 minutes at
distances of a few hundred miles. Further, there is a danger of develop-
ing resonant conditions for structures with natural periods of oscillation
near those of the predominant surface motion. Nuttli has estimated the
acceleration with distance for region 1 (7.2 magnitude) as shown in
Figure 6-16. The acceleration given in Figure 6-16 for 0.3, 1, and 3
cycle per second waves are the resultants of vertical and horizontal
components of the sustained maximum surface wave motion. (The resultant
is the vector sum of two horizontal and one vertical component.) This
work notes the attenuation as a function of wave frequency. If the
horizontal motion is considered as two-thirds of the resultant, Figure 6-8
can be plotted as shown in Figure 6-16 to compare Western attenuation
with Central attenuation. As can be seen for distances of less than
60 miles there is fair agreement. Within these distances attenuation is
controlled by geometric spreading rather than absorption so that the
attenuation of surface waves in the near field region does not vary much
with geographic area. However at greater distances, lower level long
duration shaking may be a significant problem causing liquefaction.

Table 6-5 from Nuttli (1973b) gives displacement velocity and
acceleration resultant data for hard rock ground motion. It is important
to note that the active fault zones in the central United States are not
well-delineated, in contrast to California. There is no known evidence
of surficial fault breakage for any central United States earthquake
except possibly those of 1811 and 1812.

167

Table 6-4. Attenuation Equations for Acceleration

Data Source	Equation[a]
1. San Fernando Earthquake February 9, 1971 Donovan (1974)	$y = 186206\,R^{-1.83}$
2. Housner (1965)	Graphical Presentation California Earthquakes
3. California and Japanese Earthquakes Kanai (1966)	$y = \dfrac{5}{\sqrt{T_G}}\,10^{0.61m\ -\ P\log R + Q}$ where $P = 1.66 + \dfrac{3.60}{R}$ $Q = 0.167 - \dfrac{1.83}{R}$ T_G = fundamental period of site
4. Cloud (1963)	$y = \dfrac{6.77\,e^{1.64m}}{1.1\,e^{1.1m} + R^2}$
5. Cloud (1963) Housner (1962)	$y = 1230\,e^{0.8m}\,(R + 25)^{-2}$
6. Schnabel and Seed (1973)	Graphical Presentation 11 Selected Records
7. 303 Instrumental Values Donovan (1974)	$y = 1300\,e^{0.67m}\,(R + 25)^{-1.6}$
8. Western U.S. Records Donovan (1974)	$y = 18.9\,e^{0.8m}\,(R^2 + 400)^{-1}$

[a] y is cm/s^2.
R is distance to causative fault (km).
m is magnitude.
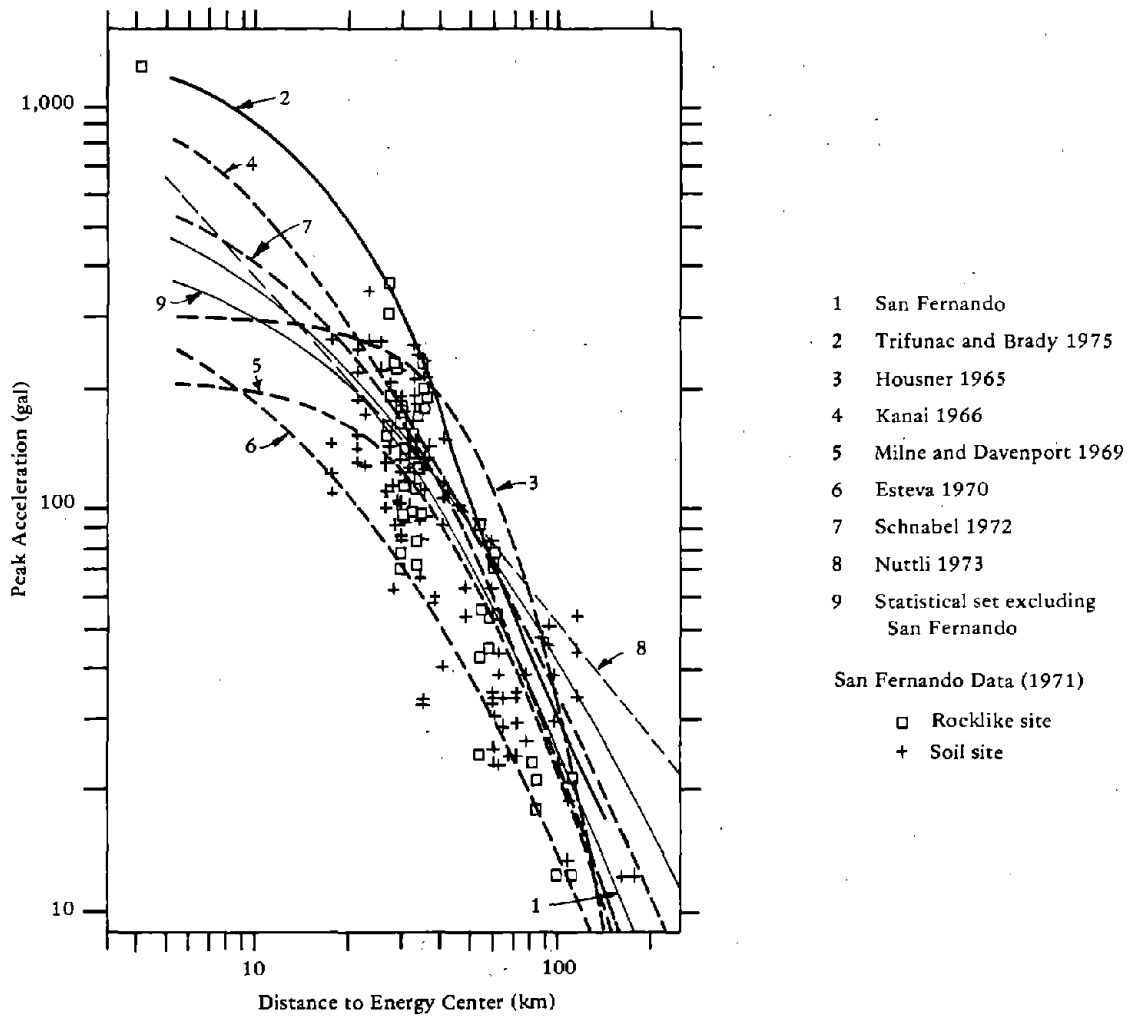
Figure 6-14. Attenuation equations for magnitude 0.5 compared
to data from strong motion stations, recording the
February 9, 1971 San Fernando earthquake.

169
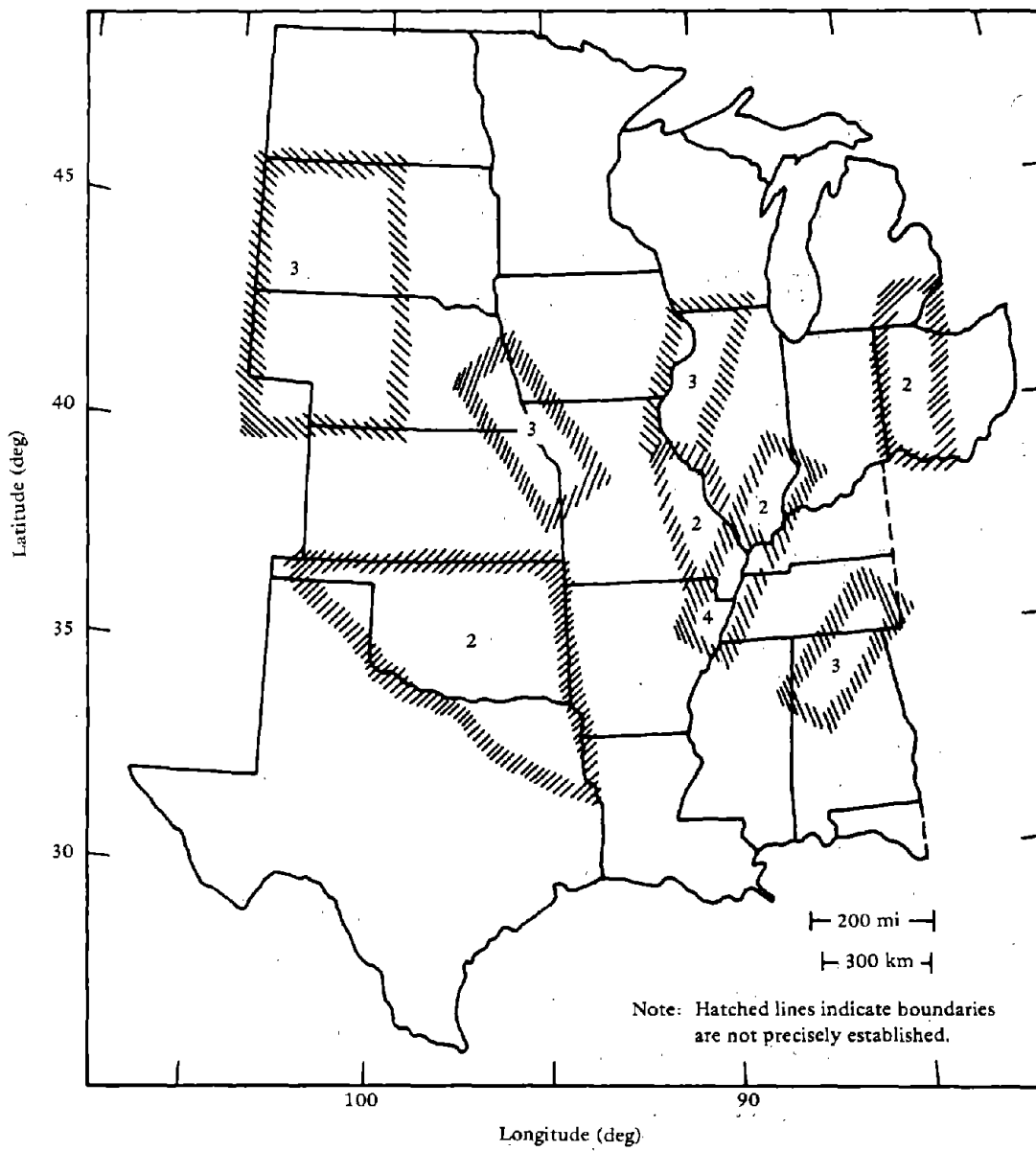
Figure 6-15. Approximate boundaries of seismic regions
1, 2, and 3 in the central United States.

170

Figure 6-16. Ground accelerations on hard rock for the maximum credible earthquake of seismic region 1 (New Madrid faulted zone). (Accelerations for wave frequencies of 0.3, 1, and 3 Hz are the resultants of the vertical and horizontal components of the sustained maximum surface-wave motion.)

Table 6-5. Design Earthquake for Regions 1, 2, and 3[a]

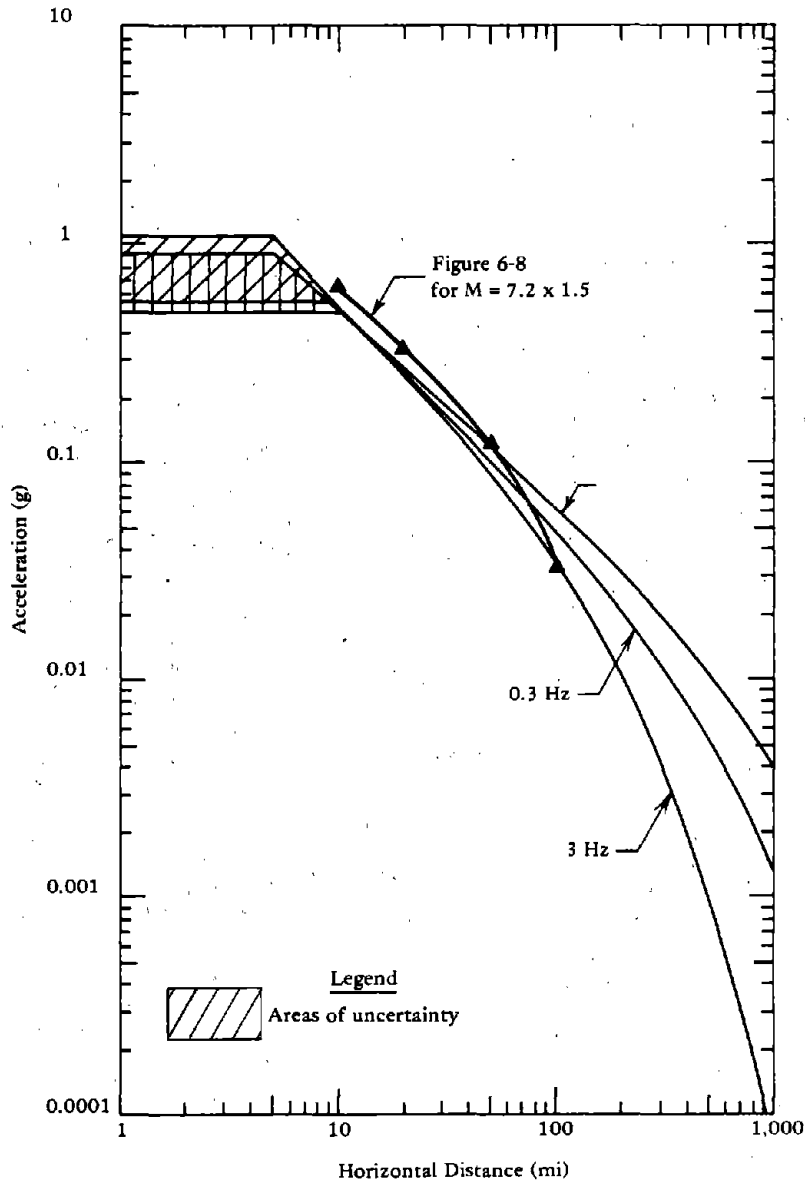| Distance (miles)	0.3-Hz Waves			1-Hz Waves			3-Hz Waves		
	Displacement (cm)	Particle Velocity (cm/s)	Acceleration (g)	Displacement (cm)	Particle Velocity (cm/s)	Acceleration (g)	Displacement (cm)	Particle Velocity (cm/s)	Acceleration (g)
Region 1									
5	120–260	260–540	0.56–1.1	12–21	78–140	0.48–0.88	1.2–2.4	26–52	0.54–1.1
10	120	260	0.56	12	78	0.48	1.2	26	0.54
15	80	170	0.35	8.2	54	0.34	0.80	17	0.35
20	60	130	0.26	6.3	42	0.26	0.60	12	0.26
25	48	100	0.21	5.2	35	0.22	0.47	9.8	0.21
35	34	72	0.15	3.9	26	0.16	0.39	6.7	0.14
50	24	50	0.10	2.8	19	0.12	0.21	4.4	0.095
75	15	32	0.066	2.0	13	0.083	0.12	2.5	0.055
100	11	23	0.047	1.6	10	0.065	0.072	1.7	0.037
150	6.5	14	0.029	1.1	6.8	0.044	0.043	0.85	0.019
200	4.6	9.8	0.020	0.80	5.2	0.033	0.026	0.53	0.012
300	2.7	5.7	0.012	0.52	3.4	0.021	0.012	0.24	0.005
Region 2									
5	12–26	26–54	0.056–0.11	1.2–2.1	7.8–14	0.048–0.088	0.12–0.24	2.6–5.2	0.054–0.11
10	12	26	0.056	1.2	7.8	0.048	0.12	2.6	0.054
15	8.0	17	0.035	0.82	5.4	0.034	0.080	1.7	0.035
20	6.0	13	0.026	0.63	4.2	0.026	0.060	1.2	0.026
25	4.8	10	0.021	0.52	3.5	0.022	0.047	0.98	0.021
35	3.4	7.2	0.015	0.39	2.6	0.016	0.039	0.67	0.014
50	2.4	5.0	0.010	0.28	1.9	0.012	0.021	0.44	0.0095
75	1.5	3.2	0.0066	0.20	1.3	0.0083	0.012	0.25	0.0055

Table 6-5. Continued

Distance (miles)	0.3-Hz Waves			1-Hz Waves			3-Hz Waves		
	Displacement (cm)	Particle Velocity (cm/s)	Acceleration (g)	Displacement (cm)	Particle Velocity (cm/s)	Acceleration (g)	Displacement (cm)	Particle Velocity (cm/s)	Acceleration (g)
Region 2 (continued)									
100	1.1	2.3	0.0047	0.16	1.0	0.0065	0.0072	0.17	0.0037
150	0.65	1.4	0.0029	0.11	0.68	0.0044	0.0043	0.085	0.0019
200	0.46	0.98	0.0020	0.080	0.52	0.0033	0.0026	0.053	0.0012
300	0.27	0.57	0.0012	0.052	0.34	0.0021	0.0012	0.024	0.0005
Region 3									
5	4.0–8.6	8.6–18	0.019–0.037	0.40–0.70	2.6–4.7	0.016–0.029	0.040–0.080	0.86–1.7	0.018–0.037
10	4.0	8.6	0.019	0.40	2.6	0.016	0.040	0.86	0.018
15	2.7	5.7	0.012	0.27	1.8	0.011	0.027	0.57	0.012
20	2.0	4.3	0.0087	0.21	1.4	0.0087	0.020	0.40	0.0087
25	1.6	3.3	0.0070	0.17	1.2	0.0073	0.016	0.33	0.0070
35	1.1	2.4	0.0050	0.13	0.87	0.0053	0.013	0.22	0.0047
50	0.80	1.7	0.0033	0.093	0.63	0.0040	0.0070	0.15	0.0032
75	0.50	1.1	0.0022	0.067	0.43	0.0028	0.0040	0.083	0.0018
100	0.37	0.77	0.0016	0.053	0.33*	0.0022	0.0024	0.057	0.0012
150	0.22	0.47	0.00097	0.037	0.23	0.0015	0.0014	0.028	0.00063
200	0.15	0.33	0.00067	0.027	0.17	0.0011	0.00087	0.018	0.00040
300	0.090	0.19	0.00040	0.017	0.11	0.0007	0.00040	0.008	0.00017

[a] The hard-rock ground motions (displacement, particle velocity, and acceleration) are the vector resultants of the vertical and horizontal components of the sustained maximum surface wave motion. At distances of 75 miles, the duration of this motion will be as much as 30 s. At distances of 100 miles and greater, the duration can be as much as 1 to 2 minutes, generally increasing with increasing epicentral distance.

173

EARTHQUAKE CHARACTERISTICS

In developing a ground motion prediction, it is necessary to define the distance from the point of interest to the fault under consideration. If the fault break is short in length and the site is located a considerable distance from the fault, the significant distance from the site to the zone of energy release can be expressed by the epicentral distance. In the case of a long fault this can be grossly misleading. The rupture of the fault propagates along its length. When the site is close to a fault the distance should consider the release of energy as the rupture propagates along the fault length. In such a case, the distance to the site from the zone of energy release is more appropriately characterized by the shortest distance to the causative fault rather than the distance to the epicenter. To give perspective to this, consider Table 6-6 which gives tentative relationships between magnitude and length of slipped fault.

·Table 6-6. Magnitude Versus Length of Slipped Fault

Magnitude	Length of Slip (miles)
8.8	1,000
8.5	530
8.0	190
7.0	25·
6.0	5
5.0	2.1
4.0	0.83

After the design earthquake magnitudes and site ground motion levels have been defined by the geological and seismological studies, characteristics of the earthquake motions must be defined for use in engineering liquefaction studies. Time-motion records are used with complex computer programs as input to analyses which predict the response of overlying soils.

The important characteristics of the acceleration record are its duration, predominant period, and peak acceleration. The present practice is to scale these characteristics from an existing record to provide the

design earthquake motion. The general problem of scaling earthquake records is treated by Seed, Idriss and Kiefer (1969) and summarized here. The acceleration is linearly scaled to provide the design peak accelerations.

The duration of strong motion has been related in a general way to fault length and the time required for the fault to shear, which can also be related to earthquake magnitude. Figure 6-17 provides a relationship between duration of strong motion and earthquake magnitude developed by Lee and Chan (1972). Note the definition of duration on the graph. Data from Page et al. (1972) for near fault horizontal motion is given in Table 6-4. Studies by Bolt (1974) and Kobayashi (1974) have developed similar duration versus magnitude correlations incorporating more recent data (Figures 6-18 and 6-19). In general the studies presented in Figures 6-17, 6-18 and 6-19 show good agreement. Duration defined as motion greater than 0.05g can be estimated by an average of the data shown. The rate of rupture is believed to be on the order of magnitude of 2 mps so that, for example, a magnitude 7 earthquake resulting from a 25-mile fault break would have at least 12.5 seconds duration. Nuttli (1973c) suggests that central United States earthquakes do not have the same duration (of felt motion) characteristics as western earthquakes as a result of the increased dispersion effects and weak attenuation. However, for distances less than 100 miles from the fault this may not be significant. Once the duration is established, segments of strong· motion of an existing record can be repeated, or deleted, in order to adjust the duration to the proper time length for the design earthquake.

Figure 6-20 provides a relationship between predominant periods of maximum acceleration, earthquake magnitude, and distance from the causative fault. A constant period is indicated for a given earthquake magnitude out to a distance of 25 miles from the causative fault. Figueroa (1960), however, indicates a very wide scatter in predominant period data out to a distance of 50 miles.

An acceleration time history for use in seismic design studies can also be generated with desired characteristics by use of random number programs shaped to the desired spectral characteristics.

Scaling an individual earthquake record has the disadvantage that each record is representative of a specific event and site. Each individual record will be deficient in some response frequencies. An ensemble of scaled earthquake records can be used as a better average of the individual records. Scaled artificial earthquake records that do not exhibit a specific bias can also be used. Procedures for selecting an ensemble of real or artificial records are provided in Werner (1970) and Guzman and Jennings (1975).
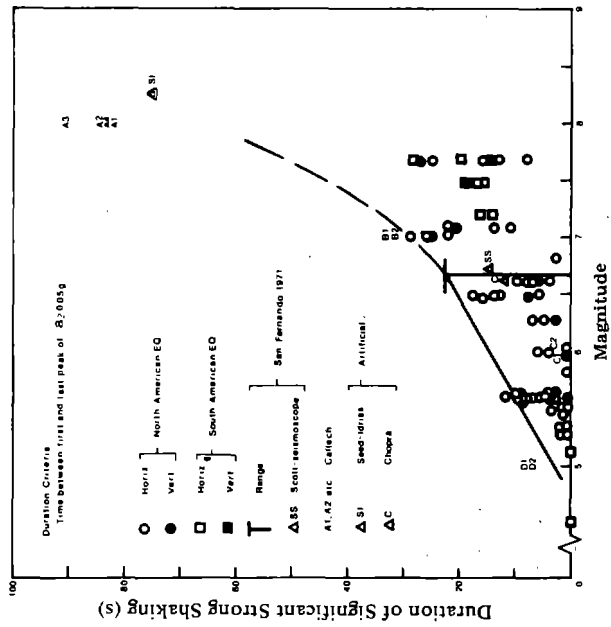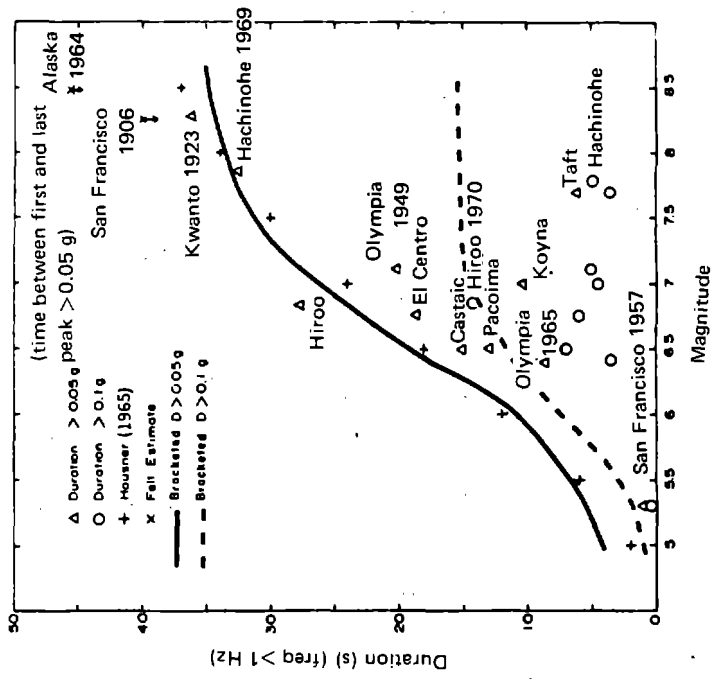
Figure 6-18. Bolt (1974) results for duration.

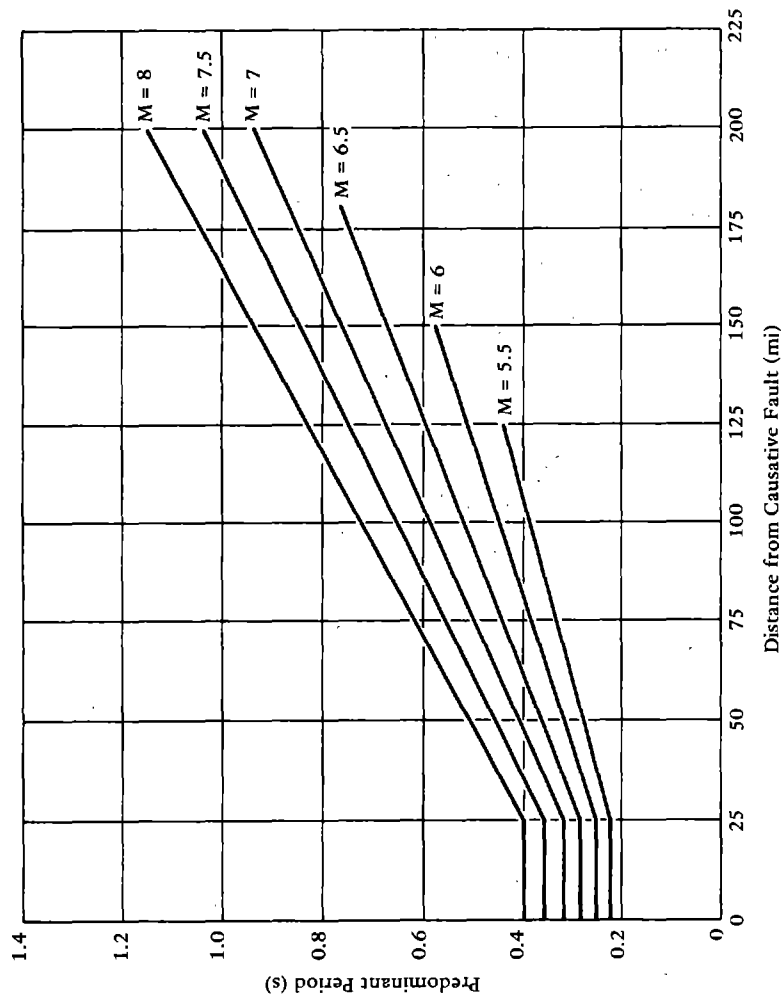Figure 6-17. Lee and Chan (1972) results for duration.

176

Figure 6-20. Predominant periods for maximum accelerations in rock (from "Characteristics of Rock Motions During Earthquakes," by H. B. Seed, I. M. Idriss, and F. W. Kiefer, in Journal of the Soil Mechanics and Foundations Division, ASCE, vol. 95, no. SM5, Sep 1969, Figure 2.6).
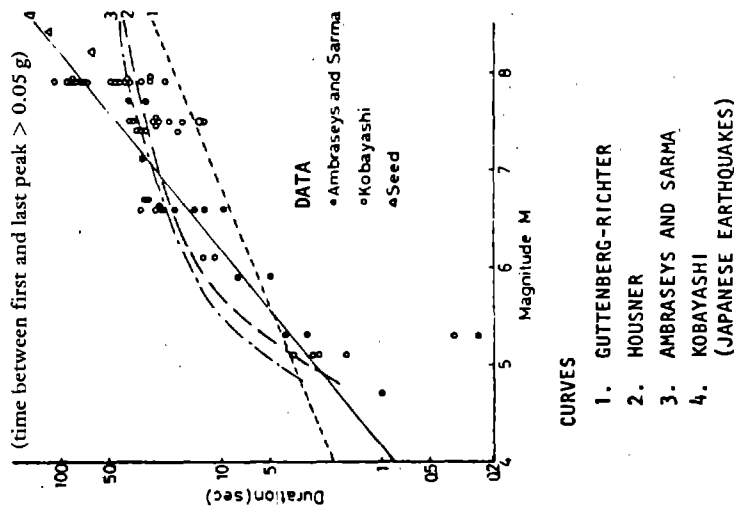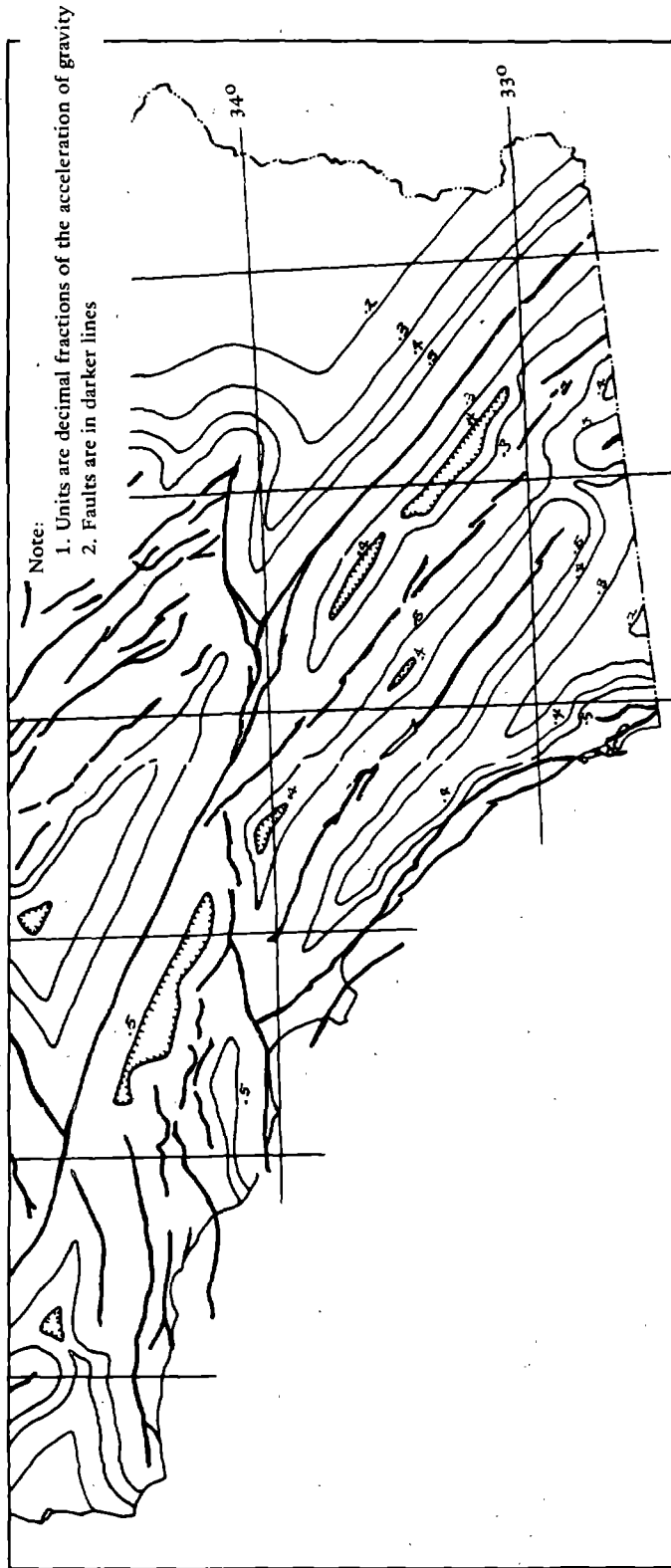

Figure 6-19. Kobayashi results for duration.

Figure 6-21. Maximum credible rock acceleration.

The liquefaction analysis procedures are not very sensitive to the type of earthquake record used. A record on a similar site should be used if available; otherwise, an artificially generated earthquake may be used.

SEISMIC STUDIES

Figure 6-21 presents a portion of a map summary of a study by Greensfelder (1974) which shows contours of possible peak acceleration from active faults using the attenuation after Schnabel and Seed (1972). The probability of occurrence is not considered other than the fact that the faults considered active include Quaternary movement. The National Oceanographic and Atmospheric Administration is in the process of developing a similar map for the entire United States. When available it may assist in predicting site motion. However, the relatively large area coverage of the maps may not be sufficiently detailed for specific site studies.

DISCUSSION

An in-depth geological and seismological investigation is desirable at proposed bridge sites to locate faults and evaluate the site soil profile. When historical data is available the design earthquake magnitude should be determined in terms of the bridge life and earthquake recurrence. For liquefaction analysis, use of the Poisson model should be adequate in most cases. For distances from the site to the fault of between 10 and 100 miles, Figure 6-8 and Tables 6-1 to 6-3 should be adequate. Figure 6-16 shows that although the attenuation in central and eastern United States is less than in the west within the range less than 60 miles, Figure 6-8 is probably adequate since this is the range of most engineering interest. The earthquake duration can be approximated from Figures 6-17, 6-18, and 6-19.

REFERENCES, CHAPTER 6

Bolt, B. A. (1970) "Causes of earthquakes," Earthquake Engineering, R. L. Wiegel ed. Englewood Cliffs, N.J., Prentice Hall, 1970.

Bolt, B. A. (1974) "Duration of strong motion," in Proceedings of the Fifth World Conference on Earthquake Engineering, Rome, Italy, Jun 1974. Rome, Italy, Rome International Association for Earthquake Engineering, 1974.

Chou, E. H. and Fisher, J. A. (1975) "Earthquake hazards and confidence," in Proceedings of the U. S. National Conference on Earthquake Engineering, Ann Arbor, Mich., Jun 1975.

Cornel, C. T. (1974) Stocastic process models in structural engineering, Stanford University, Technical Report 34. Palo Alto, Calif., May 1974.

Culver, C. G. et al. (1975) Natural hazards evaluation of existing buildings, National Bureau of Standards, NBS BSS 61. Washington, D.C., Jan 1975.

Donovan, N. C. (1974) Earthquake hazards for buildings, Dames and Moore, Engineering Bulletin 46. Los Angeles, Calif., Dec 1974.

Environmental Development Agency (1975) Seismic safety element, San Diego Council General Plan, County of San Diego. San Diego, Calif., Jan 1975.

Estana, L. (1968) Bases para la formulacion de decisiones de diseno dismico, Universidad Nacional Autonoma de Mexico, Instituto de Inginieria, no. 182. Mexico City, Mexico, May 1968.

Figueroa, J. A. (1960) "Some considerations about the effect of Mexican earthquakes," in Proceedings of the Second World Conference on Earthquake Engineering, Tokyo and Kyoto, Japan, vol 3, Jul 1960. Tokyo, Japan, Science Council of Japan, 1960, pp 1553-1561.

Greensfelder, R. W. (1974) Maximum credible rock accelerations from earthquakes in California, California Division of Mines and Geology, map sheet 23. Sacramento, Calif., 1974.

Guzman, R. and Jennings, P. C. (1975) Determination of design earthquakes for nuclear power plants, Fugro Inc., Consulting Engineers, Technical Report 50. Long Beach, Calif., 1975.

Housner, G. W. (1965) "Intensity of earthquake ground shaking near the causative fault," in Proceedings of Third World Conference on Earthquake Engineering, New Zealand, vol 1. Wellington, New Zealand, New Zealand National Committee on Earthquake Engineering, 1965, pp III:95-115.

Hudson, D. E. (1972) "Strong motion seismology," in Proceedings of the International Conference on Microzonation for Safer Construction Research and Application, Seattle, Wash., 30 Oct - 3 Nov 1972. Seattle, Wash., National Science Foundation, 1972, pp 39-60.

Knopoff, L. (1964) "The statistics of earthquakes in southern California," Bulletin of the Seismological Society of America, vol 54, no. 6-a, 1964, pp 1871-1873.

Kobayashi, Y. (1974) "Prepared discussion on duration of strong motion by B.A.B.H.," in Proceedings of the Fifth World Conference on Earthquake Engineering, Rome, Italy, Jun 1974. Rome, Italy, Rome International Association for Earthquake Engineering, 1974.

Krinitzsky, E. (1974) Fault assessment in earthquake engineering, Army Engineer Waterways Experiment Station, Miscellaneous Paper S73-1. Vicksburg, Miss., May 1974.

Lamar, D. L., Merifield, P. M. and Proctor, R. J. (1973) Earthquake recurrence intervals on major faults in southern California, geology seismicity and environmental impact, Association of Engineering Geologists, Special Publication. Los Angeles, Calif., University Publishers, 1973.

Lee, K. L. and Chan K. (1972) "Number of equivalent significant cycles on strong motion earthquakes," in Proceedings of the International Conference on Microzonation for Safer Construction Research and Applications, Seattle, Wash., 30 Oct - 3 Nov 1972. Seattle, Wash., National Science Foundation, 1972.

Milne, A. and Davenport, A. G. (1969) "Distribution of seismic risk," Canada Bulletin of Seismological Society of America, vol 59, no. 2, Apr 1969.

Newmark, N. and Rosenblueth, E. (1971) Fundamentals of earthquake engineering. Englewood Cliffs, N.J., Prentice Hall, 1971.

Nuttli, O. W. (1973a) State-of-the-art for assessing earthquake hazard in the United States, design earthquakes for the central United States, Army Engineering Waterways Experiment Station, Miscellaneous Paper S-73-1. Vicksburg, Miss., Jan 1973.

Nuttli, O. W. (1973b) "Seismic wave attenuation and magnitude relations for eastern North America," Journal of the Geophysical Research Division, ASCE, vol 75, no. 5, Feb 1973, pp 876-885.

Nuttli, O. W. "The Mississippi Valley earthquakes of 1811 and 1812: intensities, ground motion and magnitudes," Bulletin of the Seismological Society of America, vol 63, no. 1, Feb 1973, pp 227-248.

Nuttli, O. W. (1974) "Magnitude-recurrence relations for central Mississippi Valley earthquakes," Bulletin of the Seismological Society of America, vol 64, no. 4, Aug 1974, pp 1189-1207.

Nuttli, O. and Zellweg, J. (1974) "The relation between felt area and magnitude for central United States earthquakes," Bulletin of the Seismological Society of America, vol 64, no. 1, Feb 1974, pp 73-35.

Oliveira, C. S. (1975) Seismic risk analysis for a site and a metropolitan area, University of California, Earthquake Engineering Research Center, EERC Report No. 75-3. Berkeley, Calif., Feb 1975.

Page, R. A., et al. (1972) Ground motion values for use in the seismic design of the trans-Alaska pipeline system, U. S. Geological Survey, Circular 672. Washington, D.C., 1972.

Schnabel, P. B. and Seed, H. B. (1972) Accelerations in rock for earthquakes in the western United States, University of California, Earthquake Engineering Research Center, EERC Report No. 72-2. Berkeley, Calif., Feb 1972.

Seed, H. B., Idriss, I. M. and Kiefer, F. W. (1969) "Characteristics of rock motions during earthquakes," Journal of the Soil Mechanics and Foundations Division, ASCE, vol 95, no. SM5, Sep 1969, pp 1199-1218.

Seed, H. B., Murarka, R., Lysmer, J. and Idriss, I. M. (1975) Relationships between maximum acceleration, maximum velocity distance from source, and local site conditions for moderately stray earthquakes, University of California, Earthquake Engineering Research Center, EERC Report No. 75-17. Berkeley, Calif., Jul 1975.

Shannon-Wilson and Agbabian Associates (1975) Procedures for evaluation of vibratory ground motions of soil deposits at nuclear power plant sites, Nuclear Regulatory Commission, NUREG 75/072. Seattle, Wash., Jun 1975.

Tocher, D. (1958) "Earthquake energy and ground breakage," Bulletin of the Seismological Society of America, vol 48, 1958, pp 147-153.

Trifunac, M. D. and Brady, A. G. (1975a) "On the correlation of seismic intensity scales with the peaks of recorded strong ground motion," Bulletin of the Seismological Society of America, vol 65, no. 1, Feb 1975, pp 139-162.

Trifunac, M. D. and Brady, A. G. (1975b) "On the correlation of peak acceleration of strong motion with earthquake magnitude epicentral distance and site condition," in Proceedings of the U. S. National Conference of Earthquake Engineering, Ann Arbor, Mich., Jun 1975. Oakland, Calif., Earthquake Engineering Research Institute, 1975.

Wentworth and Yerkes (1971) Geological setting and activity of faults in the San Fernando area in the San Fernando, California earthquake of February 9, 1971, U. S. Geological Survey, Professional Paper 733. Washington, D.C., 1971, pp 6-16.

Werner, S. D. (1970) A study of earthquake input motions for seismic design, Agbabian Jacobsen Associates, Report No. 6912-925. Los Angeles, Calif., Jun 1970.

Wesson, R. L. et al. (1975) Faults and future earthquakes studies for seismic zonation of the San Francisco Bay Region, U. S. Geological Survey, Professional Paper 941-A. Reston, Va., 1975.

Chapter 7

CONSEQUENCES OF LIQUEFACTION

GENERAL

The magnitude of the foundation problems associated with liquefaction are directly related to the amount of ground movement or ground failure. Ground failures may be of three basic types: flow landslides, landslides with limited displacement, and bearing capacity failures. Liquefaction of a layer at depth which does not undergo large displacements may actually act as an isolator impeding the transmission of vibration energy from underlying layers to structures at the surface. Seed and Idriss (1967) show an earthquake record at Niigata, Japan, in which the surface motion significantly changes from a predominantly short-period motion to a long-period motion after about 8 seconds of motion. Presumably this indicates the time of the onset of liquefaction (Figure 7-1).

Niigata Earthquake Accelerogram (SMAC-A Type) at Basement
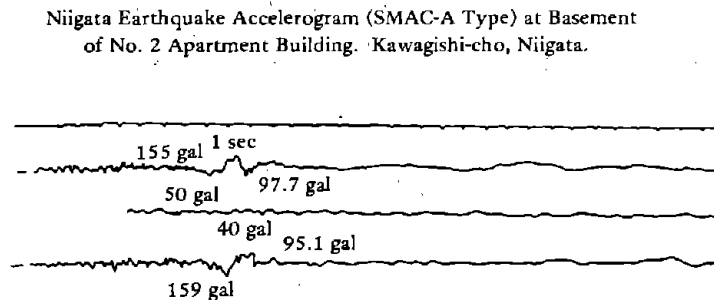of No. 2 Apartment Building. Kawagishi-cho, Niigata.

Figure 7-1. Record of ground accelerations during
Niigata earthquake (from "Landslides During
Earthquakes due to Soil Liquefaction," by
H. B. Seed in Journal of Soil Mechanics
and Foundations Division, ASCE, vol.
95, no. SM5, May 1968, Figure 6).

LIQUEFACTION FLOW LANDSLIDES

When the *in situ* relative density of the soil is low enough ($D_r < 45\%$), unlimited flow may occur. If the soil is unrestrained, sizable masses of earth materials may travel long distances. The principal restraint is only a function of the viscous restraining forces. The flow velocity can be estimated by the following equation for a case where liquefaction propagates to the surface.

$$U = \frac{\gamma_t}{2N} (b^2 - s^2) \sin \theta$$

where
- U = horizontal flow velocity (ft/s)
- N = viscosity (lb-s/ft^2) (Chapter 2)
- γ_t = total unit weight of soil
- b = depth to bottom of liquefiable layer
- S = depth to top of liquefiable layer
- θ = angle of slope

For example, if the depth to the bottom of a liquefiable layer was 20 feet and it propagated to the surface when the ground slope was 2 degrees, the viscosity was 55,000 lb-s/ft^2; and the total unit weight of the soil above the liquefiable layer was 120 lb/ft^2; then,

$$U = \frac{120}{2(55,000)} (20^2) \sin(2^\circ)$$

$$= 0.0152 \text{ ft/s}$$

$$= 0.18274 \text{ in./s}$$

If the liquefiable condition were to last for 7 minutes, the displacement would be over 6 feet.

The above methodology and example, although far from exact, can be used to give qualitative evaluations of the amount of flow displacement. One of the problems here is that the viscosity data on real soils is limited. The example shows that very slight slopes are capable of causing large deformations; conversely, horizontal deformation would not

be expected on truly flat ground. Flow landslides have occurred under seismic conditions and have been reported in the literature (Crandall, 1908; Seed, 1968). Flow continues as long as pore pressures remain high enough to maintain liquefaction. This is a function of the drainage conditions of the site and porosity of the soil and will be discussed later. The duration of liquefaction will also be discussed later.

LIQUEFACTION WITH LIMITED DISPLACEMENTS

For relative densities greater than about 45%, the data tends to indicate that limited flow rather than unlimited flow might be expected. DeAlba, Chan, and Seed (1975) have conducted shake-table tests, Figures 7-2 and 7-3, which suggest limiting horizontal shear strain as a function of relative density. The value of 45% relative density is shown as the approximate division between limited and unlimited flow. Figure 7-3 could presumably be used to estimate shear strains within the soil layer undergoing liquefaction for use in predicting the horizontal transient displacement for level ground not experiencing flow (note that in Figure 7-3 shear strain is expressed independent of ground motion level). This fact and the paucity of data at this time make these results preliminary and in need of further verification.

On sloping ground, increments of finite downslope movements could cause dilatancy-induced solidification. Thus, flow could be interrupted by solidification stages which would limit the displacement. There have been numerous cases of limited displacements, also called lateral spreading, reported (Richter, 1958; McCulloch and Bonilla, 1970; Oldham, 1899; Youd, 1973a and b). Observed cases in these references noted movements of several feet on ground sloping from 0.5 to 2%. Youd (1975) deduces several points of interest based on laboratory soil behavior. Episodes of limited flow would be expected to be most prevalent where shear stress reversals occur; thus, limited flow would be expected to occur as long as strong ground shaking exists. The shear stress reversals associated with limited flow are more easily developed beneath mild slopes where static stresses are small, rather than steep slopes. At the conclusion of a series of limited flow cycles, the soil in the failure zone may be denser or looser or at the same condition as it was before the disturbance, depending on whether pore water migrated into or out of the liquefied soil during shear.

BEARING CAPACITY FAILURES

When liquefaction occurs in soils beneath structures, flow deformations may develop, allowing vertical motion to occur. Loss of foundation support and buoyant rise of buried tanks are possible types of failures.

Several major failures of these types occurred during the 1964 Niigata earthquake, including the spectacular settling and tipping of several high-rise apartment buildings.

DeAlba, Chan, and Seed (1975) conducted model footing tests on a shake table; Figure 7-4 gives vertical velocity of settlement for a model footing in liquefied sand.

Considering flow, for an equilibrium condition the drag force of the footing must equal the footing weight; therefore

$$C_D \; A \; \rho \; \frac{V^2}{2} \;\; = \;\; pA$$

where C_D = footing drag coefficient

  A = footing plan area

  ρ = soil density

 V = footing velocity

  p = footing contact pressure

Solving for V:

$$V \;\; = \sqrt{\frac{2p}{C_D \rho}}$$

Thus, the footing settlement velocity is proportional to the square root of the footing contact pressure. The data in Figure 7-4 was obtained for footing pressures of 25 psi. Figure 7-4 may be used to crudely estimate vertical settlement knowing the duration of liquefaction. Caution must be used since the results are based on a few very small scale model tests of limited scope.

DURATION OF LIQUEFACTION, PROPAGATION TO SURFACE AND BEARING CAPACITY

The duration and propagation of liquefaction in a subsurface layer is controlled by the drainage path for the built-up pore pressure, the coefficients of permeability, and the coefficient of consolidation, which dictates the volume change characteristics of the soil layers.
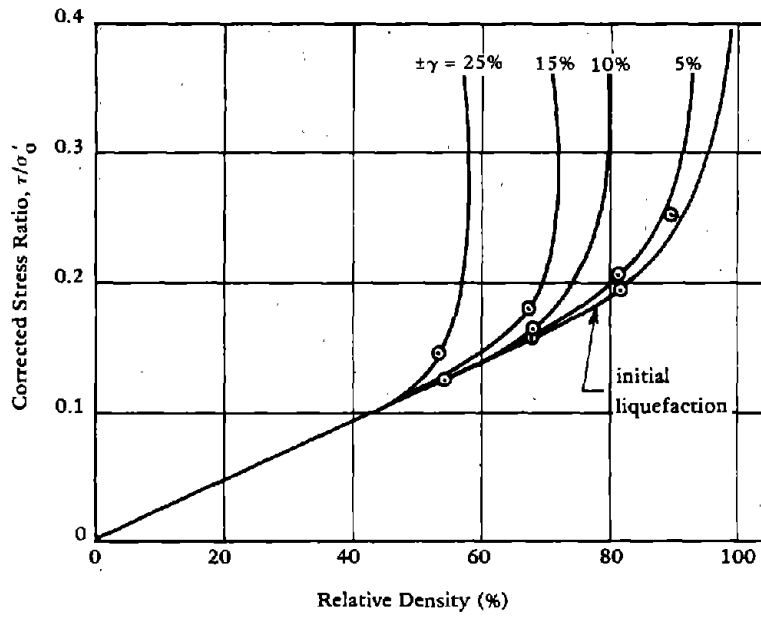
187
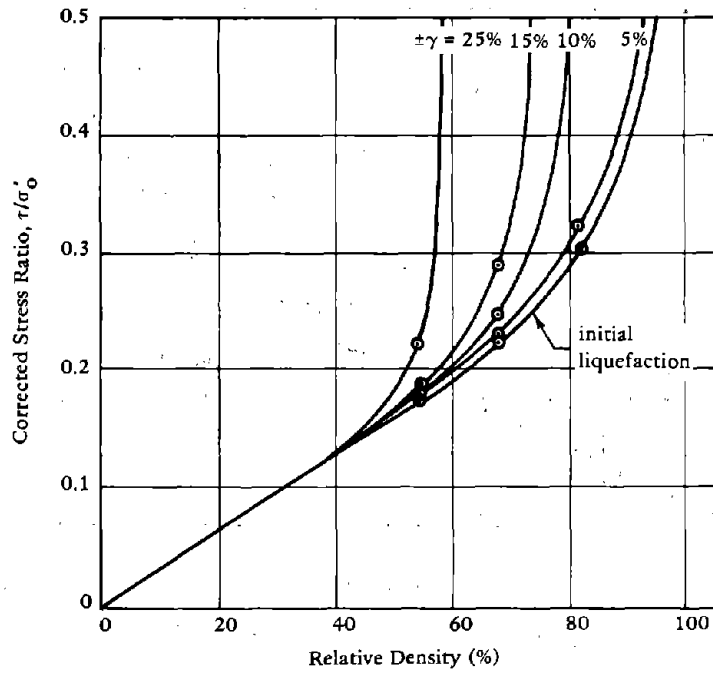
(a) Five stress cycles.
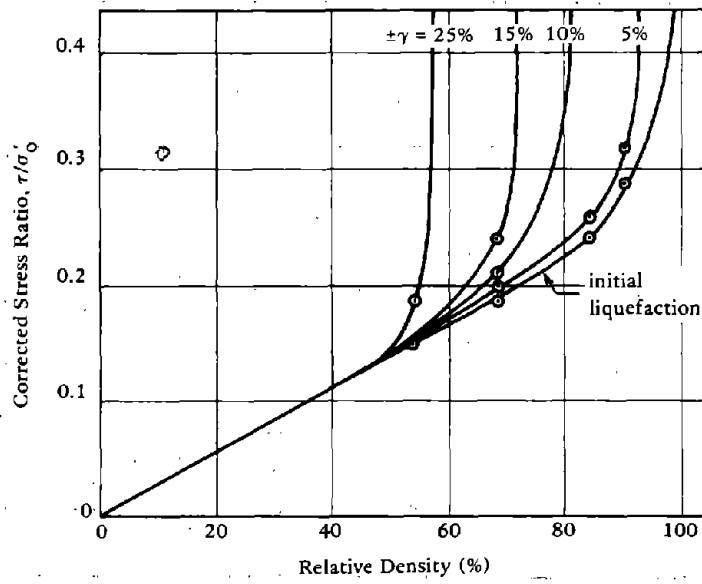
(b) Ten stress cycles.

Figure 7-2. Limiting shear strains (from H. B. Seed,
P. P. Martin, and J. Lysmer, 1975).

188

(c) Thirty stress cycles.
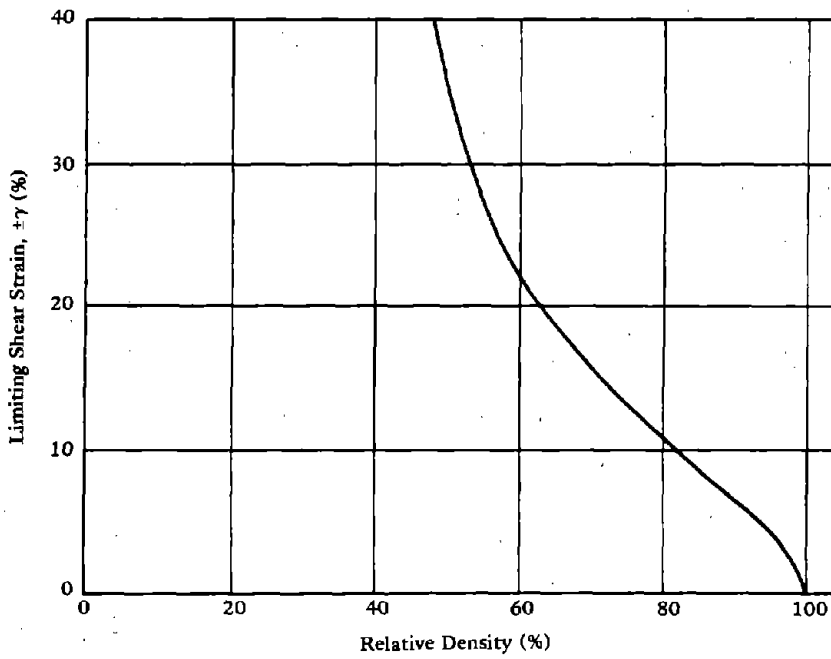
Figure 7-2. Continued

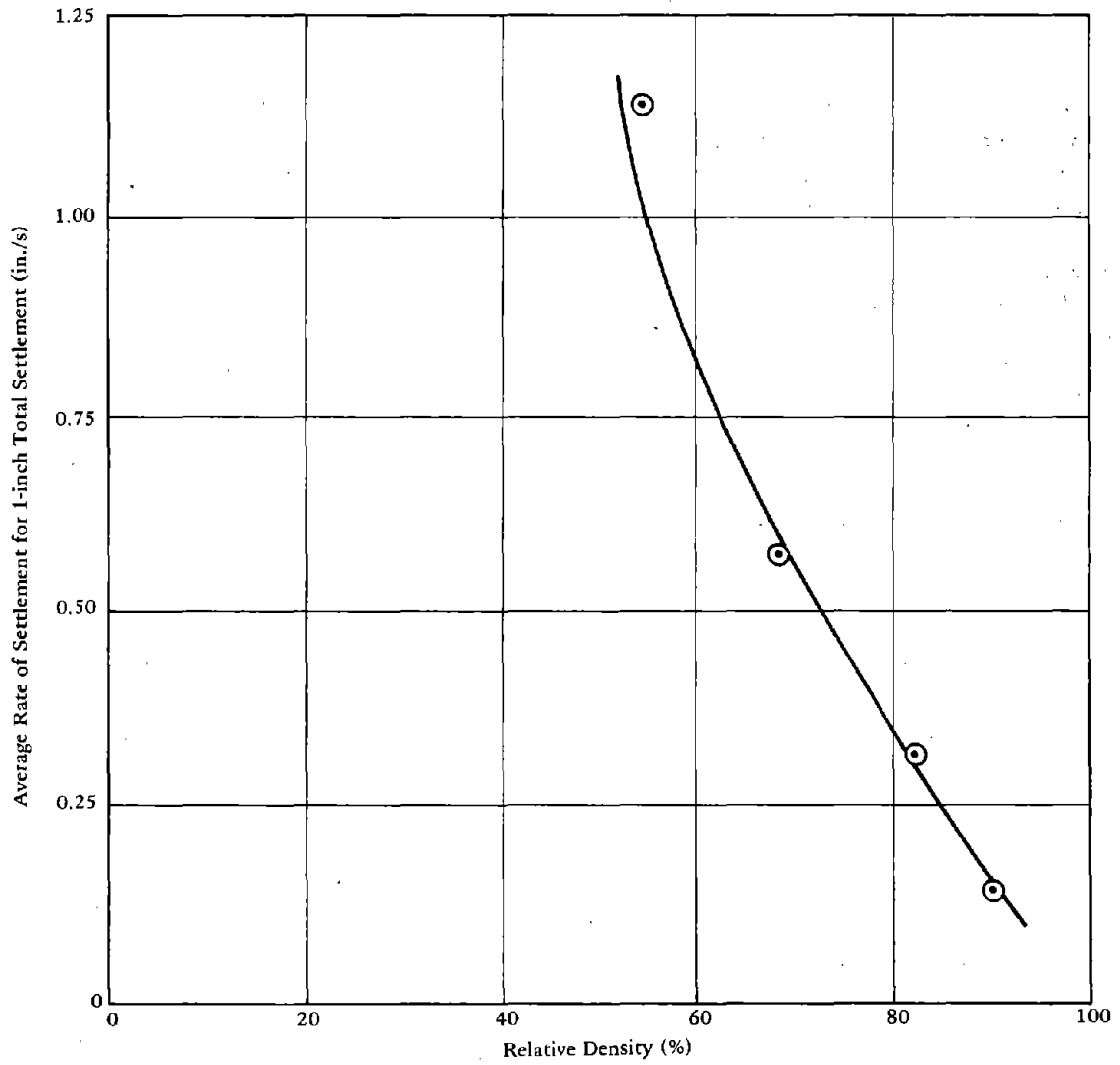Figure 7-3. Limiting shear strains independent of loading.

189

Figure 7-4. Average rate of footing settlement (from H. B.
Seed, P. P. Martin, and J. Lysmer, 1975).

Yoshimi and Kuwabara (1973) have investigated pore pressure dissipation using a finite element analysis, assuming one-dimensional flow (using Darcy's law) and layer II undergoing liquefaction. They assumed that the induced seismic shear stress terminates at the onset of liquefaction, that the soil in layer I undergoes rebound and recompression with a constant coefficient of volume change, and that the soil in layer II undergoes virgin compression with a constant coefficient of volume change.

An example of the results of their analysis is shown in Figure 7-5 in which the pore pressure buildup in the top layer is given as a function of time for the case where: (1) the coefficient of permeability in both layers are equal and (2) the coefficient of volume change in the bottom layer is 10 times greater than in the top layer. As shown in Figure 7-5 the pore pressure builds up in the top layer to a value almost equal to the effective vertical stress at a time determined as a function of the thickness of the layer and the coefficient of consolidation (nondimensionalized time factor). The effect of different thicknesses of the soil layers on the peak pore pressure buildup in the top layer is shown in Figure 7-6 for two compressibility ratios. The effect of the relative thickness of layer I on the maximum pore pressure depends on the compressibility ratio (coefficients of volume change). Yoshimi and Kuwabara (1973) have noted that the presence of a permeable layer beneath layer II has a negligible effect on the pore pressures in layer I.

It is possible that an initial excess pore pressure in layer I has been generated by the same seismic action causing liquefaction in layer II. For this case, Figure 7-7 shows the pore pressure with time for various values of initial pore pressure. It can be seen that the initial pore pressure in layer I has little effect on the peak pore pressure in that layer.

Figure 7-8 shows the results of variation of permeability and compressibility on pore pressure in the top layer. Also shown is the ratio of shear strength at any time S to initial shear strength S_o defined as

$$\frac{S}{S_o} = 1 - \frac{u}{\sigma_{vo}'}$$

Since the maximum pore pressure varies nearly linearly with depth in layer I, the minimum strength ratio S_{min}/S_o corresponding to the maximum pore pressure may be considered a constant throughout layer I

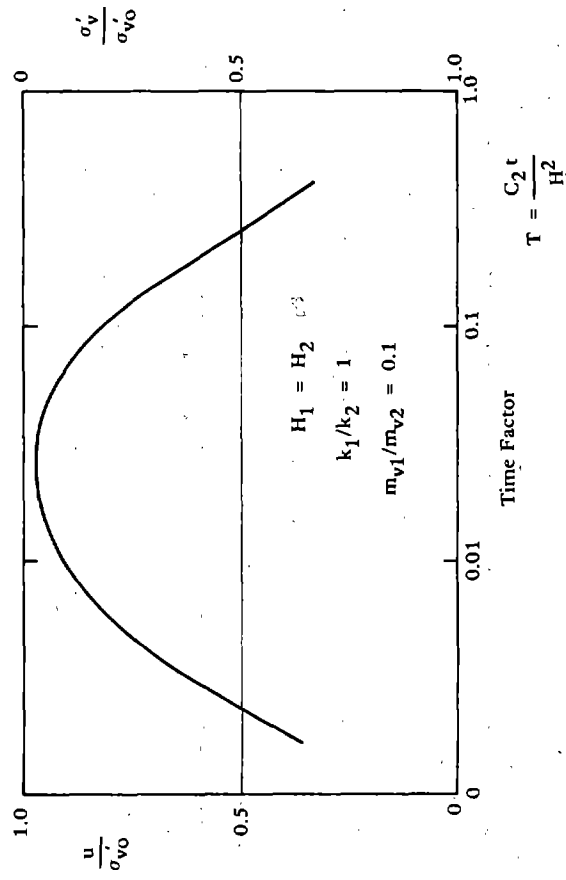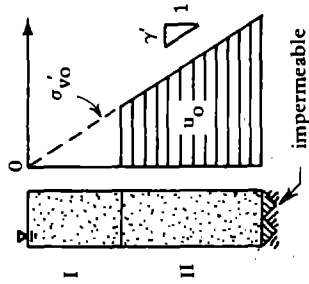$$\frac{S_{min}}{S_o} = 1 - \frac{u_{max}}{\sigma_{vo}'} = 1 - \frac{i_{max}}{i_{cr}'}$$

191

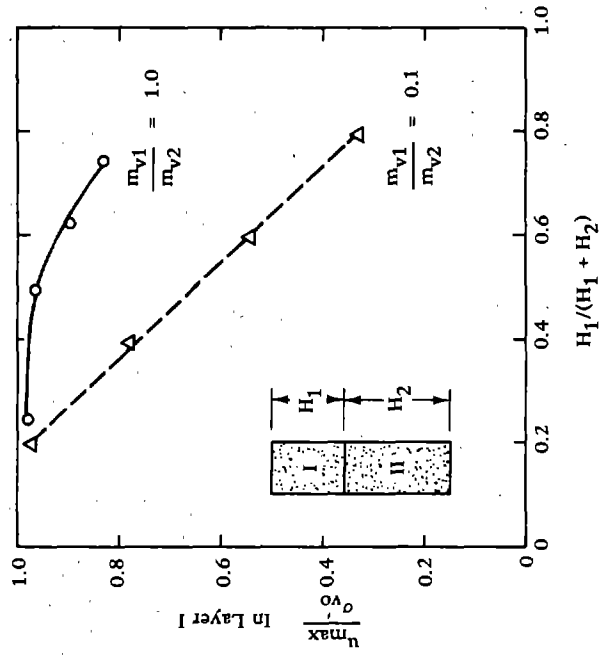Figure 7-6. Effect of relative thickness of layer I on maximum pore pressure in layer I (from Y. Yoshimi and F. Kuwabara, 1973).

Figure 7-5. Pore pressure at middepth layer I (from Y. Yoshimi and F. Kuwabara, 1973).

where i_{max} = maximum hydraulic gradient

i_{cr} = critical hydraulic gradient

Figure 7-9 shows the minimum strength in layer I for use in estimating the liquefaction of that layer. The data is replotted in Figure 7-10 to show areas where complete liquefaction in layer I occurs. It should be noted that the critical hydraulic gradient corresponding to $u_{max}/\sigma_{vo}' = 1$ in a field situation probably cannot be maintained without causing fissures and local eruption of sand and water. The presence of a foundation will affect the state of stress and seepage conditions; however, the strength ratio S_{min}/S_0 may still give a crude indication of the bearing capacity. The time to the minimum strength as noted in Figure 7-8 depends upon the coefficient of permeability, the compressibility, and the thickness of the soil. These may be in seconds or in minutes, depending on site conditions. Observations during the Niigata earthquake of 1964 noted most of the surface movement occurred minutes after the earthquake strong motion ended. Note that densification causes a reduction in k_1 and m_{v1} of the top layer and a reduction of S/S_0, which is not favorable; however, densification will cause an increase in the initial shear strength S_0, which is beneficial. The net effect of densification of layer I may or may not be advantageous, depending on the initial soil properties and the degree of densification. Increasing the permeability of the top layer markedly increases the stability of the soil. Thus, vibroflotation, sand drains, or using a coarse backfill should be more effective than densification methods in which density alone is increased.

Seed, Martin, and Lysmer (1975) have more recently investigated the distribution of hydrostatic pore pressure in the soil by use of the equation

$$\frac{\partial u}{\partial t} = C_v \left(\frac{\partial^2 u}{\partial z^2} \right) + \frac{\partial u_g}{\partial t}$$

where C_v = coefficient of consolidation of the soil

z = depth within soil

$\partial u_g/\partial t$ = rate of pore pressure generation caused by earthquake

This is the diffusion equation used in Terzaghi's classical consolidation theory, with a pressure-generating term added. The solution of this equation is accomplished by the finite-difference technique using incremental time steps. The pore pressure generation is estimated by Figure 7-11 as a function of the number of cycles to cause liquefaction.
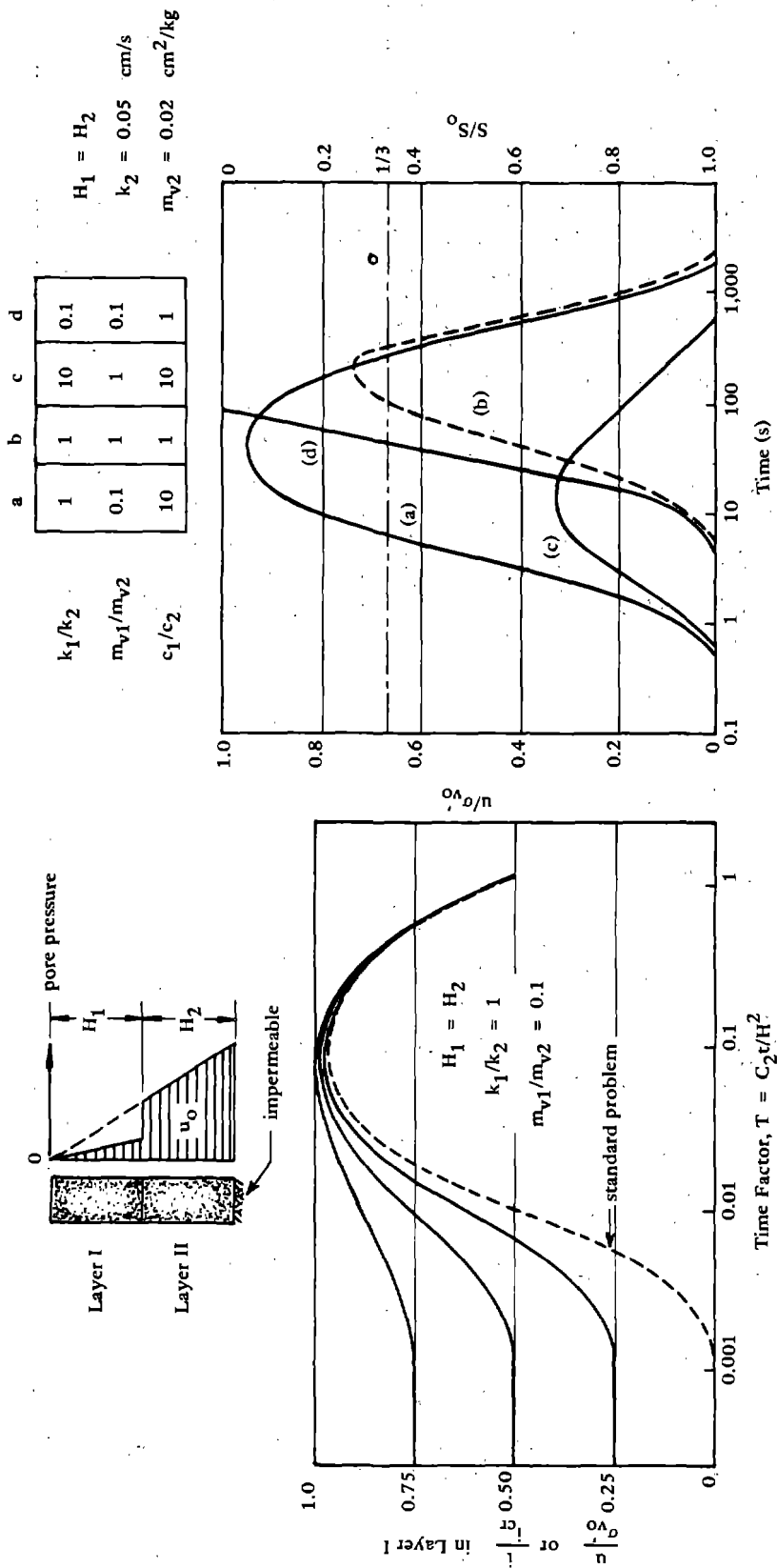
Figure 7-8. Time histories of excess pore pressure at middepth of layer I (from Y. Yoshimi and F. Kuwabara, 1973).
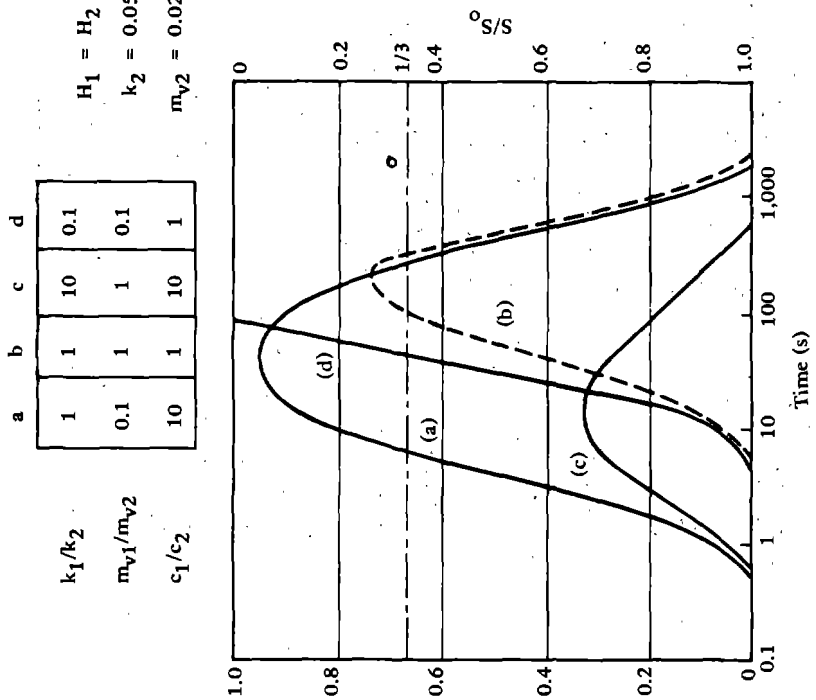

Figure 7-7. Effect of initial excess pore pressure in layer I (from Y. Yoshimi and F. Kuwabara, 1973).
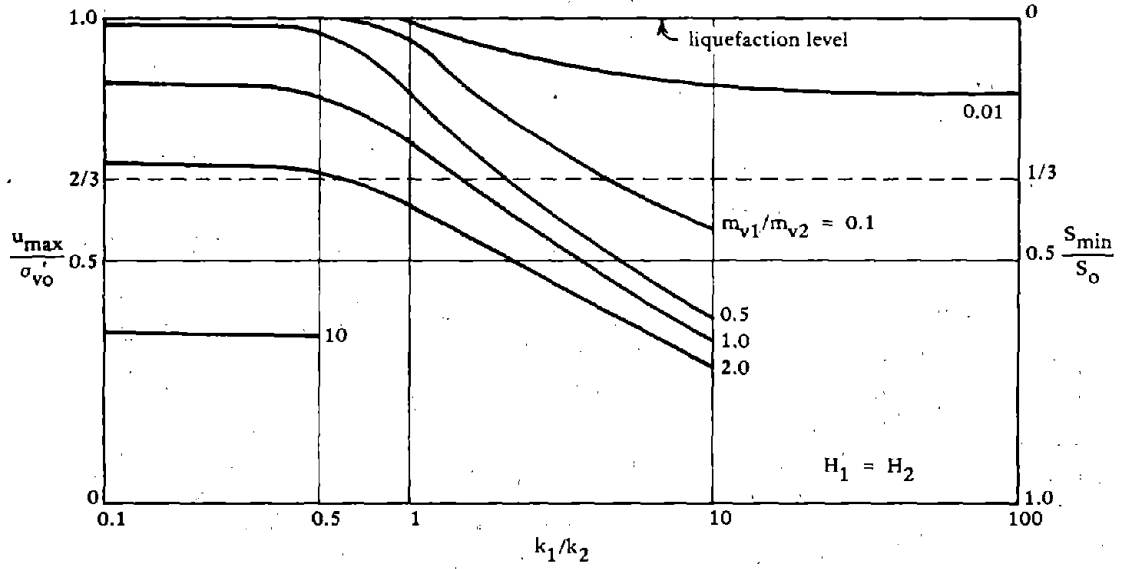
Figure 7-9. Maximum pore water pressure or minimum strength
in layer I (from Y. Yoshimi and F. Kuwabara, 1973)..
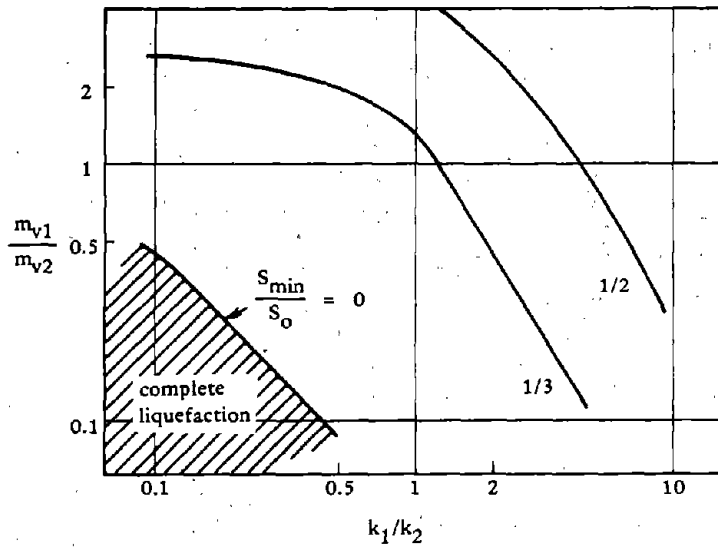
Figure 7-10. Minimum strength ratio in layer I (from
Y. Yoshimi and F. Kuwabara, 1973).
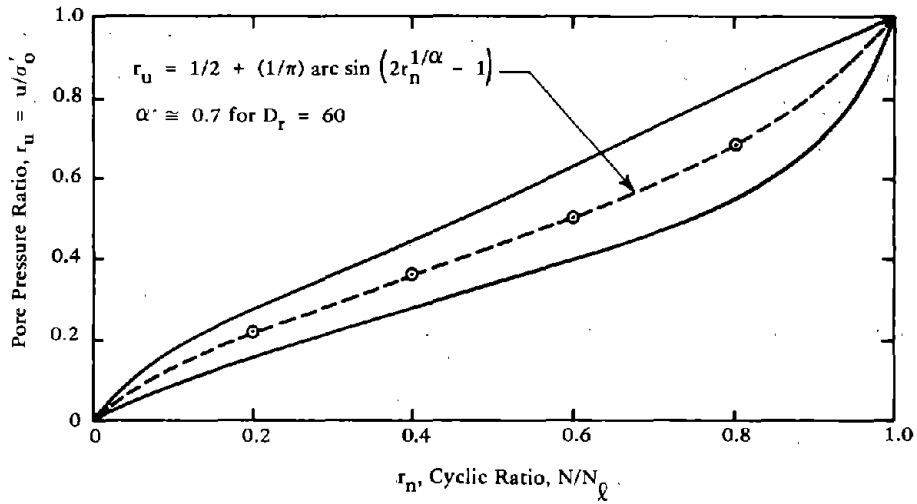
Figure 7-11. Rate of pore water pressure buildup in cyclic
simple shear tests (after P. DeAlba, C. Chan,
and H. B. Seed, 1975).

The equation shown in the figure:

$$r_u = 1/2 + (1/\pi) \arcsin \left(2r_n^{1/\alpha} - 1 \right)$$

$$\alpha \cong 0.7 \text{ for } D_r = 60$$

Figure 7-12. Theoretical relationships between compressibility
of sands and pore pressure buildup (from H. B. Seed,
P. P. Martin, and J. Lysmer, 1975).

196

The coefficient of consolidation C_v, which is defined in terms of the coefficient of volume compressibility m_v and the coefficient of permeability k, may be estimated by means of Figures 7-12 and 7-13.
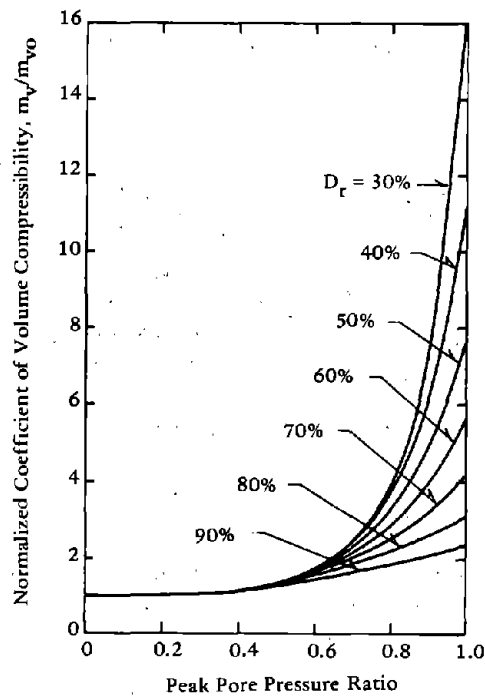
$$C_v = \frac{k}{m_v \gamma_w}$$

The rise in the water table is given by:

$$\Delta H = \frac{-k \left(\frac{\partial u}{\partial z}\right) \Delta t}{n_e}$$

where n_e = the effective porosity
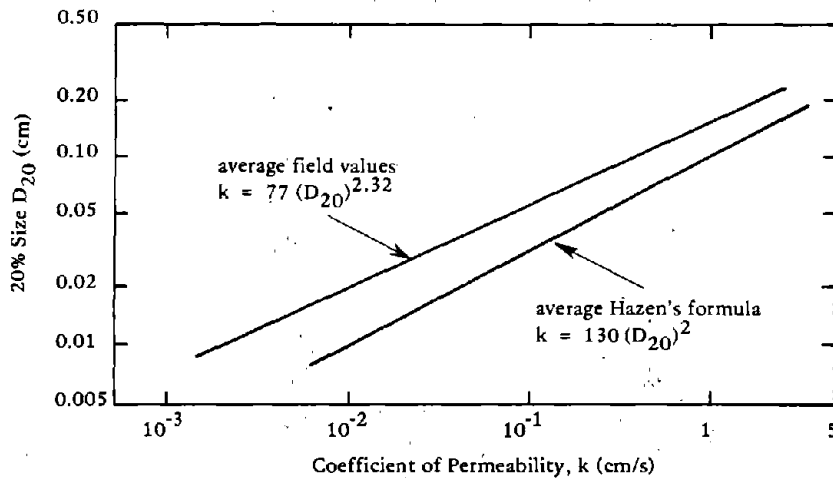
Figure 7-13. Relationships between grain size and coefficient of permeability for sands (from H. B. Seed, P. P. Martin, and J. Lysmer, 1975).

This procedure has been automated in the form of the computer program APOLLO prepared by Martin (1975) and may be used in conjunction with the analysis using the computer program SHAKE described in Chapter 3. SHAKE is used to produce the equivalent uniform cyclic stress (τ_{eq}) and the equivalent number of uniform stress cycles (n_{eq}) for various depths

of soil. From strength data the number of cycles to cause liquefaction at each depth is determined. Using this information program APOLLO solves the pore pressure generation-dissipation equation.

The pore pressure generation function is based on undrained test data. This application is deemed sufficiently accurate when small time steps are used to properly account for drainage. The elastic response analysis used to determine the number of cycles to liquefaction can be made to consider the isolation effects of subsurface liquefaction on near surface shaking and the reduction in pore pressure generation when iteration techniques are used.

A typical example from Seed et al. (1975) from the Niigata earthquake of 1964 is shown in Figures 7-14 and Figure 7-15. The computed variations of pore water pressure with time are given. Figure 7-15 shows the buildup of pore pressures. It may be seen that the sand layer at a depth of 15 feet liquefies after about 21 seconds of shaking; liquefaction extends to depths of 20, 30, and 40 feet after about 23, 32, and 40 seconds of shaking. Although the layers above 15 feet depth continue to increase in pore pressure as the shaking progresses, the rate of increase is very low after the 15-foot level liquefies. It has been noted in Seed, Martin, and Lysmer (1975) that when the pore pressure ratio in the top foot of soil reaches 60%, the ground will become soft, and a man will sink. This occurs after about 8.5 minutes in the Niigata analysis. The pore pressure ratio at the ground surface begins to decrease after about 20 minutes but would not support a man until about 40 to 50 minutes after the earthquake. The results of the computer analysis are in general agreement with observed reports.

If the water table were located at a depth of 15 feet, no significant pore pressure increases would occur in the upper 10 feet of soil even though the soil is liquefied between 15 and 40 feet. Thus, in this situation the bearing capacity of small shallow footings near the surface might well be essentially unaffected by the dissipation of pore water pressures in the liquefied zone.

Program APOLLO has been expanded into a two-dimensional computer program called GADFLEA (Booker et al., 1976). The approach is very similar to the one-dimensional analysis requiring as input information the number of cycles causing liquefaction by soil element. The number of cycles causing liquefaction is a function of the applied shear stress loading and soil confinement. These may be determined from a conventional two-dimensional elastic or inelastic finite element analysis. Using the input data program GADFLEA computes the two-dimensional pore pressure generation and dissipation from the earthquake.

Programs APOLLO and GADFLEA provide a significantly improved picture as to what is occurring to the soil and as such represents very useful tools to an engineer. The programs require values of the coefficient of permeability, coefficient of volume compressibility, and porosity. These values may be obtained for tests but are often assumed based on soil characteristics. The occurrence of liquefaction on near surface regions above the water table was found to be very sensitive to the location of the line of full saturation. Unfortunately, in field conditions a clean demarcation is not always present. As with other one-dimensional representations, the program APOLLO assumes infinite horizontal layers. This may present a problem in areas where discontinuities or slopes are present, since horizontal drainage is usually an order of magnitude greater than vertical drainage. Program GADFLEA should be used in cases requiring a two-dimensional analysis.

OBSERVATIONS OF LIQUEFACTION

Oldham (1899) reports that during the Assam, India, earthquake of 12 June 1897, a large number of jets of water rose to heights of 2 to 4 feet from fissures on the plains, carrying sand with them. The ejection of water and sand began during the earthquake and continued for 20 to 30 minutes after the shaking of ground had ceased. In many places drainage channels 15 to 20 feet deep had their bottoms forced up until they became level with the tops of their sides. Houses settled until only the roofs remained above ground.

Ambraseys and Sarma (1969) report that after the Kanto earthquake of 1923 in Japan, numerous fissures and mud volcanoes spurted intermittently. In a paddy field near the Sagami River, seven vertical wooden poles 20 feet in length suddenly emerged, finally reaching a height of about 4.5 feet above ground level. These piles, previously unknown to the local people before the earthquake, were the foundation for an old bridge built in 1182 and abandoned over 600 years earlier. In most cases, little or no damage was done to structures directly as a result of ground shaking, but rather from foundation failures.

Table 7-1 from Seed and Idriss (1971) summarizes 35 cases where available data was used in evaluation of liquefaction potential. One of the earthquakes that was well-studied occurred at Niigata, Japan in 1964.
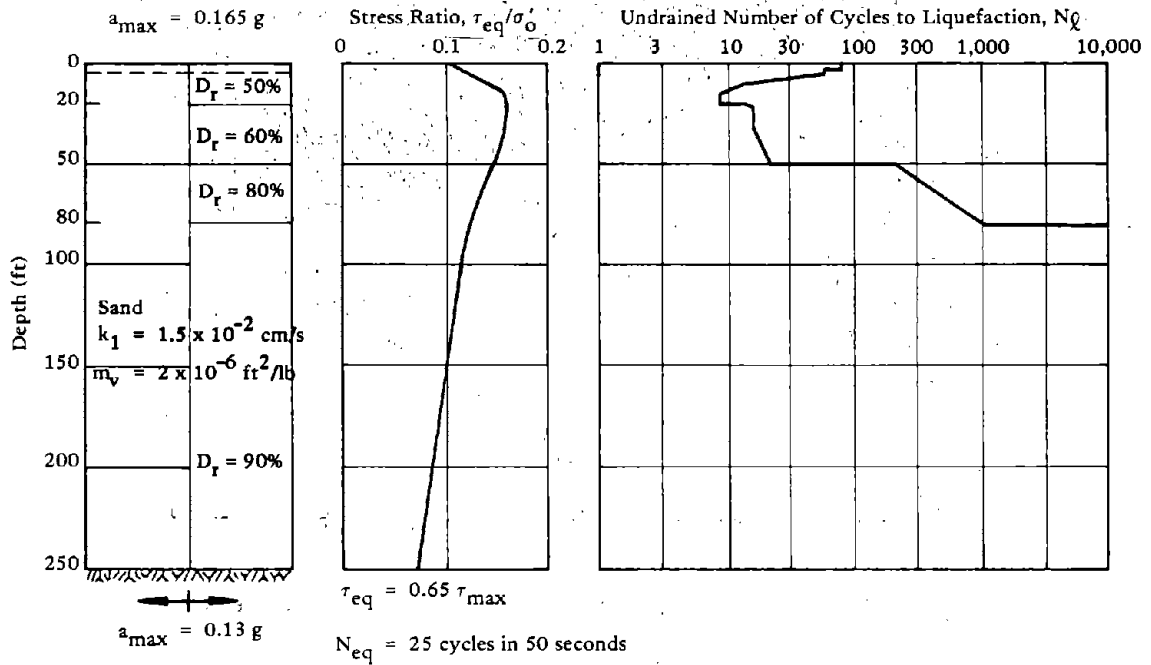
Figure 7-14. Soil profile and stress conditions used for analysis (from H. B. Seed, P. P. Martin, and J. Lysmer, 1975).
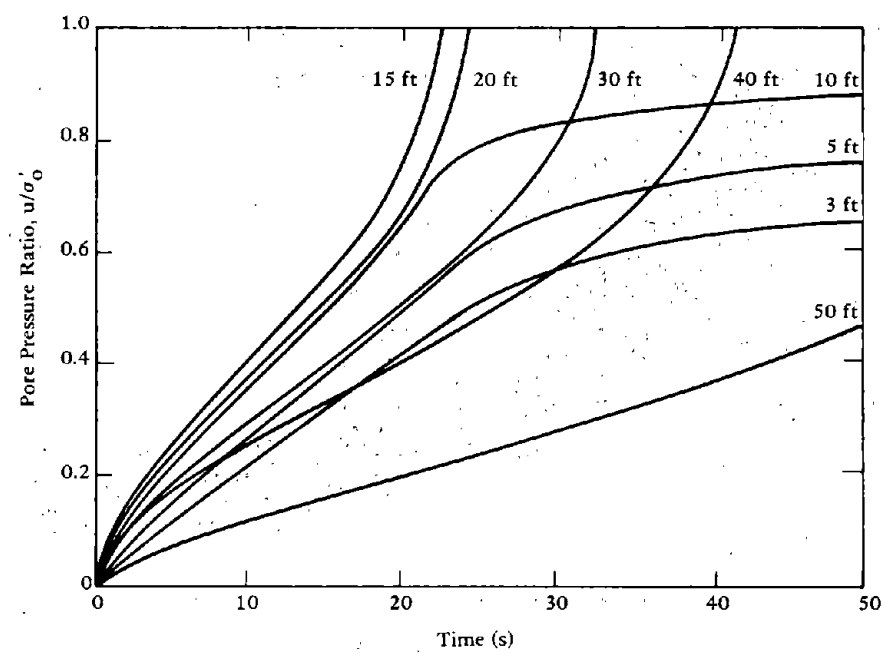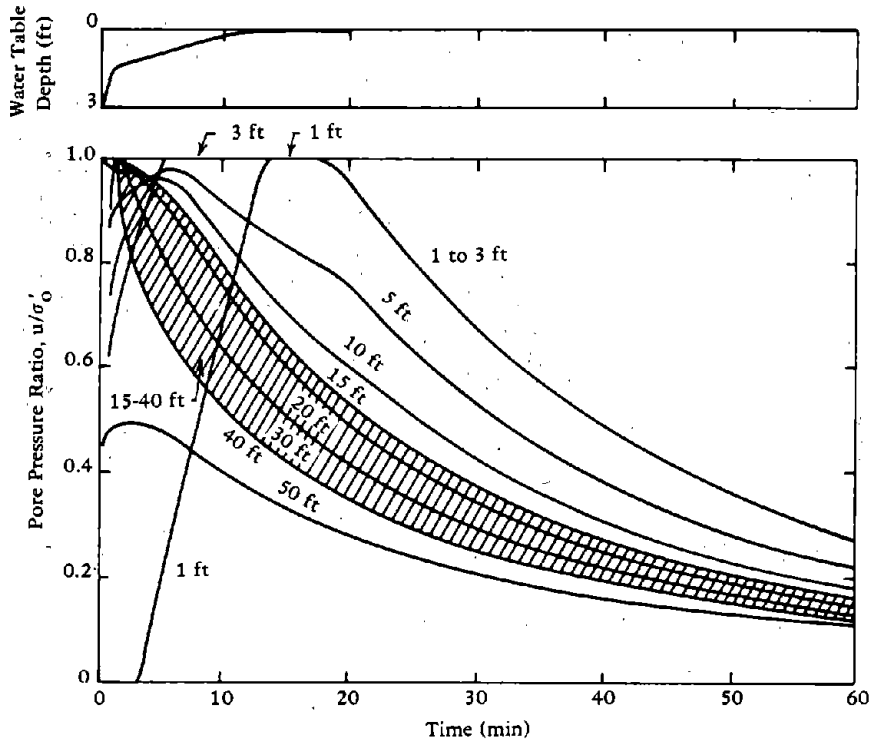

(a) During earthquake shaking.

Figure 7-15. Computed development and variation of pore water pressures for soil profile shown in Figure 7-8 (from H. B. Seed, P. P. Martin, and J. Lysmer, 1975).

200
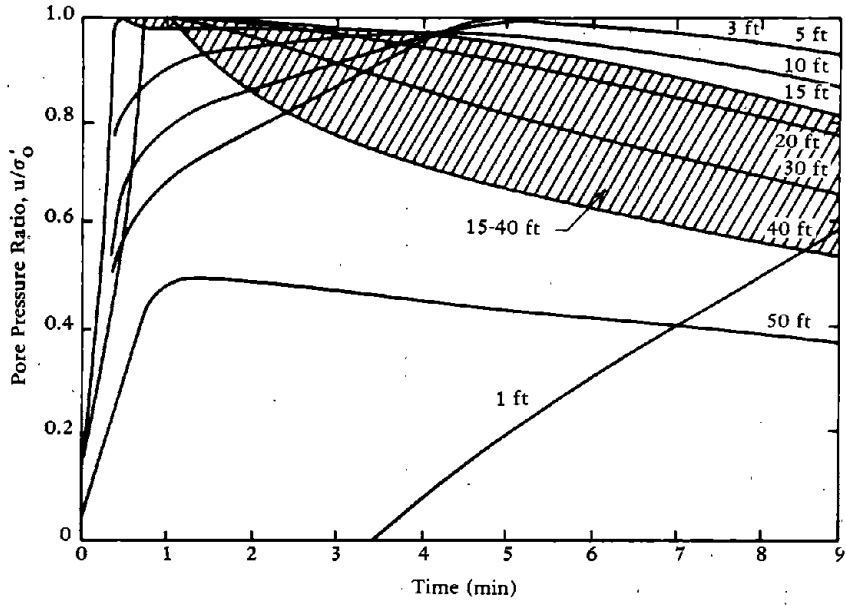
(b) In 8-minute period following earthquake.

(c) In 60-minute period following earthquake.

Figure 7-15. Continued

Table 7-1. Site Conditions and Earthquake Data for Known Cases of Liquefaction and Nonliquefaction

Earthquake	Year	Magnitude	Site	Distance From Source of Energy Release (miles)	Soil Type	Depth of Water Table (ft)	Critical Depth (ft)	Average Penetration Resistance at Critical Depth, N	Relative Density (%)	Maximum Ground Surface Acceleration (g)	τ_{av}/σ'_o	Duration of Shaking (s)	Field Behavior
Niigata	1802	6.6	Niigata	24	Sand	3	20	6	53	0.12	0.135	~20	Nonliquefaction
			Niigata	24	Sand	3	20	12	64	0.12	0.135	~20	Nonliquefaction
Niigata	1887	6.1	Niigata	29	Sand	3	20	6	53	0.08	0.09	~12	Nonliquefaction
			Niigata	29	Sand	3	20	12	64	0.08	0.09	~12	Nonliquefaction
Mino Owari	1891	8.4	Ogaki	20	Sand	3	45	17	65	~0.35	0.39	~75	Liquefaction
			Ginan West	20	Sand	6	30	10	55	~0.35	0.37	~75	Liquefaction
			Unuma	20	Sand and Gravel	6	25	19	75	~0.35	0.35	~75	Nonliquefaction
			Ogase Pond	20	Sand	8	20	16	72	~0.35	0.35	~75	Liquefaction
Santa Barbara	1925	6.3	Sheffield Dam	7	Sand	~15	25	—	40	~0.2	0.16	15	Liquefaction
El Centro	1940	7.0	Brawley	5	Sand	~15	~15	—	58	~0.25	0.155	30	Liquefaction
			All-Am. Canal	5	Sand	~20	~25	—	43	~0.25	0.155	30	Liquefaction
			Solfatara Canal	5	Sand	5	~20	—	32	~0.25	0.26	30	Liquefaction
Tohnankai	1944	8.3	Komei	100	Sand	5	13	4	40	~0.08	0.08	~70	Liquefaction
			Meiko St.	100	Silt and Sand	2	8	1	30	~0.08	0.09	~70	Liquefaction
Fukui	1948	7.2	Takaya	4	Sand	11	23	18	72	~0.30	0.30	~30	Liquefaction
			Takaya	4	Sand	3	23	28	90	~0.30	0.32	~30	Nonliquefaction
			Shonenji Temple	4	Sand	4	10	3	40	~0.30	0.29	~30	Liquefaction
			Agr. Union	4	Sand and Silt	3	20	5	50	~0.30	0.33	~30	Liquefaction
San Francisco	1957	5.5	Lake Merced	4	Sand	8	10	7	55	~0.18	0.13	18	Liquefaction
Chile	1960	8.4	Puerto Montt	~70	Sand	12	15	6	50	~0.15	0.15	~75	Liquefaction
			Puerto Montt	~70	Sand	12	15	8	55	~0.15	0.15	~75	Liquefaction
			Puerto Montt	~70	Sand	12	20	18	75	~0.15	0.15	~75	Nonliquefaction
Niigata	1964	7.5	Niigata	32	Sand	3	20	6	53	0.16	0.175	40	Liquefaction
			Niigata	32	Sand	3	25	15	70	0.16	0.175	40	Liquefaction
			Niigata	32	Sand	3	20	12	64	0.16	0.175	40	Nonliquefaction
			Niigata	32	Sand	12	25	6	53	0.16	0.16	40	Nonliquefaction
Alaska	1964	8.3	Snow River	60	Sand	0	20	5	50	~0.15	0.18	180	Liquefaction
			Snow River	60	Sand	8	20	5	44	~0.15	0.15	180	Liquefaction
			Quartz Creek	70	Sandy Gravel	0	~25	40–80	100	~0.12	0.145	180	Nonliquefaction
			Scott Glacier	55	Sand	~20	~20	10	65	~0.16	0.185	180	Liquefaction
			Valdez	35	Sand and Gravel	5	~20	13	68	~0.25	0.25	180	Liquefaction
Tokachioki	1968	7.8	Hachinohe	45 to 110	Sand	3	12	14	78	0.21	0.23	45	Nonliquefaction
			Hachinohe	45 to 110	Sand	3	12	6	58	0.21	0.73	45	Liquefaction
			Hachinohe	45 to 110	Sand	5	10	15	80	0.21	0.185	45	Nonliquefaction
			Hakodate	100	Sand	3	15	6	55	0.18	0.205	45	Liquefaction

NIIGATA EARTHQUAKE OF 1964

Seed and Idriss (1967) describe the extensive damage from the magnitude 7.5 earthquake which occurred 35 miles north of the city of Niigata, Japan on 16 June 1964. The acceleration level at the city was about 0.16. Observed damage may be divided into four groups, as shown in Table 7-2.

Table 7-2. Niigata Earthquake

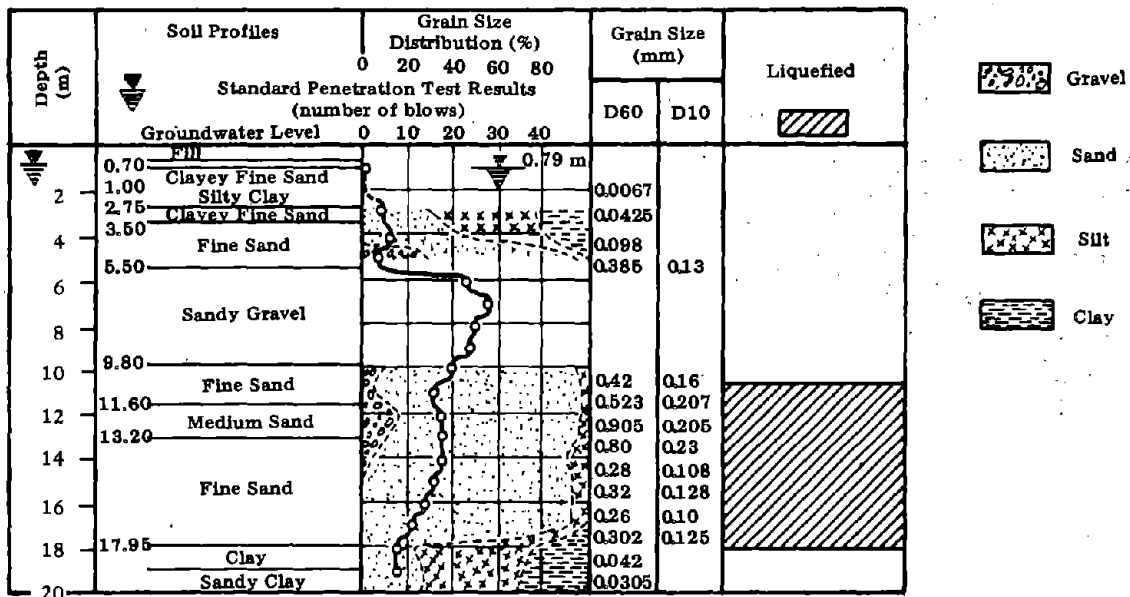| Damage to Foundation	Maximum Settlement (in.)	Angle of Tilt (deg)	Average Relative Density (%)	Range of Relative Density (%)
None	0-8	0-0.3	75	60-90
Slight	8-20	0.3-1	67	50-85
Intermediate	20-40	1-2.3	60	45-75
Heavy	>40	>2.3	45	30-60

The determination of the relative density of the *in situ* sands is extremely crude as extrapolated from the data presented by Seed and Idriss (1971).

It was noted that piles driven through loose zones into firm zones experienced significant horizontal displacement. When liquefaction occurs around the upper portion of the pile the pile loses its lateral resistance, producing movement. There were many cases of bending of piles supporting buildings in Niigata.

Kishida (1969) reports that the upper surface of the liquefied soil layer in the most severely damaged area was situated at a depth of less than 25 feet below the ground surface and that soils as deep as 75 feet were liquefied.
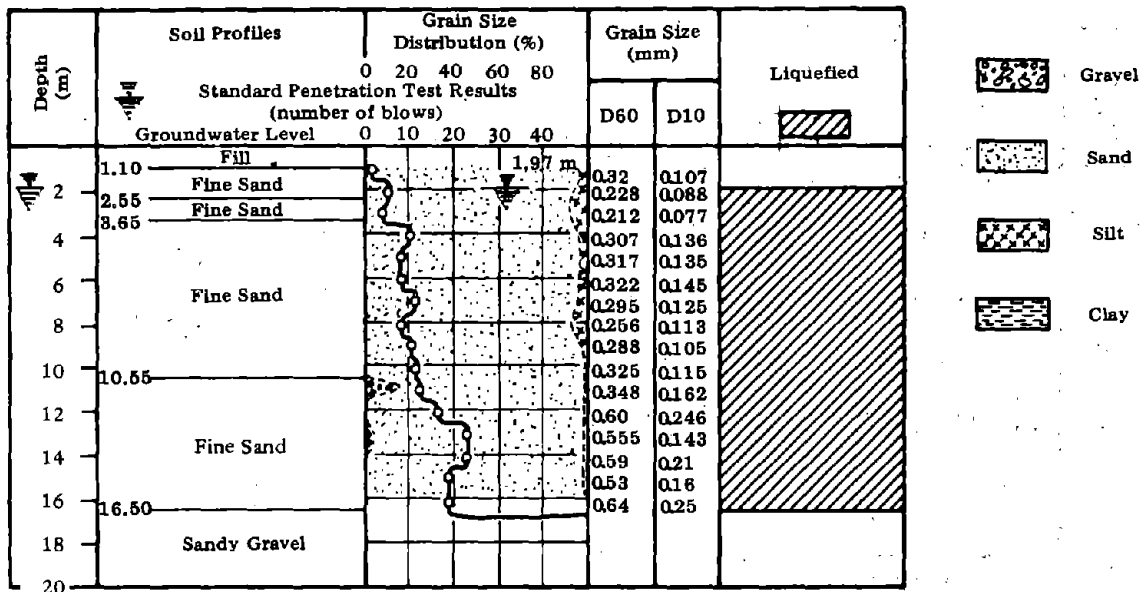
MINO OWARI EARTHQUAKE OF 1891

The Mino Owari earthquake of 28 October 1891 was a shock of 8.4 magnitude located 18.6 miles from the city of Gifu, Japan. Kishida (1969) has studied the effects of this earthquake and gives profiles of four locations (Figures 7-16 to 7-19) which show various degrees of liquefaction ranging from none to complete. Note that fine sands were most vulnerable.

Figure 7-16

Depth (m)	Soil Profiles	Grain Size Distribution (%) / Standard Penetration Test Results (number of blows)	D60	D10	Liquefied
0.70	Fill	▼ 0.79 m			
1.00	Clayey Fine Sand		0.0067		
2.75	Silty Clay				
3.50	Clayey Fine Sand		0.0425		
5.50	Fine Sand		0.098		
			0.385	0.13	
9.80	Sandy Gravel				
11.60	Fine Sand		0.42	0.16	
13.20	Medium Sand		0.523	0.207	
			0.905	0.205	
			0.80	0.23	
17.95	Fine Sand		0.28	0.108	
			0.32	0.128	
			0.26	0.10	
	Clay		0.302	0.125	
	Sandy Clay		0.042		
			0.0305		

Partial Liquefaction Eruption of Water and Soil

Gravel | Sand | Silt | Clay

Figure 7-16. Soil profile, Ogaki City, Bangoku town (from H. B. Kishida, 1969).

Figure 7-17

Depth (m)	Soil Profiles	Grain Size Distribution (%) / Standard Penetration Test Results (number of blows)	D60	D10	Liquefied
1.10	Fill	▼ 1.97 m	0.32	0.107	
2.55	Fine Sand		0.228	0.088	
3.65	Fine Sand		0.212	0.077	
			0.307	0.136	
			0.317	0.135	
	Fine Sand		0.322	0.145	
			0.295	0.125	
			0.256	0.113	
			0.288	0.105	
10.55			0.325	0.115	
			0.348	0.162	
			0.60	0.246	
	Fine Sand		0.555	0.143	
			0.59	0.21	
			0.53	0.16	
16.50			0.64	0.25	
	Sandy Gravel				

Complete Liquefaction Many Sand Volcanoes

Gravel | Sand | Silt | Clay

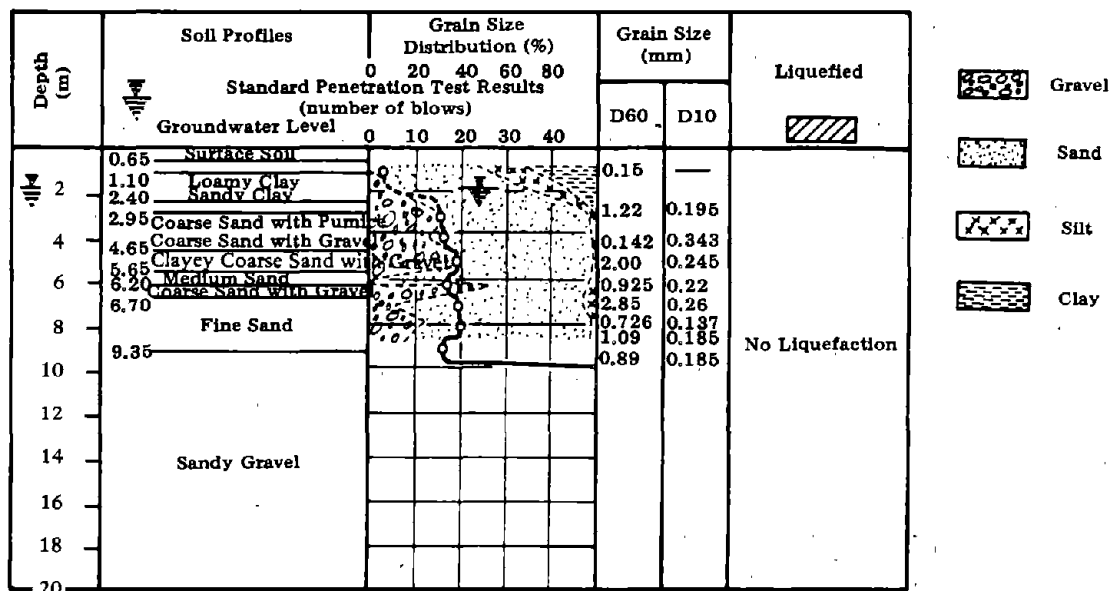Figure 7-17. Soil profile, Ginan West Primary School (from H. Kishida, 1969).

204

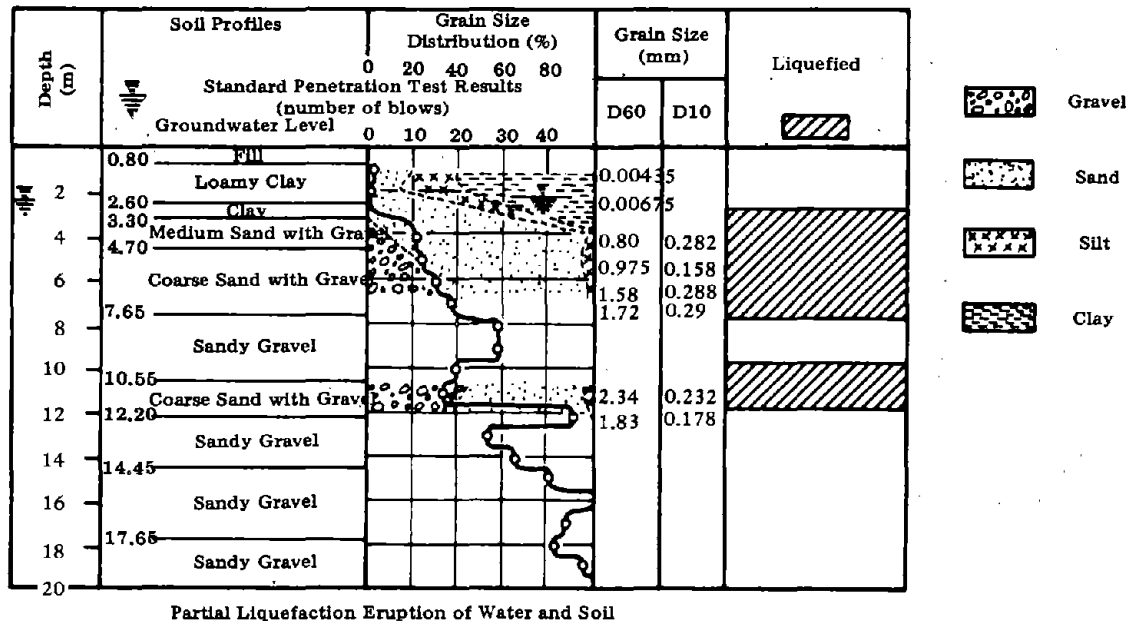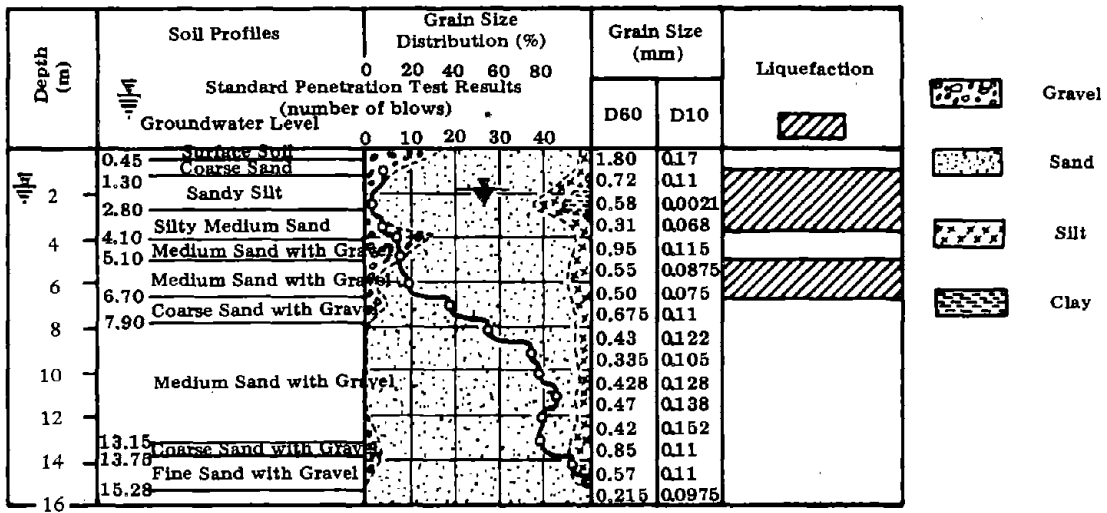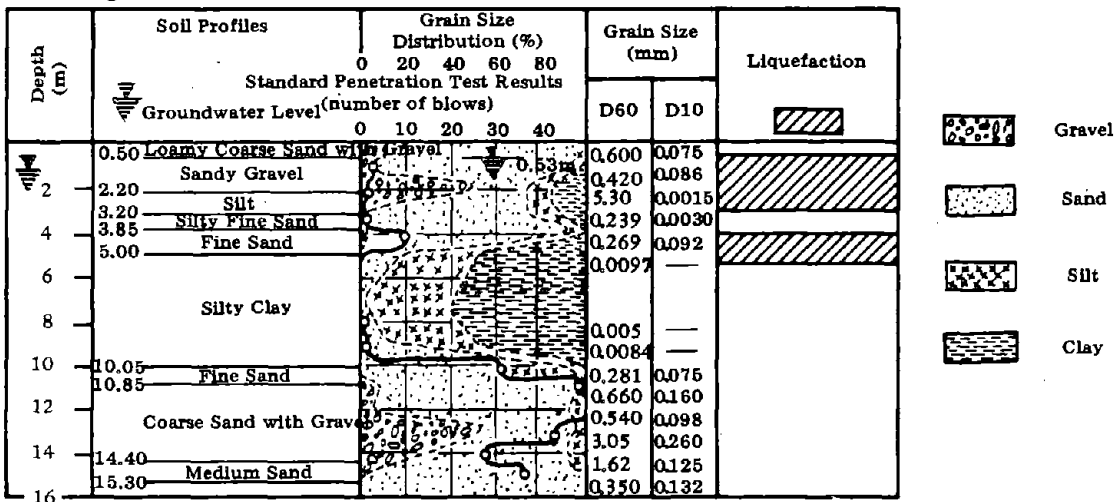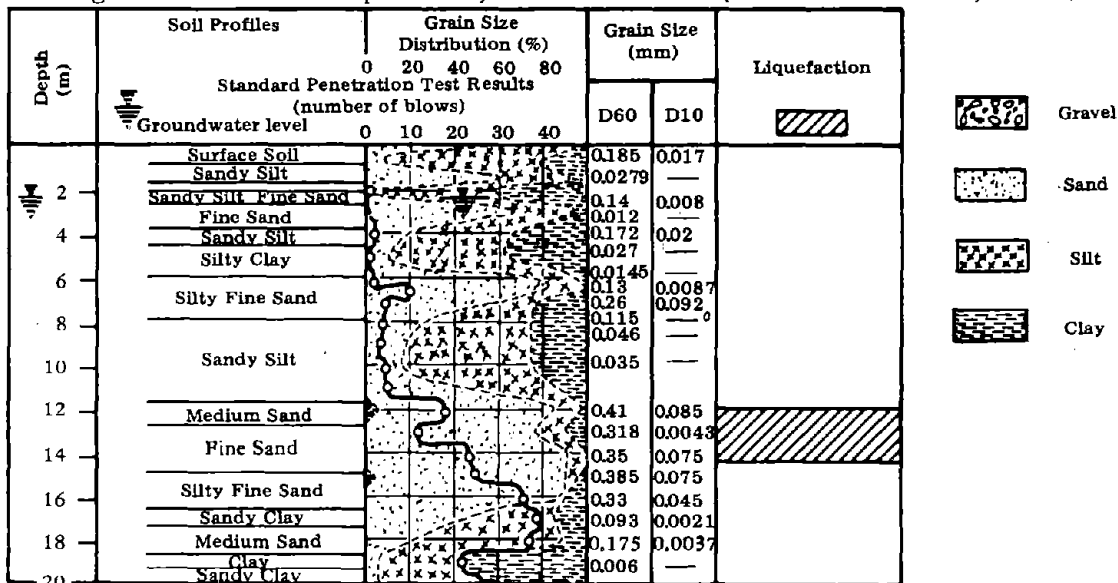Figure 7-18. Soil profile, Unuma town (from H. Kishida, 1969).

Partial Liquefaction Eruption of Water and Soil

Figure 7-19. Soil profile, Ogase Pond (from H. Kishida, 1969).

205

Figure 7-20

Depth (m)	Soil Profiles	D60	D10
0.45	Surface Soil	1.80	0.17
1.30	Coarse Sand	0.72	0.11
	Sandy Silt	0.58	0.0021
2.80			
	Silty Medium Sand	0.31	0.068
4.10	Medium Sand with Gravel	0.95	0.115
5.10		0.55	0.0875
	Medium Sand with Gravel	0.50	0.075
6.70	Coarse Sand with Gravel	0.675	0.11
7.90		0.43	0.122
		0.335	0.105
	Medium Sand with Gravel	0.428	0.128
		0.47	0.138
		0.42	0.152
13.15	Coarse Sand with Gravel	0.85	0.11
13.78	Fine Sand with Gravel	0.57	0.11
15.28		0.215	0.0975

Complete Liquefaction

Gravel · Sand · Silt · Clay

Figure 7-20. Soil profile, Komei town (from H. Kishida, 1969).

Figure 7-21

Depth (m)	Soil Profiles	D60	D10
0.50	Loamy Coarse Sand with Gravel	0.600	0.075
	Sandy Gravel	0.420	0.086
2.20		5.30	0.0015
3.20	Silt	0.239	0.0030
3.85	Silty Fine Sand		
5.00	Fine Sand	0.269	0.092
		0.0097	—
	Silty Clay		
		0.005	—
		0.0084	—
10.05	Fine Sand	0.281	0.075
10.85		0.660	0.160
	Coarse Sand with Gravel	0.540	0.098
		3.05	0.260
14.40		1.62	0.125
15.30	Medium Sand	0.350	0.132

Complete Liquefaction

Gravel · Sand · Silt · Clay

Figure 7-21. Soil profile, Meiko Street (from H. Kishida, 1969).

Figure 7-22

Depth (m)	Soil Profiles	D60	D10
	Surface Soil	0.185	0.017
	Sandy Silt	0.0279	—
	Sandy Silt Fine Sand	0.14	0.008
	Fine Sand	0.012	—
	Sandy Silt	0.172	0.02
	Silty Clay	0.027	—
		0.0145	—
	Silty Fine Sand	0.13	0.0087
		0.26	0.092
		0.115	—
		0.046	—
	Sandy Silt	0.035	—
	Medium Sand	0.41	0.085
	Fine Sand	0.318	0.0043
		0.35	0.075
		0.385	0.075
	Silty Fine Sand	0.33	0.045
	Sandy Clay	0.093	0.0021
	Medium Sand	0.175	0.0037
	Clay	0.006	—
	Sandy Clay		

Partial Liquefaction Eruption of Water and Soil

Gravel · Sand · Silt · Clay

Figure 7-22. Soil profile, Ienaga Shinden (from H. Kishida, 1969).

206

TOHNANKAI EARTHQUAKE OF 1944

The Tohnankai earthquake of 7 December 1944 was a magnitude 8.3 earthquake located about 100 miles south-southwest of Nagoya City, Japan. Kishida (1969) studied the effects of this earthquake at three locations (Figure 7-20 to 7-22). At the location noted in Figure 7-20 a Buddhist Temple which was supported on piles did not show any settlement but the ground around the temple subsided about 1-1/3 feet, and water erupted during the earthquake. The tips of the piles were at a depth of about 5 meters below the surface (26.7 feet). Figure 7-21 shows a soil profile where houses settled as much as 3.3 feet. Fine sand was expelled from the ground. Figure 7-22 shows a soil profile where differential settlement occurred as a result of partial liquefaction.

FUKUI EARTHQUAKE OF 1948

The Fukui earthquake of 18 June 1948 was a magnitude 7.2 earthquake with its epicenter 3 miles east of Fukui City, Japan. Kishida (1969) studied the effects of this earthquake and gives four profiles (Figures 7-23 to 7-26) where liquefaction was observed in varying degrees. It is interesting to note that although the distance between locations of the soil profiles in Figure 7-23 and 7-24 was only about 1,800 feet, one underwent complete liquefaction with sand volcanoes noted on the surface and the other only partial limited liquefaction, the latter being an older area approximately 3.3 feet higher in elevation with more silt. Figure 7-25 shows a site where water and sand volcanoes were quite prevalent and the main building of a temple settled 1 foot. The distance between the locations shown in Figures 7-25 and 7-26 is about 1,800 feet. The site in Figure 7-26 did not show eruptions of sand and water and only partial liquefaction. This site is again in older ground slightly higher than that of Figure 7-25.

NONLIQUEFACTION (PRE-LIQUEFACTION) SUBSIDENCE

Lee and Albasia (1974), using cyclic triaxial tests, have investigated the settlements from volume change due to the dissipation of increased pore pressures. Their work is intended to represent general ground subsidence which might be expected from soil compaction and water drainage at stresses less than that required to induce complete liquefaction. Figure 7-27 shows a series of triaxial test results, considering the effects of confining pressure, relative density, and grain size on volumetric strain. Using Figure 7-11 or 7-28, the increase in pore pressure at any cycle less than N_L may be estimated. This increase in pore pressure can be used in conjunction with Figure 7-27 to estimate the volumetric strain from the rise in pore pressure and resulting drainage.
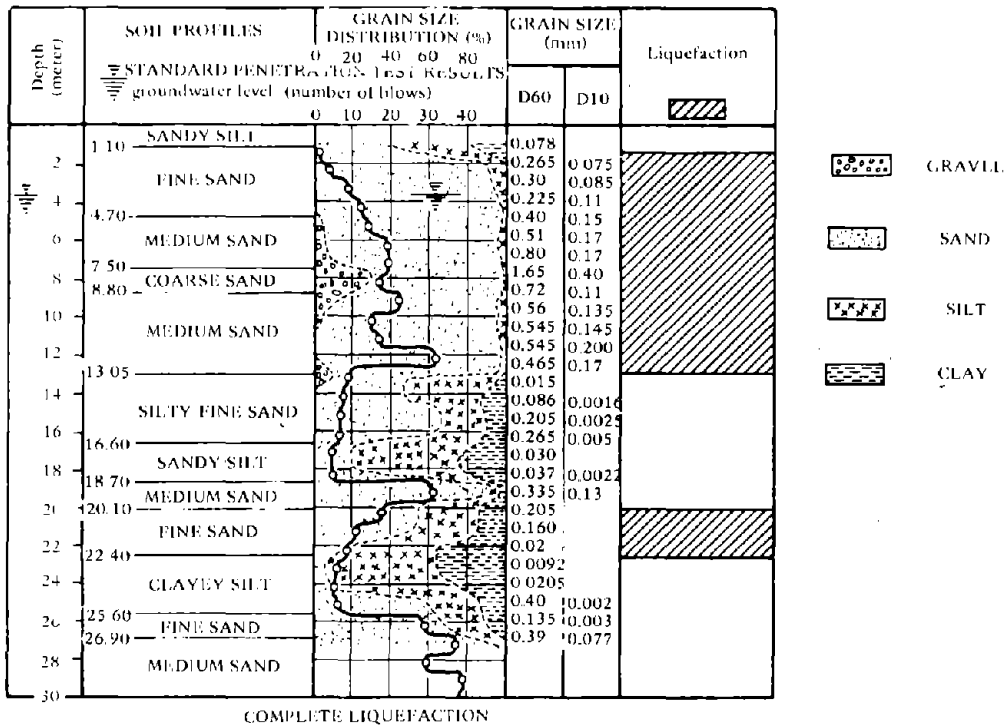
Figure 7-23. Soil profile, Takaya town 45-35 (from H. Kishida, 1969).
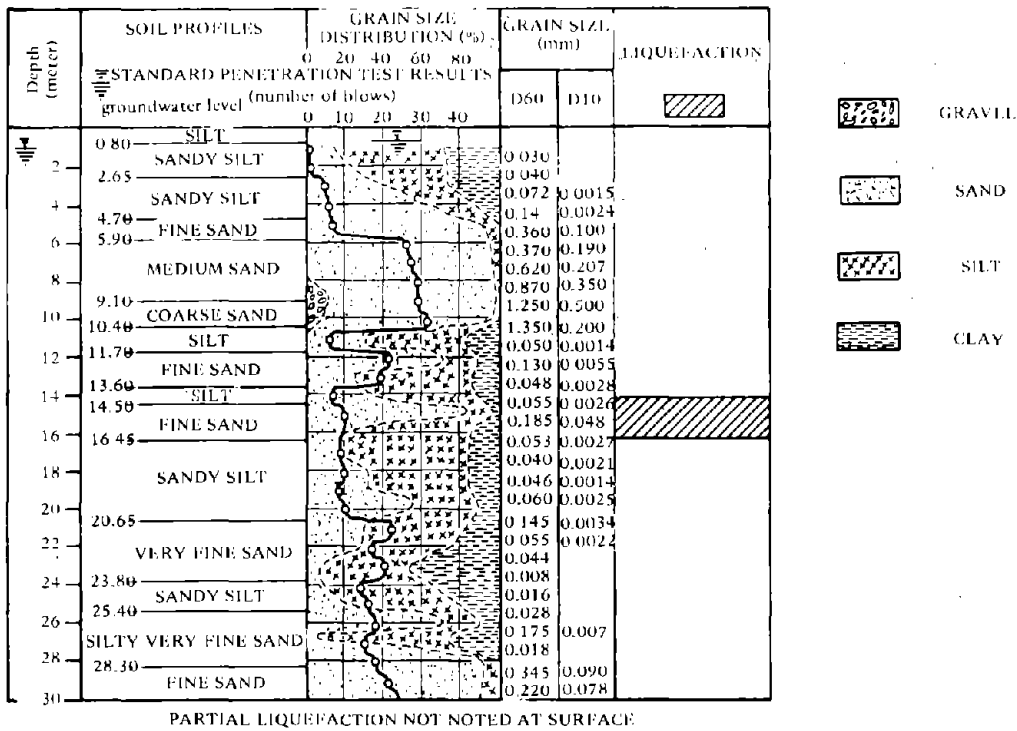
Figure 7-24. Soil profile, Takaya town 2-168 (from H. Kishida, 1969).

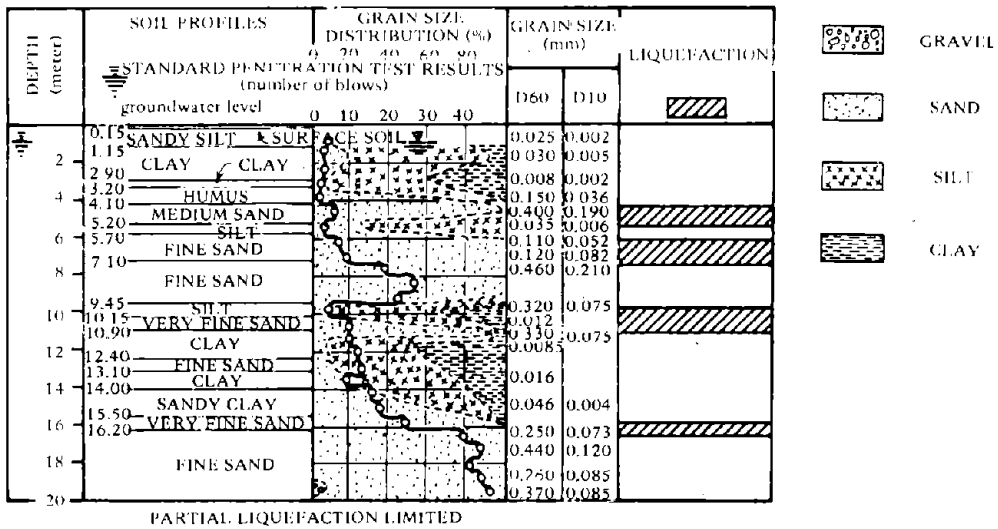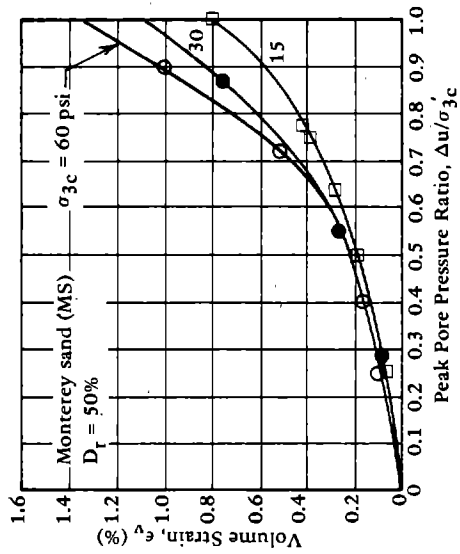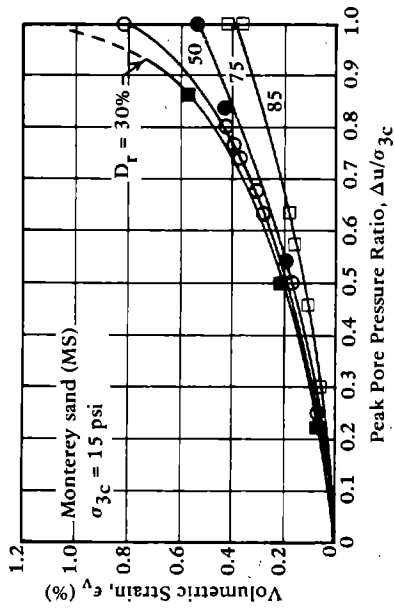**Figure 7-25. Soil profile, Shonenji Temple (from H. Kishida, 1969).**
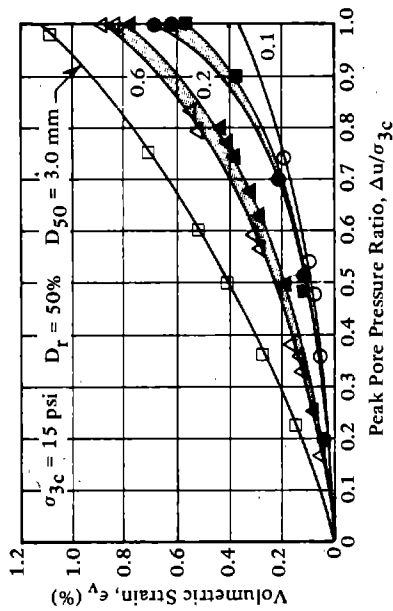
DEPTH (meters)	SOIL PROFILES	GRAIN SIZE (mm) D60	GRAIN SIZE (mm) D10
1.20	VERY FINE SAND	0.140	0.090
1.80	FINE SAND	0.250	0.085
	FINE SAND	0.460	0.330
3.60	FINE SAND	0.410	0.270
4.20	MEDIUM SAND	7.500	0.450
5.60	COARSE SAND WITH GRAVEL	5.300	0.700
		8.500	0.550
		5.800	0.800
9.50	SANDY CLAY	0.220	0.072
10.90		0.190	0.090
		0.230	0.085
		0.220	0.100
	FINE SAND	0.380	0.180
		0.390	0.150
		0.400	0.200
		0.320	0.120
		0.44	0.720
		0.570	0.130
		0.610	0.200

COMPLETE LIQUEFACTION

Legend: GRAVEL, SAND, SILT, CLAY

Figure 7-25. Soil profile, Shonenji Temple (from H. Kishida, 1969).

Figure 7-26. Soil profile, agricultural union (from H. Kishida, 1969).

DEPTH (meter)	SOIL PROFILES	GRAIN SIZE (mm) D60	GRAIN SIZE (mm) D10
0.15	SANDY SILT & SURFACE SOIL	0.025	0.002
1.15	CLAY	0.030	0.005
2.90	CLAY	0.008	0.002
3.20	HUMUS	0.150	0.036
4.10	MEDIUM SAND	0.400	0.190
5.20	SILT	0.035	0.006
5.70	FINE SAND	0.110	0.052
7.10	FINE SAND	0.120	0.082
		0.460	0.210
9.45	SILT	0.320	0.075
10.15	VERY FINE SAND	0.012	
10.90	CLAY	0.330	0.075
12.40	FINE SAND	0.0085	
13.10	CLAY	0.016	
14.00	SANDY CLAY		
15.50	VERY FINE SAND	0.046	0.004
16.20	FINE SAND	0.250	0.073
		0.440	0.120
		0.260	0.085
		0.370	0.085

PARTIAL LIQUEFACTION LIMITED

Legend: GRAVEL, SAND, SILT, CLAY

Figure 7-26. Soil profile, agricultural union (from H. Kishida, 1969).

209

(b) Relative density on reconsolidation volumetric strain.

(d) Relative density on volumetric strain following complete liquefaction.

(a) Confining pressure on reconsolidation volumetric strain.

(c) Grain size on reconsolidation volumetric strain.

Figure 7-27. Effect of various factors on volumetric strain (from "Earthquake Induced Settlements in Saturated Sands," by K. L. Lee and A. Albasia, in Journal of the Geotechnical Division, ASCE, vol. 100, GT4, Apr 1974).
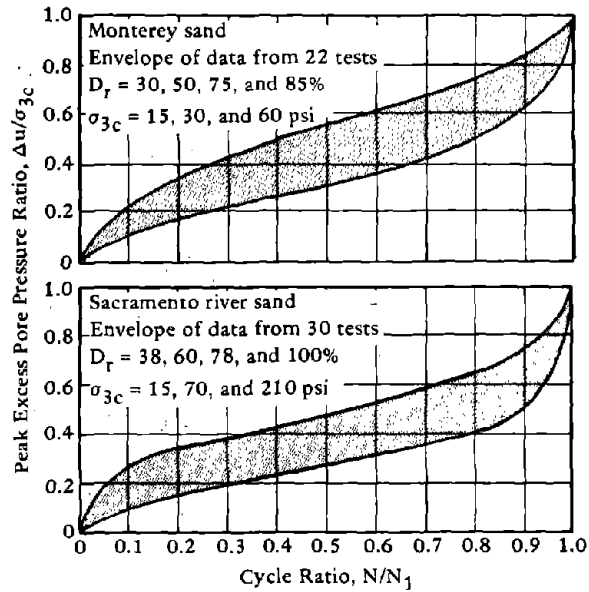
Figure 7-28. Compilation summary of pore pressure buildup data
(from "Earthquake Induced Settlements in Saturated Sands,"
by K. L. Lee and A. Albasia, in Journal of the
Geotechnical Division, ASCE, vol. 100,
no. GT4, Apr 1974).

Figures 7-27a, b, and c are limited to conditions in which complete liquefaction does not occur. The volumetric strain and the thickness of the layer can be used to estimate the vertical settlement. This is intended for level areas without concentrated footing loads which may cause shear displacements. The volumetric settlements from pore pressures lower than those causing liquefaction are generally less than 1%. Lee and Albasia (1974) have also investigated cases when liquefaction occurs. Their data, Figure 27d, indicates that vertical settlements from drainage effects may be as much as 3% of the height of the affected soil layer. This does not consider the effects of soil bearing failures but only the "regional" subsidence.

BRIDGE RESPONSE TO LIQUEFACTION

Figure 7-1 shows a three-component record of ground acceleration during an earthquake. It was pointed out that the level' of motion was significantly reduced at the onset of liquefaction; the liquefied soil acts as an isolating medium separating the structure from the driving "bedrock" layer. Further, it was previously shown that there is a delay

211
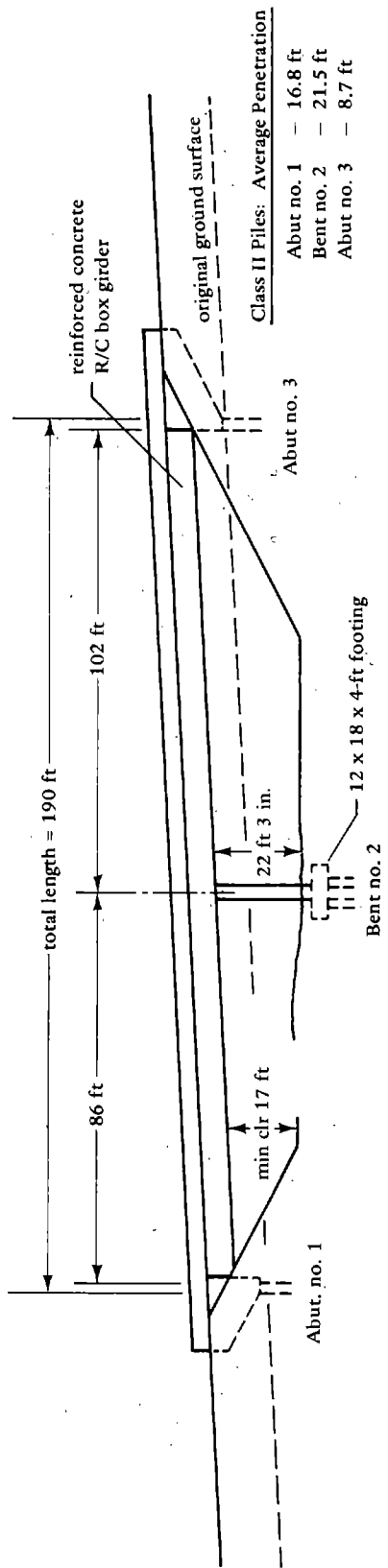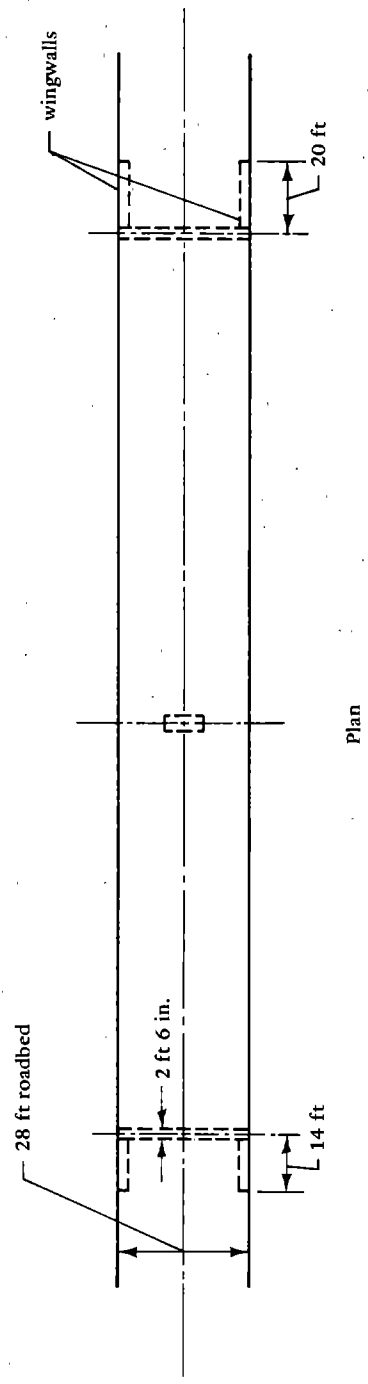
Figure 7-29. Bahia overcrossing (BS 23-161) near Benecia, California.

212

time for propagation of liquefaction of a subsurface layer to the surface.
Figure 7-5 shows this in terms of the pore pressure buildup in a top
layer of a two-layer model. Considering the shock isolation effect and
the time delay for liquefaction propagation it is reasonable to treat
the bridge analysis as a static displacement or foundation support
failure problem. This greatly simplifies the problem but should give
reasonable evaluations of the bridge response. Conventional static
structural analysis techniques may be used to estimate induced bridge
structure stresses from support displacement.

Rigid Frame-Type Structure

Figure 7-29 gives a typical continuous two-span bridge. Data for
this analysis was taken from Robinson et al. (1975). The standard
H20 S16 loading acting with the actual deadload was used. It was first
assumed that liquefaction occurred in a subsurface layer and did not
propagate to the surface to cause a loss of adequate bearing resistance.
Settlement of the center column was analyzed, and the results are shown
in terms of the reduction of the load factor (Figure 7-30). The formation
of the first hinge was taken as the basis for the load factor. As shown
in Figure 7-30, the load factor drops from 2.28 to 1.0 with the occurrence
of 13 inches of vertical deflection or 0.33 inch of horizontal deflec-
tion or 0.0022 degree of rotation. It is thus obvious that the formation
of the first hinge is very sensitive to horizontal displacement and
rotation.

The second case assumed that the liquefaction propagated to the
surface and that the support capacity of the center column was signifi-
cantly reduced. A hinge was formed in the girder at a load factor of
0.73 with a column vertical deflection of 13 inches. At a load factor
of 1.0 the vertical displacement of the column was great (about 8 feet).

It is interesting to note that the deadload represented 85% of the
total load. It is obvious that the bridge cannot maintain its own
deadweight and will collapse in the event liquefaction eliminates the
bearing capacity of the center column. For the case of a subsurface
liquefied layer, Table 7-2 based on a Niigata type earthquake 7.5 magni-
tude, indicates relative densities of at least 70% would be required to
prevent formation of the first hinge.

Simply Supported Structure

Figure 7-31 shows a four-span prestressed concrete bridge; each
span is simply supported. Figure 7-32 shows the anchorage at the supports.
Depending upon the amount of slip provided for, the anchor bolts would
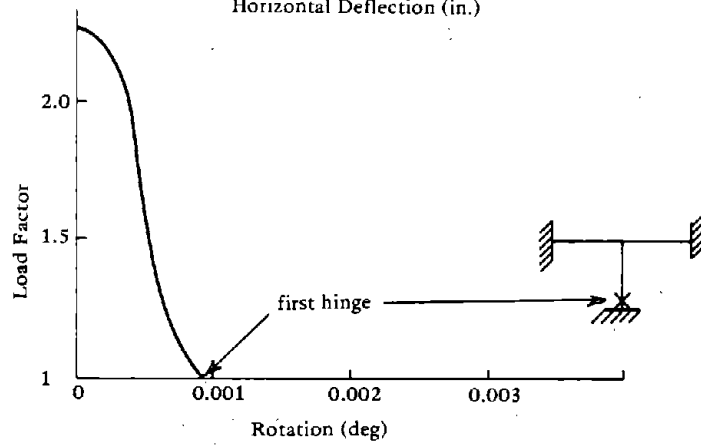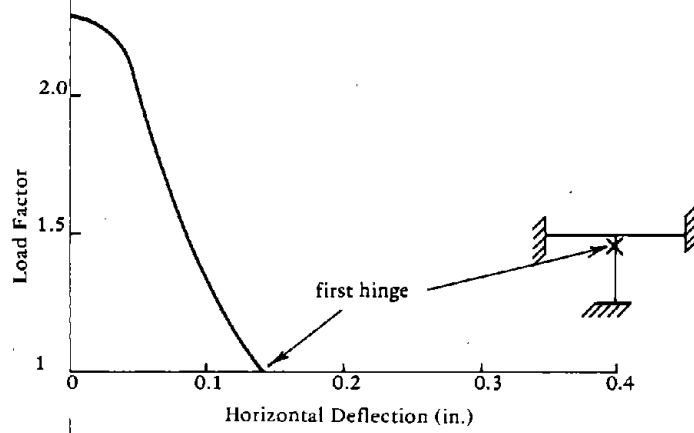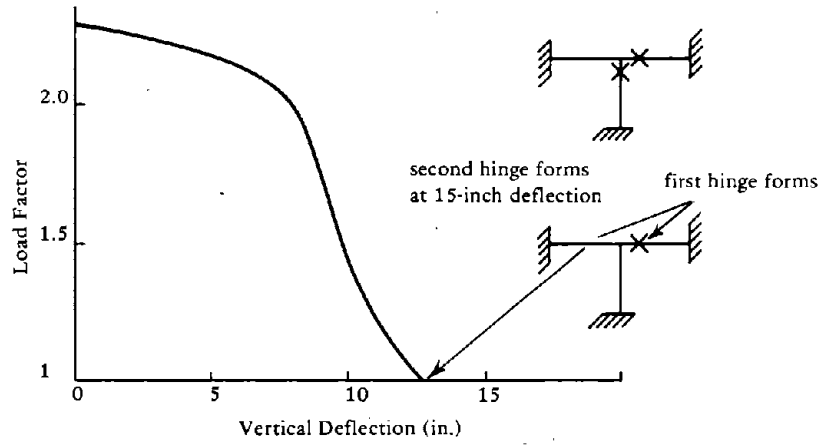
Figure 7-30. Displacement analysis of Bahia overcrossing.

fail with a relatively small vertical displacement of the center column. Figure 7-33 shows conditions in which combinations of differential settlements would cause the unrestrained simply supported girders to fall from their supports. The structure is more sensitive to horizontal differential motion and foundation rotation than vertical differential motion. The amounts of acceptable differential settlement are larger than those of the rigid frame-type bridge. However, the loss of bearing capacity at the center column results in the collapse of the structure.

EFFECT OF FOUNDATION ON LIQUEFACTION

Yoshimi and Oh-Oka (1974) performed a two-dimensional elastic analysis of a foundation under dynamic load. They conclude that the presence of the structure causes the dynamic shear stress ratio to increase at shallow depths outside the foundation. It was suggested that the region on a diagonal away from the edge of a footing would undergo liquefaction before the free field (area away from effects of the structure).

So significant is this hypothesis, if true, that this problem will be discussed here. It appears the gravity static stresses were not considered in the analysis of Yoshimi and Oh-Oka (1974). Furthermore, the choice of shear stress and confining stress were horizontal shear stress and vertical normal stress, rather than those of a principal stress orientation. The horizontal and vertical axis in the presence of initial static stress is an arbitrary choice.

In Chapter 2 a methodology was presented for computing an equivalent dynamic stress which would consider the effects of initial static shear stress from a foundation. In this analysis principal planes are used. This methodology was used in the following study.

To study the bridge foundation problem, an elastic finite element analysis was performed. The soil was modeled by plane strain two-dimensional quadrilateral elements. The footing was also modeled using the same type of element with different material properties. To attempt to model the bridge loading correctly, a typical bridge column extended vertically above the footing. The top of the column was restrained by horizontal one-dimensional elements (springs) whose stiffness and mass were typical of the lateral restraint and mass provided by a bridge deck. Figure 7-34 shows the finite element mesh.

The linear elastic analysis was performed in segments and the results combined. The static gravity analysis was combined with the results of a dynamic ground-motion analysis. In the dynamic analysis, the equivalent stress level was determined in terms of the principal stresses for each element.

215
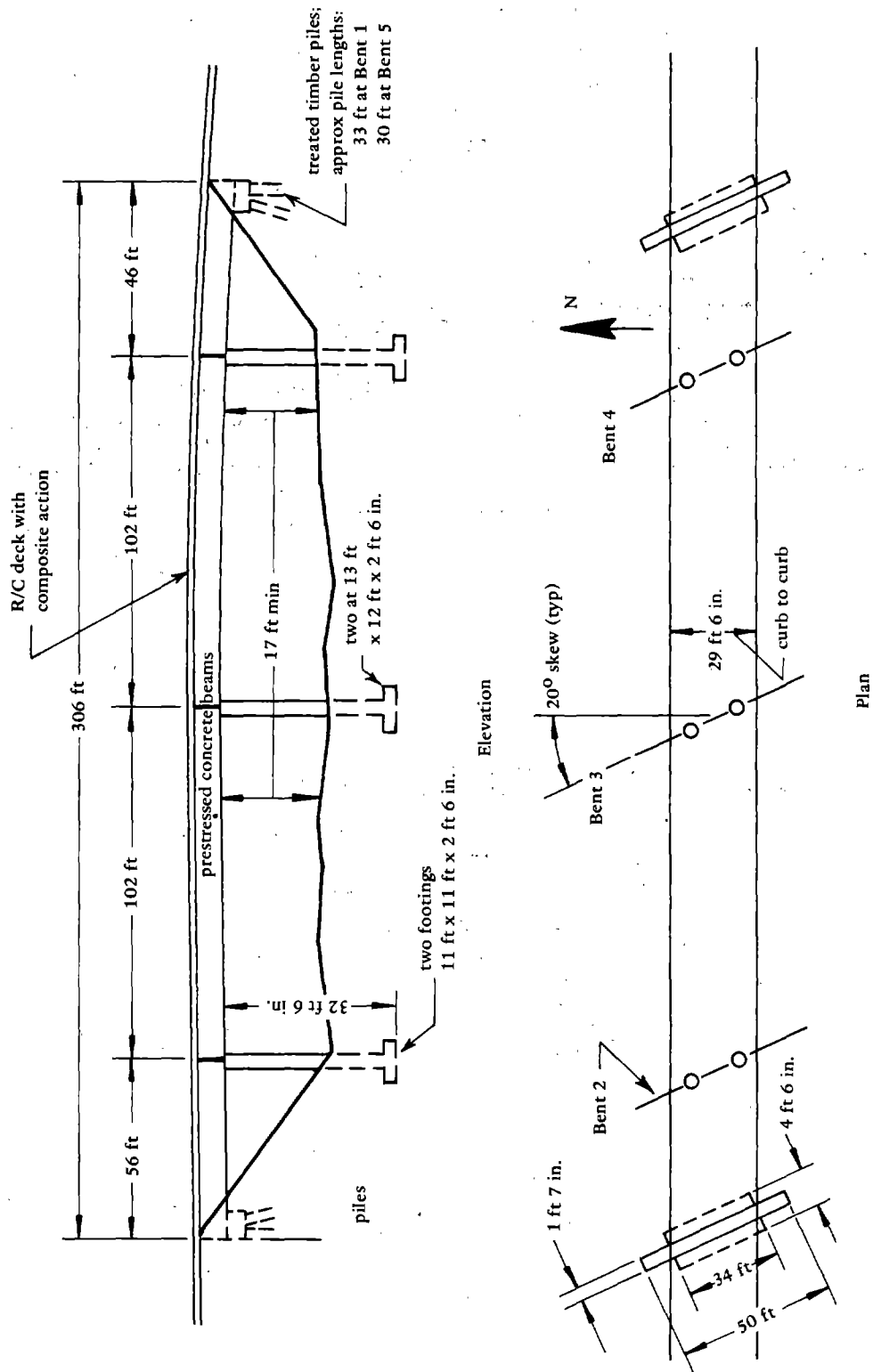
Figure 7-31. County road separation structure over Interstate 15 near Dillon, Montana.

End View

5 in. x 2 ft 8 in.

1/2

1-1/4 in. x 6 in. x 2 ft 8 in.

8.485 in.

6 in.

2 ft 5 in.

2 ft 8 in.

Swedged anchor bolt:

1-1/4 diam x 1 ft 4 in. set 1 ft into cap at Bent 1, east side of Bent 2, both sides of Bent 3, and west side of Bent 4

1 in. diam x 1 ft 2 in. set 10 in. into cap at west side of Bent 2, east side of Bent 4, and at Bent 5

Section C-C

perpendicular to grade of beam

centerline bearing

two no. 6 x 2 ft 2 in. long reinforcing bars welded to 1-1/4 in. x 6 in. x 2 ft 2 in. plate

6 in.

1 ft

8.485 in.

1 in. at centerline bearing

1-1/4 in.

drill 1-1/2 in. holes

2 ft radius

5 in.

6 in.

Figure 7-32.   Bearing shoe details of structure over Interstate 15.

Based on stiffness of bridge girder
and deck; a deflection of about
7.5 inches fails the anchor bolts
denoted by shaded section at
origin
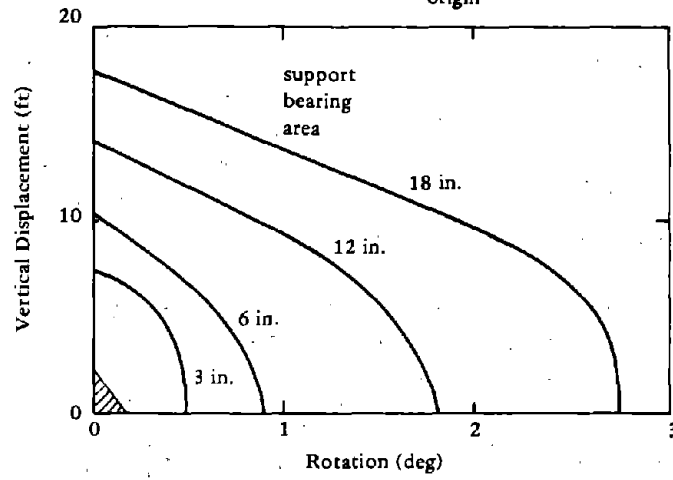
Note that full loss of
bearing capacity
results in collapse
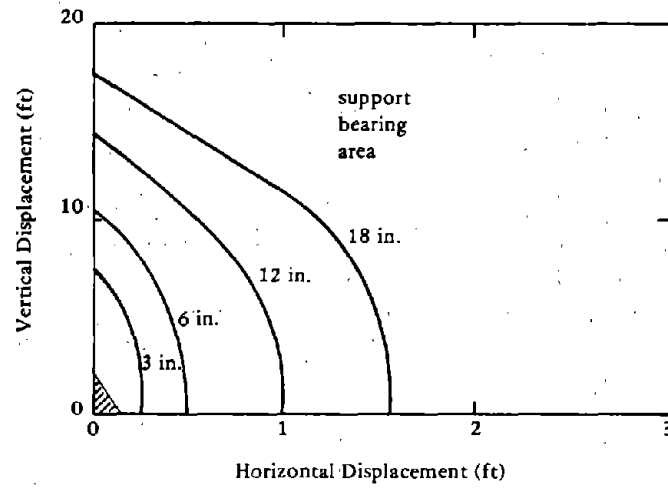
Figure 7-33. Support displacements.
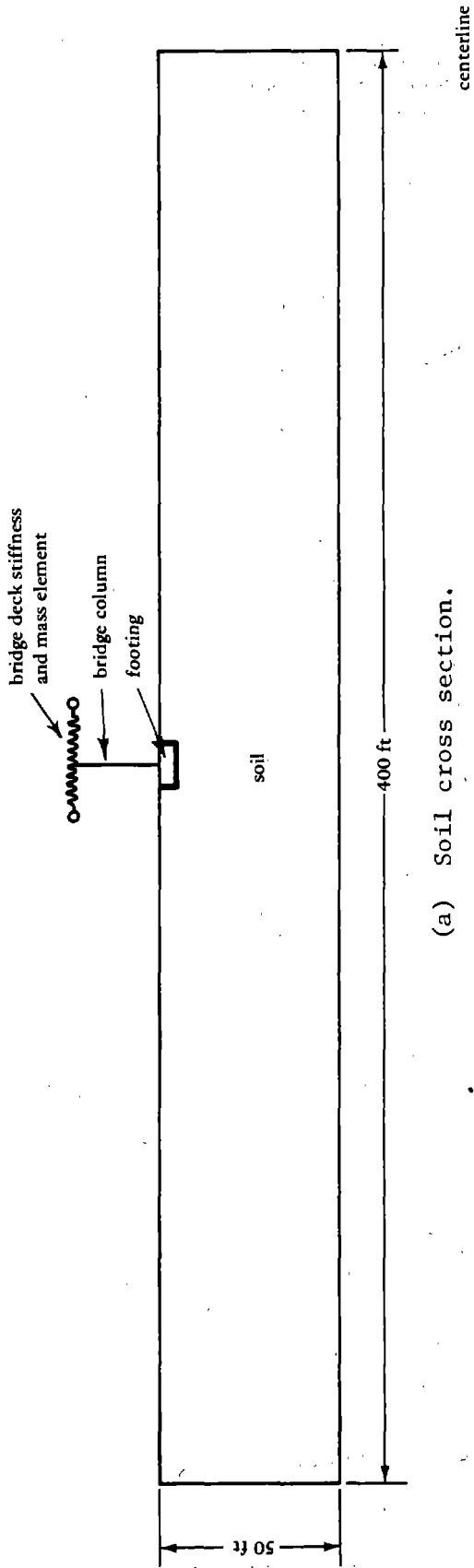
(a) Soil cross section.
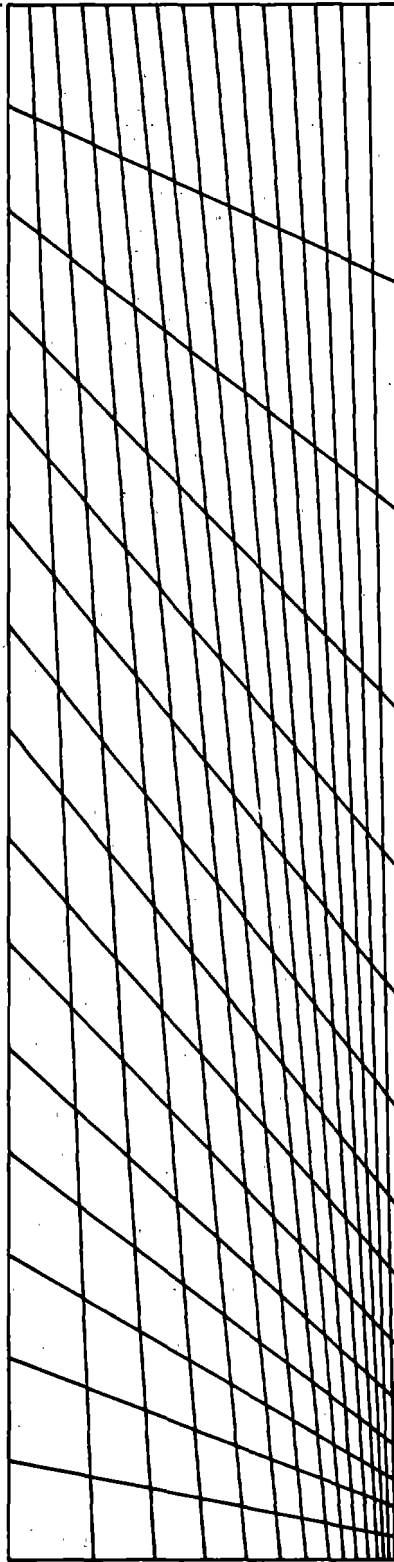
(b) Half of finite element mesh of soil field.

Figure 7-34. Finite element analysis of soil field.

Figure 7-36. Octahedral normal static stress σ_o.

Figure 7-35. Vertical static stress σ_v.

Figure 7-35 shows the vertical static effective stress. Figure 7-36 shows the effective static octahedral normal stress, and Figure 7-37 gives a static K (the ratio of minor to major principal stress). Figure 7-38 shows the static shear stress on the former principal plane, and Figure 7-39 shows the dynamic shear stress level. Figure 7-40 shows the dynamic shear stress computed by the methodology discussed in Chapter 2; i.e., the shear stress determined on the principal plane orientation before application of the dynamic load. Thus, this stress rotation eliminates the complexities of considering initial shear stress level and, hence, nonsymmetric stress reversals. Figure 7-41 shows a plot of equivalent shear stress ratio and Figure 7-42 gives the relative number of cycles to cause liquefaction using the modified approach. The specific numbers are not as important as the general shape of the contour lines, since the specific numbers represent the selection of earthquake record amplitude and frequency and the choice of soil material properties. The shape of the general contours appear independent of earthquake loading or soil parameters.

The significant conclusion is that, based upon a more realistic assessment of the actual stress conditions, it appears that the area beneath a foundation is less sensitive to liquefaction than the free-field area (the opposite of what Yoshimi and Oh-Oka, 1974, concluded). Thus, liquefaction analysis techniques which are based on free-field conditions are conservative when applied to areas beneath footings. The present state-of-the-art of direct computation of pore pressure (similar to Appendix A) is very limited. The present two-dimensional stress-analysis, finite-element programs only attempt to answer the problem of pore pressure distribution indirectly in terms of the shear-stress/confining-stress ratio.

REDUCTION IN FOUNDATION CAPABILITY DUE TO LIQUEFACTION

There is essentially no quantitative experimental data available for evaluating reductions in foundation load-carrying capability due to partial liquefaction of subfoundation soils. It has been tacitly assumed in most instances that foundation load support is not critical up until the point at which initial liquefaction has occurred in the free-field regions. Limited test data on small scale model footings by DeAlba, Chan, and Seed (1975) has tended to support this assumption, at least for homogeneous sands under undrained conditions. The analysis of liquefaction beneath load discontinuities (discussed earlier) further suggests the noncritical nature of the subfoundation material response (again for homogeneous soils).
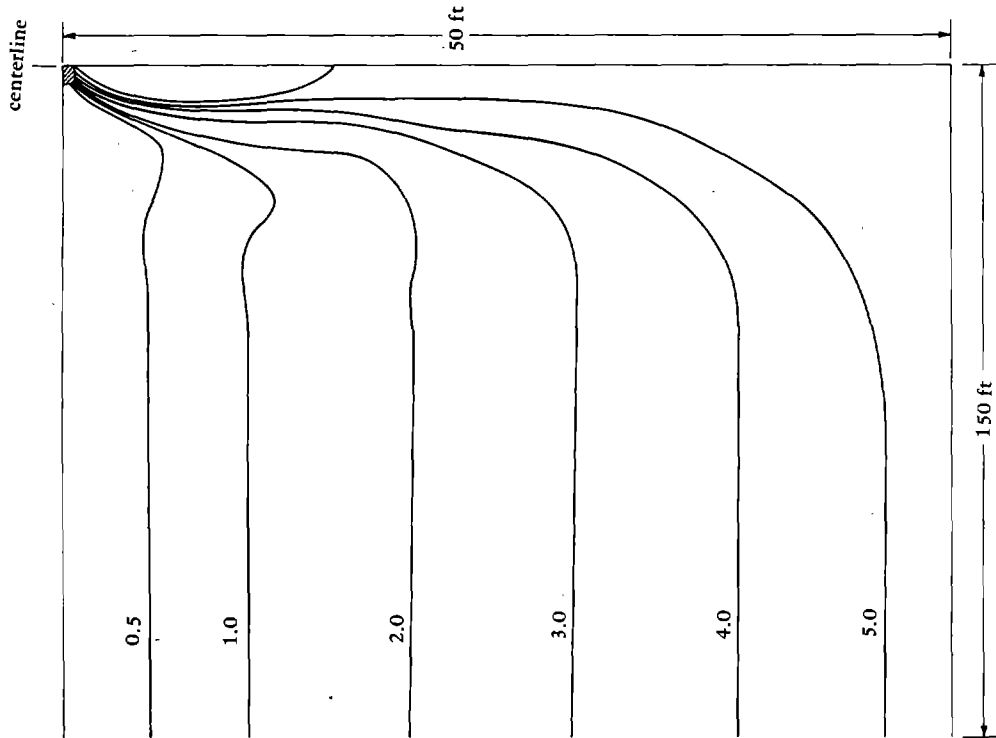
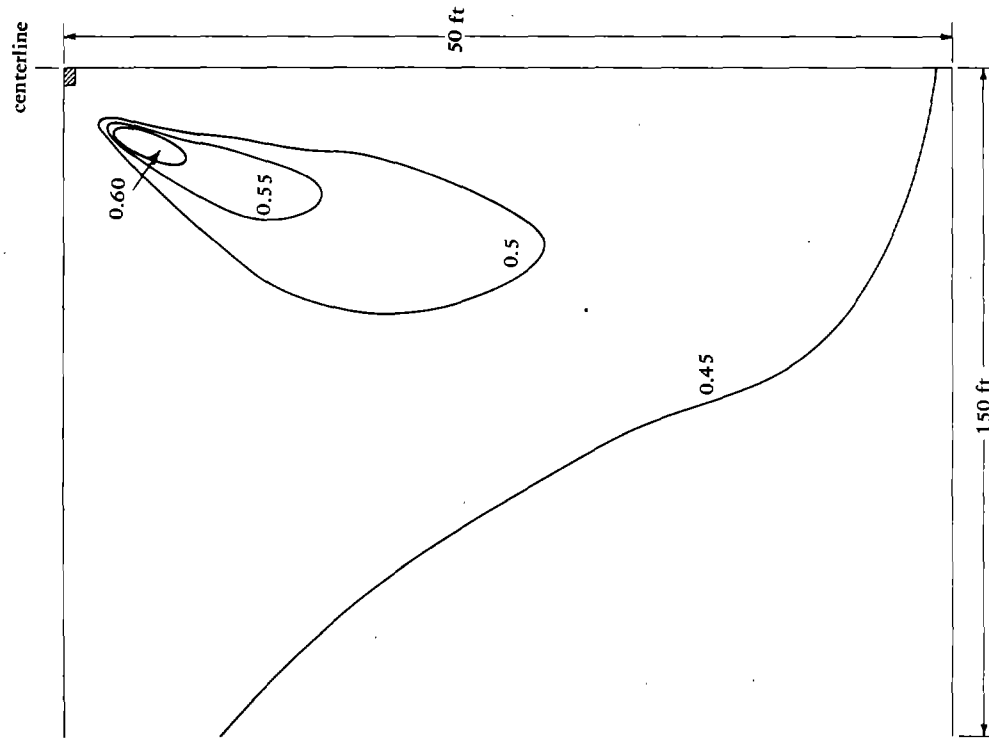Figure 7-38. Static shear stress τ_{static} on what was formerly the principal plane.
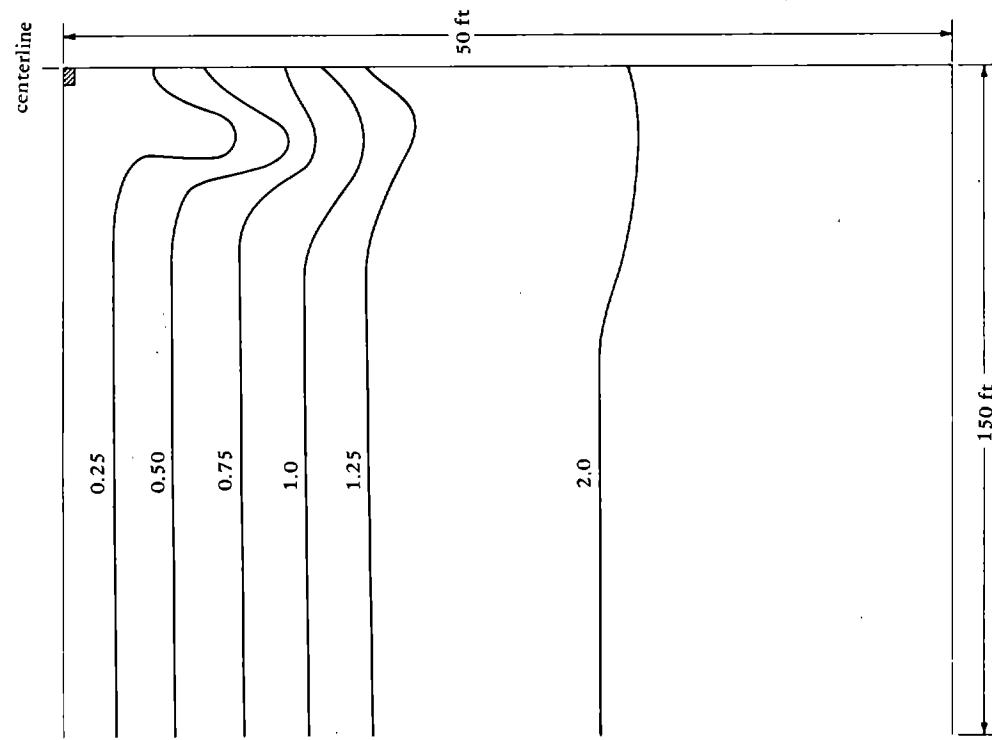

Figure 7-37. Ratio of principal stresses K_o.
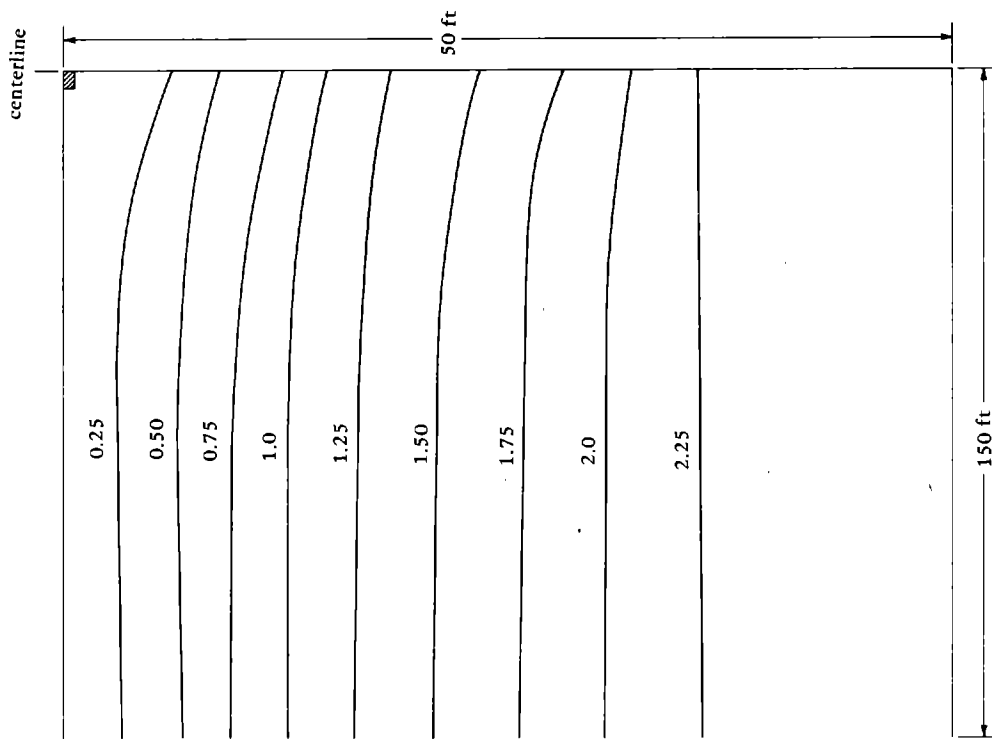
Figure 7-40. Dynamic shear stress on what was the principal plane prior to dynamic loading.

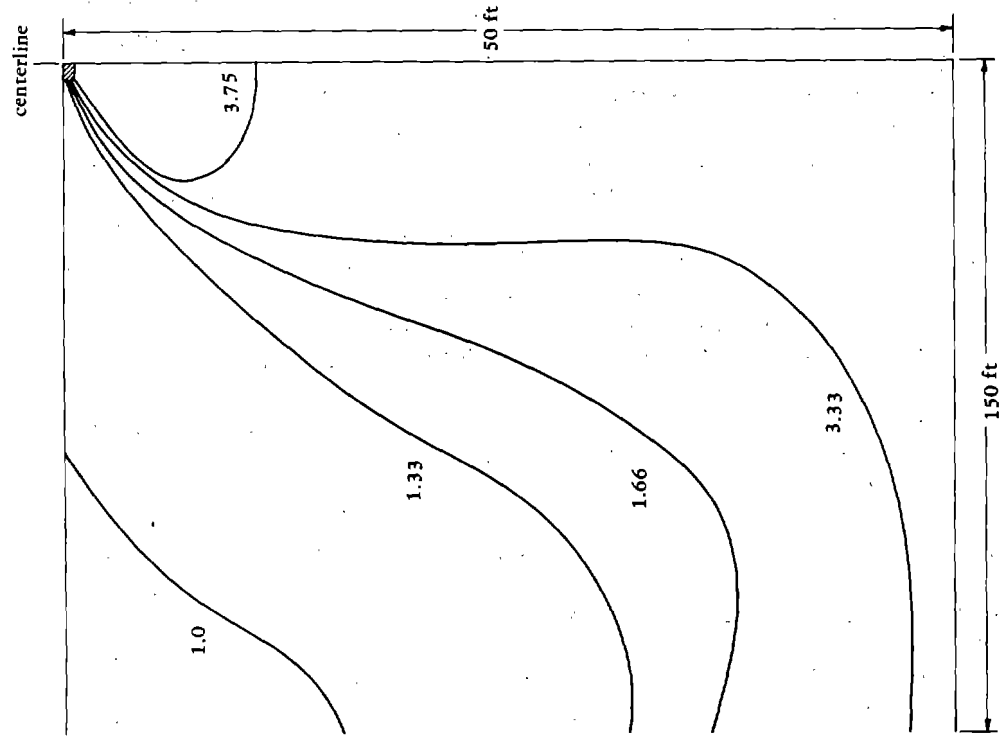Figure 7-39. Dynamic shear stress $\tau_{dynamic}$.

223

Figure 7-42. Relative number of cycles to cause liquefaction.

Figure 7-41. Shear stress ratio.

It is generally agreed that structures on homogeneous deposits of sand fail because of excessive settlement rather than by bearing capacity failure. However, in many cases typical soil profiles contain layers of different material, significant parts of which may exhibit cohesive behavior. Bearing capacity failures are common modes of failure in cohesive soils. It is also conceivable that situations could be encountered in the field where strongly stratified soil profiles have horizontal permeabilities many times greater than those in the vertical direction (see Terzaghi and Peck, 1967, page 334). Under such cases it is possible that rapid horizontal equalization of excess pore water pressure might permit settlement or even failure of the foundation following the cessation of earthquake motion under somewhat quasi-static conditions.

Under such conditions, it might be desirable to consider a reduced-foundation capability in order to avoid either foundation failure (outright collapse or shear failure) or unacceptable settlement.

For granular soils, the static-load factor of safety against collapse is generally well over 3, and allowable bearing capacity is generally governed by permissible settlement of the supported structure. In some cases of earthquake-induced loading, a high degree of foundation damage due to settlement might be considered tolerable provided total collapse of the structure did not occur. In these cases ultimate bearing capacity might become a limiting design factor.

The ultimate bearing capacity of a foundation resting upon soil may be approximated by relationships such as the following proposed by Terzaghi and Peck (1967), for continuous footings:

$$q = c N_c + \gamma' D_f N_q + \gamma' B N_\gamma \qquad (1)$$

where

q = bearing capacity of a footing per unit of footing area

c = cohesion of the soil

D_f = depth of embedment of the footing below the ground surface

B = one-half the minimum footing dimension

γ' = effective weight of the soil (i.e., buoyant weight below the water table)

N_c, N_q, N_γ = bearing capacity factors, defined as a function of the frictional resistance of the soil (see Terzaghi and Peck, 1967)

225

Since the type of liquefaction of interest herein is limited to cohesionless soils, the factor N_c may be neglected and the bearing capacity expressed in the form

$$q = \gamma'D_fN_q + \gamma'BN_\gamma \qquad (2)$$

The factor N_q is intended to account for the strength contribution due to the confinement offered by the surcharge, or the soil above the foundation base level $\gamma'D_f$. The factor N_γ accounts for the frictional resistance of the soil beneath the base of the footing represented by the term $\gamma'B$. A reduction in either N_γ or $\gamma'B$ caused by generation of excess pore water pressure would then cause a reduction in ultimate bearing capacity. Thus, the allowable load following generation of a pore water pressure increment u might be approximated by:

$$q = (\gamma'D_f - \Delta u)N_q + (\gamma'B - \Delta u)N_\gamma \qquad (3)$$

where the unit load reduction is $\Delta u(N_q + N_\gamma)$. The increase in pore pressure may be estimated by use of the program GADFLEA cited earlier in this chapter. To maintain the same factor of safety as under nonearthquake loading, the allowable bearing capacity must be reduced by multiplying it by the factor:

$$R = \frac{(\gamma'D_f - \Delta u)N_q + (\gamma'B - \Delta u)N_\gamma}{\gamma'D_fN_q + \gamma'BN_\gamma} \qquad (4)$$

Defining Δu in terms of the ratio of excess pore pressure generated to initial effective stress, $\Delta u/\sigma'$, Equation 4 may be written as:

$$R = \frac{\gamma'D_f\left(1 - \frac{\Delta u}{\sigma'} N_q\right) + \gamma'B\left(1 - \frac{\Delta u}{\sigma'}\right)N_\gamma}{\gamma'D_fN_q + \gamma'BN_\gamma} \qquad (5)$$

where the critical region for $\Delta u/\sigma'$ could be taken as that beneath the foundation base within a depth of one and one-half times the foundation width. Equation 5 may be further simplified by the assumptions:

(1) Water table at the surface (i.e, $\gamma' = \gamma_b$)

(2) $N_q \approx N_\gamma$

(3) $h = \Delta u / \gamma_w$ (where γ_w is the weight of water)

Hence, the reduction factor may be roughly estimated as:

$$R = \frac{(D_f - h) + (B - h)}{D_f + B} \qquad (6)$$

The ultimate bearing capacity of a pile group in cohesionless soils may be estimated in terms of that of a pier of similar dimensions. Thus, the bearing capacity is the same as for a footing plus the contribution of skin friction along the sides of the equivalent pier (of depth D). The D-term contributes to ultimate load capacity as a diminishing multiple of D for values of D greater than five times the foundation width, [5 x (2B)]. For D values beyond 15 x (2B), this contribution becomes essentially constant. Thus, an increase in unit bearing capacity due to this latter term may be estimated as:

$$\frac{D^2 \gamma'}{2A} P \tan \psi \qquad (7)$$

where D = pile group length

   γ' = soil effective weight

   P = perimeter of the pile group

   A = plan area of pile group

   ψ = friction angle between the pile group and the surrounding soil

Under this situation the load reduction factor would be roughly equal to

$$R = \frac{(\gamma'D - \Delta u)N_q + (\gamma'B - \Delta u)N_\gamma + \frac{D}{2}(\gamma'D - \Delta u)\frac{P}{A}(\tan \psi)}{DN_q + BN_\gamma + D^2 \tan \psi} \qquad (8)$$

or in terms of the ratio $\Delta u/\sigma'$ and assuming $P/A = 8B/4B = 2$;

$$R = \frac{D\left(1 - \frac{\Delta u}{\sigma'}\right)N_q + B\left(1 - \frac{\Delta u}{\sigma'}\right)N_\gamma + D\left(1 - \frac{\Delta u}{\sigma'}\right)\tan\psi}{DN_q + BN_\gamma + D^2\tan\psi} \qquad (9)$$

Settlements of foundations on granular materials are commonly assumed to be roughly proportional to the applied loading. Thus, a prescribed reduction in allowable load capacity due to partial liquefaction could serve to maintain settlement levels within acceptable limits.

To provide a slightly more detailed treatment of the effect of partial liquefaction on allowable settlements, it will be interesting to consider work by Schimming (1962) dealing with the settlement of footings on cohesionless soils. With the use of dimensional analysis combined with model test data, a relationship has been developed between $q/\gamma B$ and δ/B for circular footings resting upon the surface of a cohesionless soil. This relationship when plotted in the hyperbolic form outlined by Kondner (1962) provides the relationship,

$$\delta_1 = \frac{q_1 \, aB}{\gamma B - bq_1} \qquad (10)$$

where
  q = unit loading
  B = footing radius
  γ = effective weight of the soil
  δ = settlement
  a = constant
  b = constant

Under an increase in dynamic pore pressure Δu, the revised settlement δ_2 may be estimated in terms of:

$$\delta_2 = \frac{q_2 \, aB}{(\gamma B - \Delta u) - bq_2} = \frac{q_2 \, aB}{\gamma B\left(1 - \frac{\Delta u}{\sigma'}\right) - bq_2} \qquad (11)$$

Assuming it is necessary to permit no increase in settlement under partial liquefaction (δ_2) over that permitted for the normal case of no earthquake loading, then,

$$\delta_2 = \delta_1 \quad \text{or} \quad \frac{q_1 \, aB}{\gamma B \, - \, bq_1} = \frac{q_2 \, aB}{\gamma B \, 1\left(- \frac{\Delta u}{\sigma'}\right) \, - \, bq_2} \tag{12}$$

Therefore,

$$q_2 = q_1 \left(1 - \frac{\Delta u}{\sigma'}\right) \tag{13}$$

or the reduction in allowable load to provide no increase in settlement under partial liquefaction is seen to be merely:

$$R = \frac{q_2}{q_1} = 1 - \frac{\Delta u}{\sigma'} \tag{14}$$

(i.e., proportional to the reduction in initial effective confining stress).

DISCUSSION

A bridge designer should have an estimate of the magnitude of ground displacement that might be expected if liquefaction were to occur; however, the information available to date is extremely limited. The methods for estimating displacements given in this chapter are crude and approximate. Further work in this area may show their need for modification; they are presented here as a first guess to alert the bridge designer to a potential hazard. CEL is presently investigating this problem by several approaches, one of which is the two-phase finite element program described in Chapter 3. Hopefully, the results of this work can yield better estimates of ground displacement (see Appendix A).

REFERENCES, CHAPTER 7

Ambraseys, N. and Sarma, S. (1969) "Liquefaction of soils induced by earthquake," Bulletin of the Seismological Society of America, vol 59, no. 2, Apr 1969, pp 651-664.

Booker, J. R., Rahman, M. S. and Seed, H. B. (1976) GADFLEA: A computer program for the analysis of pore pressure generation and dissipation during cyclic or earthquake loading, University of California, Earthquake Engineering Research Center, EERC Report No. 76-24. Berkeley, Calif., Oct 1976.

Crandall, R. (1908) The San Francisco peninsula in the California earthquake of 1906, vol 1. Washington, D. C., Carnegie Institute, pp 246-254.

DeAlba, P., Chan, C. and Seed, H. B. (1975) Determination of soil liquefaction characteristics by large-scale laboratory tests, University of California, Earthquake Engineering Research Center, EERC Report No. 75-14. Berkeley, Calif., May 1975.

Kishida, H. (1969) "Characteristics of liquefied sands during Mino-Owari, Tohnankai, and Fukui earthquakes," Soils and Foundations (Japan), vol 9, no. 1, Mar 1969.

Kondner, R. L. (1962) "Hyperbolic stress-strain response, cohesive soils," Journal of the Soil Mechanics and Foundations Division, ASCE, vol 89, no. SM1, Feb 1963, pp 115-143.

Lee, K. L. and Albasia, A. (1974) "Earthquake induced settlements in saturated sands," Journal of the Geotechnical Division, ASCE, no. GT4, Apr 1974.

Martin, P. P. (1975) Non-linear methods for dynamic analysis of ground response, Ph.D. thesis, University of California. Berkeley, Calif., Jun 1975.

McCulloch, D. S. and Bonilla, M. G. (1970) Effects of the earthquake of March 27, 1964, on the Alaska railroad, U. S. Geological Survey, Professional Paper 545-D. Washington, D.C., 1970, 161 pp.

Oldham, R. D. (1899) Report on the great earthquake of 12th June 1897, Memorandum Geological Survey, India, vol 49, 379 pp.

Richter, C. F. (1958) Elementary seismology. San Francisco, Calif., W. H. Freeman, 1958, 786 pp.

Robinson, R., et al. (1975) Structural analysis and retrofitting of existing highway bridges subjected to strong motion seismic loading, Illinois Institute of Technology, Research Institute Report J-6320. Chicago, Ill., May 1975.

Schimming, B. B. (1962) An analytic and experimental study of footings resting on a cohesionless soil, Ph.D. thesis, Northwestern University. Evanston, Ill., 1962.

Seed, H. B. (1968) "Landslides during earthquakes due to soil liquefaction," Journal of the Soil Mechanics and Foundations Division, ASCE, vol 93, no. SM5, May 1968, pp 1053-1122.

Seed, H. B. and Idriss, I. M. (1967) "Analysis of soil liquefaction, Niigata earthquake," Journal of the Soil Mechanics and Foundations Division, ASCE, vol 93, no. SM3, May 1967.

Seed, H. B. and Idriss, I. M. (1971) "A simplified procedure for evaluating soil liquefaction potential," Journal of the Soil Mechanics and Foundation Division, vol 97, no. SM6, Sep 1971.

Seed, H. B., Martin, P. P. and Lysmer, J. (1975) The generation and dissipation of pore water pressures during soil liquefaction, University of California, Earthquake Engineering Research Center, EERC Report No. 75-26. Berkeley, Calif., Aug 1975.

Terzaghi, K. and Peck, R. B. (1967) Soil mechanics in engineering practice. New York, N.Y., John Wiley and Sons, 1967.

Yoshimi, Y. and Kuwabara, F. (1973) "Effect of sub-surface liquefaction on the strength of surface soil," Soils and Foundations (Japan), vol 13, no. 2, Jun 1973.

Yoshimi, Y. and Oh-Oka, H. (1974) "Influence of degree of shear stress reversal on the liquefaction of potential of saturated sand," Soils and Foundations (Japan), vol 15, no. 3, Sep 1974.

Youd, T. L. (1973a) Liquefaction, flow and associated ground failure, U.S. Geological Survey, Circular 688. Reston, Va., 1973, 12 pp.

Youd, T. L. (1973b) Ground movements in the Van Norman Lake vicinity during San Fernando, California, earthquake of February 9, 1971, in San Fernando, California, Department of Commerce, National Oceanic and Atmospheric Administration, vol 3. Washington, D.C., 1973, pp 197-206.

Youd, T. L. (1975) "Liquefaction, flow and associated ground failure," in Proceedings of the U. S. National Conference on Earthquake Engineering, Ann Arbor, Mich., Jun 1975. Earthquake Engineering Research Institute, Oakland, Calif., 1975, pp 146-155.

Chapter 8

DAMAGE TO BRIDGE STRUCTURES CAUSED BY
EARTHQUAKE INDUCED LIQUEFACTION

This chapter will present examples of typical bridges damaged by
liquefaction of the soil foundation. The description of the earthquake
damage in Japan is based on a summary by Iwasaki, Penzien, and Clough
(1972). The Alaska earthquake damage is based on reports by Ross, Seed,
and Migliaccio (1973) and from the U.S. Geological Survey (Kachadoorian,
1968; McCulloch and Bonilla, 1970; and Waller, 1966). It is thought that
by showing the reader the effects of earthquake-induced liquefaction
damage he will be better equipped for future designs.

KANTO EARTHQUAKE OF 1923

A severe earthquake of magnitude 7.9 occurred in Sagomi Bay off the
southern coast of the Kanto area of Japan. Nearly 2,000 bridges suffered
light to heavy damage.

The Banyu Bridge was located 15 miles northeast of the epicenter.
The bridge substructures were under construction at the time of the
earthquake. Both abutments were of gravity-type reinforced concrete
with pile foundations and were completed at the time of the earthquake.
The piers were reinforced concrete rigid frames with concrete caisson
foundations. Among the total of 56 piers, only 6 had been completed
near the left bank of the river. The caisson foundations of 42 piers
had either just been completed or were under construction at the time
of the earthquake.

The superstructures, consisting of 57 single span-reinforced concrete
T-shape girders of a total length of 620 m (57 x 10.9 m) and a width of
7.3 m, had not been erected at the time of the earthquake.

During the earthquake, the substructure sustained extensive damage
(Figure 8-1). The right and left abutments tilted about 20 and 4 degrees,
respectively, toward the center of the river. Major failures occurred

232

in the horizontal beams of the piers. Insufficient curing of the concrete could have been an important factor in the amount of damage. Large displacements and floating of several caisson foundations were observed. In view of the behavior it appears that liquefaction of the soils occurred.

NIIGATA EARTHQUAKE OF 1964

The Niigata earthquake which occurred in the northwestern part of Honshu Island on 16 June 1964 registered 7.5 on the Richter scale. Its epicenter was under the sea near Awashima Island about 55 km north of Niigata City and its hypocenter depth was estimated to be in the range of 20 to 30 km.

Severe damage was caused on the alluvial plain near the mouths of the Shinano River and the Agano River in Niigata City, especially in the area near the mouth of the Shinano River where loose sand layers with a high water table existed. In this area, highway bridges and other structures sustained considerable damage due to liquefaction of the ground soils. The maximum acceleration was about 0.15 g (predominant period 2 seconds) horizontally and about 0.05 g (predominant period 0.3 second) vertically. Based on extensive damage surveys, it was observed that (1) although damage to bridge structures was observed in Akita, Fukushima, Niigata, and Yamagata Prefectures, major damage was concentrated near the mouths of the Shinano and Agano Rivers in Niigata City where soil conditions were bad; (2) the degree of damage to bridges was roughly proportional to the Japanese seismic intensity (however, in some areas with the same intensity, different ground conditions considerably affected the degree of damage); (3) abutments generally suffered more damage than did piers, due to the pressures developed by backfills; (4) the degree of substructure damage appeared to be independent of foundation type; (5) the soft saturated sandy soils near ground surface liquefied (thus reducing bearing capacities, which allowed substructures to slide, settle, and tilt); (6) those bridges having deep foundations resting on hard sandy layers with standard penetration values N greater than 25 sustained only minor damage; and (7) superstructure damage was indirectly caused by failures of the substructures. Additional information is given in Chapter 7.

The Showa Bridge crossed the Shinano River about 1.2 km up the river from the Bandai Bridge which was approximately 55 km south of the epicenter. Construction was completed in May 1964 just 1 month prior to the earthquake.

Figure 8-1. Damage to the Banyu Bridge (from T. Iwasaki, J. Pienzien, and R. Clough, 1972).

(a) Design.

(b) Damage to pier at Chigasaki side.
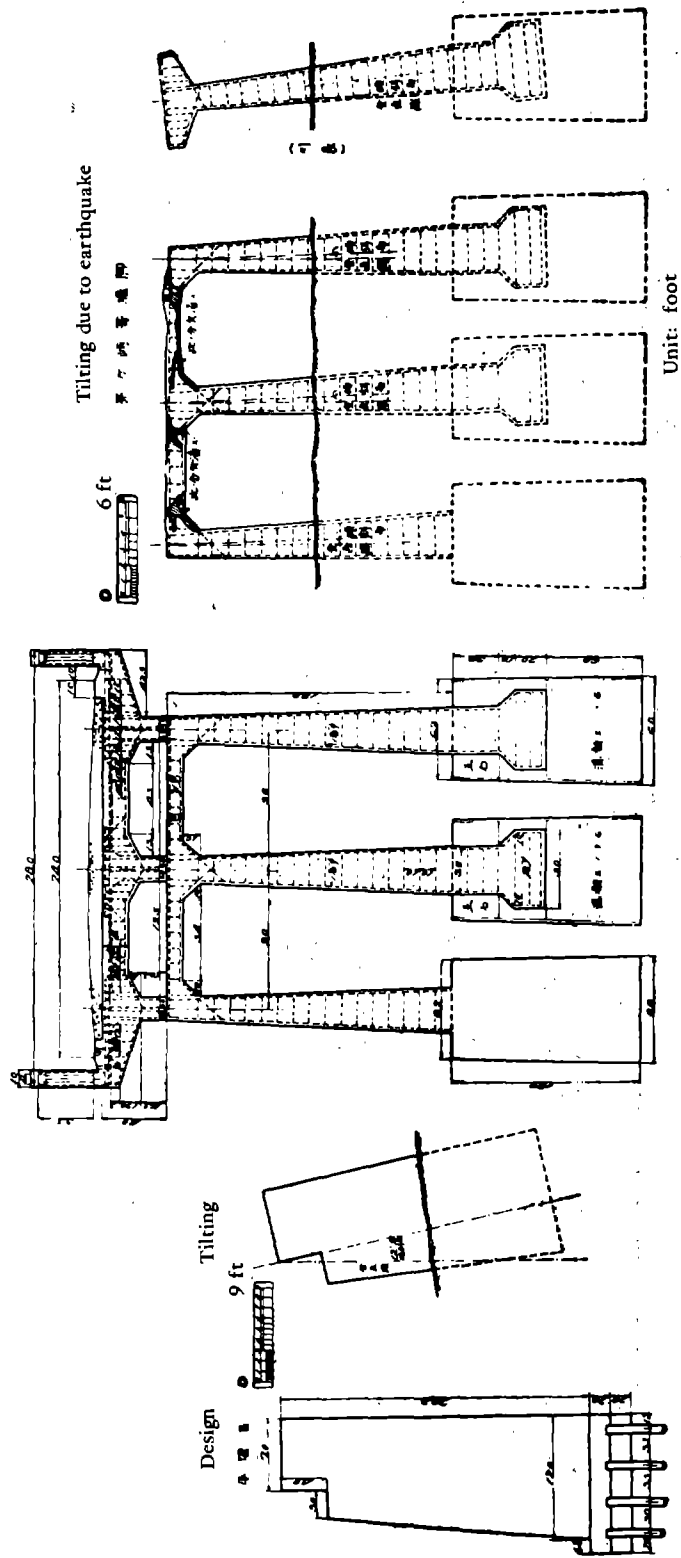
(c) Damage to abutment of Hiratsuka side.

234

The ground at this site consisted of sandy soils which were comparatively soft near the left bank and comparatively hard near the right bank (Figures 8-2 through 8-5). The abutments were pile bents (nine single-row piles 609 mm in diameter and 22 m in length) as were the piers (nine single-row piles 609 mm in diameter and 25 m in length). These bents had collar braces and cap beams (Figure 8-3). The seismic design coefficient for the substructures was 0.2. The superstructures consisted of 12 composite-steel simple span girders.
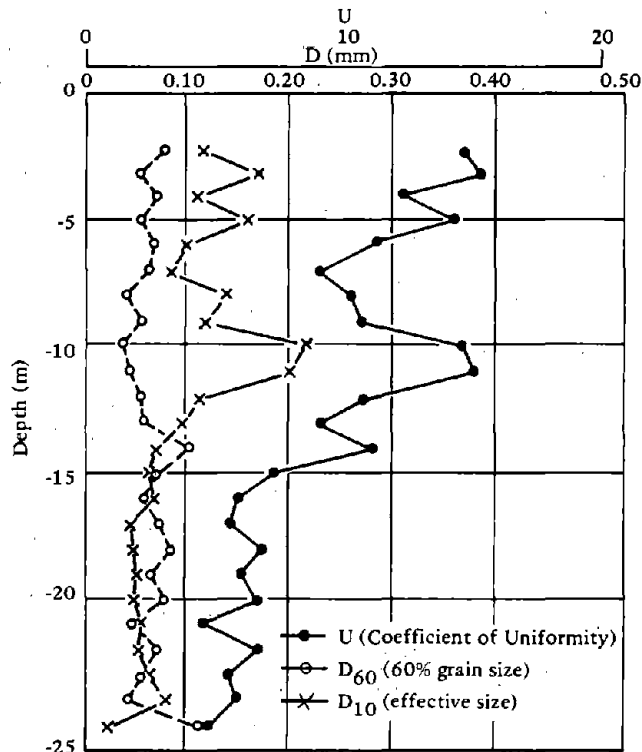
Figure 8-2. General view of the Showa Bridge (from T. Iwasaki, J. Pienzien and R. Clough, 1972).

During the earthquake, the bridge sustained severe damage (Figure 8-6). The left abutment moved about 1 m toward the center of the river, and its approach road settled considerably. In contrast with this behavior, the right abutment and its approach road sustained no significant damage. The first to fourth piers from the left bank tilted toward the right bank. The magnitudes of permanent deformation were 13 to
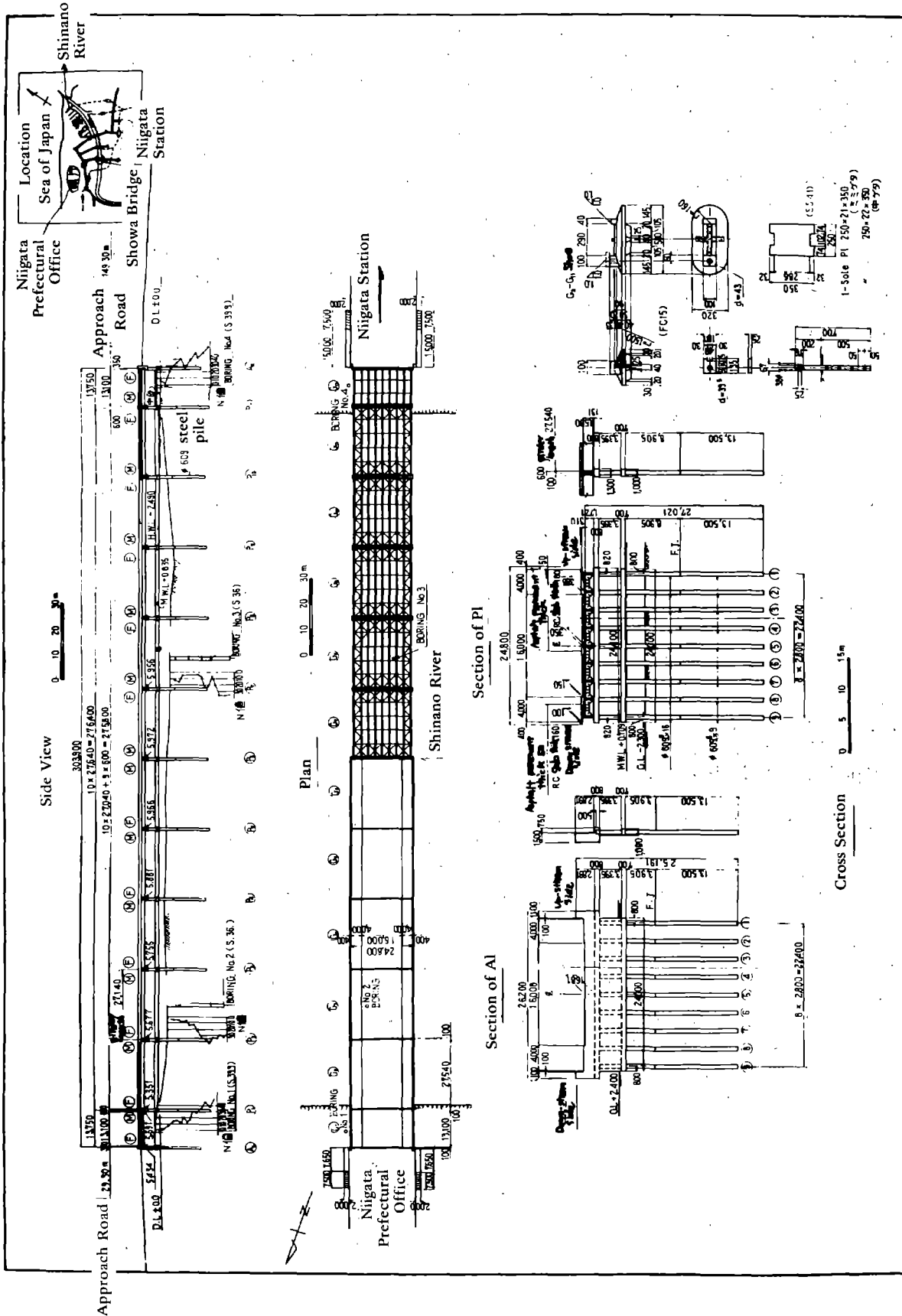
Figure 8-3. General view of the Showa Bridge (from T. Iwasaki, J. Pienzien and R. Clough, 1972).

42 cm at their caps. The fifth and sixth piers collapsed completely into the river while the seventh through the eleventh piers suffered only slight damage. Five girders (third through seventh from left bank) out of twelve fell into the river. Only the sixth span fell at both ends which was caused by failure of the fifth and sixth piers.

Damage characteristics of the bridge are shown in Figures 8-6 and 8-7. These reveal the following main causes of damage: (1) the sub-structures consisting of single-row steel piles were too flexible, (2) liquefaction of the soils occurred (except near the right bank), (3) both bearing supports of the sixth span were movable, (4) the super-structures consisted of simple girders which were not connected together, and (5) catastrophic sliding of the ground occurred near the left bank.

EBINO EARTHQUAKE OF 1968

An earthquake occurred near Ebino, Mishiamorokate County, Miyazaki Prefecture, in the southern part of Ryushu Island on 21 February 1968, registering 6.1 on the Richter scale.

About 2 hours prior to the main shock, a foreshock with a magnitude of 5.6 occurred. Many aftershocks also occurred, including three major ones: One on February 22 (magnitude 5.5) and two on March 25.

Within a radius of about 5 km in the area of Ebino, Miyazaki Prefec-ture, and Hoshimatsu, Kagoshima Prefecture, where the ground is made up of volcanic sandy soils, several major landslides occurred on steep slopes. The bridge, completed in 1964, crosses the Ikejima River on a municipal road in Ebino.

The abutments and the two piers were of reinforced concrete solid-slab-type construction with spread footings and pile foundations. The superstructures, having a total length of 49.6 m and a width of 6 m, consist of steel H-shape simple girders over three spans.

The first pier from the left bank settled about 25 cm during the earthquake. No significant damage was observed to other portions of the bridge. Near the bridge, the river bed surface cracked and settled considerably; some sandy materials from the deeper layers boiled out through cracks. Therefore, it is believed that liquefaction occurred at this site.
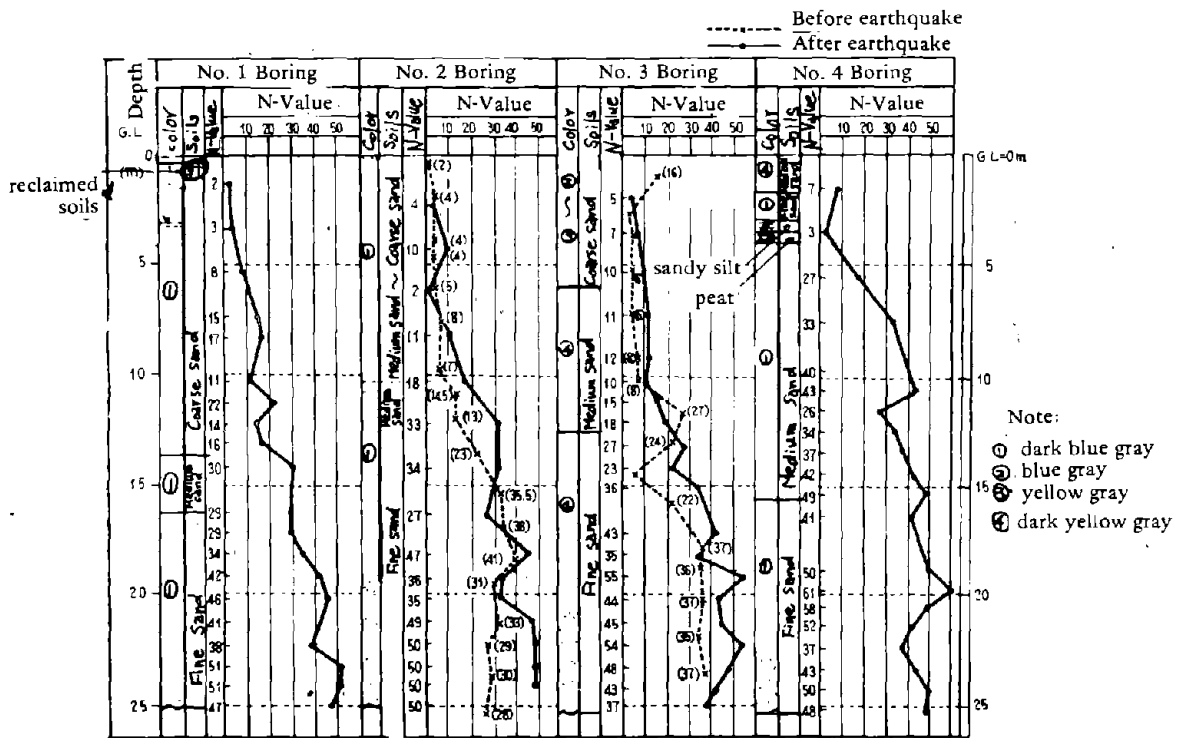
Figure 8-4. Boring logs at the Showa Bridge (from
T. Iwasaki, J. Pienzien and R. Clough, 1972).
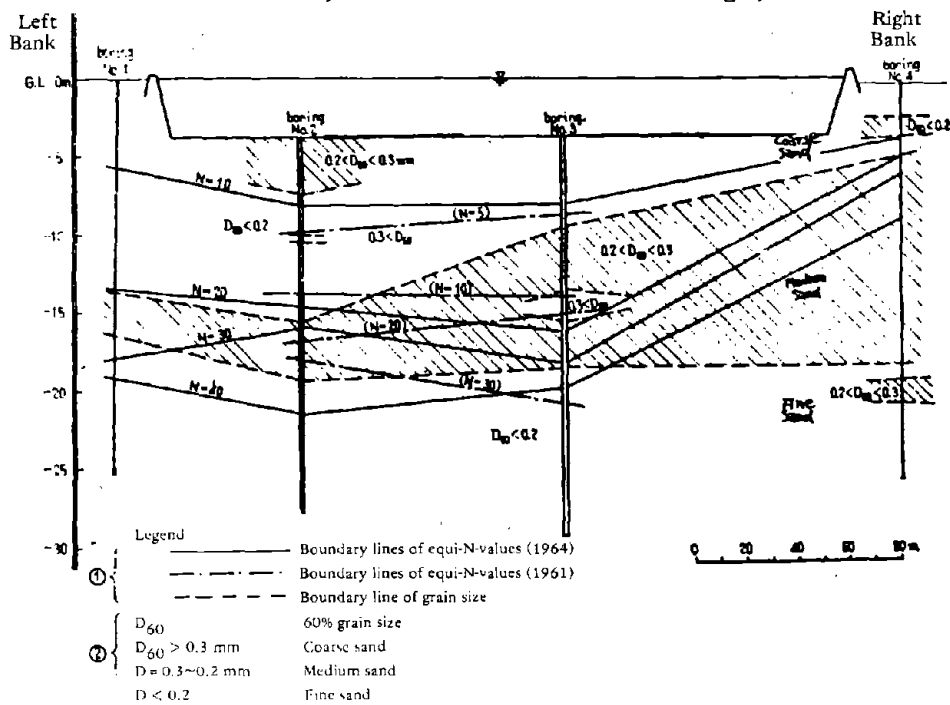
Figure 8-5. Soil profile at the Showa Bridge (from
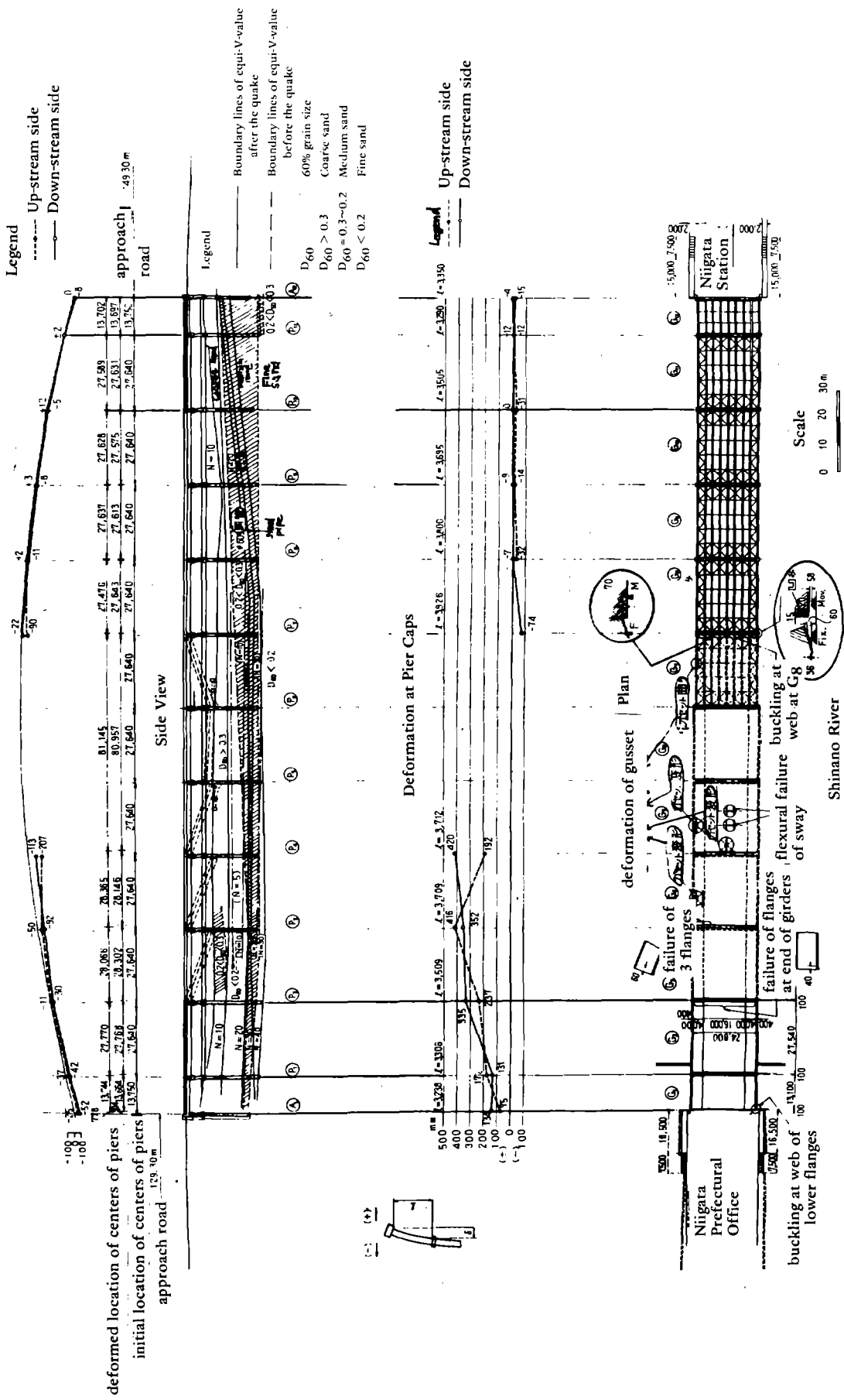T. Iwasaki, J. Pienzien and R. Clough, 1972).

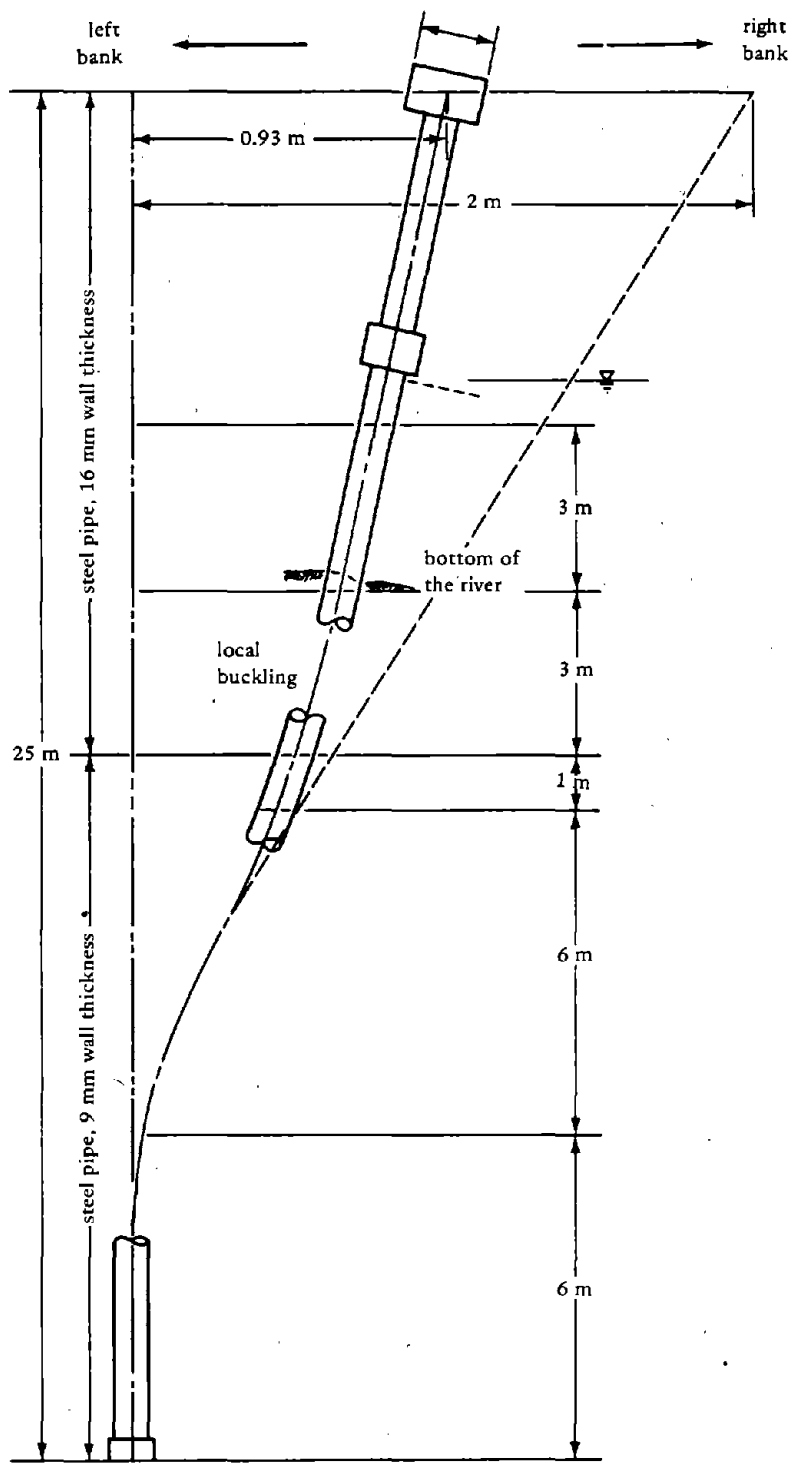Figure 8-6. Damage to the Showa Bridge (from T. Iwasaki, J. Pienzien and R. Clough, 1972).

Figure 8-7. Permanent deformation of a pile pulled out at
the Showa Bridge (T. Iwasaki, J. Pienzien and
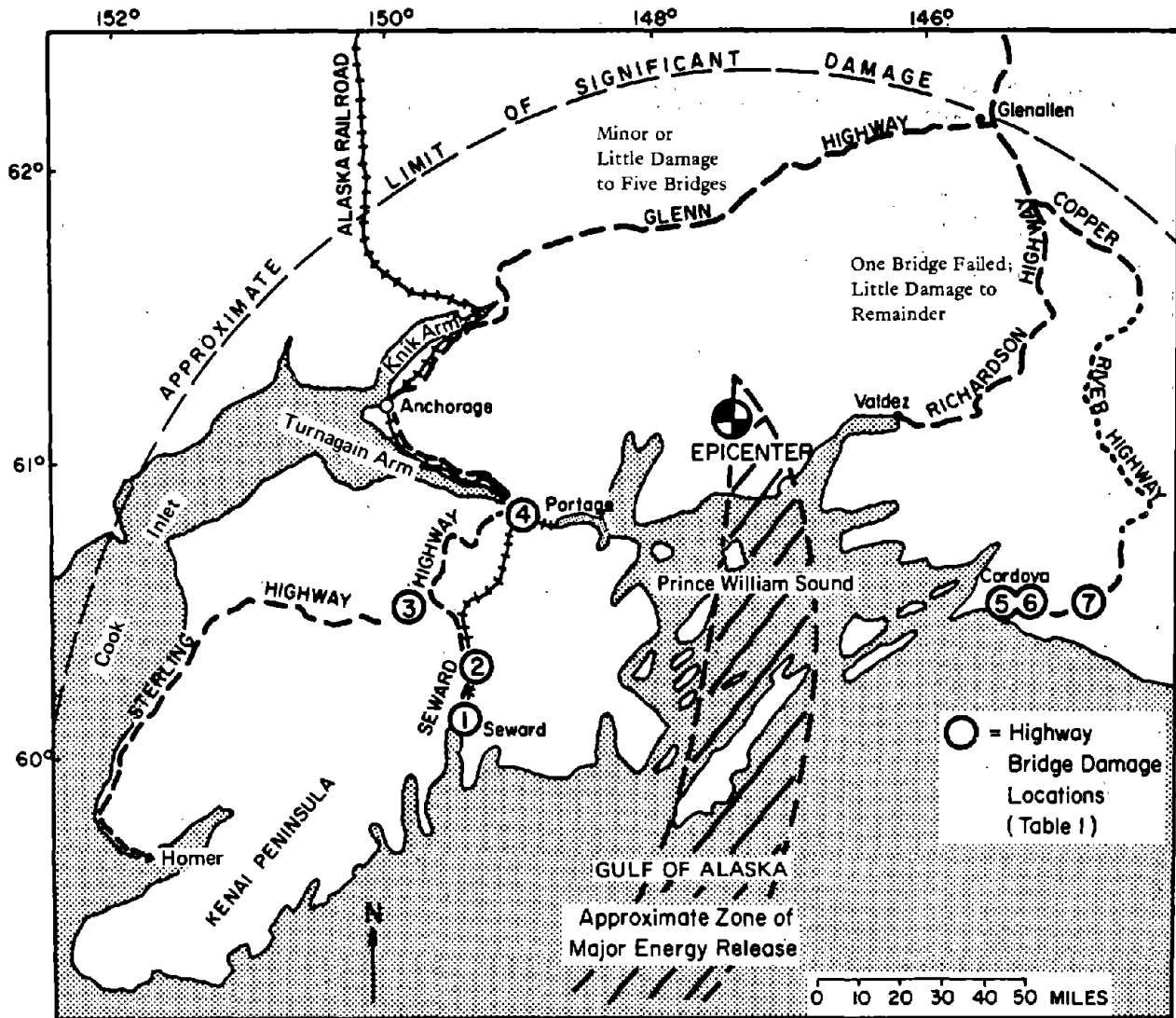R. Clough, 1972).

ALASKA EARTHQUAKE OF 1964

On 27 March 1964, a major earthquake (magnitude 8.4) occurred with
its epicenter located approximately 80 miles east-southeast of Anchorage
(Figure 8-8). Numerous bridges were destroyed. Ross, Seed and Migliaccio
(1973) give a summary of the performance of highway bridge foundations.
Kachadoorian (1968) reported on the Alaska Highway System. McCulloch
and Bonilla (1970) reported on the Alaska Railroad damage which totaled
$46 million (over $25 million to bridges). Of the 204 bridges in south-
central Alaska, 141 were damaged (92 severely). The earthquake damaged
186 of the 830 miles of roadway. Some typical cases where liquefaction
occurred are described here.

Resurrection River

Two bridges (596 and 598) on the Resurrection River, located about
1,500 feet from each other, are shown in Figures 8-9 and 8-10. Both
bridges were located on a silty sandy gravel. Bridge 596 suffered
severe damage, but bridge 598 suffered only moderate damage. The major
difference in the two bridges is the location of the piers in relation
to the channel margins. In bridge 596 the abutment fills extended
almost to the piers so that a movement of soil from beneath the abutment
fills would exert high lateral loads on the pier footings and piers,
causing rotation. In bridge 598 a clearance of 20 feet between the toes
of the abutments and the piers provided space for soil displacement.
The location of abutments is significant.

Snow River

A cross section of the valley is shown in Figure 8-11. The river
crosses an alluvium-filled, glaciated trough in bedrock. There were
four bridges in service and one under construction at the time of the
earthquake. Figure 8-11 gives their location and shows the depth of the
pile foundations. Bridge 603 penetrated bedrock on the west side. The
east embankment settled, but the bridge remained in service. Bridge 604
experienced settlement of the abutments and approach fills in relation
to the midstream piers and resulted in a humped configuration. Bridge
605 (Figure 8-12) was destroyed by the earthquake which caused the deck
to collapse to the streambed. Many of the timber bents settled or were
driven downward as much as 10 feet. The abutments moved toward one
another compressing and buckling the superstructure. The piles extended
40 to 60 feet into sands and silts having penetration resistance of 5 to
10 blows. This soil is very susceptible to liquefaction, and liquefaction
would be expected.

Minor or Little Damage to Five Bridges

LIMIT OF SIGNIFICANT DAMAGE

ALASKA RAIL ROAD

GLENN HIGHWAY

Glenallen

APPROXIMATE

62°

One Bridge Failed; Little Damage to Remainder

COPPER RIVER HIGHWAY

RICHARDSON HIGHWAY

Knik Arm

Anchorage

Valdez

EPICENTER

61°

Turnagain Arm

Cook Inlet

HIGHWAY

④ Portage

HIGHWAY

③

Prince William Sound

Cordova

⑤⑥ ⑦

STERLING

SEWARD

②

① Seward

○ = Highway Bridge Damage Locations (Table 1)

60°

KENAI PENINSULA

Homer

N

GULF OF ALASKA

Approximate Zone of Major Energy Release

0 10 20 30 40 50 MILES

Location	Approximate Distance From Zone of Major Energy Release (mi)	Approximate Acceleration
Seward Highway		
① Resurrection River	60	0.12
② Snow River	60	0.12
③ Kenai River (on Sterling Highway near junction with Seward Highway)	80	0.085
④ Turnagain Arm (Portage area)	50	0.143
Copper River Highway		
⑤ Scott Glacier streams	50	0.143
⑥ Sheridan Glacier streams	55	0.13
⑦ Lower Copper River	70	0.095

Figure 8-8. Highway routes of seven main bridge-damage locations.
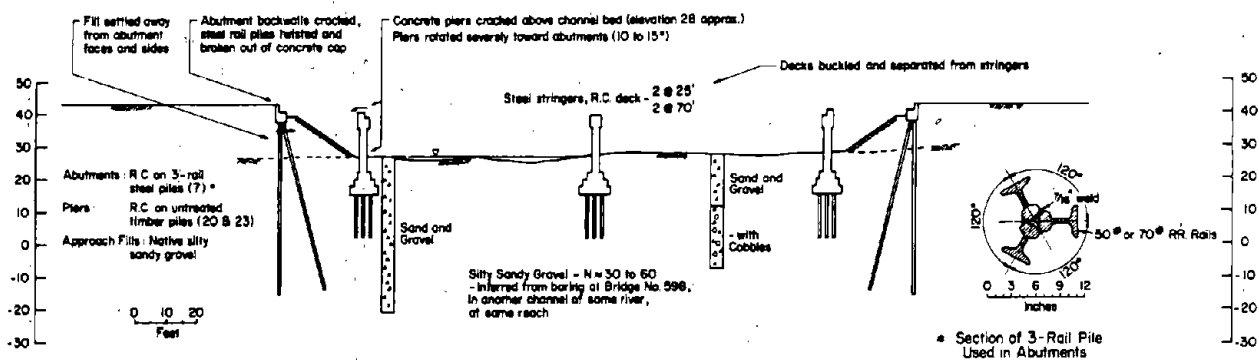
Figure 8-9. Bridge 596: Resurrection River (centerline section looking
upstream - natural scale).
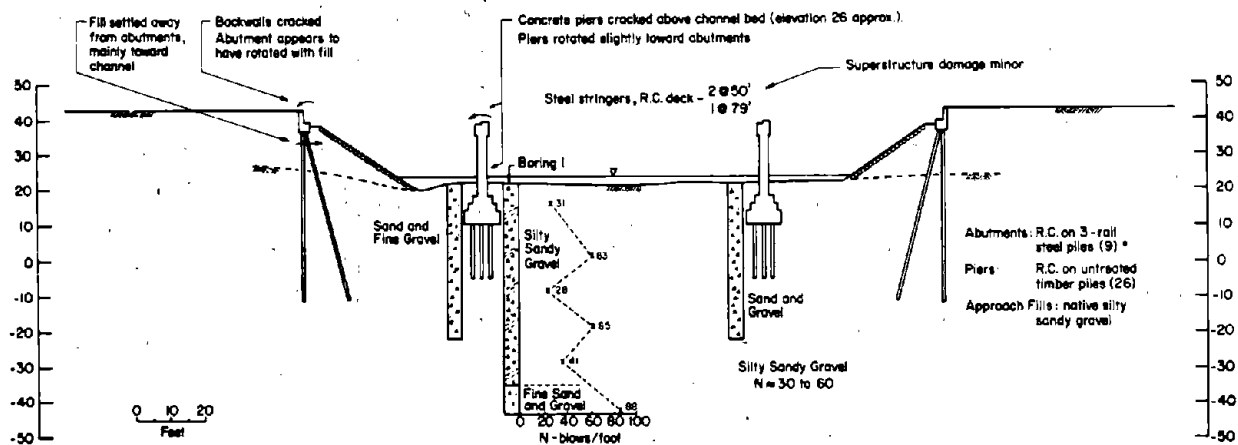
Figure 8-10. Bridge 598: Resurrection River (centerline section looking
upstream - natural scale).

243
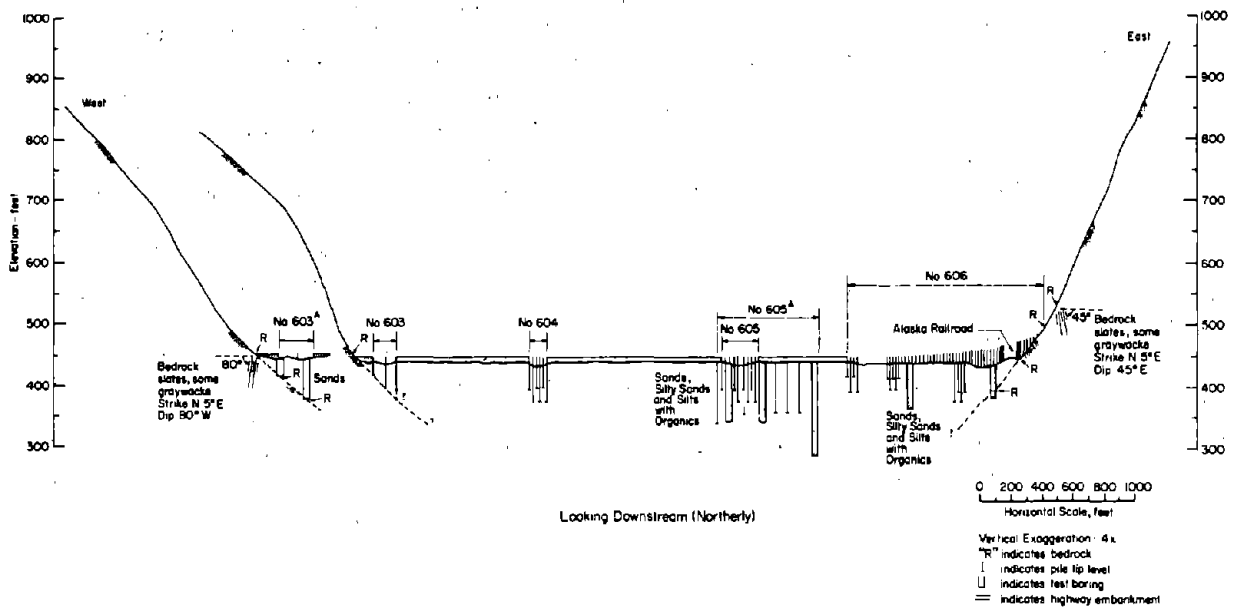
Figure 8-11. Composite section across snow river valley (relative positions of Snow River bridges and foundation materials).
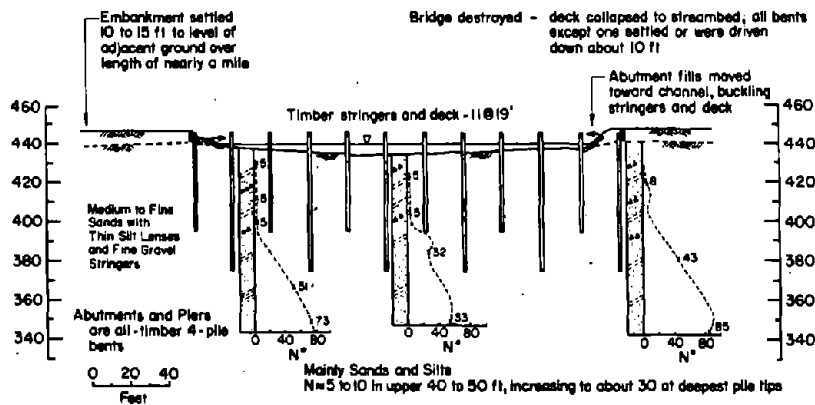
Figure 8-12. Bridge 605: Snow River (centerline section looking downstream – natural scale).

244

Bridge 605A was under construction (Figure 8-13). The 11 steel-tube piles for one abutment had been driven to a depth of about 100 feet, cut off to a common level and filled with concrete. During the earthquake these piles underwent relative vertical displacement up to 7 feet and also experienced tilting. Four of the concrete bridge piers had been completed. These piers, each supported on 21 concrete-filled steel-tube piles, underwent tilting up to 15 degrees and lateral displacement up to 8 feet (Figure 8-14). Liquefaction of a zone below the ground surface occurred with mud oozing up in cracks. The 10-foot high road embankment was reduced to the level of the flood plain.

Bridge 606 was a long overpass structure similar to bridges 604 and 605. The timber bents were founded on bedrock for a distance of about 400 feet from the eastern abutment. The westerly two-thirds of the timber trestle was founded on granular soils. Post earthquake evaluation showed that the trestle and rigid frame collapsed from the eastern abutment for a distance of 600 feet and the damage reports state the westerly abutment settled as much as 2 feet.

Copper River

The 22-mile stretch of highway on the Copper River includes 19 bridges, all of which were damaged to some extent — most moderate to severe. The prevalent types of failure were severe abutment deformation and relative vertical displacement. Considerable evidence of liquefaction was noted in the form of fissures and subsidence craters with adjacent ejected soil.

Portage Creek

A typical bridge and the grain-size distribution of the foundation soils are shown in Figures 8-15 and 8-16. The soil conditions are a loose, surficial sandy gravel over interbedded sands and silts underlain by silt. The bridge was destroyed, with the abutments settling and moving toward the channel. The pile bents twisted and were displaced. Liquefaction would have been expected. The extensive longitudinal fissuring and spreading of the highway embankment reported are typical of foundation soil liquefaction.
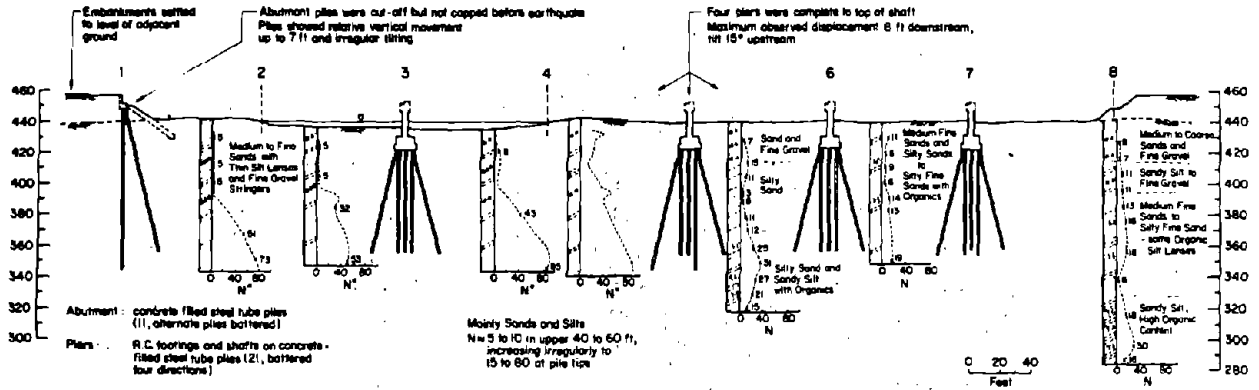
Figure 8-13. Bridge 605A (during construction): Snow River (centerline
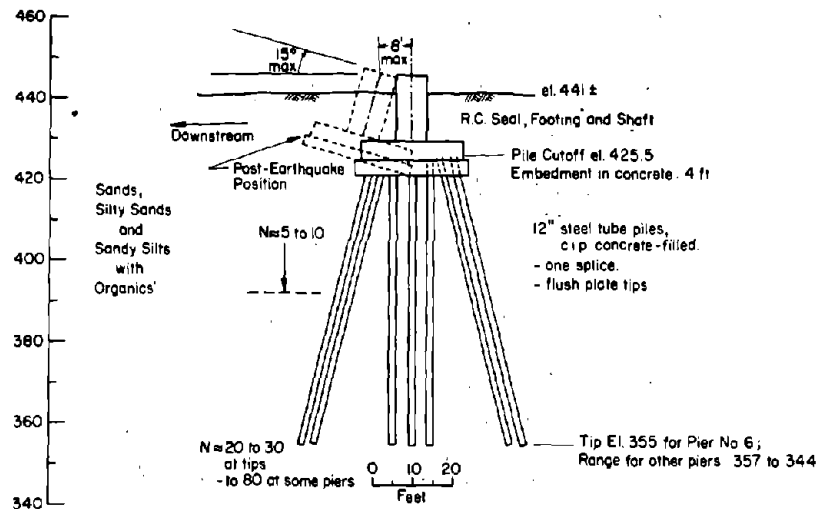section looking downstream - natural scale).

Figure 8-14. Bridge 605A (during construction): Snow River
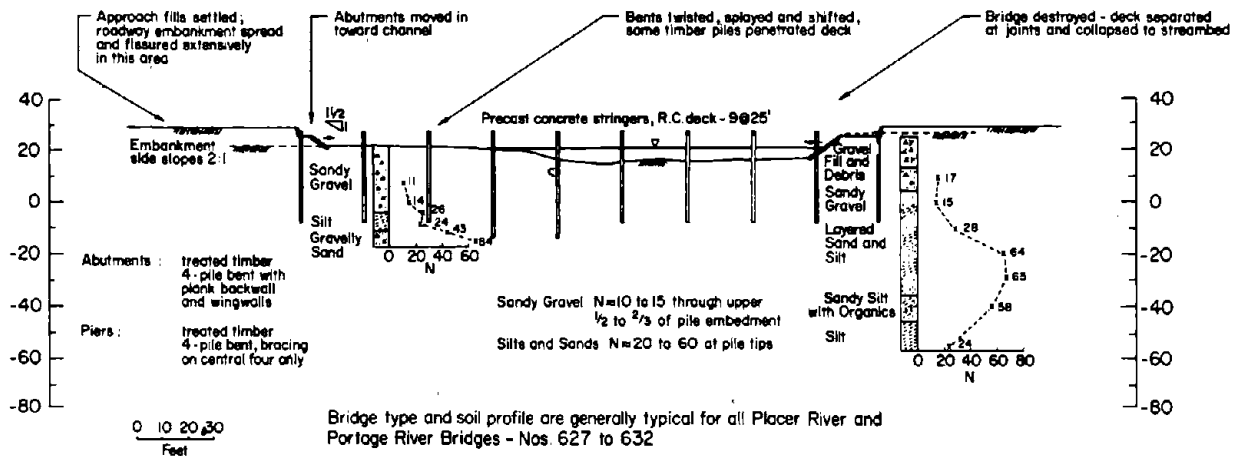(lateral elevation of pier 6 as constructed
at time of earthquake).

246

Figure 8-15. Bridge 631: Portage Creek (centerline section looking downstream - natural scale).

Scott Glacier

Eleven bridges spanned the channels of the Scott Glacier outwash. The western five were founded on timber bents with precast concrete caps and the remainder were on steel-rail bents with cast-in-place caps (Figure 8-17). Loose to medium-dense material extended below the piles. In most cases, damage was severe, with liquefaction as the major cause of damage. Bridge 348 (Figures 8-18 and 8-19) is typical of such damage.

Summary of Alaskan Damage

The most prevalent damage was shortening of the overall span between abutments. This is associated with settlement of abutment fills. In many cases the superstructure of the bridge had ridden up over both abutments. The effects of liquefied soil were noted in the longitudinal and lateral displacement of bridge piers. Many bridges showed a final configuration in which the piers were higher than the abutments. In other cases, this was reversed. Ross, Seed and Migliaccio (1973) compare foundation support conditions for 60 bridges (Figure 8-20). They conclude the following for the Alaska bridges observed:

1. No foundation failures were observed on bedrock.

2. Bridges with distinctly different support conditions along the bridge such as bedrock at one end and piling into cohesionless soils at the other resulted in moderate to heavy damage.

247
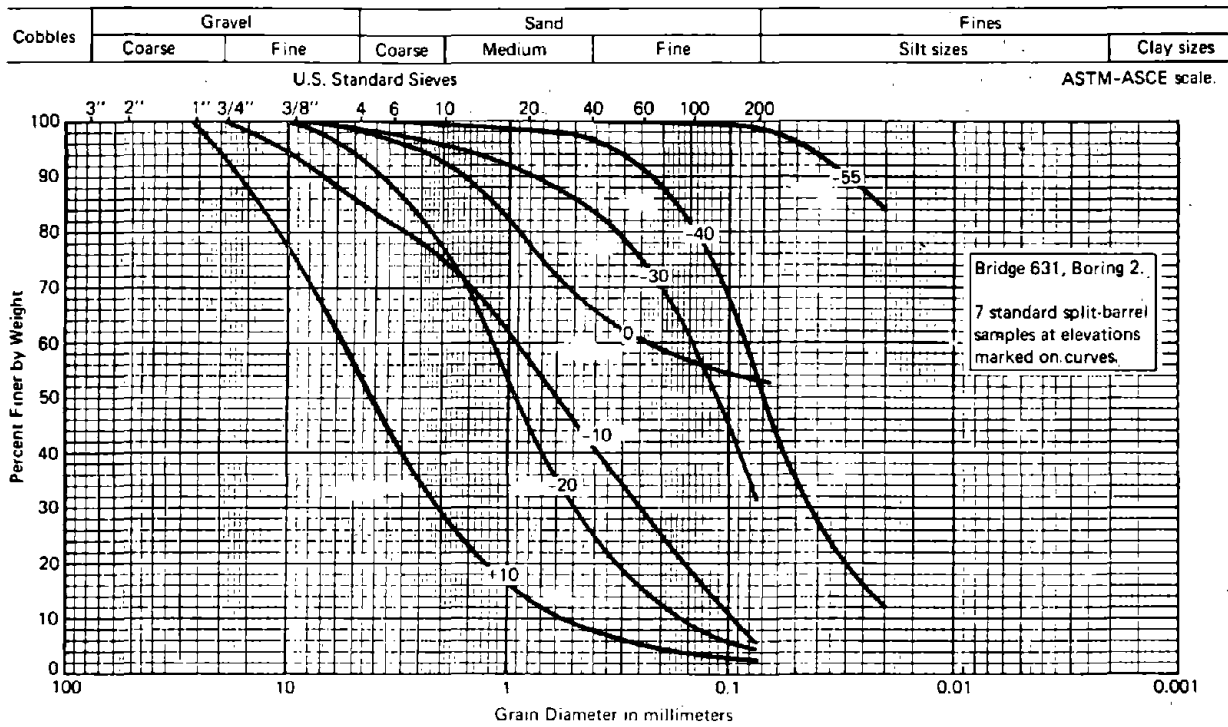
Figure 8-16. Grain-size distributions for soils at Bridge 631: Portage Creek.

3. Bridges with piles driven through saturated sands and silts to low-to-medium relative density (N<20) soils suffered severe foundation displacement.

4. Bridges founded on piles driven through loose to medium dense sands and silts into denser sands and silts also suffered severe damage.

5. Bridges founded in gravels and gravelly sands behaved well.

McCulloch and Bonilla (1970) found similar results for railway bridges. Most bridges on sand and gravel suffered moderate to severe damage. They noted that damage was more severe as the thickness of alluvium increased. They describe the damage to several bridges, noting large vertical and horizontal displacements. They further note that piles were shifted with little tilting, indicating movement of the foundation material was probably as deep or deeper than the pile tips; so liquefaction occurred at depth. They point out that the Alaska earthquake record indicated a long period of compression-wave (P-wave) generation which may have increased pore water pressures sufficient to produce liquefaction. The deep sediments associated with river beds form bowl-like formations which, when excited, may resonate. If resonance occurs, the magnitude of surface motions would be increased. It was noted that in many places where there was no surface evidence of liquefaction in adjacent areas, highway embankments still settled indicating high pore water pressure in the underlying sediments. Major land spreading was observed in which liquefaction occurred at depth but did not propagate to the surface; surface layers displaced horizontally as a unit carrying all structures with it.


CONCLUSIONS

Although it is difficult to generalize the consideration of damage because of the diversity of bridge and foundation designs, one thing is observed consistently: the behavior of bridges on loose soil deposits is associated with a high probability of significant damage. Any methodology described in Chapter 3 would indicate the potential for liquefaction at most of the sites reviewed here.
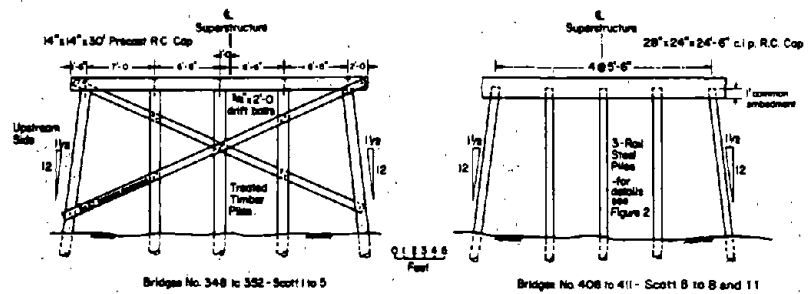
Although it was not evident that any specific type of foundation is best-suited to withstand liquefaction, it was noted that foundations resting on sandy soil with N values greater than 25 experienced minimal damage (provided they were rigid enough to withstand lateral displacement). Piles, especially, must be designed to withstand buckling in the event of loss of side restraint in the near surface regions. Clearance should be provided between abutments and piers to minimize the effect of abutment soil displacement in pier movement. Severe differential settlement has occurred where abutments were on dissimilar materials. Checks should also be made to insure that vertical loads are sufficient to prevent floating or rising of buoyant foundations as a result of liquefaction.
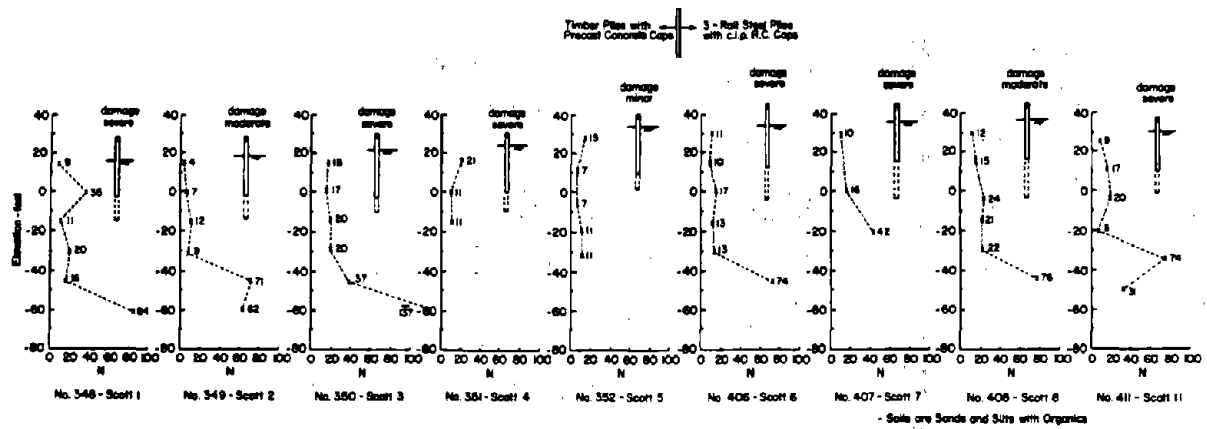
(a) Relationship of bridge piling to standard penetration
test logs across outwash plain.
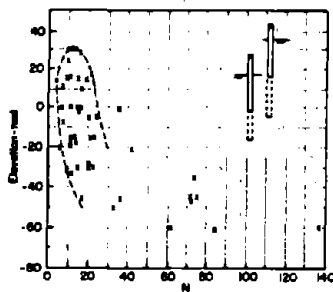
b. Combined Standard Penetration Test Data (9 Bridge Sites)

(b) Combined standard penetration
test data (nine bridge sites).

(c) Bent elevations.

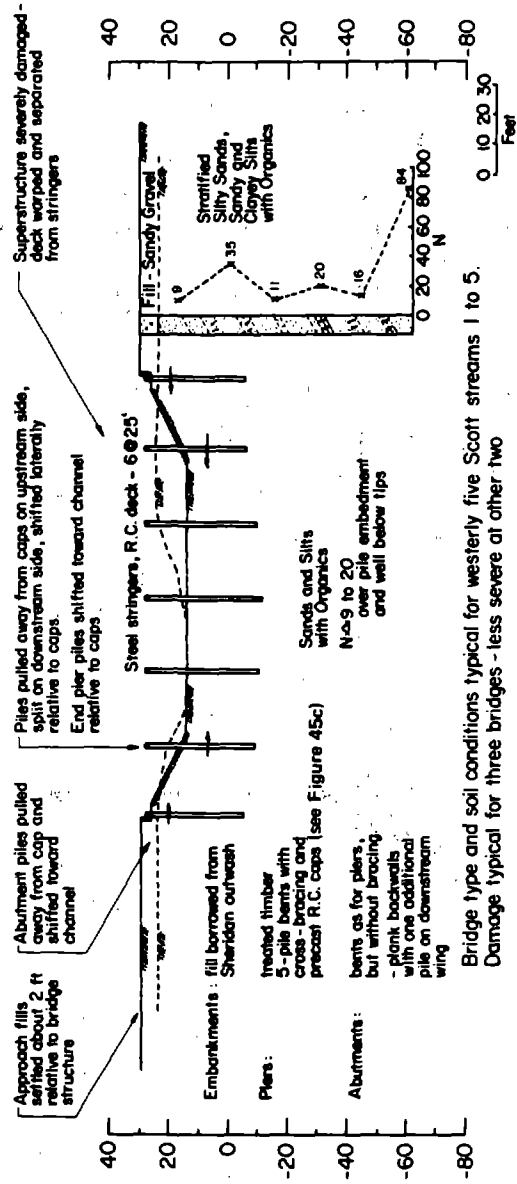Figure 8-17.   Bridges 348 to 352 and 406 to 411:   Scott Glacier streams.

250

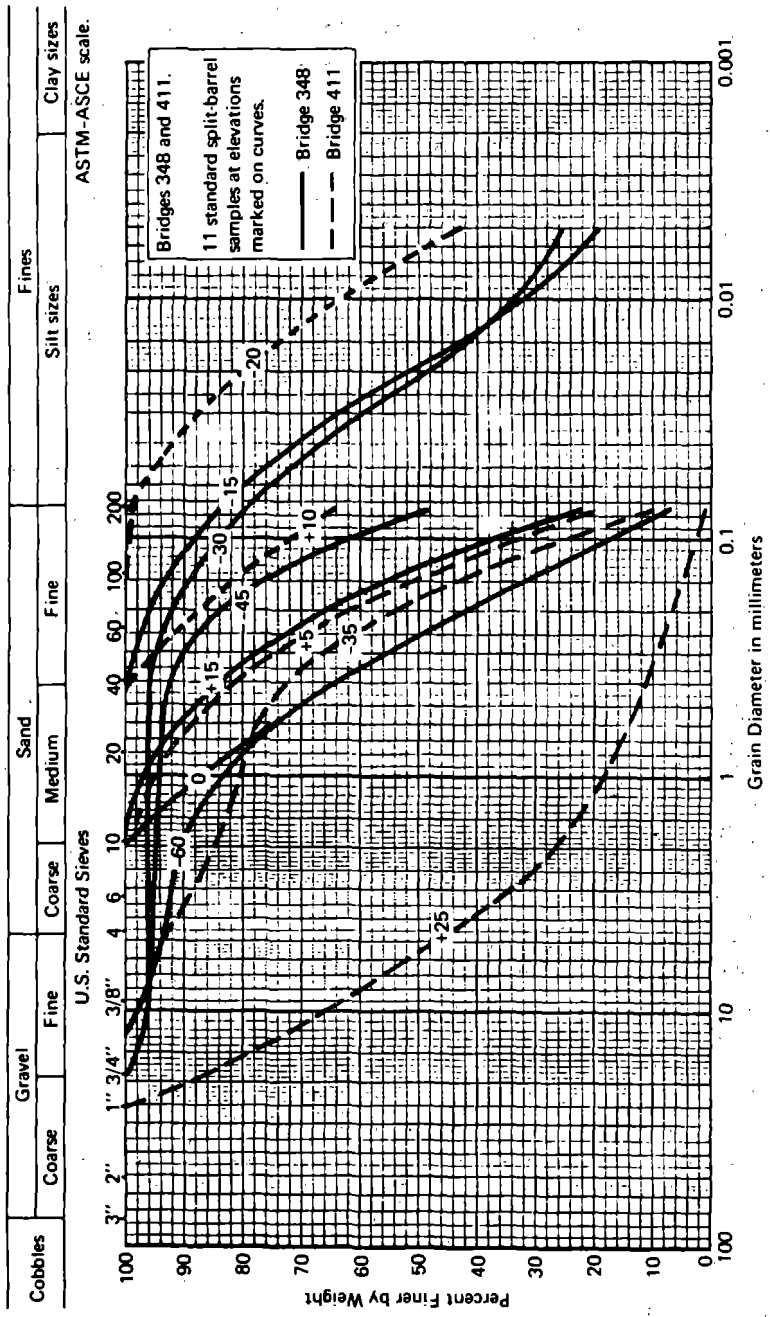Figure 8-18. Bridge 348: Scott Glacier stream (centerline section looking upstream — natural scale).

251

Figure 8-19. Grain-size distributions for soils sampled at Bridges 348 and 411:
Scott Glacier streams 1 and 11 (less the fraction > 1.4 inch).

252

Foundation Support Conditions	Foundation Displacements			
	Severe	Moderate	Minor	Nil
Founded directly on bedrock				● ● ● ● ● ● ●
Piling to bedrock through cohesionless soils				●
Founded on bedrock at one end of bridge, directly or via piles; piling embedded in cohesionless soils over remaining length	●	●		
Piling embedded in gravels and gravelly sands		● ● ● ● ● ●	● ● ● ● ● ●	● ● ● ● ● ●
Piling embedded in saturated medium to dense sands and silts (20 < N < 40 approx)	● ● ●			
Piling driven into medium to dense sand and silts (N > 20) through saturated loose to medium-dense sands and silts (N < 20)	● ● ● ● ● ● ● ●			
Piling embedded in saturated loose to medium-dense sands and silts (N < 20)	● ● ● ● ● ● ● ● ● ●	●	● ●	

Figure 8-20. Correlation between foundation displacements sustained and foundation support conditions at bridges on the Seward, Sterling, and Copper River Highways (data available from only 60 of a total of approximately 120 bridges on the three highways).

REFERENCES, CHAPTER 8

Iwasaki, T., Penzien, J. and Clough, R. (1972) An investigation of the effectiveness of existing bridge design methodology in providing adequate structural resistance to seismic disturbances, Federal Highway Administration Offices of Research and Development, Report No. FHWA-RD 73-13. Washington, D.C., Nov 1972.

Kachadoorian, R. (1968) Effects of the earthquake of March 27, 1964 on the Alaska highway system, U. S. Geological Survey, Professional Paper 545-C. Washington, D.C., 1970.

McCulloch, D. and Bonilla, M. (1970) The Alaskan earthquake, March 27, 1964: effects on transportation and utilities, The Alaskan Railroad, U. S. Geological Survey, Professional Paper 545-D. Washington, D.C., 1970.

Ross, G. A., Seed, H. B. and Migliaccio, R. R. (1973) "Performance of highway bridge foundations: the great Alaska earthquake of 1964," Engineering, National Academy of Sciences. Washington, D.C., 1973.

Waller, R. M. (1966) Effects of the March 27, 1964 earthquake on the hydrology of south central Alaska, U. S. Geological Survey, Professional Paper 544-A. Washington, D.C., 1966.

Chapter 9

RECOMMENDATIONS FOR LIQUEFACTION CRITERIA FOR BRIDGE SITES

RISK ASSESSMENT

A dictionary definition of the term "calculated risk" states: "A
hazard or chance of failure whose degree of probability has been estimated
before some undertaking is entered upon." Casagrande (1965), in a study
of the role of risk in soil mechanics, states that the calculated risk
is the type of risk that nobody knows how to calculate, bringing out the
ambiguity of the adjective "calculated." He defines the term calculated
risk as: the use of imperfect knowledge guided by judgment and experience
to estimate the probable ranges for all pertinent quantities that enter
into the solution of a problem and to base a decision on an appropriate
margin of safety.

The margin of safety that we use should bear a direct relationship
to the magnitude of the potential losses and the range of uncertainties
at a site. Projects with the potential for catastrophic loss of lives
and property should always be planned with an awareness of the responsi-
bility involved. Therefore, the best knowledge and judgment, coupled
with the most sophisticated techniques, must be used to ensure the best
design. Detailed site investigations should be undertaken to provide
all the required information for an analysis. This, along with conserva-
tive factors of safety, minimizes the risk. However, when failure of
smaller projects involves a tolerable financial loss and no loss of
life, the extent or degree of risk must take into consideration economic
factors and magnitude of losses that would result from failures. The
effort spent in the design is obviously reduced. It is in these routine
projects where the calculated risk is greatest. Obviously, the extent
of site definition is more limited for smaller projects. It is in these
areas that this report attempts to provide most guidance.

Casagrande (1965) divides risk into two groups: engineering risk
and human risk. He further divides engineering risk into two groups,
unknown risks and calculated risks. Unknown risks are, by definition,
those risks which cannot be identified until they reveal themselves by
failure. Calculated risks are areas where the state of knowledge is
limited, requiring judgment. Significant progress has been made in our

understanding of the seismic liquefaction phenomenon. However, uncertainties exist in the determination of site motion, the determination of site soil profile and parameters, and the evaluation of the soil strength. Table 9-1 summarizes the design philosophy suggested.

Table 9-1. Philosophy of Earthquake-Resistant Design

Structural Criteria	Liquefaction Behavior
1. Prevent nonstructural damage in minor earthquake ground shakings which may frequently occur in the service life of the bridge.	1. No liquefaction. Factor of safety >1.3.
2. Prevent structural damage and minimize nonstructural damage in moderate earthquake ground shaking which may occur occasionally.	2. No liquefaction. Factor of safety >1.1.
3. Avoid collapse or serious damage in severe earthquake ground shakings which may rarely occur.	3. Liquefaction limited to confined subsurface layer which does not propagate to surface to cause bearing failure. Horizontal flow potential limited to acceptable level.

SITE INVESTIGATION

Chapter 6 presents the requirements for evaluating a potential bridge site to determine the design earthquake ground motion. Detailed surface and subsurface geological information, when available, can aid in evaluation of a site by giving evidence of fault offset, earthquakes associated with faults, determination of age of most recent movement on faults, determination of relationships between site area faults and regional faults, and the identification and description of the faults capable of producing an earthquake. Use should be made of all available geologic maps and data. The time period for active faults should include the Holocene period and perhaps as much as several hundred thousand years in areas of low seismicity to ensure recognition of all potentially active faults.

256

The detailed site investigation must, as a minimum, provide information on the type and *in situ* condition of the soil with depth and the location of the water table so that a soil profile may be constructed. The extent of the investigation is controlled by the importance of the structure. For conventional bridges of normal importance where large-scale soil-test programs are not possible, it is suggested that at least standard penetration tests be used in conjunction with the recovery and classification of borings.

Since the amount of money that might be spent on a site investigation may be limited for a simple bridge, the emphasis should be placed on field tests rather than laboratory tests. Also to be considered is that although the bridge structure by itself might not be costly, it may represent a link in a transportation network which would become useless if the bridge should fail.

SITE MOTION

The ground motion should be determined based on a design level earthquake as described in Chapter 6. A design magnitude should be selected in relation to a probability of occurrence during the life of the structure. In most cases, historical data is limited and additional data from the National Bureau of Standards Study (see Chapter 6) may be needed to provide guidance in selecting design level earthquakes. The design level earthquake should be checked with design earthquake levels assigned to specific faults that have occurred in the past and were thought possible for the future. The present state-of-the-art of liquefaction analysis is limited to ground-motion analysis represented by shear waves.

Figure 6-8 is probably representative of most data, although accelerations may be greater than shown. Tables 6-1 to 6-4 should be used in conjunction with Figure 6-8. The figure and tables may be used for the entire United States in view of the limited data available in the central and eastern portion (see Chapter 6). For engineering usage at distances less than 60 miles, the western United States data are probably adequate since attenuation within this range is controlled by geometric spreading rather than absorption.

CONSTRUCTION IN AREAS OF POTENTIAL LANDSPREADING

Regional land movement — landspreading — may occur during earthquakes as a result of increased pore pressures and reduced soil strength. Structures which cannot undergo differential settlements of high magnitudes should not be built where landspreading is expected, such as on

topographically low areas where the water table is high. The process of
site selection should give preference to areas where soils are at higher
relative densities and unconsolidated sediments are thinnest. Landspread-
ing may be reduced by elimination of surface depressions. The practice
of side borrowing to build embankments increases lateral spreading and
should be avoided. Narrow fills for highways, even on well-compacted
areas, can settle as a result of ground cracks. Outward flow of soils
on the embankment can be expected if the underlying native soils undergo
limited flow from liquefaction. Then settlements of highway embankments
will occur: the wider the fill, the less chance of damage. Parallel
fills for opposite lanes of highways should be combined into one fill to
reduce damage in areas where subsurface soil indicates potential for
liquefaction.

In site selection the toes of alluvial fans and deltas should be
avoided. Crossings should be made in the older, higher, better drained
upper segments of fans and deltas, which are probably more stable.

PRELIMINARY EVALUATION OF LIQUEFACTION POTENTIAL

A preliminary analysis should be made to determine if a liquefaction
problem exists and to what extent a site investigation should be planned.
Figure 9-1 outlines the decision process, and the following information
is required: (1) design earthquakes and (2) a preliminary soil profile
and an estimate of *in situ* soil conditions.

The site profile may be estimated from standard penetration test
results. The simplified hand-computation procedures described in Chap-
ter 3 should be used to define the liquefiable region. For typical
soils the soil strength may be estimated from Figure 3-12 reduced by 10%
to account for multidirectional shaking. The extent of the investigation
is controlled by the magnitude of the project; a bridge might not justify
a large exploration and testing program unless it is of key importance.
Generally, a moderate program of standard penetration field tests and
cyclic triaxial laboratory tests may cost $10,000 to $15,000 (in 1976
dollars) by the time the samples are collected and data reduced, evalu-
ated, and presented in a usable form, provided the site is easily acces-
sible to a local soils laboratory.

DETAILED ANALYSIS OF BRIDGE VULNERABILITY TO LIQUEFACTION

The methods for predicting the occurrence of liquefaction have been
described in Chapter 3. By use of either the simplified hand computation
or the more complex computer one-dimensional or two-dimensional method,

the number of cycles to cause liquefaction at various depths is determined. The soil information required to accomplish this includes a detailed soil profile of the site with estimates of layer density, shear modulus, and strength. Having established a pore pressure generation parameter in terms of the number of cycles to liquefy (N_L), the pore pressure generation/dissipation equation (see Chapter 7) may be solved by the computer programs APOLLO or GADFLEA resulting in a time history of the bearing capacity of the soil, or approximated by Figures 7-9 and 7-10. Estimates of soil compressibility and permeability are required. The adequacy of bridge support in bearing may now be estimated. Using consolidation analysis and viscous flow, support motions of the bridge may be estimated. These support motions may be evaluated by a static structural displacement analysis. The structure should have the design dead weight and live load acting on it in conjunction with the displacements. As shown in Chapter 7, a static displacement analysis is satisfactory since the occurrence of liquefaction isolates the bridge from ground motion and the support displacements are delayed until the liquefaction has time to propagate to the surface.

MINIMIZATION OF BRIDGE DAMAGE

Three basic ingredients are available to reduce the possible damage to a bridge from liquefaction: (1) site selection, (2) site improvement, and (3) bridge design.

Site Selection

As noted in the Alaskan earthquake, bridges located on bedrock suffered least while bridges on deep fine-grained soils suffered most. The geologic and engineering characteristics of a highway route should be thoroughly investigated and evaluated. In some cases, the geologic and hydrologic factors may dictate a route selection that may initially be more expensive than an alternate route over liquefiable soils. However, if repair costs after an earthquake are considered, the overall cost may be less for the more expensive route. Whenever possible, bridge sites should be selected that avoid areas where thick, unconsolidated, young, water-laid, noncohesive sediments occur. Liquefaction requires a high water table; the probability of occurrence can be reduced be selecting an area with a water table below 10 or 20 feet, if possible. Areas where the ground is sloping offer the possibility of horizontal flow if liquefaction occurs. As noted in Chapter 7, slopes of only a few degrees are capable of creating flows of several feet. Sites with sloping ground and topographically low areas should be avoided as much as possible.
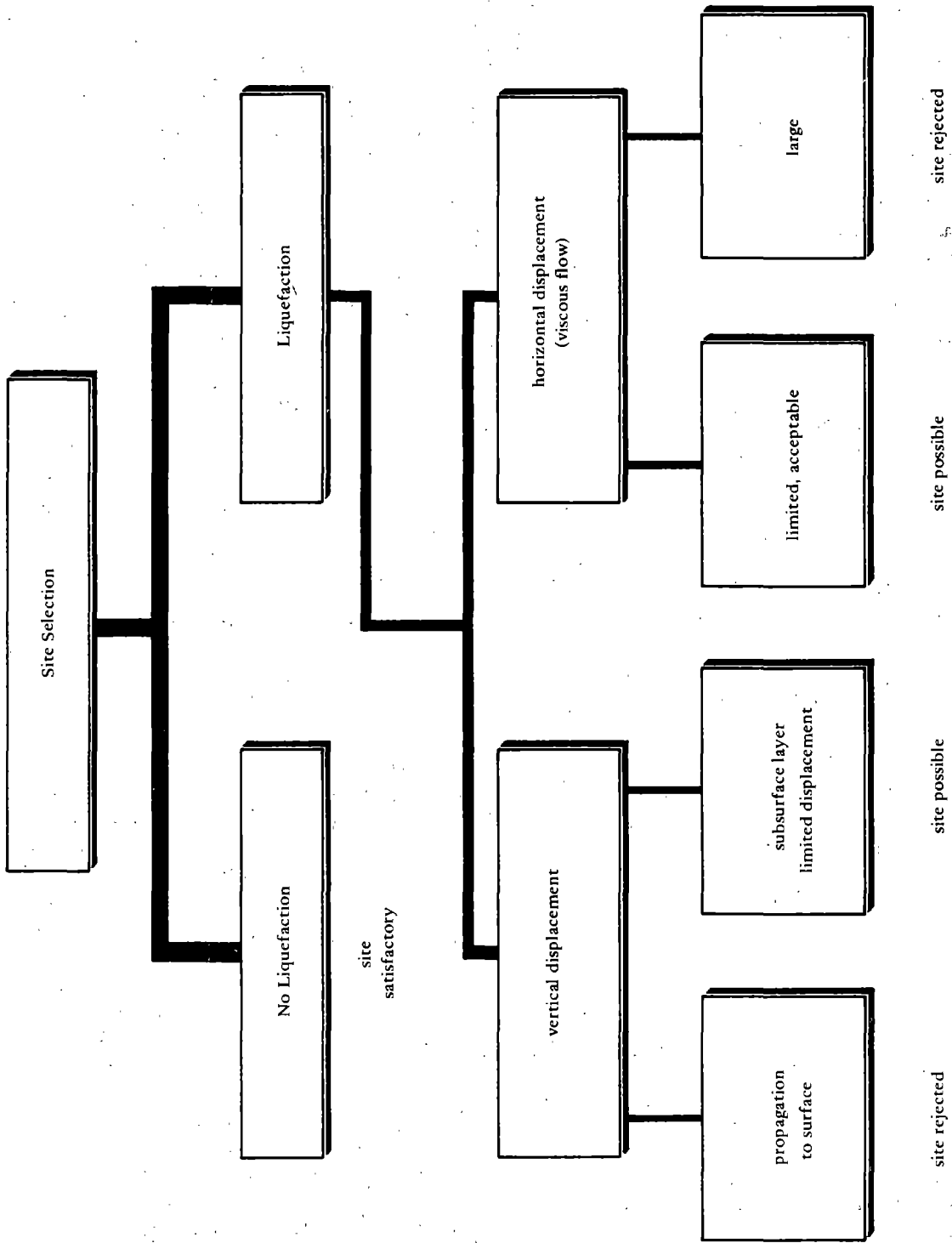
Figure 9-1. Outline of decisions for site selection.

Specifically, the propagation of liquefaction must be evaluated. If the region in which liquefaction occurs propagates to the surface from an earthquake, large motions can be expected and the site should not be considered as satisfactory. If the region in which liquefaction occurs is limited and confined to subsurface layers which do not affect the bearing of the bridge foundation, the site may be considered acceptable if regional subsidence is not large.

Sites where calculations for horizontal and vertical movement must be made using viscosity calculations are probably not well-suited for bridges since large deformations would be expected.

Bridges should be oriented perpendicular to streams and not be skewed. This should minimize differential abutment motion and bridge twisting.

As shown in Chapter 7, soils with relative densities less than 45% can undergo unlimited flow and should be avoided at bridge sites. Soils with relative densities of 80% or greater will probably have limited displacements if liquefaction occurs. Bridges which are sited on these soils must be designed to withstand the displacements expected. Soils with relative densities between 45% and 80% may or may not be suitable for bridge sites; therefore, an extensive analysis should be performed to estimate the potential soil strain which might occur.

Site Improvement

It has been noted previously that a high groundwater table contributes markedly to liquefaction potential. Lowering the water table has a twofold effect: first, it lowers the region in which liquefaction can be initiated; second, it increases the effective confining stress on the potentially liquefiable soil zone. From a practical point of view, it may not be economical to permanently lower the water table at a bridge site.

Next to lowering the groundwater table, the most important method of reducing the liquefaction potential is by increasing the relative density of the soil. Densification increases the initial shear strength of the soil; however, as pointed out in Chapter 7, densification may cause a reduction in permeability of the top layer of soil resulting in an unfavorable condition. Increasing the permeability of the near surface soil improves it. Vibroflotation or sand compaction piles both densifies the soil and improves drainage when porous material is used. Thus, these methods should be more effective than other densification methods in which density alone is increased. Increased confinement through use of highly porous surcharges such as coarse backfill are also extremely effective in reducing liquefaction potential.

Bridge Design

Both structurally indeterminant and determinant structures can
be designed to withstand stresses and displacements without failure.
However, the more indeterminant a structure is, the more the stresses
in the structure are influenced by support displacement. A typically
designed continuous-span bridge is limited to significantly less dis-
placement than a corresponding determinant structure. However, loss of
the support capacity of a column bent for either structure will probably
result in collapse of both structures. In general, structures should be
designed to be articulated to maintain static determinancy. This is not
meant to require expansion joints or other similar devices which have
given designers problems in earthquakes; the intent is to make super-
structure component stress levels independent of support displacements.

In the Alaskan earthquake, it was noted that in short bridges the
bridge decks restrained by the abutments, buckled upward and the center
columns usually rose with the bridge. For short spans only, consideration
should be given to elimination of center columns. As pointed out, loss
of bearing capacity of the center column usually results in collapse of
the structure. A bridge supported at the abutments by comparison would
be much less displacement-vulnerable provided it could accommodate
relative horizontal motion between abutments. The bridge deck should
extend past the abutment supports to allow sufficient relative motion.
The bridge girders should be tied together transversely to allow the
bridge deck to function as a unit.

In multispan bridges, the first column bents should be located as
far away from abutment embankments as feasible. It was noted that
embankment subsidence caused the bent foundation to move toward the
center of the bridge. It was noted that when liquefaction occurred,
bridge piles near the center tended to group closer together and rise.
The distance between piles increased nearer the abutments since the
motion was toward the center. Appropriate horizontal and vertical
superstructure displacements should be planned into the structure. A
movement of 2 feet was quite common in the Alaskan earthquake. Provisions
should be made for wide abutments, and allowing the superstructure to
overhang the abutment supports.

In areas where bedrock is near the surface, caissons to rock provide
the most reliable, although probably the most expensive, type of founda-
tion. In regions where liquefaction will occur, vertical piles have
been found to have insufficient lateral stability. When the soil becomes
liquefied, the horizontal restraint is lost, and the pile may experience
large lateral displacements. This is not surprising considering the
long unbraced length of the pile and its load. Thus piles, even though
driven into competent material below a potentially liquefiable zone and
designed not to rely on friction in the liquefiable zone, may still fail
because of excessive horizontal motion or from buckling over its unsup-
ported length.

Shallow, low pressure footings might be suited for liquefaction which does not propagate to the surface and cause bearing failure. The bridge engineer must make foundation choice based on the specifics of the site, the types of structure, and loads. In any case, the bridge must be designed such that the combination of dead and live load and liquefaction displacement do not result in overstressing at any point (formation of first hinge).

PROBABILITY OF OCCURRENCE

To evaluate the risk of liquefaction at·a site, both the damage from liquefaction and the probability of occurrence must be reviewed together. To accomplish this, the designer should prepare a list of magnitudes of earthquakes from results of liquefaction analyses showing: (1) no liquefaction, (2) liquefaction of subsurface layer withoutt widespread propagation, (3) liquefaction of subsurface layer with propagation to foundation support level, and (4) liquefaction propagating to surface. These levels of liquefaction should then be correlated to the probability that a specific magnitude earthquake occurs. Depending on the method for analysis, uncertainties in acceleration, relative density, and soil strength may be included.

An example of this will be shown. Let us consider a site at a known distance from a fault. The site acceleration and standard deviation may be estimated from Chapter 6. The number of earthquake cycles and standard deviation may be estimated from Figure 3-24. The soil's relative density and standard deviation may be determined, as discussed in Chapters 4 and 5, from laboratory or field tests, and the soil strength and standard deviation, in the absence of actual data, may be estimated from Figure 3-12. Using the simplified calculation procedure, a factor of safety may be determined directly. However, a Monte Carlo simulation can be performed taking the four variables (soil strength, relative density, site acceleration, and number of earthquake cycles) as random, normally distributed values, shaped by their means and standard deviations.

Consider the following case where the distance to the fault is 40 miles; then the ground motion for various magnitude earthquakes is given in Table 9-2.

Assume a case where the relative density is 0.60 with standard deviation of 0.06 and the soil strength as indicated in Figure 3-7; then, by using simple Monte Carlo simulation, the probability of liquefaction may be determined as a function of earthquake magnitude, as shown in Table 9-3. The probability of an earthquake occurring and causing liquefaction may be estimated by use of recurrence data for a fault

263

(usually expressed as a number of events per year for magnitude greater than or equal to M). The recurrence data is used to determine the number of events expected between a magnitude increment, M_i to $M_i + 1$. The expected number of earthquake events per year is multiplied by the number of years for the life of the structure and by the average probability of liquefaction occurring for the magnitude range M_i to $M_i + 1$ to yield the expected number of earthquakes causing liquefactions for the fault, time period and magnitude increment. The expected number of earthquakes causing liquefaction, λ, is used to compute the probability of an earthquake occurring and causing liquefaction by a Poisson's distribution

$$P_{LE} = 1 - e^{-\lambda}$$

Assuming the fault to be a typical fault system in California with specific recurrence intervals (number of earthquakes per year), the probability of an earthquake occurring and causing liquefaction is shown in Table 9-4.

For this example the highest probability of liquefaction in the 50-year span is 0.046 from a magnitude 8 earthquake. The most probable earthquake causing liquefaction may occur at any magnitude and is a function of fault activity and site conditions. The consequences and extent of liquefaction for the most probable magnitude earthquake should be determined. (Although the consequences from other magnitude earthquakes will be greater, the probability is lower.) Thus, levels of damage and extent of propagation of liquefaction can be determined as a function of magnitude and probability of occurrence.

The overall risk to a structure may be determined based on the probability of occurrence of liquefaction and the consequences should it occur. It is also obvious that the uncertainty associated with the ability to predict earthquake motion and to determine site properties results in some probability of liquefaction even though the median factor of safety is greater than 1.0. Thus, a degree of conservatism must be exercised until more accurate site definition and earthquake-motion data become available.

Using the Monte Carlo simulation technique, graphs may be developed which show the factor of safety and probability of liquefaction as a function of earthquake magnitude, distance from the fault, and relative density of the soil at the site (Figures 9-2 through 9-6). The groundwater table is assumed to be at a depth of 5 feet and the occurrence of liquefaction at a depth of 20 feet. Figure 9-2 shows the factor of safety for various confidence limits.

Table 9-2. Ground Motion

Earthquake Magnitude	Number of Cycles	Number of Cycles Standard Deviation	Acceleration (g)	Acceleration Standard Deviation (g)
5.0	3.67	3.64	0.005	0.0056
5.5	4.86	3.92	0.0143	0.0146
6.0	6.43	4.11	0.0303	0.0309
6.5	8.51	4.14	0.0516	0.0527
7.0	11.27	5.81	0.0711	0.0725
7.5	14.92	8.19	0.0790	0.0806
8.0	19.76	11.52	0.0790	0.0806

Table 9-3. Probability of Liquefaction

Earthquake Magnitude, M	Probability of Liquefaction, $P_L(M)$	Median Factor of Safety
5.0	0.000	>10
5.5	0.000	>10
6.0	0.007	5.38
6.5	0.047	3.06
7.0	0.097	2.22
7.5	0.165	1.81
8.0	0.218	1.67

Table 9-4. Probability of Earthquake Causing Liquefaction

Magnitude	Recurrence Interval, U(M)[a]	Number of Events/Yr, U(M)	Expected Events 50 Years	P_L	Expected Events Causing Liquefaction	P_{LE}
5.0	0.26	0.13	6.5	0	0	0
5.5	0.13	0.063	3.15	0	0	0
6.0	0.067	0.033	1.65	0.007	0.01155	0.011
6.5	0.034	0.017	0.85	0.047	0.03995	0.039
7.0	0.017	0.0076	0.38	0.097	0.03686	0.036
7.5	0.0094	0.0050	0.25	0.165	0.04125	0.040
8.0	0.0044	0.0044	0.22	0.218	0.04796	0.046

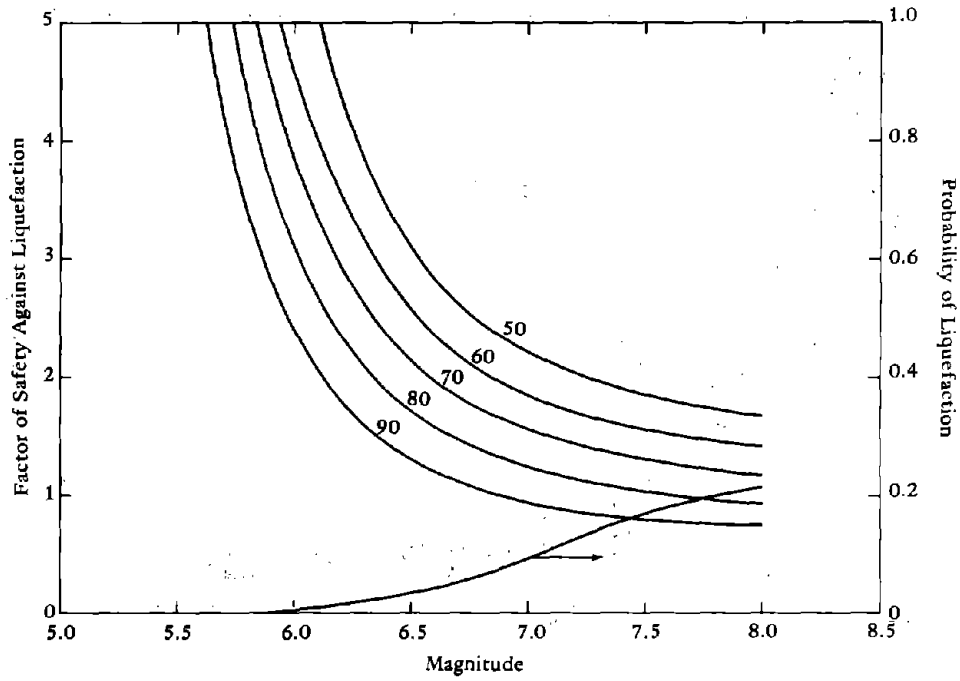[a] Number of events per year $\geq M$ and assumed that $t = 50$ years.
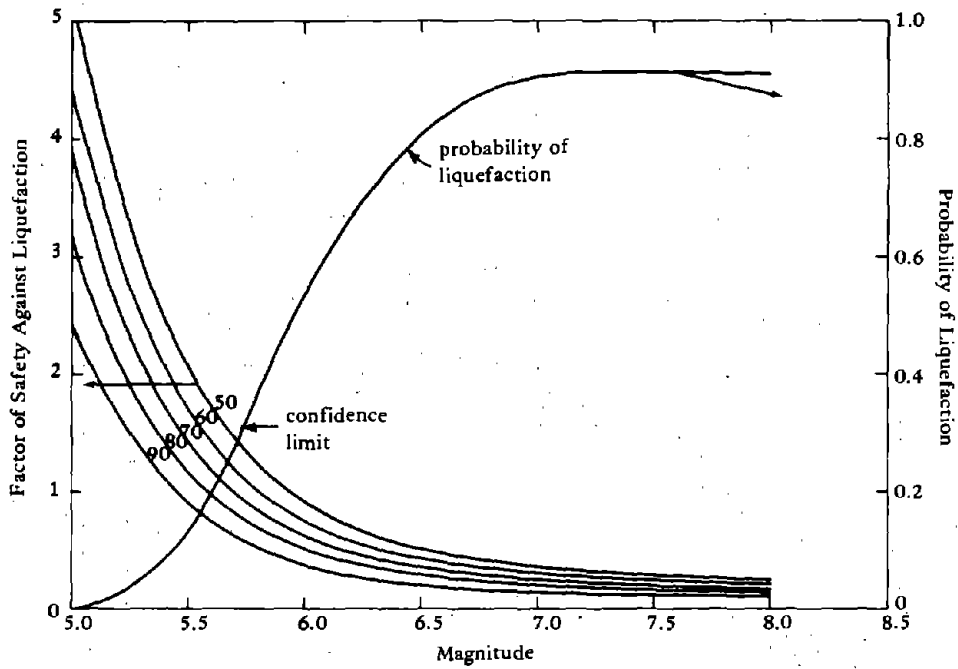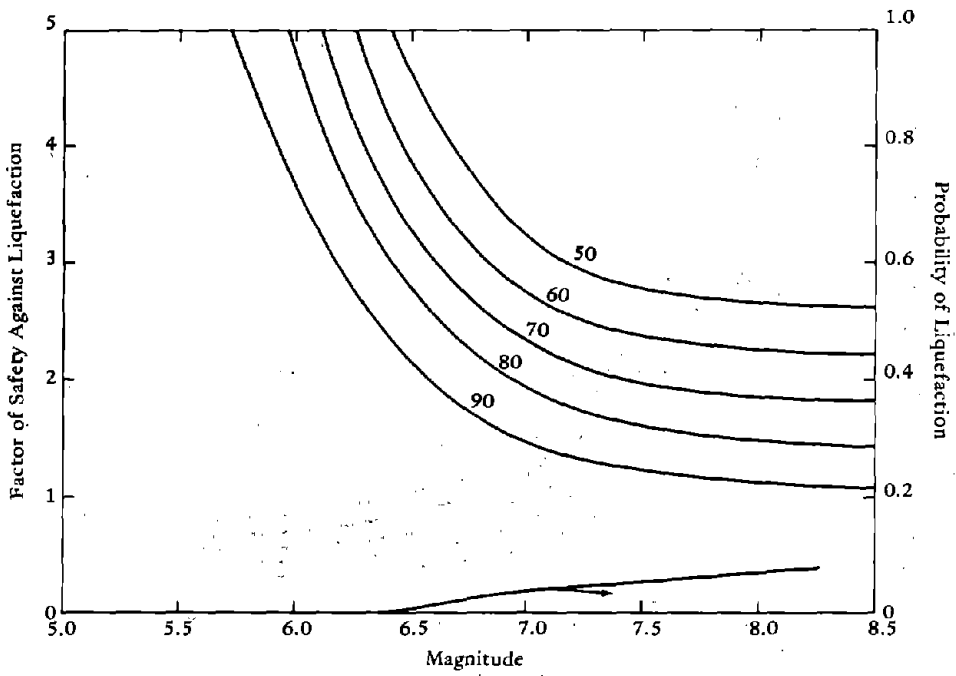
(a) Distance to fault - 20 miles.
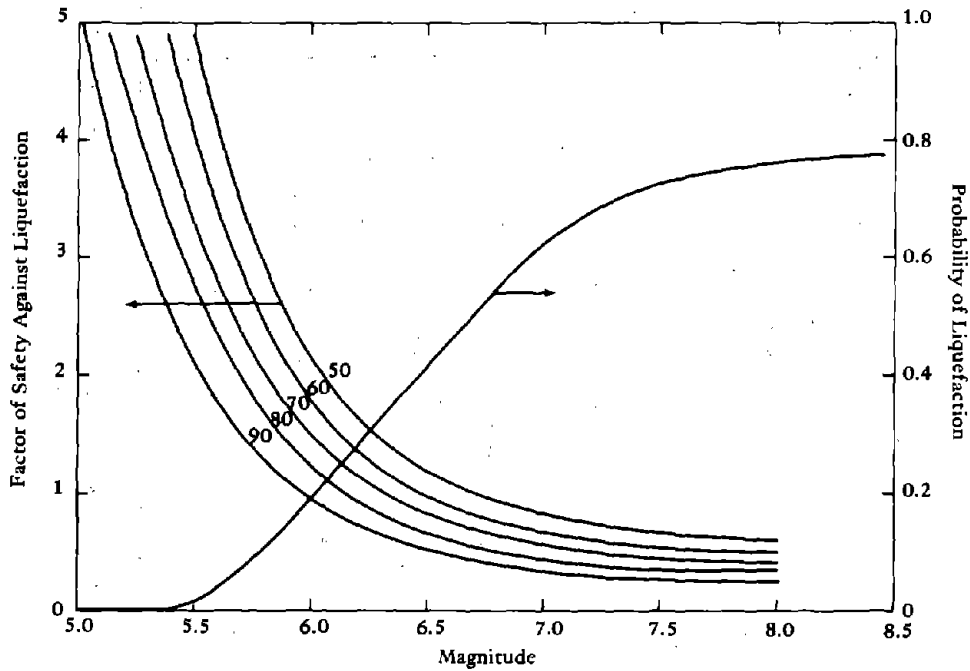
(b) Distance to fault - 30 miles.

Figure 9-2. Factor of safety for various confidence limits
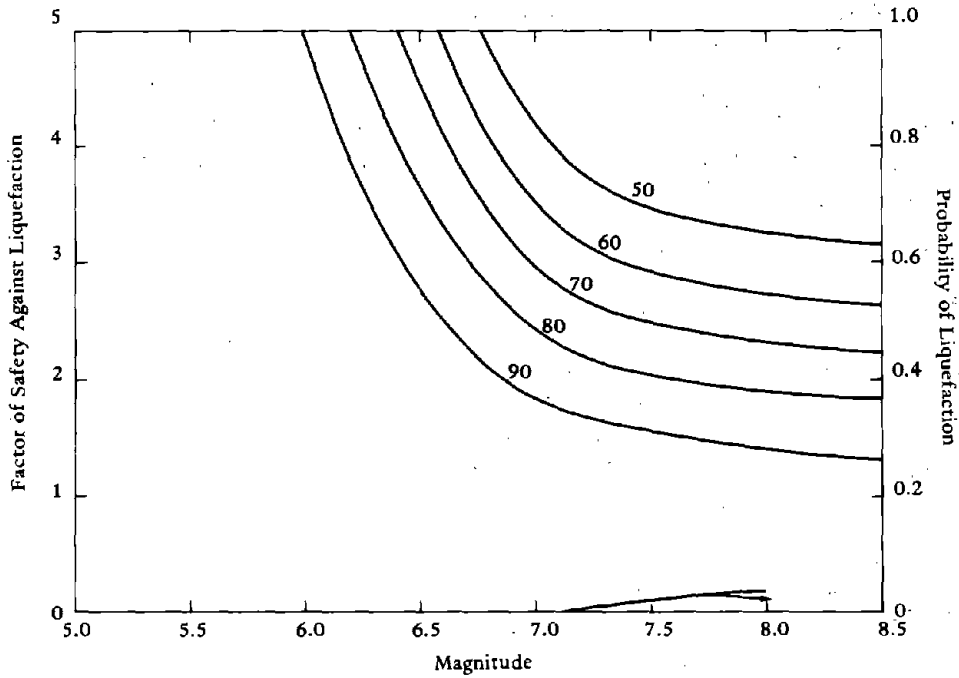and probability of liquefaction at relative
density of 0.4.

267
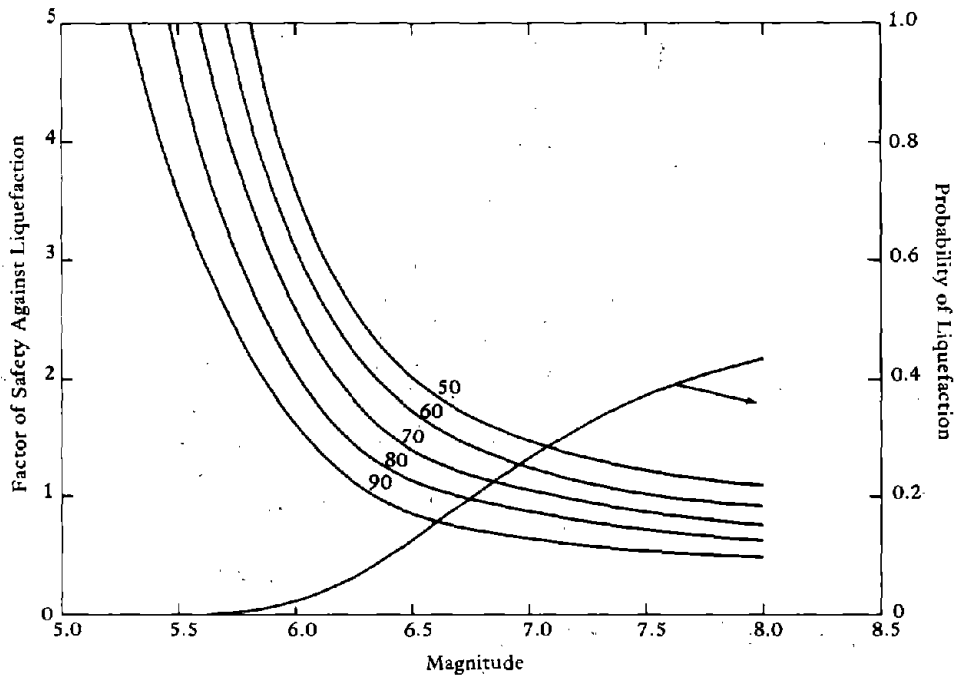
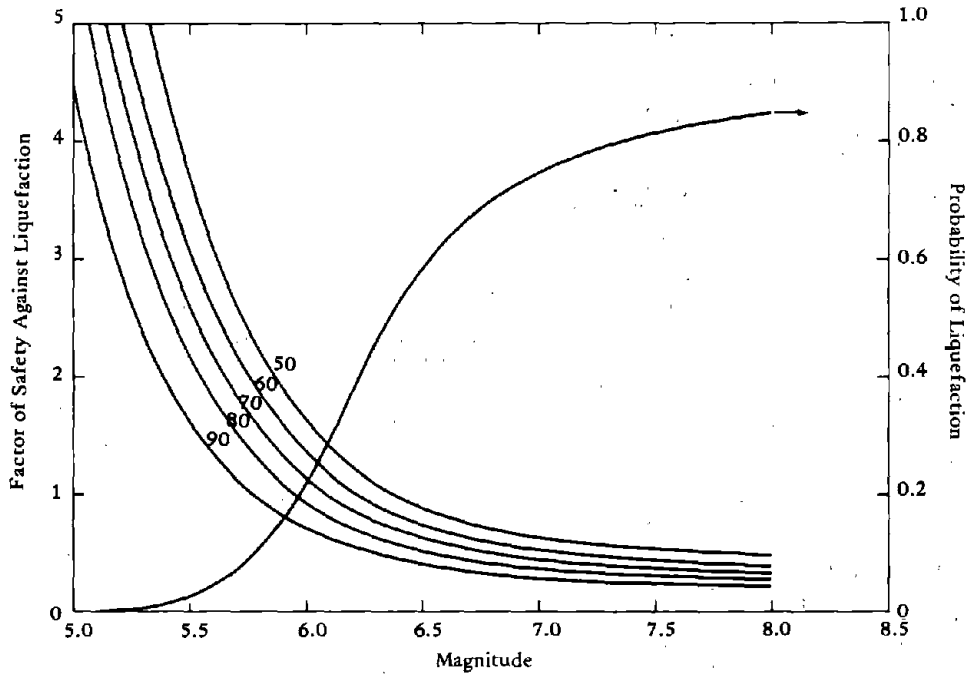(c)   Distance to fault – 40 miles.
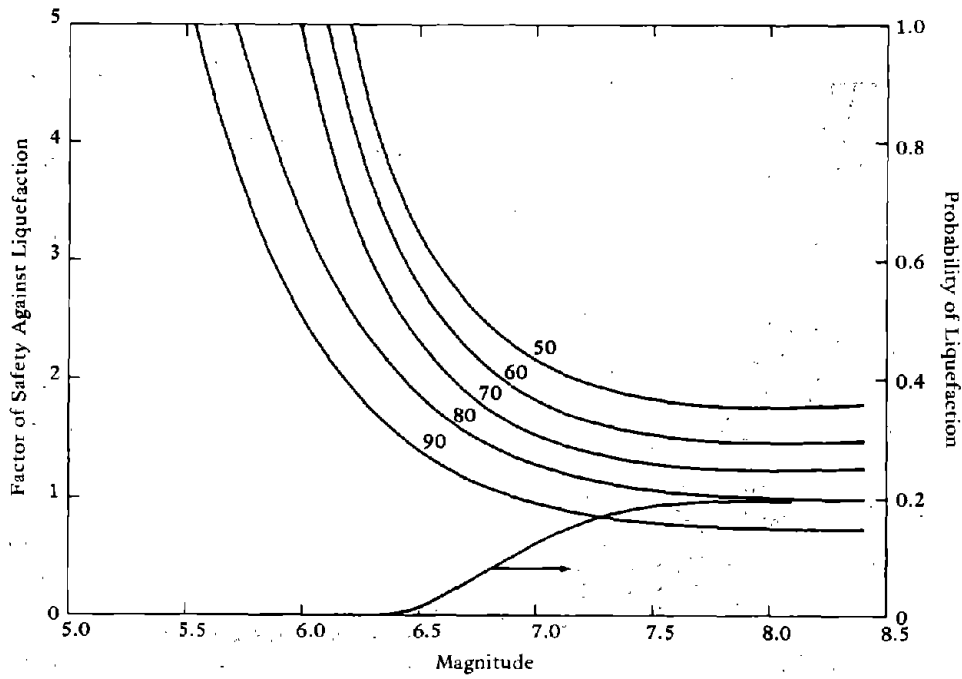
(d)   Distance to fault – 50 miles.
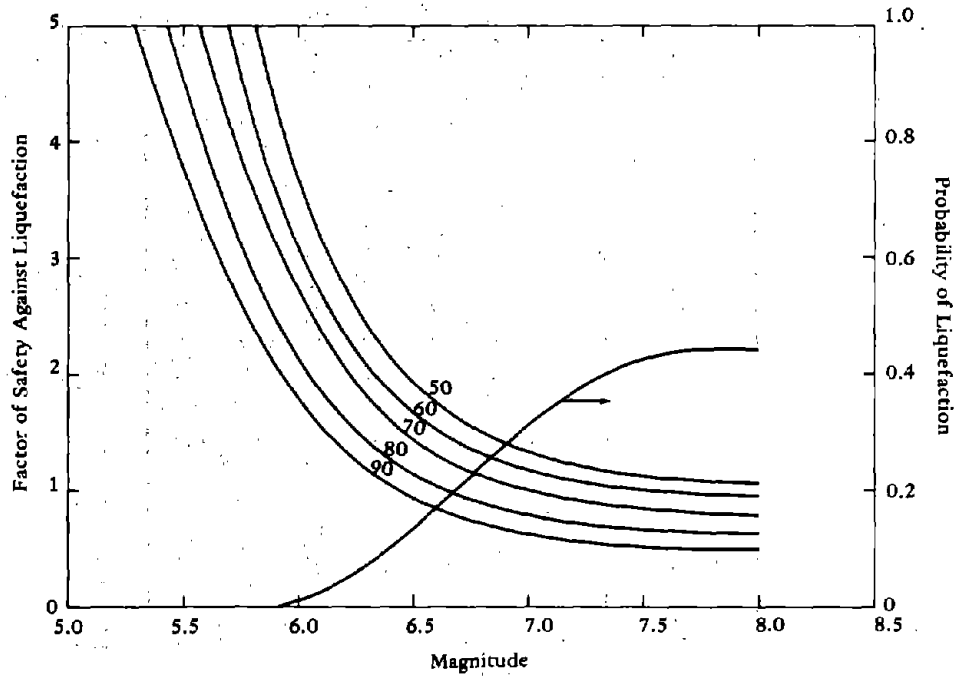
Figure 9-2.   Continued

268
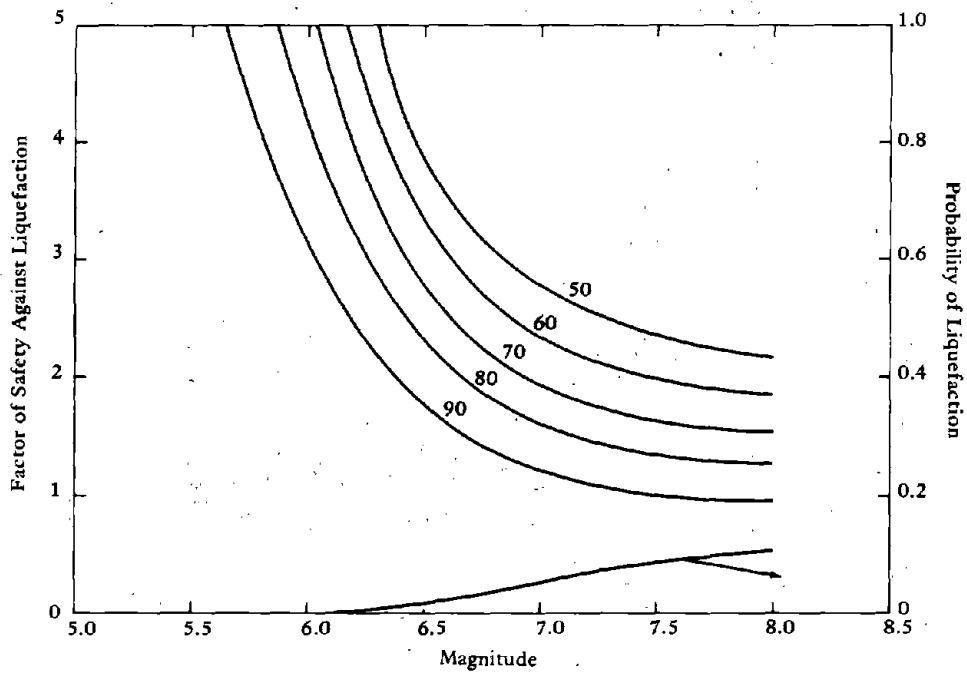
(e) Distance to fault - 60 miles.

Figure 9-2. Continued
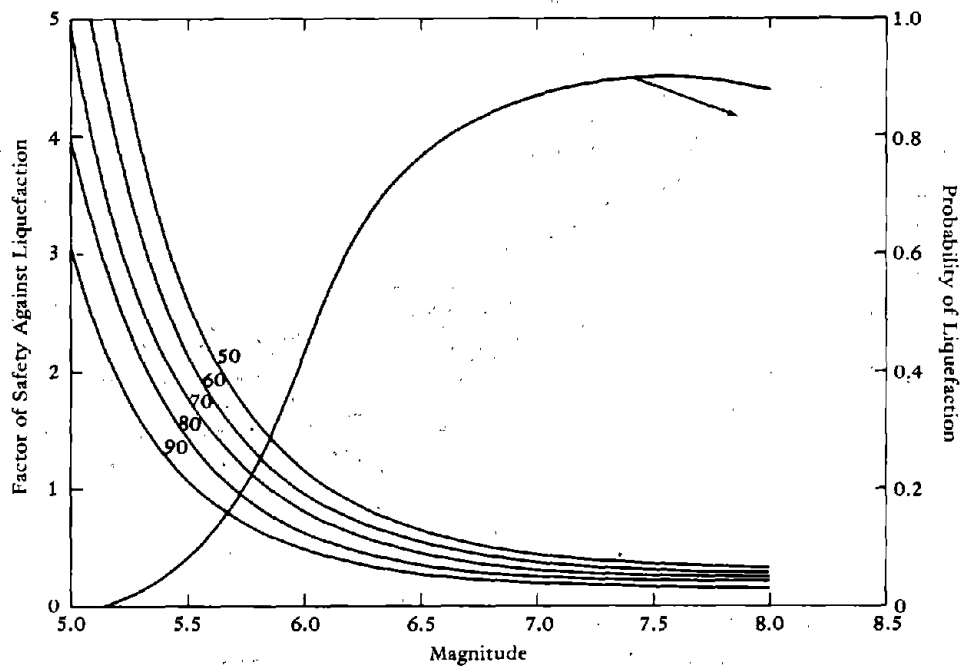
(a) Distance to fault - 20 miles.

Figure 9-3. Factor of safety for various confidence limits
and probability of liquefaction at relative
density of 0.5.
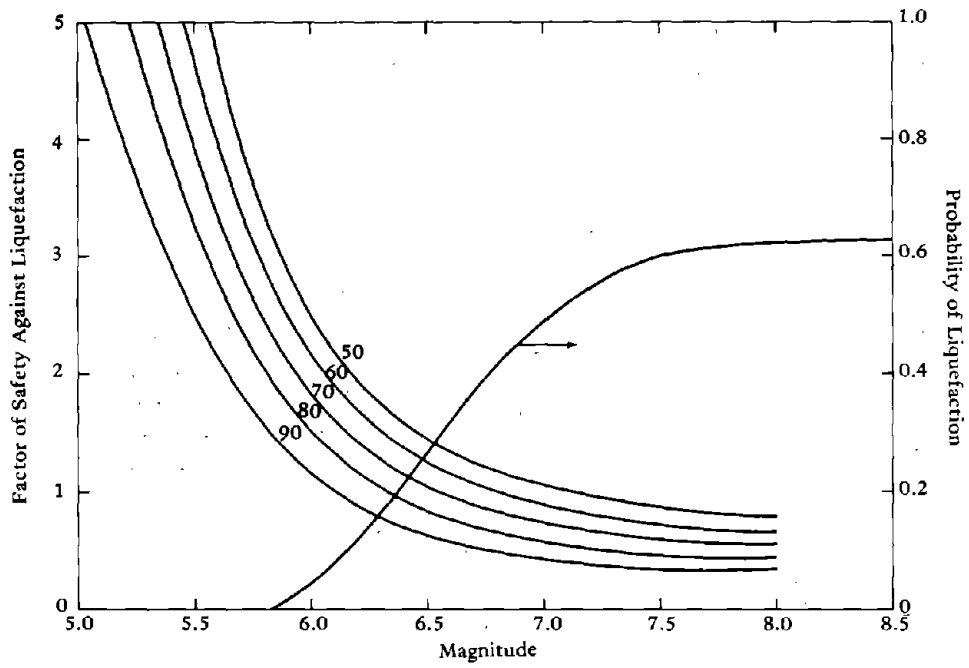
(b) Distance to fault – 30 miles.
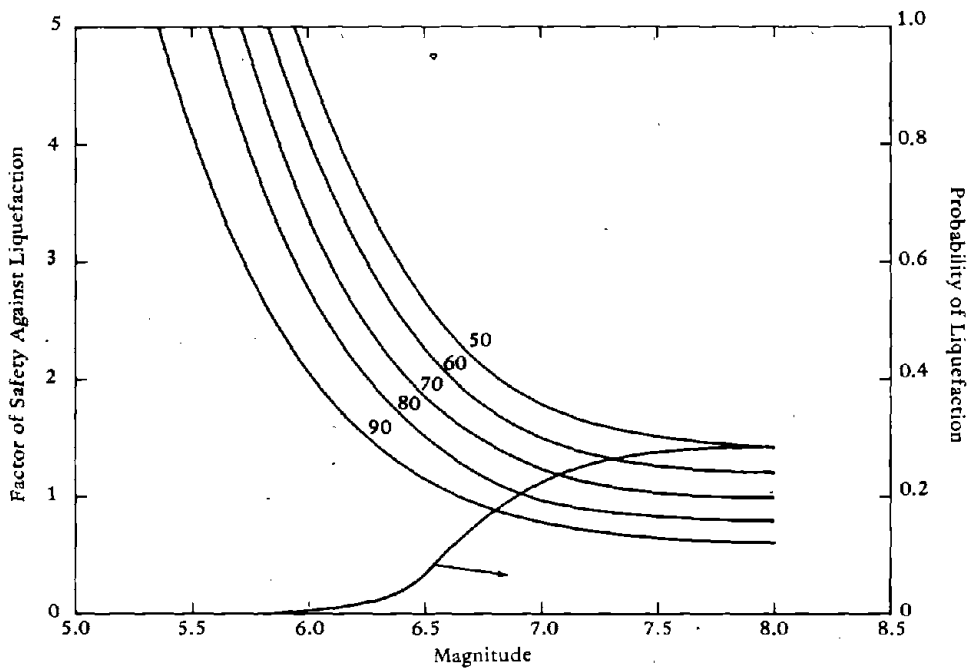
(c) Distance to fault – 40 miles.

Figure 9-3. Continued

270
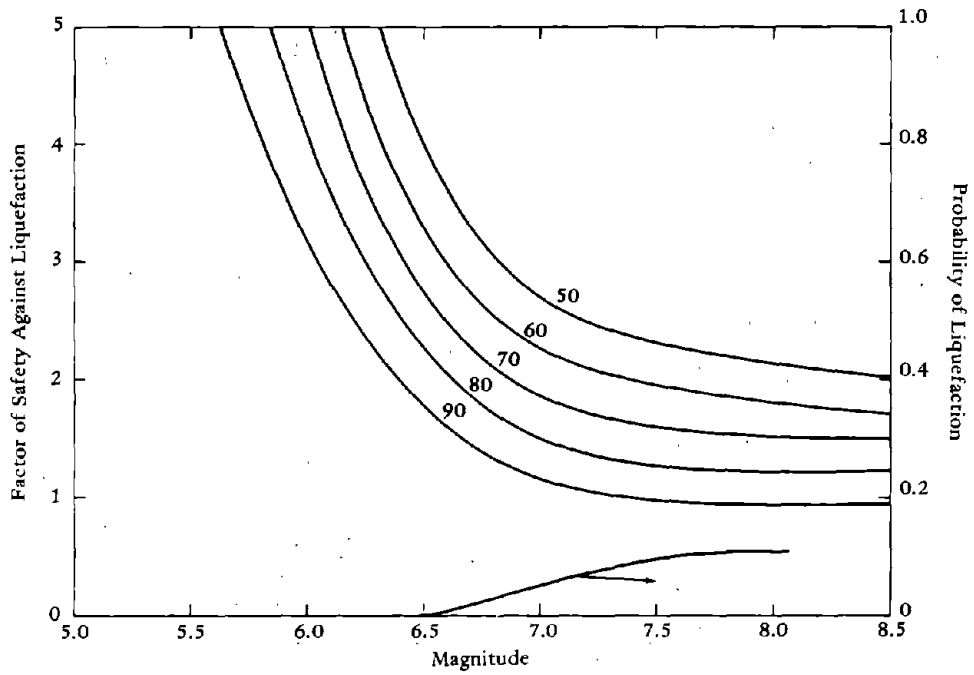
(d)   Distance to fault - 50 miles.
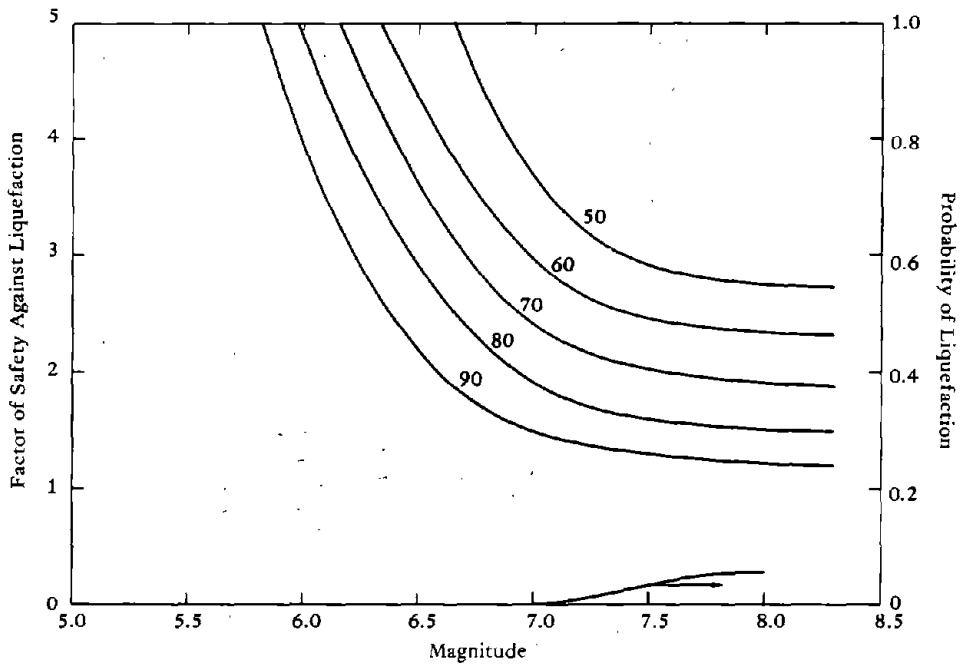
(e)   Distance to fault - 60 miles.

Figure 9-3.   Continued
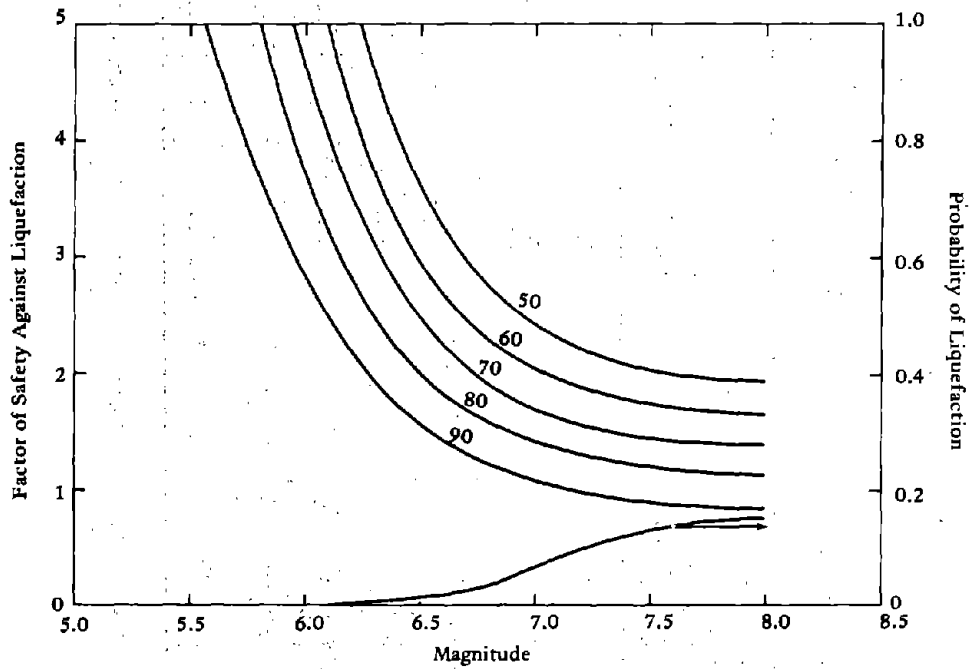
271
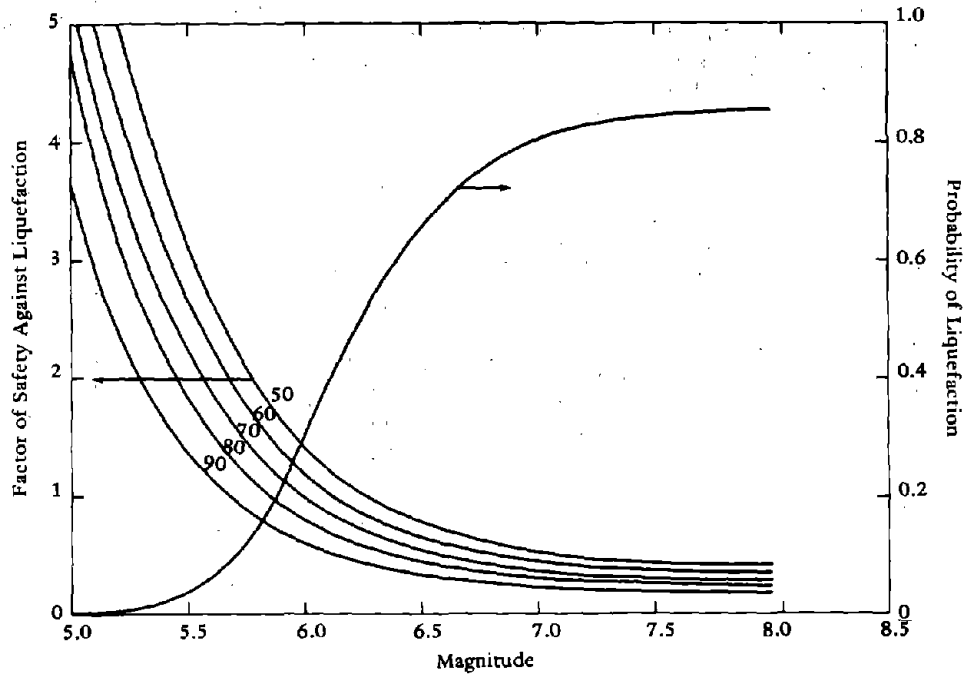
(a) Distance to fault - 20 miles.
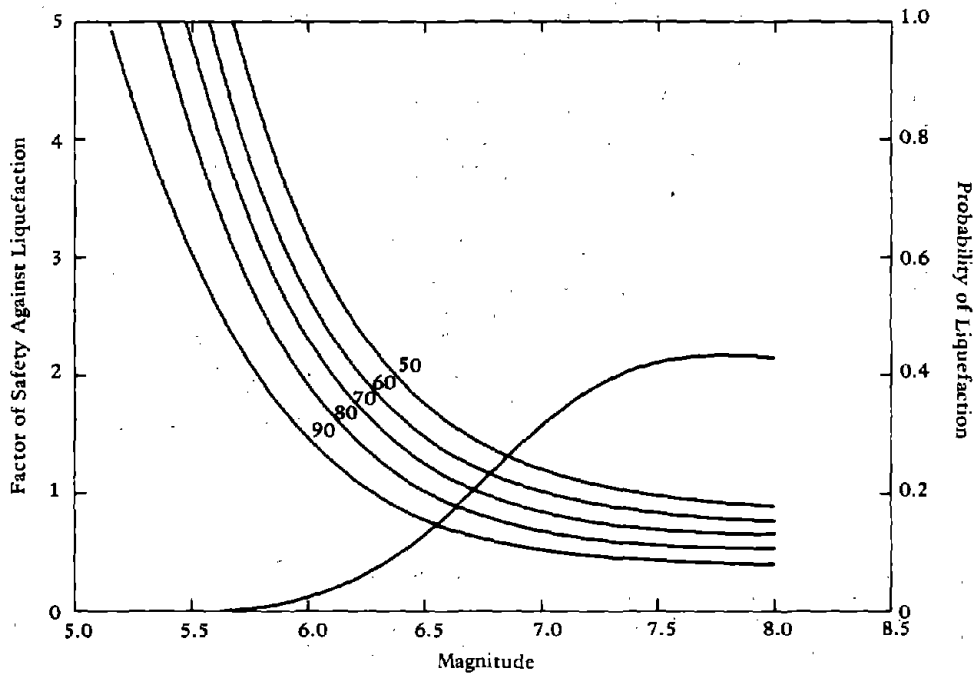
(b) Distance to fault - 30 miles.

Figure 9-4. Factor of safety for various confidence limits
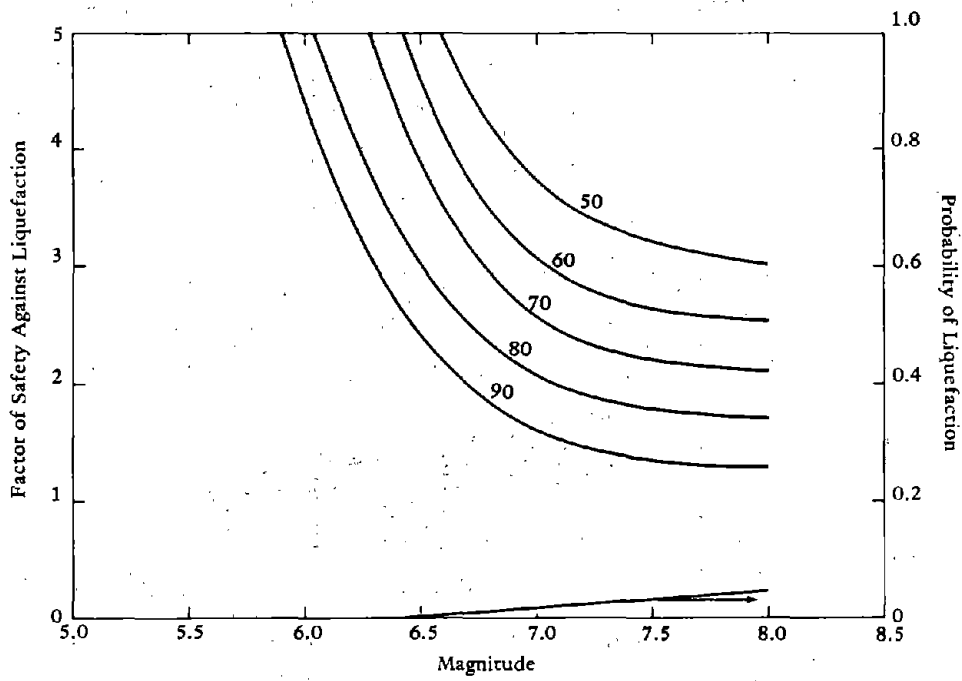and probability of liquefaction at relative
density of 0.6.

(c) Distance to fault - 40 miles.

(d) Distance to fault - 50 miles.

Figure 9-4. Continued

273.

(e)   Distance to fault - 60 miles.

Figure 9-4.   Continued

(a)   Distance to fault - 20 miles.

Figure 9-5.   Factor of safety for various confidence limits
and probability of liquefaction at relative
density of 0.7.
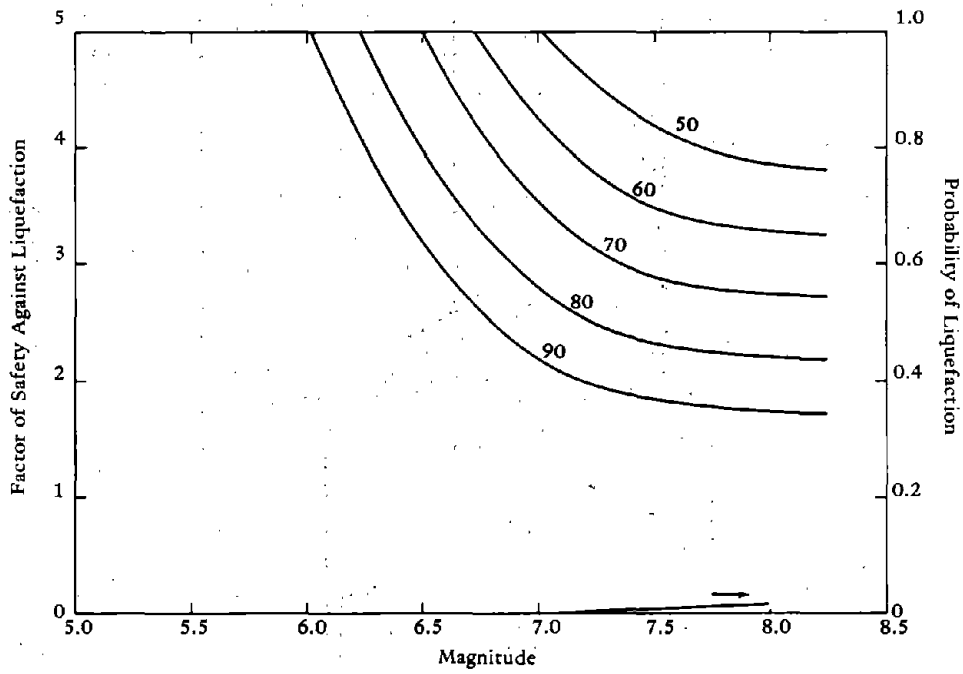
(b) Distance to fault - 30 miles.

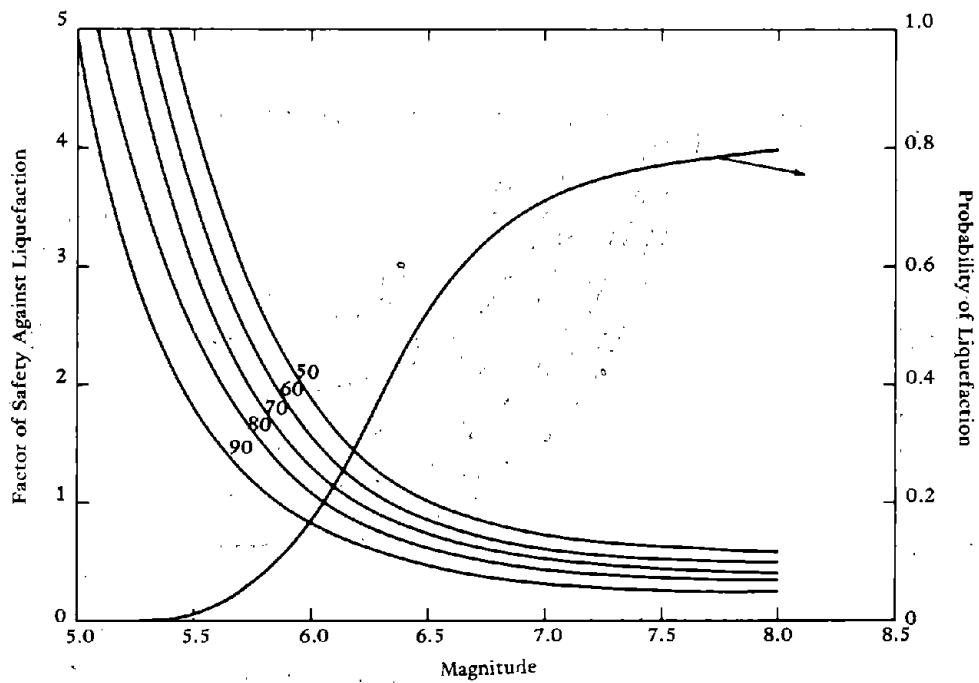(c) Distance to fault - 40 miles.

Figure 9-5. Continued
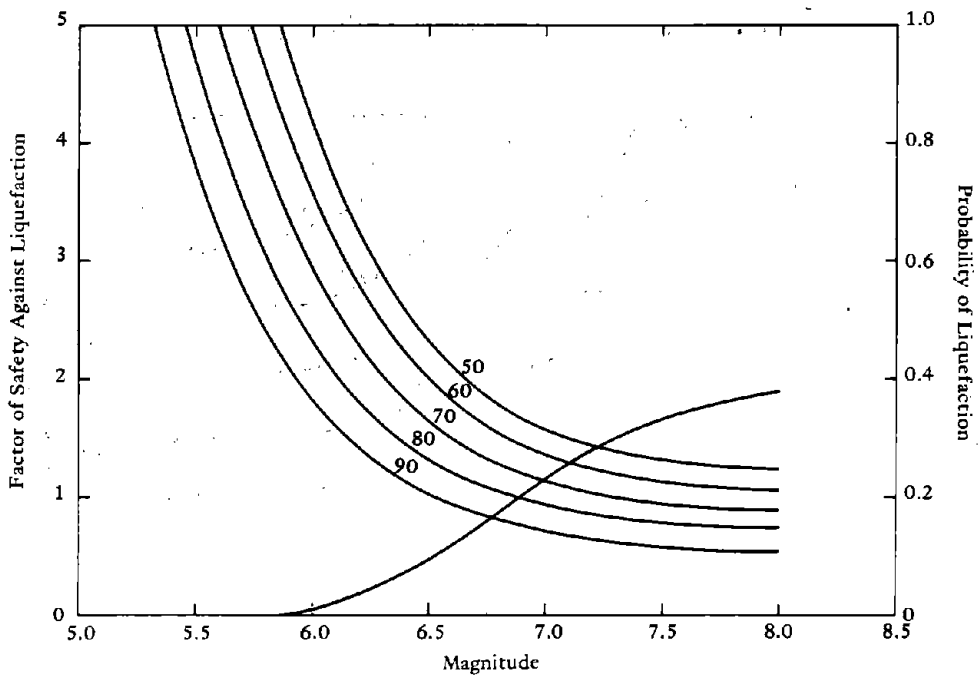
275

(d) Distance to fault - 50 miles.

(e) Distance to fault - 60 miles.
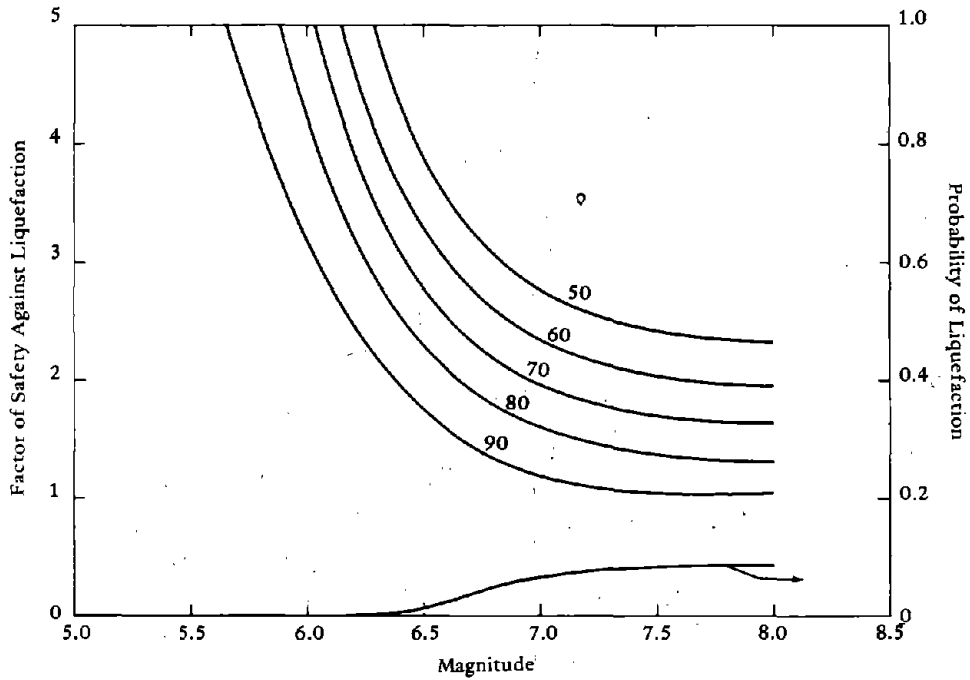
Figure 9-5. Continued
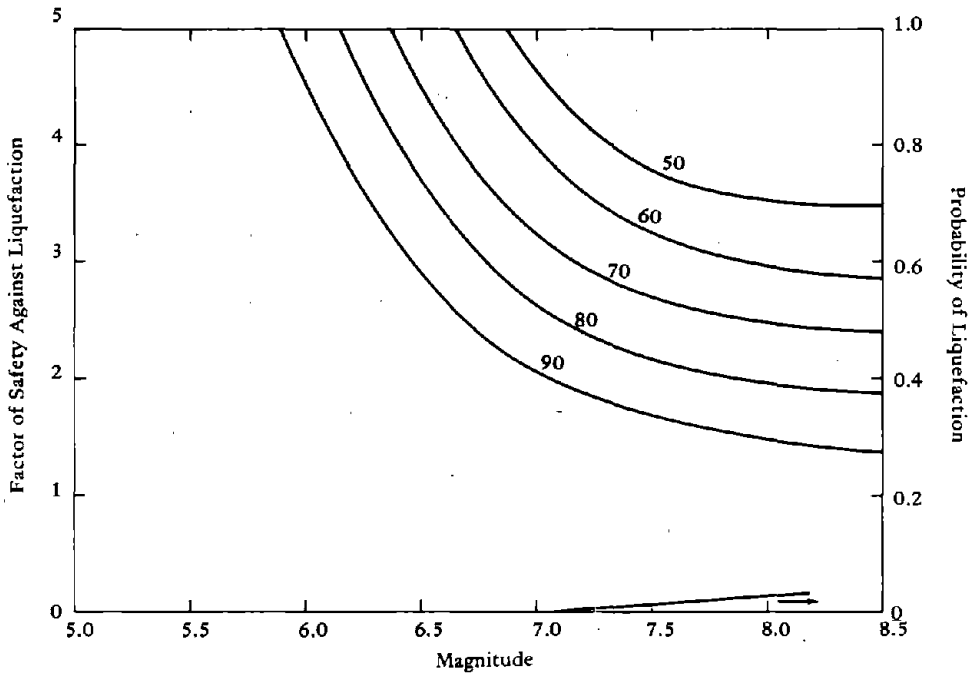
276

(a) Distance to fault – 20 miles.

(b) Distance to fault – 30 miles.

Figure 9-6. Factor of safety for various confidence limits
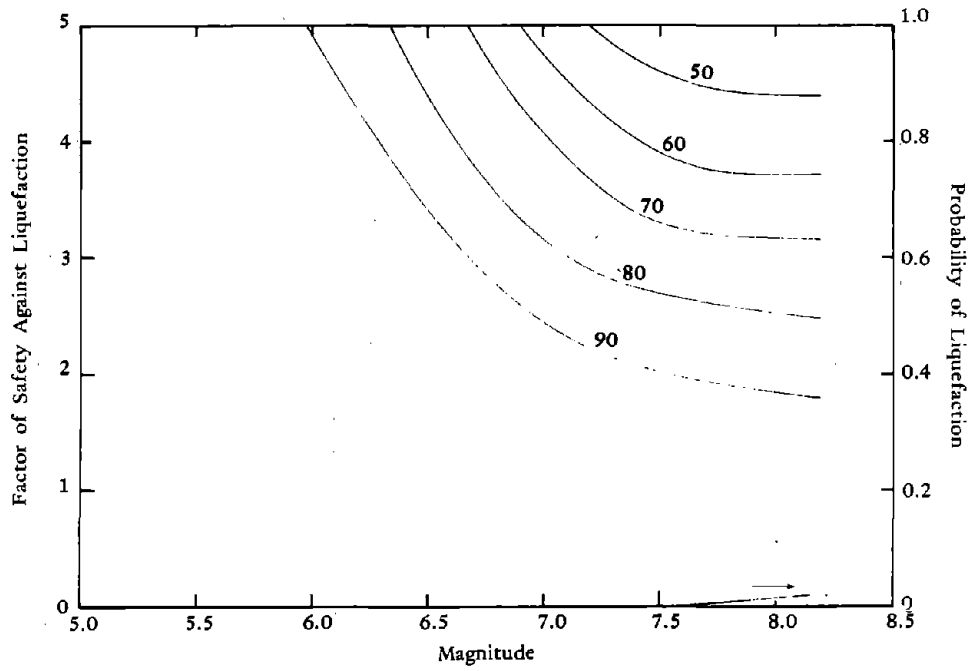and probability of liquefaction at relative
density of 0.8.

277

(c) Distance to fault - 40 miles.

(d) Distance to fault - 50 miles.

Figure 9-6. Continued

278

(e) Distance to fault - 60 miles.

Figure 9-6. Continued

CRITERIA FOR BRIDGE SITES

The criteria for selection of bridge sites should be based on earthquakes with the following magnitudes:

M_A = recurrence, once in 10 years

M_B = recurrence, once in 25 years

M_C = recurrence, once in 50 years, or design level earthquake

M_D = recurrence, once in 200 years, or the maximum credible earthquake

Under the proposed criteria the site is considered acceptable if the mean-minus-one-standard-deviation factor of safety $FS_{m-\sigma}$ (84% confidence limit) and the probability of an earthquake causing liquefaction P_{LE} are as shown in Table 9-5. Note that the probability includes the occurrence of an earthquake and is not simply the probability of liquefaction.

It should be noted that in the proposed criteria liquefaction is allowed to occur for the M_D earthquake (maximum credible earthquake) as long as it remains confined to subsurface layers, does not cause bearing failures, or produce unacceptable horizontal and vertical displacements. Since the displacements would be limited, acceptable levels of damage would be imposed on the bridge structures, and collapse would not occur.

In the proposed bridge siting criteria, the acceptability of a site depends on whether the value of the probability of an earthquake causing liquefaction is <0.10. This value is based solely on engineering judgment. By comparison, the Naval Facilities Engineering Command, as a basis for structural design, uses an earthquake with a probability of occurring, or being exceeded, of 0.1 in 25 years (the estimated life of typical Naval structures). The bridge criterion proposed here is somewhat more conservative in that it suggests use of 50 years to account for the longer life typical of bridge structures. Further, the occurrence of liquefaction does not always result in collapse of the bridge.

It is very difficult to quantify the dollar value of a functioning bridge. A key transportation link over which people must travel to reach a hospital obviously requires special consideration. The value of human life has always been of highest importance in the United States. Engineers are often faced with problems asking, "How safe is safe enough?" or "Where can extra funds be best spent to yield the greatest return?" An economic analysis may be of use in comparing alternatives to produce the best return. To attempt to put the probability value in perspective and to demonstrate an economic analysis, the following comparison is made.

Assume that there are a number of people on a typical small bridge when an earthquake occurs causing liquefaction. Assume as a worst case that the bridge collapses and some are injured and some are killed. Assume that the total injury and death is equivalent to 10 people killed. This number will be used as a basis for comparison. During a 50-year period the criteria set the probability of an earthquake causing lique-faction at 0.1. The annual rate for an earthquake causing liquefaction is 0.002. The fatality rate from motor vehicle driving is 0.00027 fatalities per person per year (National Bureau of Standards) and for 10 people is 0.0027.

In the proposed criteria there is a lower probability of the bridge's collapsing than of 10 people being killed in 50 years of driving. This is not intended to be rigorous mathematical derivation but only a simple comparison to put the value suggested in the criteria in perspective.

Assuming that 10 people were killed and that the value per individual was $100,000, the annual expected casualty loss is $2,000.00 (100,000 x 10 x 0.002). Assume the bridge structure is $400,000; its annual expected loss would be $800.00 (400,000 x 0.002).

The total annual expected loss would be $2,800. The present value of a series of $2,800 payments at a 6% interest for 50 years is $44,136. This is 11% of the bridge cost.

Assume that the site may be improved such that the probability of an earthquake causing liquefaction is 0.05 in 50 years. The annual rate of an earthquake causing liquefaction is 0.001, and the total expected loss from bridge collapse and associated deaths is $1,400. The present value of a series of payments of $1,400 at 6% interest is $22,068. Thus, up to $22,068 ($44,136 - $22,068) can be spent to accomplish the reduction in P_{LE} and still be cost effective.

As an alternative example consider the fatality rate from driving — 0.00027 fatalities per person per year. Consider an exposure per year of 340 hours (12,000 miles at 35 miles per hour), then the fatality rate per hour of exposure is 7.94×10^{-7}. The rate of an earthquake causing liquefaction — and assuming worst case bridge collapse — is 0.002 per year or 2.28×10^{-7} per hour of exposure. An hour of potential exposure to an earthquake on the bridge is safer than an hour of exposure to driving (2.28×10^{-7} is less than 7.94×10^{-7}).

Table 9-5. Criteria for Site Selection

Earthquake	Factor of Safety, $FS_{m-\sigma}$	Liquefaction Probability, P_{LE}	Liquefaction Consequences					
			Liquefaction Subsurface Layer	Propagation to Surface	Bearing Failure	Horizontal Flow Failure	Vertical Settlement Failure
M_A	≥ 1.5	≤ 0.1	No	No	No	No	No
M_B	≥ 1.3	≤ 0.1	No	No	No	No	No
M_C	≥ 1.1	≤ 0.1	No	No	No	No	No
M_D	—	—	Yes[a]	No	No	No	No

a Upper region pore pressure limited to prevent failure.

DISCUSSION

This report is intended to provide guidance to a bridge planner
with a problem of siting a bridge in an area where potentially liquefiable
soils exist. The range of methods for predicting the occurrence of
liquefaction has been given. The choice of a method is a function of
the available information and size of the study. Methods were given to
estimate soil displacement. Although these are admittedly crude, some
means of determining the consequences of liquefaction must be used. It
is in this area that existing knowledge is most limited and to which
future research should be directed. Volume II gives a more condensed
guide in a format to be of practical assistance to highway engineers.

REFERENCES, CHAPTER 9

Casagrande, A. (1965) "The role of the calculated risk in earthwork
and foundation engineering," Journal of Soil Mechanics and Foundations
Division, ASCE, vol 91, no. SM4, Jul 1965.

Appendix A

LASS-I: COMPUTER PROGRAM FOR PRE-LIQUEFACTION ANALYSIS
OF HORIZONTALLY LAYERED SATURATED SOILS

By

Jamshid Ghaboussi*

INTRODUCTION

Computer program LASS-I is being developed for pre-liquefaction earthquake analysis of horizontally layered saturated granular soil deposits. This appendix is written to familiarize the reader with one research program in progress. A column of the horizontally layered saturated soil system is modeled as an assemblage of special one-dimensional elements capable of undergoing three displacement components at each node. Separate phases of solid granular skeleton and pore water pressure are modeled individually and coupling between the two phases is taken into account. The system can be, in general, subjected to three components of earthquake base acceleration; however, the present version of the computer program uses only one horizontal component and one vertical component of base motion. The response of the system computed by program LASS-I consists of time histories of motions of the two separate phases and the time histories of effective stresses and pore water pressure. A nonlinear material model is used to represent the behavior of the solid granular skeleton. A criterion for initial liquefaction in terms of effective stresses is provided to monitor the onset of liquefaction within each element, thereupon the material properties of such element is modified accordingly to correspond to post initial-liquefaction behavior.

The theoretical basis of the methodology has been reported in Ghaboussi and Wilson (1973a) and will only be discussed very briefly here.

---

* Associate Professor, University of Illinois, Urbana, Illinois.

METHOD OF ANALYSIS

The saturated granular soil system is treated as a two-phase medium with constituent materials being the granular solid skeleton and pore water. The two phases are coupled through volumetric strains. The method is general and has been applied to two-dimensional cases in previous studies of Ghaboussi and Wilson (1972 and 1973b). However, linearly elastic material properties were used for modeling the behavior of the solid skeleton. With this type of material model the pore pressures result only from transient elastic volumetric strains, which neglects the residual reduction in effective pressure (increase in pore water pressure) caused by dilatancy or volumetric coupling of granular soils under shear deformation. An appropriate nonlinear material capable of accounting for the changes in pore pressure under shear strains has been used in this study.

The horizontally layered system of saturated soils is assumed to consist of horizontal layers with specified thicknesses and material properties. Each layer is subdivided into a number of "layer elements," which consist of the medium contained between two horizontal planes a distance h apart. The plane separating two adjacent elements is referred to as the "nodal plane." The motion of the system is described by nodal-displacement degrees of freedom. In a general case each node has four displacement degrees of freedom; three components of displacement of the solid portion (u_x, u_y, u_z) and a vertical displacement of pore water w_y with respect to the solid. A schematic representation of a layered system and a typical layer element are shown in Figures A-1 and A-2.

The nodal planes remain horizontal during the motion of the systems, and they can only undergo parallel displacements. Torsional motion of the system is neglected. As a result of these assumptions there are only three nonzero strain components. The strain-displacement relations are:

$$\varepsilon_{yy} = u_{y,y}$$
$$\varepsilon_{xy} = u_{x,y} \qquad \qquad \text{(A-1)}$$
$$\varepsilon_{zy} = u_{z,y}$$

and the volumetric strain of pore water is given by the following relation:

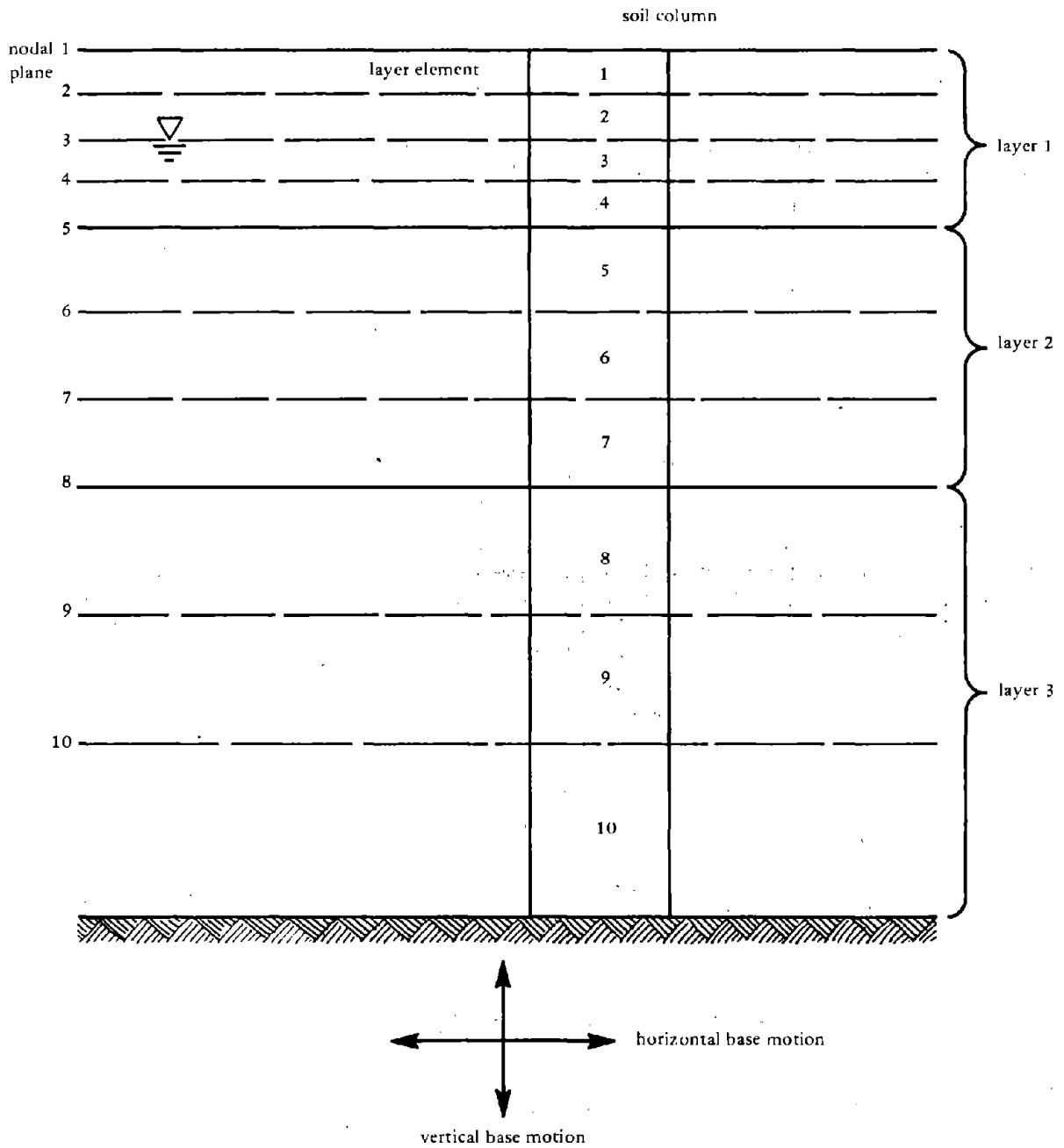$$\zeta = w_{y,y} \qquad \qquad \text{(A-2)}$$

285

Figure A-1. Schematic representation of layered soil.
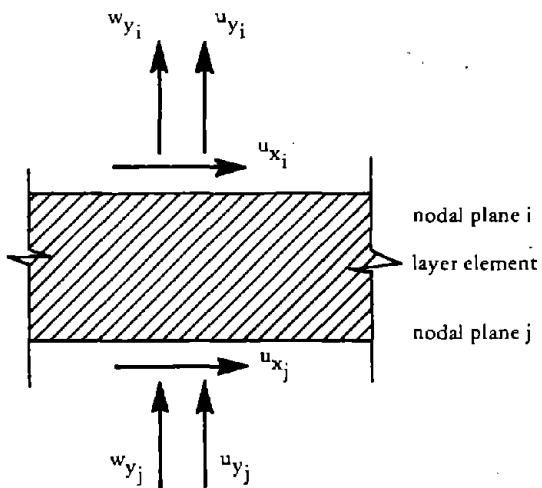

Figure A-2. Typical layer element.

286

For a typical layer element (shown in Figure A-2) the components of displacement are assumed to vary linearly between the nodal planes i and j. With this assumption on variation of displacements for each element, the stiffness matrix, mass matrix, and "dissipation resistance" matrix can be computed. The matrices for the system result from direct assembly of the element matrices.

The matrix equation of motion for the system can be written as follows.

$$\begin{bmatrix} M_s & 0 \\ 0 & M_f \end{bmatrix} \begin{Bmatrix} \ddot{u} \\ \ddot{w} \end{Bmatrix} + \begin{bmatrix} 0 & 0 \\ 0 & H \end{bmatrix} \begin{Bmatrix} \dot{u} \\ \dot{w} \end{Bmatrix} + \begin{bmatrix} K_{ss} & K_{sf} \\ K_{sf}^T & K_{ff} \end{bmatrix} \begin{Bmatrix} u \\ w \end{Bmatrix} = \begin{Bmatrix} M_{sI} \\ 0 \end{Bmatrix} \ddot{u}_g \qquad (A-3)$$

The displacement vectors u and w contain, respectively, the displacements of the solid portion and displacements of pore water with respect to solid. The subscripts s and f refer to solid and fluid, respectively. This system of equations is nonlinear. The nonlinearity is introduced only through the submatrix K_{ss} which contains the nonlinear material behavior of the solid granular skeleton. This nonlinear matrix equation of motion can be written symbolically as follows:

$$M \ddot{U} + D \dot{U} + K U = P_r \qquad (A-4)$$

The stiffness matrix K is the tangent stiffness matrix; hence, the matrix equation of motion is written in incremental form, for the purpose of time integration, as follows:

$$M \ddot{U}_t + D \dot{U}_t + K \Delta U_t = P_t - F_{t-\Delta t} \qquad (A-5)$$

The subscript t refers to time and ΔU_t is the increment of displacement. The internal resisting force vector $F_{t-\Delta t}$ is computed from stress at the end of the previous time step. The internal resisting force vector represents the forces required on the system which will equilibrate the stresses acting in the system. The incremental form of the matrix equation of motion is directly integrated in time to obtain the time history of the response of the system.

Two types of energy absorption mechanisms of equivalent damping effects are present in the analytical model used here. A hysteretic damping is introduced into the system by using the material model which will be discussed in the next section. The magnitude of energy absorbed

287

with this damping mechanism is dependent on the maximum shear strains which develop within each element. Another energy-absorption mechanism is provided through the dissipation resistance matrix which represents dissipation of pore water pressure and flow of pore water through the granular solid. These two damping effects appear to adequately represent the energy absorption in the system.

MATERIAL MODEL

The material model for the behavior of saturated sand within the range up to initial liquefaction which was used in computer program LASS-I is essentially based on experimental results and observations reported by Tatsuoka, Ishihara, and Yasuda (1973, 1974, and 1975).

The shear stress-strain relation under monotonic loading is represented by the following equation and shown in Figure A-3a.

$$\left(\frac{q}{p'}\right) = \frac{\gamma \, G_o \, S_{max}}{\gamma \, G_o + S_{max}} \tag{A-6}$$

in which q is the shear stress, p' is the effective pressure, and γ is the shear strain. This relation is assumed to apply to shear stress in the positive or negative direction. The unloading is assumed to take place linearly with the slope G_o until the previous maximum or minimum value of q is reached, whereupon stress-strain relation becomes valid again. The stress-strain relation in shear as represented by the above equation is assumed to remain constant up to the onset of initial liquefaction. This is a reasonable assumption as no significant changes occur in the void ratio of saturated sands during the earthquake prior to liquefaction. In the p'-q plane the shear yield loci take the form of straight lines radiating from the origin (Figure A-3b). Within the low stress range encountered in the earthquake analysis of soil deposits this appears to be a reasonable assumption. The existence of such yield loci for shear deformations has also been experimentally verified by Poorooshasb et al. (1967). However, it has been shown that for higher values of effective pressure the yield loci approach a state parallel to the p'-axis.

The initial effective pressures at each depth prior to application of shear stresses are denoted by p_o'. With the application of monotonically increasing shear stresses under undrained conditions, the stress point in the p'-q plane follows a path as shown in Figure A-3b which intersects the failure line at effective pressure p_ℓ'. This stress path has been approximated by a quarter of an ellipse which is given by the following equation:

288

$$f_2 = (p' - p'_\ell)^2 + \left(\frac{1}{\lambda^2}\right) q^2 - (p'_o - p'_\ell)^2 = 0 \qquad \text{(A-7)}$$

The failure line is given by

$$f_1 = q - p' \tan \phi = 0 \qquad \text{(A-8)}$$

This stress path is completely defined by the two material constants ϕ and λ. The parameter ϕ is the angle of the failure line. The material parameter λ is the ratio of the major and minor axes of the ellipse, as given by the following relation.

$$\lambda = p'_\ell \tan \left(\frac{\phi}{p'_o - p'_\ell}\right) \qquad \text{(A-9)}$$

As can be seen from Figure A-3b, under a monotonic increase in shear stress, the effective pressure p' decreases, and the pore water pressure increases in the undrained condition. In unloading the effective pressure is assumed to remain constant until the stress path reaches the curve $f_2 = 0$ at either side of the p'-axis, whereupon the stress path follows this curve to a higher maximum value of q/p'.

Ishihara and his co-workers have introduced the concept of "multiplicity of state boundary surface" which explains several aspects of the behavior of sands. As a result of this concept they have postulated that loading stress paths on each side of the p'-axis are independent of each other. In a cyclic stress situation, therefore, at each instant two values of p'_o exist, which are associated with stress paths for positive and negative values of q.

Initial liquefaction in experiments occurs at a stress point very close to the failure line, but the stress path does not quite reach the failure line. To take this into account a new material parameter is introduced which represents the maximum value of the (q/p') ratio attainable for each element of soil, and this parameter is denoted by "α".

It has long been recognized that the relative density of sand D_r is an important parameter in evaluating the liquefaction potential of saturated soils. Therefore, it is desirable to determine the model material parameters in terms of the relative density. The most important material parameter in terms of its influence on the buildup of pore water pressure is λ which defines the contractancy property of the material.
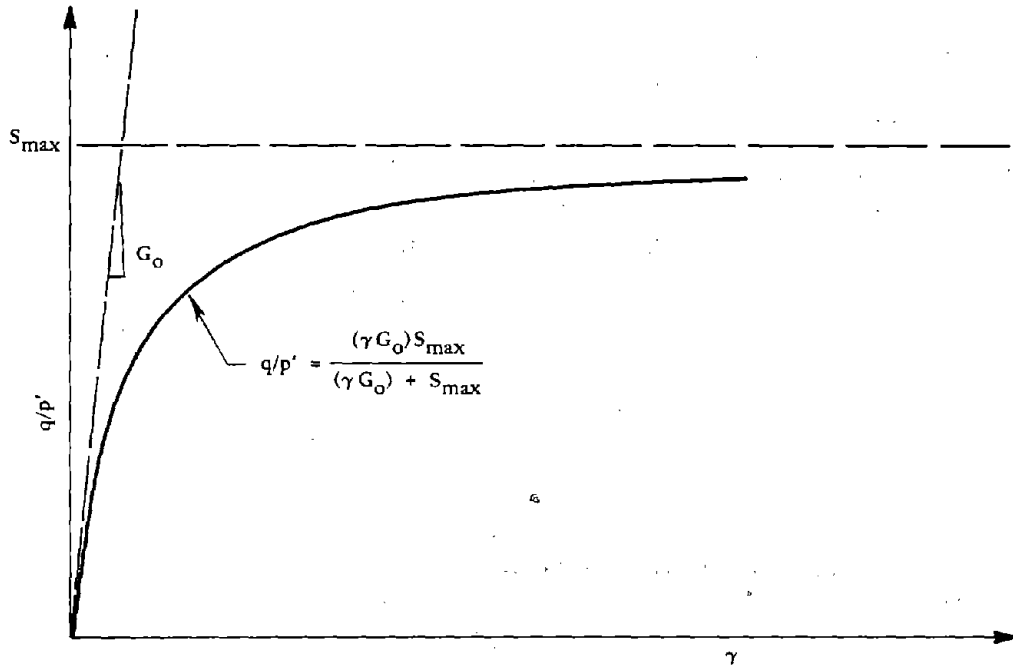
(a)   Normalized stress-strain relationship.

$$q/p' = \frac{(\gamma G_o) S_{max}}{(\gamma G_o) + S_{max}}$$
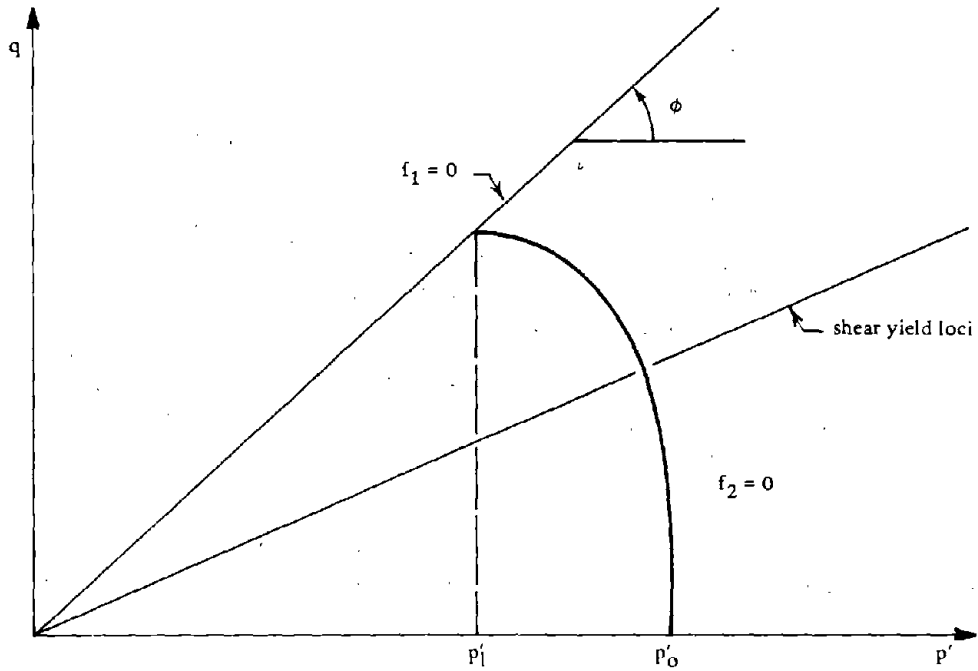
(b)   Stress path.

Figure A-3.   Material model.

The values of λ determined from various reported experimental results are shown in Figure A-4 versus the relative density. The data appears to fall within a narrow band for low and medium densities. The value of λ increases with relative density, and the value of $\lambda = 1$ occurs at about 35% relative density. This corresponds to a circular stress path $f_2 = 0$. Below 35% relative density the major axis of f_2 falls along p'-axis, and above this relative density the major axis of f_2 is parallel to q-axis. From the data in Figure A-4, which are for fairly uniform sands with rounded particles, it appears that λ is only dependent on relative density, and the effective pressure p_o' has little effect on it. Castro's (1969) data for experiments with value of $p_o' = 1.0$, 4.0, and 10.0 kg/cm^2 do not differ appreciably. As a result of this observation it can be concluded that, for fairly uniform sands with rounded particles, the shape of the stress path f_2 remains constant. Only its size changes with p_o', since λ is independent of p_o'. However, Castro also has reported the results of experiments on two types of sands with angular and subangular particles. The values of λ determined from these results are shown in Figure A-5, and it is evident that the effective pressure p_o' has a great deal of influence on λ. Therefore, for these types of sands the shape of the stress path f_2 must also be dependent on the effective pressure. However, at present there is not sufficient data to justify quantification of this phenomenon, and it is not included in computer program LASS-I.

POST-INITIAL-LIQUEFACTION BEHAVIOR

After the stress path has reached a level very close to the yield line or monotonic strain has reached a certain level, it is said that the soil element is at initial liquefaction. When using a strain criterion for initial liquefaction, it is important to distinguish between the actual strain in the cyclic environment and its monotonic strain equivalent; the latter must be used. After initial liquefaction, the material behavior of the soil element changes abruptly. Although this material behavior change is gradual in cyclic tests under monotonic loading for low relative densities (especially for dense sands), very abrupt material behavior changes have been observed. In any case, for the purpose of material modeling, this material behavior change must be considered an abrupt and discrete phenomenon.

There appears to be very little experimental data to provide insight as to the mechanism of the post-initial-liquefaction behavior of saturated sands. Limited experimental data does point to certain general material postulates, but an acceptable material mechanism must await further experimental evidence. Ishihara et al. (1976) have used a specific stress path for post-initial-liquefaction behavior which appears justified, based upon the limited experimental data. This specified stress
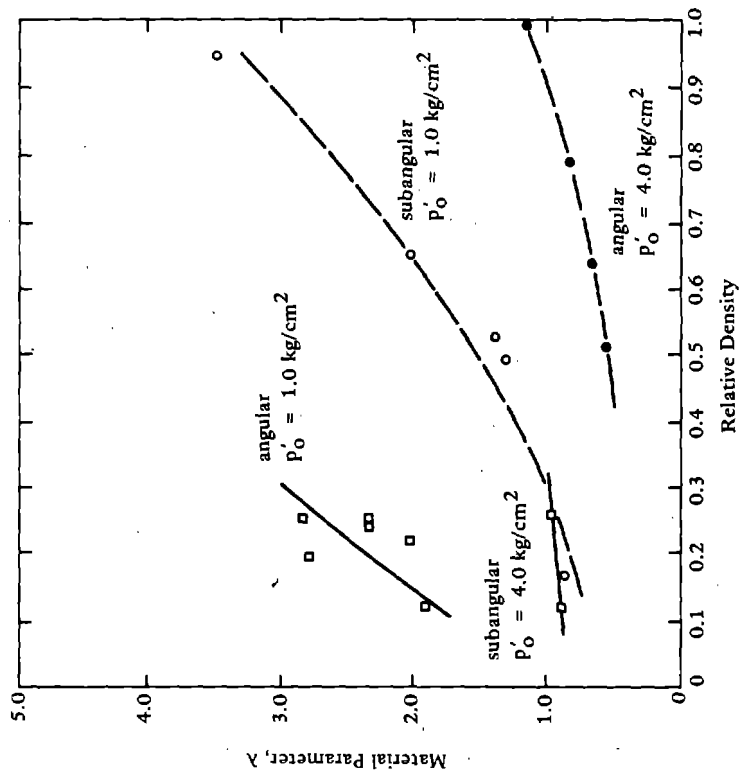
Figure A-5. Material parameter λ versus relative density, showing effects of angularity.
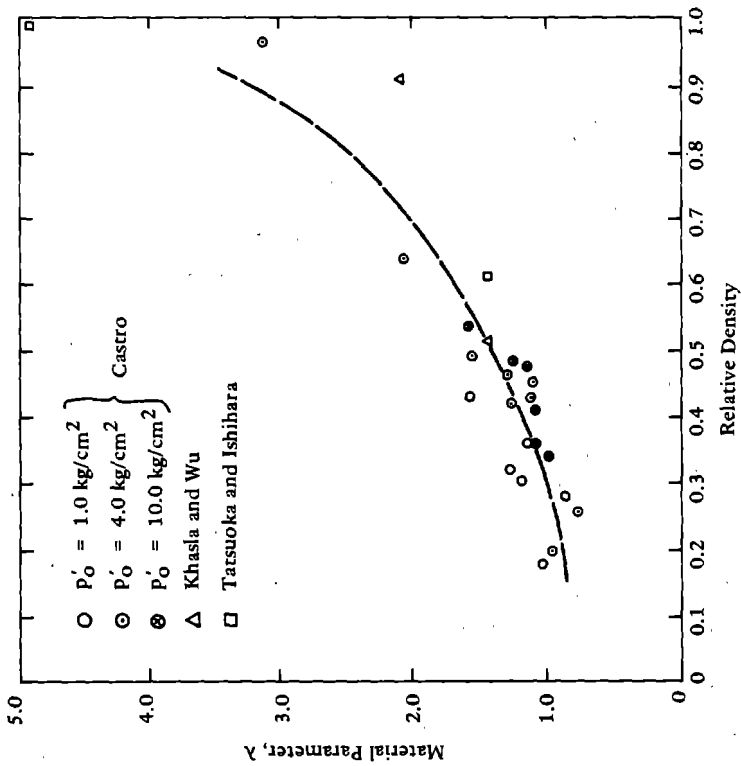

Figure A-4. Material parameter λ versus relative density.

292

path is sufficient for the type of application reported in Ishihara et al. (1976). However, a general material model needed for systematic dynamic stress analysis requires information as to the deformational characteristics of sand at post-initial-liquefaction range. Sufficient experimental data for development of such a material model does not exist at present.

All sands do not lose their strength after the initial liquefaction. It appears that only in very loose states or at low densities does complete liquefaction almost instantaneously follow initial liquefaction; the stress point in p'-q plane instantaneously follows the failure line down to the origin. At higher values of relative densities, additional stress cycles are required to further reduce the effective pressure and achieve complete liquefaction. It appears reasonable to assume that the shear loading and unloading characteristic does not change appreciably after initial liquefaction. From cyclic tests it seems that the pore pressures and effective pressures start oscillating after initial lique-faction because the stress point must move up along the failure line upon loading which reduces pore pressure, and upon unloading the pore pressure increases. The magnitude of pore pressure increase in each cycle of loading will depend on relative density of the sand and the highest magnitude of shear stress in that cycle. It seems the shear stresses after initial liquefaction cause an interlocking of particles, resulting in higher effective pressure which, upon unloading, is trans-ferred to pore pressures. A possible mechanism for explaining this phenomenon is a change in compressibility of solid skeleton.

REFERENCES, APPENDIX A

Castro, G. (1969) "Liquefaction of sands," Harvard Soil Mechanics Series, no. 81, Cambridge, Mass, Jan 1969.

Ghaboussi, J. and Wilson, E. L. (1972) "A variational formulation of dynamics of fluid saturated porous elastic solids," Journal of the Engi-neering Mechanics Division, ASCE, vol 98, no. EM8, Aug 1972.

Ghaboussi, J. and Wilson, E. L. (1973a) "Liquefaction analysis of satu-rated granular soils," in Proceedings of the Fifth World Conference on Earthquake Engineering, Rome, Italy, Jun 1973. Rome, Italy, Rome Inter-national Association of Soil Mechanics, 1974.

Ghaboussi, J. and Wilson, E. L. (1973b) "Seismic analysis of earth dam-reservoir systems," Journal of the Soil Mechanics and Foundations Division, ASCE, vol 99, no. SM10, Oct 1973, pp 849-862.

Ishihara, K., et al. (1976) "Prediction of liquefaction in sand deposits during earthquakes," Soils and Foundations (Japan), vol 16, no. 1, Mar 1976.

Ishihara, K., Tatsuoka, F. and Yasuda, S. (1975) "Undrained deformation and liquefaction of sand under cyclic stresses," Soils and Foundations (Japan), vol 15, no. 1, Mar 1975.

Poorooshasb, H. B., Holubec, I. and Sherbourne, N. (1967) "Yielding and flow of sand in triaxial compression," Canadian Geotechnical Journal, vol 4, 1967.

Tatsuoka, F. and Ishihara, K. (1973) "Stress path and dilatancy performance of a sand," in Proceedings of Eighth International Conference on Soil Mechanics and Foundations Engineering, Moscow, vol 1, Aug 1973, pp 419-424. International Society of Soil Mechanics and Foundation Engineering, 1973.

Tatsuoka, F. and Ishihara, K. (1974) "Drained deformation of sand under cyclic stresses reversing direction," Soils and Foundations (Japan), vol 14, no. 3, Dec 1974.